

Table of contents

| | |
|--|-----------|
| A. INTRODUCTION..... | 9 |
| 1. Boron..... | 10 |
| 1.1 <i>Boron trihalides.....</i> | <i>10</i> |
| 1.2 <i>Boric acid.....</i> | <i>10</i> |
| 1.3 <i>Boron hydrides.....</i> | <i>11</i> |
| 1.4 <i>Carboranes.....</i> | <i>12</i> |
| 1.4.1 <i>Medical application for Carboranes.....</i> | <i>13</i> |
| 2. Boron Neutron Capture Therapy..... | 16 |
| 2.1 <i>Epithermal neutron sources.....</i> | <i>17</i> |
| 2.2 <i>Boron delivering agents.....</i> | <i>18</i> |
| 2.2.1 <i>Approved Boron delivering agents.....</i> | <i>19</i> |
| 2.2.2 <i>Boron delivering agents under evaluation.....</i> | <i>21</i> |
| 3. Theranostic..... | 23 |
| 3.1 <i>Theranostic approach and BNCT.....</i> | <i>24</i> |
| 3.1.1 <i>Positron Emission Tomography (PET).....</i> | <i>24</i> |
| 3.1.2 <i>Single-Photon Emission Computed Tomography (SPECT).....</i> | <i>26</i> |
| 3.1.3 <i>Nuclear Magnetic Resonance Imaging (¹H-MRI).....</i> | <i>27</i> |
| 3.1.4 <i>Fluorine Magnetic Resonance Imaging (¹⁹F-MRI).....</i> | <i>28</i> |
| 4. Fluorine 18..... | 29 |
| 4.1 <i>Fluorine-18 production.....</i> | <i>30</i> |
| 4.2 <i>Labeling methods with Fluorine-18.....</i> | <i>31</i> |
| 4.2.1 <i>Electrophilic radiofluorination.....</i> | <i>31</i> |
| 4.2.2 <i>Nucleophilic radiofluorination.....</i> | <i>32</i> |
| 4.2.3 <i>Noncanonical bonds (B-¹⁸F, Si-¹⁸F).....</i> | <i>33</i> |
| B. OUTLINE OF THE THESIS..... | 35 |
| C. RESULTS AND DISCUSSION..... | 37 |
| 1. Organotrifluoroborate Sugar Conjugates – part I..... | 38 |
| 1.1 <i>Synthetic project.....</i> | <i>38</i> |
| 1.2 <i>Cytotoxicity evaluation.....</i> | <i>43</i> |
| 1.3 <i>Stability evaluation.....</i> | <i>45</i> |
| 1.4 <i>Radiolabeling optimization.....</i> | <i>47</i> |
| 1.5 <i>HR-MS stability studies for the radiolabeling optimization.....</i> | <i>49</i> |
| 1.6 <i>In vivo PET imaging.....</i> | <i>53</i> |
| 2. Organotrifluoroborate Sugar Conjugates – part II..... | 55 |
| 2.1 <i>Synthetic project.....</i> | <i>55</i> |
| 2.2 <i>Stability evaluation.....</i> | <i>66</i> |
| 3. Nanomaterial decorated with borane structures..... | 68 |
| 4. Carborane-containing drug analogs..... | 74 |

| | |
|---|------------|
| D. LIST OF PUBLICATIONS | 82 |
| E. EXPERIMENTAL DETAILS..... | 83 |
| 1. Organotrifluoroborate Sugar Conjugates – part I | 84 |
| 1.1 <i>Chemistry</i> | 84 |
| 1.1.1 General | 84 |
| 1.1.1 Abbreviations..... | 85 |
| 1.1.2 General Procedures | 86 |
| 1.1.3 Synthetic Schemes..... | 87 |
| 1.1.4 Products characterizations | 91 |
| 1.2 <i>Biology</i> | 119 |
| 1.2.1 Cell culture..... | 119 |
| 1.2.2 Cell viability assay | 119 |
| 1.3 <i>Stability evaluation</i> | 120 |
| 1.3.1 ¹⁹ F NMR kinetic analysis for Glc1..... | 120 |
| 1.3.2 ¹⁹ F NMR kinetic analysis for Glc2..... | 121 |
| 1.3.3 ¹⁹ F NMR kinetic analysis for Glc3..... | 122 |
| 1.3.4 ¹⁹ F NMR kinetic analysis for Glc4..... | 123 |
| 1.3.5 ¹⁹ F NMR Kinetic analysis for Man3 | 124 |
| 1.4 <i>¹⁸F radiolabeling and stability studies</i> | 125 |
| 1.4.1 General | 125 |
| 1.4.2 Radiolabeling with [¹⁸ F] ⁻ and solid precursor..... | 125 |
| 1.4.3 Radiolabeling with [¹⁸ F] ⁻ and solid precursor..... | 126 |
| 1.4.4 Radiolabeling with acidified [¹⁸ F] ⁻ and solid precursor..... | 126 |
| 1.4.5 Stability in vitro studies | 127 |
| 1.5 <i>In vivo PET imaging</i> | 128 |
| 2. Organotrifluoroborate Sugar Conjugates – part II | 129 |
| 2.1 <i>Chemistry</i> | 129 |
| 2.1.1 General | 129 |
| 2.1.2 Abbreviations..... | 130 |
| 2.1.3 General Procedures | 131 |
| 2.1.4 Synthesis and characterization of alkyne 11 | 132 |
| 2.1.5 Synthetic Schemes..... | 134 |
| 2.1.6 Products characterizations | 136 |
| 2.2 <i>Stability Evaluation</i> | 151 |
| 2.2.1 ¹⁹ F NMR kinetic analysis for Glc5..... | 151 |
| 2.2.2 ¹⁹ F NMR kinetic analysis for Glc6..... | 152 |
| 2.2.3 ¹⁹ F NMR kinetic analysis for Glc7..... | 153 |
| 2.2.4 ¹⁹ F NMR kinetic analysis for Glc9..... | 154 |
| 3. Nanomaterial decorated with borane structures | 155 |
| 3.1 <i>Chemistry</i> | 155 |
| 3.1.1 General | 155 |
| 3.1.2 Synthetic scheme..... | 155 |
| 3.1.3 Synthetic procedures..... | 156 |

| | |
|--|------------|
| 4. Carborane-containing drug analogs | 158 |
| 4.1 <i>Chemistry</i> | 158 |
| 4.1.1 General | 158 |
| 4.1.2 Synthetic scheme..... | 158 |
| 4.1.3 Synhtetic procedures and characterizations | 160 |
| F. REFERENCES..... | 163 |



UNIVERSITÀ DEL PIEMONTE ORIENTALE
DOTTORATO DI RICERCA
IN CHEMISTRY & BIOLOGY

Via Duomo, 6
13100 – Vercelli (ITALY)

DECLARATION AND AUTHORISATION TO ANTIPLAGIARISM DETECTION

The undersigned Laura Confalonieri student of the Chemistry & Biology Ph.D. course (XXXV°
Cycle)

declares:

- to be aware that the University has adopted a web-based service to detect plagiarism through a software system called “Turnit.in”,
- his/her Ph.D. thesis was submitted to Turnit.in scan and reasonably it resulted an original document, which correctly cites the literature;

acknowledges:

- his/her Ph.D. thesis can be verified by his/her Ph.D. tutor and/or Ph.D. Coordinator in order to confirm its originality.

Date: 12/11/2022

Signature:*Laura Confalonieri*.....

Abbreviation list (alphabetical order)

| | |
|--------------------------------|--|
| [¹⁸F]EF5 | 2-(2-nitro-1H-imidazol-1-yl)-N-(2,2,3,3,3-pentafluoropropyl)-acetamide |
| [¹⁸F]FDG | [¹⁸ F]Fluorodeoxyglucose |
| ¹⁸F-BPA | 4- ¹⁰ B-Borono-2- ¹⁸ F-fluoro-L-phenylalanine |
| 6-[¹⁸F]FDOPA | 3,4-dihydroxy-6-[¹⁸ F]fluoro-L-phenylalanine |
| ABNS | Accelerator-based neutron sources |
| BNCT | Boron Neutron Capture Therapy |
| BPA | L-Boronophenylalanine |
| BSH | Sodium borocaptate |
| CAs | Contrast agents |
| CT | Computed tomography |
| CuAAC | Copper-catalyzed azide-alkyne cycloaddition, click reaction |
| EGFR | Epidermal growth factor receptors |
| EPR | Enhanced permeability and retention effect |
| FBY | Fluoroboronotyrosine |
| FDA | Food and Drug Administration |
| GB-10 | Sodium decaborate |
| GBM | Glioblastoma multiforme |
| Gd-DTPA | Gadolinium-Diethylenetriaminepentacetate |
| GLUT | Facilitative sugar transporter |
| high-LET | High linear energy transfer |
| ICP-AES | Inductively coupled plasma-atomic emission spectrometry |
| ICP-MS | Inductively coupled plasma mass spectrometry |
| IE | Isotopic exchange |
| k | Rate constant |
| LDLs | Low-density lipoproteins |
| mAbs | Monoclonal antibodies |
| MRI | Magnetic Resonance Imaging |
| NSAID | Non-steroidal anti-inflammatory drug |
| PAMAM | Polyamidoamine |
| PEG | Polyethylene glycol |

| | |
|------------------------|--|
| PET | Positron Emission Tomography |
| RBE | Radiobiological effectiveness |
| RC | Radiochemical |
| cRDG | Cyclic Arg-Gly-Asp |
| SA | Specific activity |
| SiFA | Silicon-based fluoride acceptor |
| SPECT | Single-photon emission computed tomography |
| T₁ | Longitudinal relaxation time |
| t_{1/2} | Half-life value |
| T₂ | Transverse relaxation time |
| TBR | Tumor-to-blood concentrations ratio |
| TNTR | Tumor-to-normal tissue ratio |
| VEGFR | Vascular endothelial growth factor receptors |

A. INTRODUCTION

1. Boron¹

Boron (B) is the only nonmetallic element in Group 13. Discovered in 1808, its name derives from the Arabic “buraq” word for borax². It occurs naturally as borax and kernite and has a low cosmic and terrestrial abundance due to the unlikely nucleosynthesis reactions for light elements. Boron exists in two isotopes: ¹¹B is the most abundant (80%), while ¹⁰B counts only for 20%. Like the other first elements from the other groups, boron differs from its congeners because of its small atom radius. This property correlates with high ionization energy, high electronegativity, and a tendency to form covalent bond. Starting from an electronic configuration with three external electrons ([He]2s² 2p¹), boron can reach up to six electrons in the valence shell by forming three covalent bonds. As a result, many of its compounds act as Lewis acids, accepting a pair of electrons from a donor to complete the octet.

1.1 Boron trihalides

Boron trihalides (BX₃) are widely used Lewis acids in daily lab practice. Unlike the halides of the other elements in Group 13, they are monomeric in the gas, liquid, and solid states. Boron trifluoride and trichloride are gases, the tribromide is a volatile liquid, and the triiodide is solid. The order of acidity is contrary to the order of electronegativity of the attached halogen (BF₃<BCl₃<BBr₃). The tetrafluoridoborate anion, BF₄⁻, is used in preparative chemistry when large noncoordinating ions are needed. Both BCl₄⁻ and BBr₄⁻ can be prepared in non-aqueous solvents, but they are too unstable to be convenient. The corresponding organotrifluoroborates (R-BF₃⁻) are handy reagents in organic chemistry with a wide range of applications.

1.2 Boric acid

Boric acid, B(OH)₃, is a weak Brønsted acid in an aqueous solution. In concentrated neutral or basic solution, B(OH)₃ tends to form polynuclear anions of formula [B₃O₃(OH)₄]⁻. Boric acid reacts with alcohol in the presence of sulfuric acid and forms simple borate esters B(OR)₃. 1,2-Diols have a particularly strong tendency to form borate esters due to the chelate effects, producing cyclic structures such as the pinacol ester. Organoboronic acids, R-B(OH)₂, are of primary importance for the Suzuki-Miyaura coupling reactions. They are subjected to the formation of trimeric cyclic anhydrides called boroxines. This equilibrium has no bearing on the coupling process but can influence the reaction stoichiometry³.

1.3 Boron hydrides

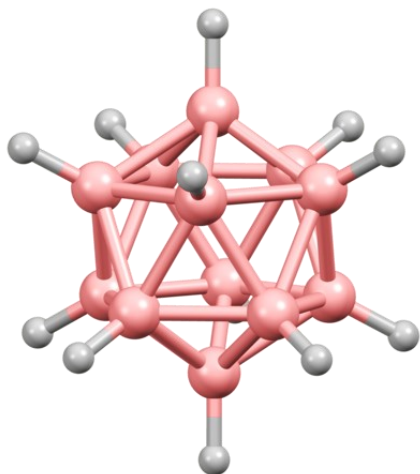


Figure 1A - $[B_{12}H_{12}]^{2-}$ structure.

By Ben Mills - 01.10.2022 Own work, Public Domain,

<https://commons.wikimedia.org/w/index.php?curid=99571007>

Among the compounds containing just B and H, the simplest hydride of boron is the gaseous diborane (B_2H_6). Controlled pyrolysis of B_2H_6 in the gas phase – extensively studied by Alfred Stock - provides a route to higher boranes and borohydrides. Boron clusters have delocalized molecular orbitals that stabilize the entire molecule, but their relative stability depends on the cage structure. According to Wade's rules - developed by Kenneth Wade in the 1970s^{4,5} - the species of formula $[B_nH_n]^{2-}$ have a *closo* structure, with a B atom at each corner of a closed deltahedron and no B-H-B bonds. This series of ions range from $n=5$ to $n=12$, with the icosahedral $[B_{12}H_{12}]^{2-}$ ion as a prominent exponent (**Figure**

1A). Boron clusters of formula B_nH_{n+4} have the *nido* structure. They can be considered as *closo*-boranes which has lost a vertex but has B-H-B bond as well as B-B bonds (**Figure 1B**). Clusters of formula B_nH_{n+6} have an *arachno* structure. They are richer in hydrogen but highly unstable even at room temperature. They can be regarded as *closo*-structures less two vertices.

Reactions of boron hydrides with Lewis bases range from cleavage of the BH_n unit from the cage to deprotonation of the cluster, cluster enlargement, and abstraction of one or more protons. Instead, the electrophilic displacement of H^+ catalyzed by a Lewis acid led to Friedel-Crafts reactions and provides a route to alkylated and halogenated species ⁶.

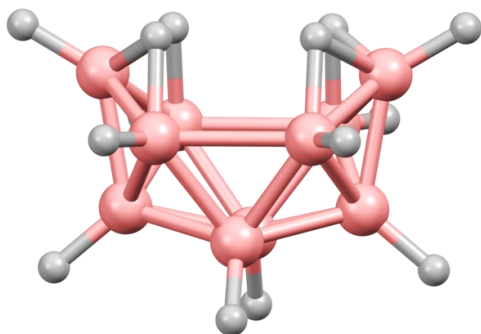


Figure 1B – $B_{10}H_{14}$ structure.

By Ben Mills - 01.10.2022 Own work, Public Domain,

<https://commons.wikimedia.org/w/index.php?curid=98714789>

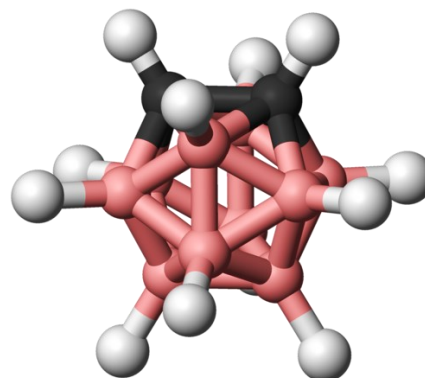


Figure 1C – $1,2-B_{10}C_2H_{12}$ structure.

Public Domain, 01.10.2022

<https://commons.wikimedia.org/w/index.php?curid=1405900>

1.4 Carboranes⁷

Closely related to the polyhedral boranes are the carboranes, a large family of clusters that contains both B and C atoms (**Figure 1C**). From the decaborane ($B_{10}H_{14}$, *nido* structure) via displacement of H_2 by a weak base (typically R_2S or CH_3CN) and subsequent addition of an alkyne is possible to obtain a *closo*-1,2- $B_{10}C_2H_{12}$ structure.

The chemistry of *closo*-carboranes is grouped in five kinds of reactions: thermal cage rearrangement, base promoted deboronation, substitution at carbon, substitution at boron, and reductive cage opening without loss of boron.

Closo-carboranes survive in the air and can be heated without decomposition, but they undergo cage isomerization upon heating. At $500^\circ C$ in an inert atmosphere, they convert into 1,7- $B_{10}C_2H_{12}$, which in turn isomerize at $700^\circ C$ to the 1,12-isomer (**Figure 2**).

Although 1,2- $B_{10}C_2H_{12}$ is stable, the cluster can be partially fragmented in strong base and deboronated to yield *nido*- $[B_9C_2H_{12}]^-$. The H atoms attached to the carbons are mildly acidic, a consequence of the polarity induced by the electron withdrawing carbon atoms. It is important to note that the electron-withdrawing character of the skeletal carbons is a local effect due to the higher electronegativity of carbon atoms compared to their boron neighbors and is not indicative of an overall electron "deficiency" of the electron density in the cage. The C-H acidity is highest in 1,2-isomers (*o*-carborane), decreases in the 1,7-isomer (*m*-carborane), and is zero in the 1,12-isomer (*p*-carborane). It is possible to obtain C-metallated derivatives by treatment with butyllithium or Grignard reagents. The resulting product undergoes many reactions characteristic of organolithium reagents to afford C-substituted organo-derivatives.

The B-H bonds exhibit virtually no acidic behavior because of the low electronegativity of boron. Moreover, the presence of ten boron vertexes in four different electronic environments in the 1,2- $B_{10}C_2H_{12}$ cage often produces complex substitutions pattern. However, the electron-delocalized character of the *o*-carborane cage renders it, much like an aromatic ring, susceptible to attack by electrophiles. Reactions with halogenating agents afford a range of B-fluoro, -chloro, -bromo, and -iodo derivatives that can be exploited in cross-coupling reactions. Usually, only the relatively negative boron atoms at vertexes 9, 12, 8, and 10 are halogenate, and no substitution takes place at carbon. B (9)-alkyl, alkenyl, or aryl derivatives can be synthesized from 1,2- $R_2B_{10}C_2H_9$ -9-I by reaction with Grignard reagents mediated by phosphino-palladium complexes.

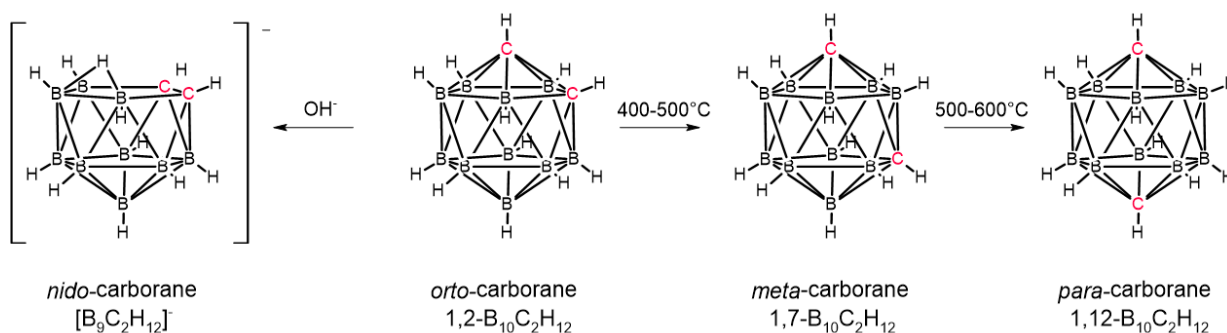


Figure 2 – Carborane structures. *Ortho-carboranes survive in the air and can be heated without decomposition, but they undergo cage isomerization upon heating. At 500°C in an inert atmosphere, they convert into meta-carboranes, which in turn isomerize at 700°C to the para-carboranes. Closo-carboranes can be partially fragmented in strong base and deboronated to yield nido-[B₉C₂H₁₂].*

1.4.1 Medical application for Carboranes

Today, medicinal chemistry heavily relies on organic chemistry; most of the marketed drugs are purely organic molecules that can incorporate nitrogen, oxygen, and halogens besides carbon and hydrogen. Commercial boron-based drugs are still rare, but there is an increasing interest in carboranes clusters due to their unique properties that are not present in organic counterparts^{8,9}. These unique properties are ascribed to the boron atoms, thanks to their inherent electron deficiency, lower electronegativity, and smaller orbital size compared to carbon¹⁰.

Currently, the main application for carboranes is the design of agents for Boron Neutron Capture Therapy (BNCT) via coupling with tumor-targeting vectors^{11–15}. Recently, carboranes were exploited as scaffolds for imaging probes and boron-dipyrromethene (BODIPY) dyes^{16–18}.

An upcoming application for carboranes clusters is their employment as pharmacophores¹⁹. A pharmacophore is a partial structure in which important functional groups and hydrophobic structures are arranged in suitable positions for binding to a receptor²⁰. Though carboranes may not intuitively appear to be appropriate moieties for incorporation into pharmaceuticals, the H₂C₂B₁₀H₁₀ carborane cage occupies approximately the same volume as a rotating phenyl ring and is likewise a hydrophobic entity⁸. Their hydrophobicity – due to the presence of hydridic B–H units – can be a beneficial property for transport across cell membranes and the blood–brain barrier (BBB) as well as for hydrophobic interactions with binding pockets in enzymes²¹. The inorganic nature of carborane clusters prevents enzymatic degradation, and their non-toxicity lowers the toxic side effects of the potential drugs¹⁰. The unique three-dimensional structure and superior synthetic flexibility of carboranes compared to aryl rings can be used to probe and optimize

protein binding in an unprecedented manner and fine-tune the pharmacokinetics of new drug candidates⁸. Moreover, the unique spatial arrangement of the cage carbon atoms in *ortho*, *meta*, and *para*-carboranes can serve as a scaffold to direct the relative orientation of substituents optimizing the binding affinity¹⁹.

Carborane-containing structures have been used in the design of numerous receptor ligands¹⁹. The pioneering studies in this field were conducted in early 2000 on the development of novel ligands for the nuclear (intracellular) estrogen receptors (ERs)²². Estrogen receptors play a central role in the treatment of breast cancers as well as other pathologies correlated to the reproductive system²³. They exist as two subtypes, α and β ^{24,25}. Over the years, carborane-containing ligands have demonstrated both agonistic and antagonistic activities, as well as a selective affinity for specific ER subtypes²⁶⁻²⁸.

Using the same approach, hundred of carborane-containing ligands have been developed for some of the most relevant receptors, including but not limited to the purinergic receptor, vitamin D receptor, and epidermal growth factor receptor¹⁹.

Among the proteins targeted with these types of structures, the cyclooxygenase (COX) enzymes are relevant for better understanding part of this thesis (see **Result and Discussion - section 4**). COX is a homodimer and integral membrane protein that exists in two isoforms: COX-1, which is constitutively expressed in most tissues and is known as a “housekeeping” enzyme, and COX-2, which is inducible and primarily associated with pain, fever, and inflammation²⁹. Most nonsteroidal anti-inflammatory drugs (NSAIDs) used for treating pain and inflammation are non-specific and target both isoforms. The side effects correlated with the non-selective inhibition of COX-1 and COX-2 range from gastrointestinal disorders to more severe consequences for long-term use²⁹. Moreover, recent studies have revealed that COX-2 is overexpressed in various cancers and is often associated to a bad prognosis^{30,31}.

The isoforms share a similar structure and high sequence identity, but the active site of COX-2 is approximately 25% larger than that of COX-1²⁹. Based on this data, the size-extension of classical NSAIDs has successfully yielded inhibitors with COX-2 selectivity. Accordingly, celecoxib and rofecoxib, larger molecules compared to other NSAIDs, were introduced as COX-2 selective inhibitors³². Unfortunately, a high number of these drugs has been withdrawn from the market after a few years due to the increased risk of cardiovascular events^{33,34}.

This fact spurred the research of new COX-2 inhibitors with better safety profiles. Some meta-analyses hinted that the more selectivity of drugs for COX-2 leads to higher risks of cardiovascular toxicities, which in turn demands moderately selective COX-2 ³⁵. In this contest, Hey-Hawkins and coworkers developed several carborane-containing analogs of indomethacin, rofecoxib, and mefenamic acid. Often, the nido-containing structures were more potent than the parent closo compounds, and the activity greatly depended on the isomer employed^{29,36,37}.

2. Boron Neutron Capture Therapy

Boron Neutron Capture Therapy (BNCT) is a cancer treatment based on a nuclear reaction between boron atoms and neutrons³⁸. ^{10}B nuclei have a very high nuclear cross section for neutron capture compared to other more abundant elements. Thanks to this property, ^{10}B has been employed both for emergency reactivity control in nuclear reactors and the BNCT development. Upon neutron capture, ^{10}B becomes ^{11}B in an excited state. This unstable species spontaneously decays to high linear energy transfer (high-LET) α particle (^4He) and a recoiling ^7Li nucleus. The fission process also frees a small amount of γ radiation and approximately 2.4 MeV of kinetic energy³⁹ (**Figure 3A**). The high-LET α particles generated show cytotoxic effects only within the cell in which they were released, as their path length in tissues is approximately 5-9 μm ⁴⁰. So, upon accumulation of the ^{10}B -containing molecules inside the cancer cells and irradiation of the area with low-energy neutrons, the malignant cells can be selectively killed sparing the surrounding healthy tissues (**Figure 3B**)³⁸. However, two requirements must be fulfilled to ensure a successful treatment: enough ^{10}B atoms (thousand) must be – exclusively – inside the cancer cells and a sufficient flux of neutrons (ten million per second) must be directed toward the tumor³⁸. Over the last 50 years, BNCT has been used in clinical trials on a variety of tumors, including but not limited to glioblastoma multiforme (GBM)⁴¹, primary and recurrent head and neck cancer^{42,43}, lung cancer⁴⁴, liver cancer, and primary and metastatic melanoma⁴⁵.

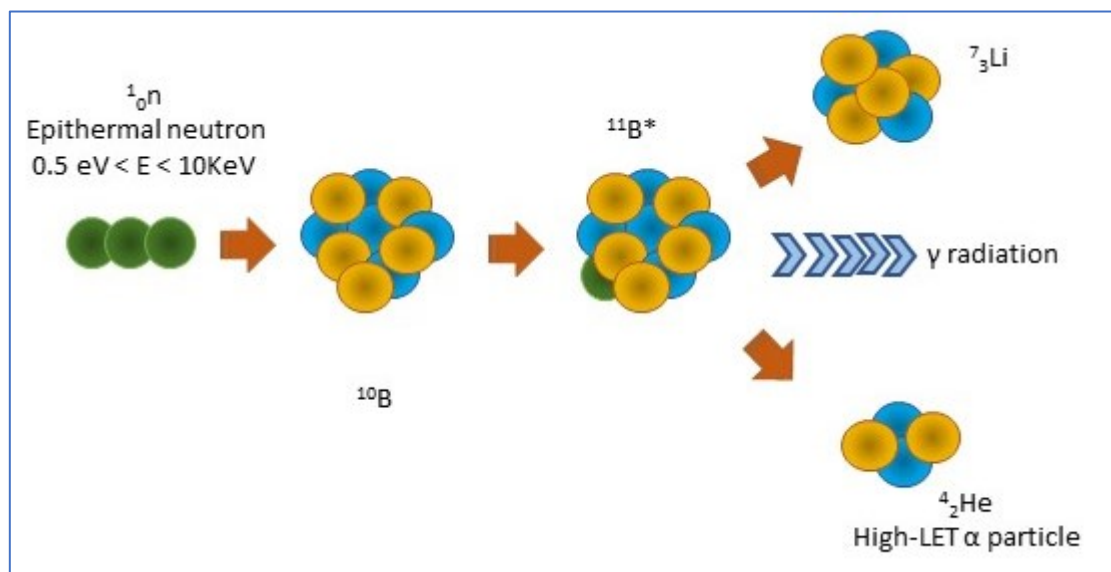


Figure 3A - Boron neutron capture reaction

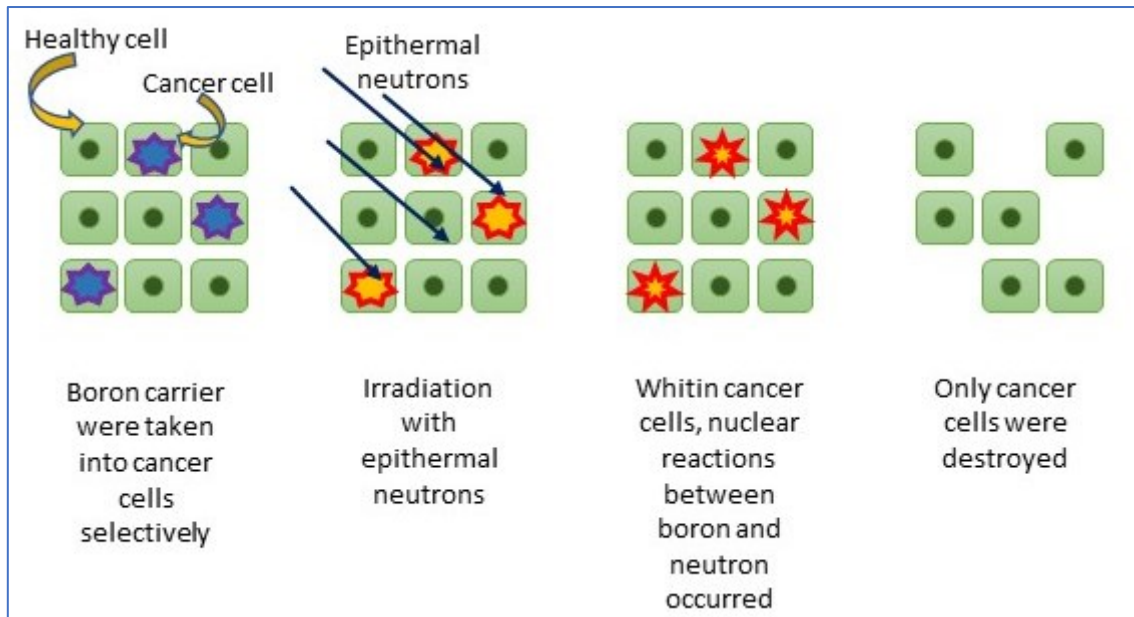


Figure 3B – The mechanism of selective killing of tumor cells with BNCT

2.1 Epithermal neutron sources

For BNCT, neutrons must be delivered with a high flow rate, at the “right” energy, and with minimal contaminants in the radiation beam. The low-energy – epithermal - neutrons required for the therapy have energy between 0.5eV and 10 KeV and can be obtained from two sources: nuclear reactors or particle accelerators⁴⁶. The former source of neutrons is the historical one, but nowadays there are fewer facilities able to carry on BNCT clinical trials, the legislation is becoming stricter, and it is not conceivable the hypothesis to install nuclear reactors in hospital environments. On the other hand, accelerator-based neutron sources (ABNS) are a rising reality in BNCT⁴⁷. They are more compact than nuclear reactors, can be sited in hospitals, and are subjected to lighter regulations. Unfortunately, the neutron beam generated from the accelerator has a lower intensity flux compared to the one from a nuclear source. However, many companies are investing in developing new technologies that are helping to bridge the gap⁴⁸.

2.2 Boron delivering agents.

The ideal boron-containing compound, or carrier, should display the following characteristics³⁹:

- Low systemic toxicity.
- Deliver therapeutics amount of ^{10}B to the tumor, estimated to be around at least 20 μg of $^{10}\text{B}/\text{g}$ of tumor or approximately 10^9 ^{10}B atoms/tumor cell.
- High tumor-to-normal tissue ratio (TNTR) and tumor-to-blood concentrations ratio (TBR).
- Rapid clearance from the blood while persisting in the tumor during the irradiation process.
- Ready quantification of tissue-localized boron.

Between these characteristics, obtaining the highest TNTR possible – for the BNCT treatment it should be greater than 4:1⁴⁸ - is the desired outcome for all cancer treatments. Targeted therapy has been one of the main goals of biotechnology research in the last 20 years. Reducing side effects and doses by delivering the drug exclusively to the tumor is slowly becoming a reality^{49,50}. However, BNCT has a second big challenge to face: quantifying the boronated compound inside the tumor cells over the time. BNCT is a binary treatment that relies on two components that have no effects by themselves. To ensure optimal therapeutic results, both the boron delivery agent and the neutrons must be present inside the cancer cells at the highest possible concentration⁵¹. To date, the concentration of boronated compounds inside the tumor can only be determined by analyzing peripheral blood samples and using pharmacokinetic models⁵². Clinically, the value of TBR is strictly correlated with TNTR⁴⁸. The inductively coupled plasma-atomic emission spectrometry (ICP-AES) is the method of choice for boron quantification in both clinical trials and basic research^{53–55}. However, as other analytic techniques proposed over the years, ICP-AES can only provide discrete data on boron concentration, limiting the BNCT applications⁵⁶. To better understand the biodistribution of boronated compounds, in the last years, several imaging techniques – like Positron Emission Tomography (PET) and Magnetic Resonance Imaging (MRI) - have been coupled to BNCT aiming to a theranostic approach (see **Introduction - section 3.1** for further details)^{48,56}.

2.2.1 Approved boron delivering agents.

To date, only three boron delivery agents have been approved for clinical trials (**Figure 4A**):

- Sodium decaborate (GB-10)
- Sodium borocaptate (BSH)
- L-Boronophenylalanine (BPA)

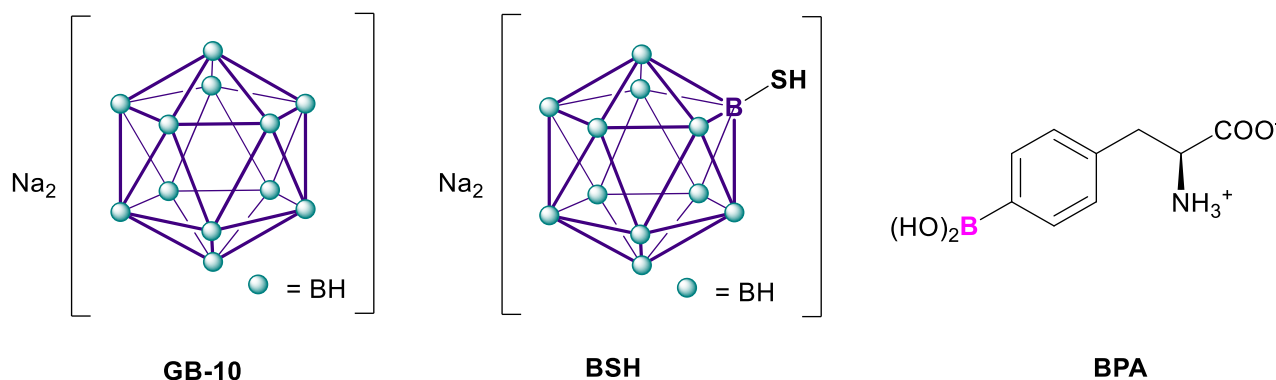


Figure 4A - Boron delivery agents approved for clinical trials.

While GB-10 has an approved FDA Investigational New Drug designation but has never been used clinically, BSH and BPA are the agents used in human clinical trials since the 1970' ⁵⁷. Both compounds have low system toxicity and recorded efficacy in BNCT treatment but are far from the ideal boronated agent⁴⁸. BSH is a *closo*-borohydride first synthesized by Miller et al. in 1964⁵⁸. It was first used clinically by Hatanaka and Nakagawa in Japan^{59,60}, and by Sauerwein and his research group in the Netherlands in Phase I/II clinical trial to treat patients with high-grade gliomas⁶¹.

L-Boronophenylalanine was first synthesized by Snyder et al. in 1958⁶². Initially, assuming that melanin-synthesizing cells would have shown a preferential uptake, BPA was employed in the BNCT treatment of patients with cutaneous melanoma^{45,63}. Then, further data suggested a potential application also in treating brain cancers.

The fructose complex of BPA⁶⁴ (**Figure 4B**) - which is definitively more soluble than BPA - rapidly entered the clinical use for high-grade gliomas, outrunning the use of BSH^{65,66}.

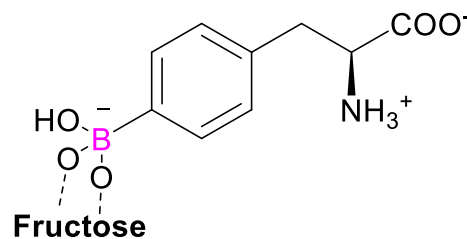


Figure 4B – BPA- fructose complex.

The main limitation of both BSH and BPA is their uneven distribution inside tumors, especially in brain tumors. It has been demonstrated that tumor boron concentrations varied both within different regions of the tumor, as well as among different patients⁶⁷. This phenomenon is more evident for BSH, but also BPA is affected⁶⁸. It is most likely due to the high histological, genomic, and epigenomic heterogeneity typical of high-grade gliomas⁶⁹, but nevertheless is a substantial drawback to the effective BNCT application⁷⁰.

2.2.2 Boron delivering agents under evaluation.

The need for more performing boron-delivering agents has led to the flourishing synthesis of hundreds of new candidates over the last fifty years. The major challenge in their design has been the requirement of selective tumor cell targeting and the delivery of a therapeutic dose of boron with minimal uptake and retention by healthy cells⁵⁷. A strategy to increase the selectivity has involved incorporating boron atoms into tumor-targeting molecules, such as amino acids, nucleosides, peptides, proteins, and sugars. On the other hand, nanomaterials – like liposomes and nanoparticles - can exploit the *enhanced permeability and retention* (EPR) effect to ensure a higher period of persistence inside the tumor cells^{71–73}.

It is possible to divide the new candidates based on their molecular weight: low-molecular-weight and high-molecular-weight compounds⁷⁴.

In the low-molecular-weight class, there are boronated amino acids containing a single boron atom or polyhedral borohydrides.^{75–77} Boron-containing cyclic amino acids, developed by Kabalka and Chandra et al., showed promising behavior in preclinical BNCT applications.^{78–80}

Boronated nucleosides could theoretically place the boron atom in the closest proximity to the DNA after their incorporation into the macromolecule. This fact can increase the radiobiological effectiveness (RBE) of BNCT⁸¹. Several groups focused on synthesizing carborane derivatives of all the canonical nucleosides. The susceptibility of the compounds to phosphorylation by cytosolic kinases can be an indication of the possible DNA incorporation^{82,83}.

Peptides able to bind receptors or transporters overexpressed in tumor cells with high affinity and selectivity have attracted tremendous interest as targeted boron delivery agents⁷⁴. Peptides targeting the epidermal growth factor receptors (EGFR)⁸⁴, or the vascular endothelial growth factor receptors (VEGFR)⁸⁵, as well as neuropeptide Y¹⁵ and cyclic Arg-Gly-Asp (cRDG),⁸⁶ have been successfully modified with boron-containing moieties. A similar approach can be applied to the conjugation with monoclonal antibodies (mAbs) able to recognize tumor-associated epitopes⁸⁷.

An increased glycolysis rate is one of the hallmarks of tumor cells⁸⁸, therefore boron-containing carbohydrates have recently sparked much interest⁸⁹. The facilitative sugar transporter (GLUT) is a family of 14 proteins that have different affinities for glucose, galactose, and mannose. GLUT1 and GLUT3 are usually overexpressed in several types of tumors and are well-known targets in many chemotherapeutic approaches^{90,91}. Substitutions on the glucose structure must be carefully evaluated to retain a good affinity for GLUT1. To date, modifications on C1, C2, and C6 have been

the most explored and seem to be well tolerated^{92,93}. Boron-containing carbohydrates have been synthesized in two ways: through the addition of a single boron atom into the monosaccharide structure or through conjugation with a polyhedral borohydride structure. In the first case, the products are boronic acid derivatives that mimic the native sugars^{94–97}, in the second instance, sugars are exploited also to increase the poor hydrophilic behavior of carboranes and borohydrides^{98,99}.

Into the category of high-molecular-weight compounds a wide range of nanomaterials can be enclosed, like dendrimers, liposomes, and nanoparticles. Nanomaterials can deliver higher concentrations of boron and can be used as multipurpose platforms⁷⁴.

Dendrimers, especially boron-rich polyamidoamine (PAMAM), have been conjugated to several cells-targeting peptides, confirming their potential applications in preclinical BNCT studies^{100,101}.

Liposomes are non-toxic nanocarriers made of cholesterol and phospholipids that can deliver both hydrophobic as well as hydrophilic bioactives¹⁰². Hydrophilic boronated compounds – like *nido*-carboranes or BSH – can be encapsulated into the aqueous core, while lipophilic molecules such as *closo*-boranes can be incorporated into the bilayer^{103–105}. These kinds of nanostructures can carry enormous quantities of boron aiding in the delivery of the required amount of 20 µg of boron for a gram of tumor tissue.

Polymeric nanoparticles¹⁰⁶, gold nanoparticles¹⁰⁷, as well as magnetic nanoparticles¹⁰⁸ have been proposed over the years as promising boron carriers to meet both the biocompatibility and the tumor-targeting requirements.

The ideal boron delivery agent has to be yet discovered, not because of the lack of trying but due to the complexity of the task at hand. Other aspects must be also addressed, normalized treatment protocols, safe neutron sources, and creation of multidisciplinary centers. Many experts in this field recommend a joint effort between very different disciplines, ranging from nuclear physics to surgery, from chemistry to radiation oncology, and from mathematics to radiation biology. Steps in this direction were made in recent years thank to the creation of the international program RENOVATE.

3. Theranostic

The term “theranostic” was coined by Funkhouser, the CEO of PharmaNetics Inc., in the early ‘2000¹⁰⁹. It identifies a material that combines the modalities of therapy and diagnostic imaging. The idea is to treat the disease while visualizing it. In this way, undesirable differences in biodistribution and selectivity that currently exist between distinct imaging and therapeutic agents would be eliminated or at least detected¹¹⁰. A generic theranostic agent consists of a carrier, a targeting ligand, a proper therapeutic compound, and a signal emitter (**Figure 5**). The last two elements have to be wisely chosen based on the therapy and imaging techniques used¹¹¹. Chemotherapy, photodynamic therapy, and radiation therapy are just examples of therapeutic approaches that have been coupled with imaging techniques to improve their precision¹¹⁰. On the other hand, magnetic resonance imaging (MRI), nuclear imaging (PET/SPECT/CT), and ultrasound imaging - among other imaging techniques - have been successfully employed in this kind of approach¹¹². Nanomaterials are often the carrier of choice as they can be easily engineered to facilitate the construction of multi-modal formulations¹¹³. Polysaccharide-based theranostic agents have recently sparked much interest thanks to their low toxicity, high biodegradability, and physiological stability^{112,114}.

One of the most renowned findings in the theranostic field has been ¹⁷⁷Lu-DOTATATE (Lutathera), a drug for peptide receptor radionuclide therapy. This agent targets the somatostatin receptors - overexpressed in the neuroendocrine tumor – and delivers the radioisotope to the cancer cells with high precision. The Food and Drug Administration approved ¹⁷⁷Lu-DOTATATE in 2018 for the treatment of neuroendocrine tumors in the gastrointestinal tract or pancreas in adults, and in 2021 it was also approved in Japan^{115–117}.

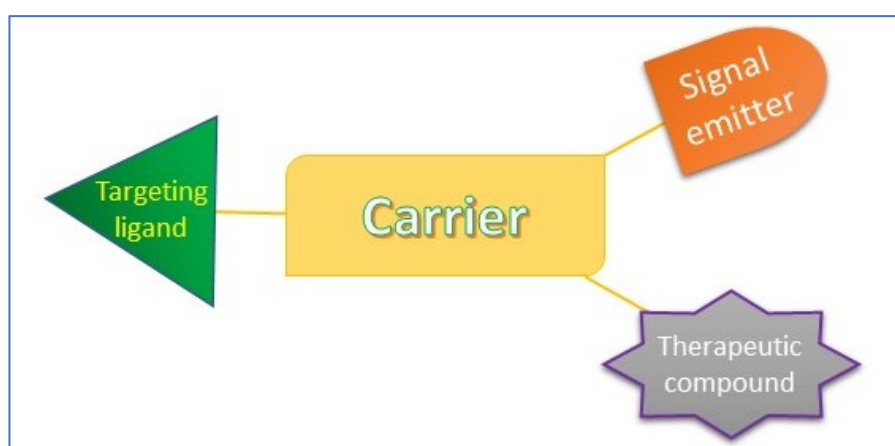


Figure 5 - A generic theranostic agent structure

3.1 Theranostic approach and BNCT

The effectiveness of BNCT strongly depends on the amount of energy locally deposited by the ^{10}B nuclear fission reaction. The energy is proportional to the product of ^{10}B concentration and the thermal neutron flux inside the tumor volume at the irradiation time¹¹⁸. In this context, a theranostic approach can be fundamental for making BNCT more effective⁵¹. As described in the **Introduction - section 2.2**, to date a direct and noninvasive way to determine the ^{10}B concentration in the tumor and surrounding tissues is still lacking. This fact is an enormous disadvantage that has been addressed by the scientific community only recently⁴⁸.

Among the imaging techniques that can be paired with BNCT, positron emission tomography (PET), single-photon emission computed tomography (SPECT), and magnetic resonance imaging (MRI) are the most promising.

3.1.1 Positron Emission Tomography (PET)

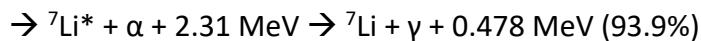
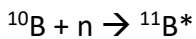
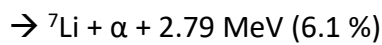
Since its introduction in the 1970s, Positron Emission Tomography (PET) has been widely used as an imaging technique in the medical field for diagnosis and therapy control¹¹⁹. The technique relies on the emission of positrons (β^+) from a neutron-deficient radionuclide and the following annihilation reaction with an electron present in the biological environment. The two high-energy photons generated from the annihilation event travel in opposite directions along an approximately straight line and reach a PET detector. The detector amplifies the signal and converts it into an image¹²⁰. The physical integration of PET and computed tomography (CT) in hybrid PET-CT scanners allows combined anatomical and functional imaging. The radionuclides most used for this kind of application are fluorine-18 (^{18}F), carbon-11 (^{11}C), nitrogen-13 (^{13}N), and oxygen-15 (^{15}O), mainly because they have a radio decay process that is almost exclusively by positron emission. They are also isotopes of elements largely present in organic molecules that can be quickly produced in a cyclotron¹²¹. Fluorine is rather uncommon in biomolecule structures, but its similarity to atomic hydrogen - Van der Waals radius and covalent bond length to carbon - makes fluorine-18 the most widely used PET radionuclide¹²².

Embedding a fluorine-18 atom into a BNCT agent permits localizing and quantifying the molecule before and after the treatment. In 1991, Ishiwata et al. developed 4- ^{10}B -Borono-2- ^{18}F -fluoro-L-

3.1.2 Single-Photon Emission Computed Tomography (SPECT)

SPECT relies on the emission of γ -radiation from specific radionuclides. The γ -decay emits a single γ -photon that is collected by the detector. The presence of a collimator ensures that only photons perpendicular to the detector surface are registered, which allows the user to trace back the spatial origin of the photons. The measurement is carried out from different angles, and with an algorithm like the one used for CT, a 2D or 3D image can be reconstructed¹¹⁴. The radionuclides of choice for this kind of application decay mainly through γ emission, like ¹²³I, ^{99m}Tc, and ¹¹¹In¹²⁸.

During BNCT the following nuclear reactions take place:



The prompt γ rays from ¹⁰B(n, α)⁷Li reactions are yielded from ⁷Li* which has about 10⁻¹⁴ s half time¹²⁹. It is possible to use the 0.478 MeV photon emitted after the ¹⁰B capture reaction as a signal to obtain a SPECT image¹³⁰. Considering the following equation $D \sim \int n_B \sigma \phi dV$ where D = the dose, n_B = the density of ¹⁰B nuclei, σ = the cross section for neutron capture, Φ = the neutron flux, and V = the tumor volume. The number of γ -photons emitted after the nuclear reaction is a direct estimation of the product Φn_B and consequently of the dose D¹¹⁸.

In this case, there is no need to develop a specific tracer, since the molecule required for the imaging technique is the same needed for the therapy, but there are other problems to face. Measuring the 478 keV gamma-rays can be troublesome due to the high background noise, which means images with poor resolution, and collateral annihilation reactions that reduce the signal^{131,132}. The detector material plays a crucial role in assuring spatial resolution and accuracy. Recent studies suggest the Cadmium-Telluride, Lutetium-Yttrium-Oxyorthosilicate, or Gadolinium-Aluminium-Gallium Garnet as promising components for new BNCT-SPECT imaging devices^{133,134}.

3.1.3 Nuclear Magnetic Resonance Imaging (¹H-MRI)

The typical MRI signal arises from the longitudinal (T_1) and transverse (T_2) relaxation times of water protons that behave differently based on the interactions with biological macromolecules and membranes. Usually, the images obtained are highly resolved and give detailed morphological and functional information without the need for any contrast agent. However, the endogenous contrast can be increased using contrast agents (CAs) that alter the T_1 and T_2 of water protons in the tissues where they distribute.

Contrast agents are usually extremely stable macrocyclic complexes of Gadolinium (III). Combining paramagnetic ions and boron structure into the same molecule can lead to a dual-modality probes, but the biodistribution profiles have to be carefully evaluated¹³⁵. In two different works, boron cluster and BPA were conjugated to the commonly used MRI contrast agent Gd-DTPA (*Diethylenetriaminepentacetate*). Their uptake was evaluated *in vivo*, but the results obtained were not completely positive^{136,137}. A further step in this field was accomplished by Geninatti Crich's group with the synthesis of a Gd-carborane compound delivered to tumor cells thanks to low-density lipoproteins (LDLs). The synthesized product tends to self-assemble in micellar aggregates, but after treatment with β -cyclodextrin, the authors were able to obtain stable supramolecular adducts with LDL. This formulation was tested *in vitro* and *in vivo*, and it was possible to draw a strict correlation between the result of the MRI assessment and the amount of boron taken up by tumor cells measured by ICP-MS^{138,139}.

3.1.4 Fluorine Magnetic Resonance Imaging (^{19}F -MRI)

^{19}F -MRI is a promising and complementary modality for ^1H -MRI. ^{19}F MRI is well-suited for functional imaging if an appropriate fluorine-containing probe is administered because fluorine-containing compounds are found only in teeth and bones, in the form of solid salts. This means the lack of background signals and the possibility to obtain high-resolution images. On the other hand, a high concentration of ^{19}F nuclei of at least 0.2–1 mM is necessary for useful MRI¹⁴⁰.

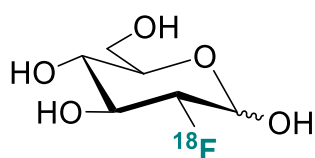
Capuani et al. have done some in deep studies over the past decade on the use of ^{19}F -BPA as a dual-modality probe for BNCT and ^{19}F -MRI^{141,142}. In their most recent work, they evaluated the ^{19}F -BPA internalization in pancreatic cancer cells using three independent techniques: neutron autoradiography to quantify boron, liquid chromatography to quantify ^{19}F -BPA, and ^{19}F -MRS to quantify fluorine-19. The internalization results obtained using ^{19}F -MRS agreed with the data obtained by the well-established techniques to quantify boron compounds, confirming the usefulness of this approach¹⁴³.

4. Fluorine 18

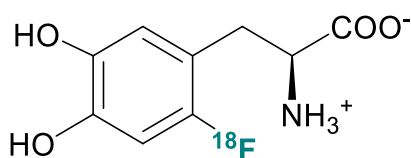
Positron Emission Tomography (PET), as mentioned in the **Introduction - section 3.1.1**, is an imaging technique suitable for diagnosing cardiac, neurological, and tumor conditions¹⁴⁴, as well as inflammatory and infectious diseases¹⁴⁵. Moreover, the technique has a sufficient speed of acquisition to allow the determination of the pharmacokinetics of radiotracer. PET imaging can provide important insights for drug discovery and development and for potentially limiting side effects due to off-target binding¹⁴⁶.

Fluorine-18 is the most widely used PET radionuclide. It has a Van der Waals radius similar to that of atomic hydrogen (atomic radii of 1.35 and 1.20 Å, respectively) and forms a covalent bond with carbon about the same length (which results in only a little steric difference when replacing hydrogen with fluorine)¹²². Additionally, it has a relatively long half-life (109.8 min) - compared to other radionuclides – which allows for multistep synthesis, extended imaging procedures, and off-site use in satellite PET facilities without a cyclotron¹²¹.

[¹⁸F]Fluorodeoxyglucose ([¹⁸F]FDG) and 3,4-dihydroxy-6-[¹⁸F]fluoro-L-phenylalanine (6-[¹⁸F]FDOPA) are the radiotracers of choice for the diagnosis of tumor and Parkinson conditions, respectively (**Figure 7**)^{147,148}. Glucose transporters actively absorb [¹⁸F]FDG into cells. Then, once it has entered the glycolytic pathway is phosphorylated by hexokinase. By this point, the metabolic pathway can't proceed further due to the fluorine atom in position two, and the [¹⁸F]-FDG-6-phosphate is trapped irreversibly inside the cells¹²⁸. Instead, [¹⁸F]FDOPA follows the classical steps of catecholamine synthesis. Upon entering the brain cells, [¹⁸F]FDOPA exhibits irreversible binding characteristics in the early hours post-injection. It is decarboxylated by aromatic amino acid decarboxylase yielding [¹⁸F]fluorodopamine, which is retained for several hours within dopamine vesicles and thereafter degraded. The resulting acidic metabolites, [¹⁸F]dihydroxyphenylacetic acid and [¹⁸F]homovanillic acid, are free to diffuse out of the brain¹⁴⁹. Alongside these two radiotracers, many other fluorine-18-containing compounds have been approved for clinical practice, while thousand have been developed over the last forty years¹⁴⁷.



[¹⁸F]FDG



[¹⁸F]FDOPA

Figure 7 - [¹⁸F]Fluorodeoxyglucose ([¹⁸F]FDG) and 3,4-dihydroxy-6-[¹⁸F]fluoro-L-phenylalanine (6-[¹⁸F]FDOPA) structures

4.1 Fluorine-18 production

Fluorine-18 is produced with a cyclotron primarily by proton (¹H) irradiation of ¹⁸O, a stable naturally occurring isotope of oxygen. When the target is liquid H₂¹⁸O, an aqueous solution of ¹⁸F-fluoride ion is obtained; when the target is ¹⁸O₂ gas, [¹⁸F]F₂ gas is obtained¹⁵⁰. ¹⁸F-fluoride ions act as nucleophiles in a range of reactions, while [¹⁸F]F₂ behaves as an electrophile¹²¹. The key difference between these two chemical forms is the specific activity (SA = radioactivity/mol) of the produced ¹⁸F isotope. Nucleophilic ¹⁸F-fluoride is obtained with high SA, thanks to the efficient nuclear reaction ¹⁸O (p, n) ¹⁸F. Electrophilic [¹⁸F]F₂ has much lower specific activity because fluorine-19 gas must be added as a carrier to extract the [¹⁸F]F₂ from the cyclotron. Moreover, since only one of the fluorine atoms carries the ¹⁸F label the maximum theoretical radiochemical yield (RCY) is limited to 50%^{128,151}.

4.2 Labeling methods with fluorine-18

Irrespective of the isotope used, all synthetic routes to radiolabeled compounds require that the incorporation of the expensive or unstable isotope is carried out at a late stage of the synthesis. Hence, the utilization of the isotope is maximized¹⁵². Generally, the synthesis and purification timeframe should not exceed two to three times the half-life of the radionuclide in use¹²⁸. The labeling methods with fluorine-18 can be divided into two main categories based on the reagent used, $[^{18}\text{F}]\text{F}_2$ or $[^{18}\text{F}]\text{F}^-$. Electrophilic approaches are less common due to the difficulties in obtaining $[^{18}\text{F}]\text{F}_2$ with a high specific activity. Nevertheless, new types of reagents have been developed to overcome this issue¹²¹. Instead, nucleophilic approaches are well established and can be applied to aromatic as well as nonaromatic compounds. Usually, fluorine-18 is introduced on carbon atoms, but an interesting application for $[^{18}\text{F}]\text{F}^-$ is the formation of noncanonical bonds with other elements like boron, silicon, or aluminium¹²¹.

The direct fluorination of biomolecules – like proteins or peptides - is not always possible due to the harsh conditions typically required for such reactions (e.g. high temperatures, and nonaqueous solvents). In these cases, indirect fluorination employing a suitable prosthetic group can help solve the problem¹⁵³. This approach requires the installation of a prosthetic group on the biomolecule, the radiosynthesis of the ^{18}F -radiolabelled motif that will react with the prosthetic, and a final coupling step¹⁵⁴.

4.2.1 Electrophilic radiofluorination

For years, the use of $[^{18}\text{F}]\text{F}_2$ has been burdensome due to its poor chemo- and regioselectivity. These characteristics are a consequence of its high chemical reactivity and usually resulted in low RCYs. Despite this fact, $[^{18}\text{F}]\text{F}_2$ has been successfully employed for the synthesis of $[^{18}\text{F}]\text{FDG}$ ¹⁵⁵, 6- $[^{18}\text{F}]\text{FDOPA}$ ¹⁵⁶, and 2-(2-nitro-1H-imidazol-1-yl)-N-(2,2,3,3,3-pentafluoropropyl)-acetamide ($[^{18}\text{F}]\text{EF5}$)¹⁵⁷, a promising radiotracer for which no route from $[^{18}\text{F}]\text{F}^-$ has been reported to date¹⁵⁴. **Figure 8** shows some electrophilic ^{18}F -fluorinating reagents prepared from $[^{18}\text{F}]\text{F}_2$. These reagents provided new opportunities for enantio- and diastereoselective ^{18}F -fluorination leading to new chemical space¹⁵⁴.

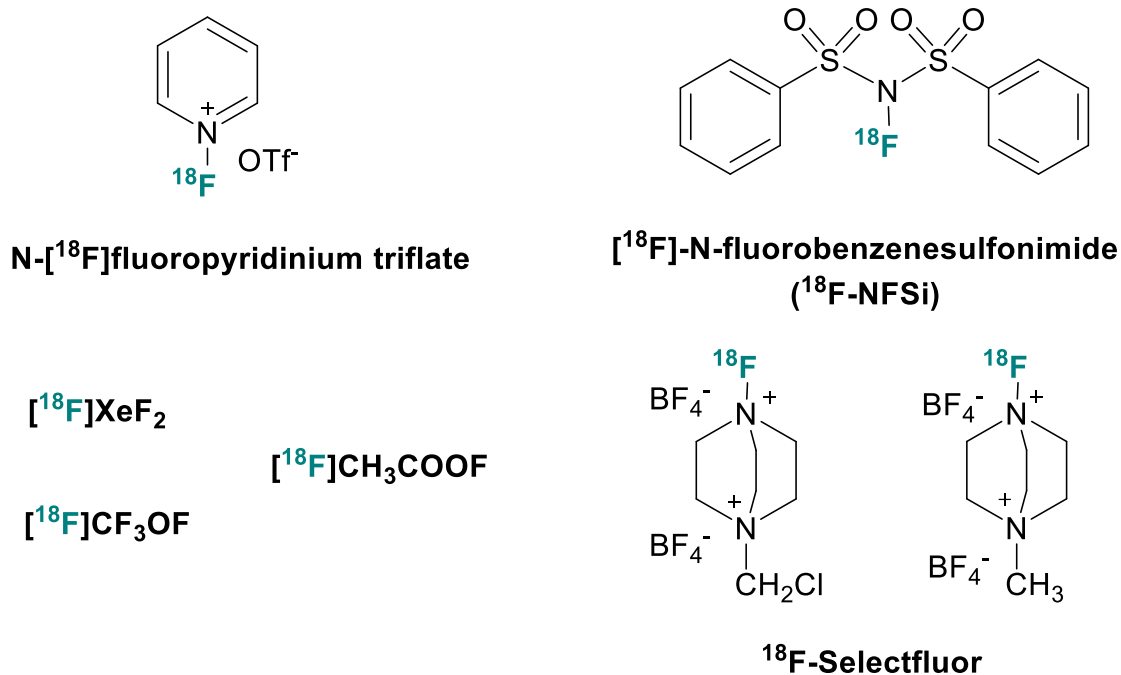


Figure 8 – Structures of some electrophilic ¹⁸F-fluorinating reagents.

4.2.2 Nucleophilic radiofluorination

Both aliphatic or aromatic substrates can undergo nucleophilic substitution leading to C(sp³)-¹⁸F or C(sp²)-¹⁸F bonds¹²¹. In both cases, [¹⁸F]F⁻ can not be used directly from the cyclotron but need a pretreatment. Although fluoride ion is a strong nucleophile, in aqueous solutions it forms hydrogen bonds with the surrounding water molecules and becomes unreactive for nucleophilic substitution. To be useful, the ¹⁸F-fluoride must be dehydrated by evaporation of the water and then treated with a phase transfer catalyst - such as the cryptand Kryptofix222 - or by the addition of bulky tetrabutylammonium cation. The second step is needed to enhance the solubility and nucleophilicity of fluoride ions in organic solvents since nucleophilic fluorinations are typically conducted in polar aprotic organic solvents with poorly nucleophilic bases (carbonate or bicarbonate ions). Thus, the aqueous solution of [¹⁸F]F⁻ obtained from the cyclotron target is treated with the desired salt before evaporation of the water; water removal is assisted by azeotropic distillation of water using CH₃CN¹⁵⁰.

Aliphatic nucleophilic substitutions usually follow an S_N2 mechanism. These kinds of reactions are greatly influenced by temperature, base, and leaving group used¹⁵⁸. This is the synthetic approach

of choice to [^{18}F]FDG, in which the axial triflate on the C-2 of mannose is replaced by the [^{18}F]F $^-$ with epimerization¹⁵⁵.

^{18}F nucleophilic aromatic substitution requires sufficient activation of the phenyl ring, which can be achieved by electron-withdrawing groups (such as $-\text{NO}_2$, $-\text{CN}$, $-\text{CF}_3$, or carbonyl groups) in the ortho or para position to the leaving group. Aromatic nucleophilic substitutions are usually conducted in a polar aprotic solvent and require higher temperatures than aliphatic substitution (typically above 100 °C)¹⁴⁶.

4.2.3 Noncanonical bonds ($\text{B-}^{18}\text{F}$, $\text{Si-}^{18}\text{F}$)

In the last decades, many noncanonical ^{18}F -labelings through bond formations with Si, B, Al, and Ga have been proposed as valid alternatives to the C- ^{18}F approach. Numerous groups have become interested in harnessing the inherently high fluorophilicity of these elements as a way to introduce ^{18}F into molecules of biological interest¹⁵⁹.

The use of silicon as a fluoride acceptor dates back to 1985 when Rosenthal et al. proposed [^{18}F]fluorosilanes as labeling synthons. They treated chlorotrimethylsilane with $^{18}\text{F}^-$ in aqueous acetonitrile isolating the corresponding [^{18}F]fluorosilane in 65 % yield. A preliminary *in vivo* evaluation revealed fast hydrolysis of the compound accompanied by high radioactivity (^{18}F) uptake by the bone making it unsuitable as a labeling synthon¹⁶⁰. In 2006 Schirrmacher et al. reported the syntheses of substituted [^{18}F]organofluorosilanes and their *in vitro* and *in vivo* stability. They described two approaches: one using organochlorosilanes as labeling precursors and a second based on the ^{18}F - ^{19}F isotopic exchange (IE) using [^{19}F]di-tert-butylphenyl fluorosilane as a highly efficient silicon-based fluoride acceptor (SiFA compound)^{161,162}.

Almost concomitantly, Perrin et al. published a paper on the boron- ^{18}F chemistry together with the synthesis of a [^{18}F]-tetrafluoroborate. The radiolabeling procedure was performed through IE in aqueous solvent at room temperature¹⁶³. From 2005 on, the same group focused on the development of organotrifluoroborates (R-BF_3) as prosthetic groups for a single-step ^{18}F -labeling¹⁶⁴. In particular, the *in vivo* stability of these kind of molecules has been studied for years since the hydrolysis of R-BF_3 to their corresponding boronic acids (B(OH)_2) can be problematic in an aqueous biological environment. Hydrolytic release of ^{18}F -fluoride *in vivo* should be avoided since it would result in accumulation in calcium-rich fluorophilic bones, increasing background

noise, and obscuring imaging results¹⁶⁵. Both Perrin and Gabbai investigated the solvolytic lability of aryltrifluoroborates (Ar-BF_3) and discovered that electron withdrawing substituents retard the rate of Ar-BF_3 solvolysis, while electron-donating groups enhance it^{166,167}. In 2015, Perrin's group studied the solvolysis rates of aliphatic trifluoroborates; in this case, too, they discovered increased stability for molecules bearing electron-withdrawing substituents¹⁶⁸. The rate of R-BF_3 hydrolysis is governed by the dissociation of the first fluorine atom, followed by rapid hydrolysis to the boronic acid with no detectable mono- or difluoroborate intermediates. Thus, complete hydrolysis can be approximated as pseudo-first order where the observed kinetic rate is congruent with the rate of initial defluorination¹⁶⁶.

The higher stability toward hydrolysis due to electron-withdrawing substituents has been exploited in the design of new potential PET radiotracers¹⁶⁵. Among the most prominent results was the development of two $^{18}\text{F-BF}_3$ peptides that target the somatostatin type-2 receptor overexpressed by the neuroendocrine tumor, and numerous trifluoroborate probes able to target the prostate-specific membrane antigen¹⁶⁹⁻¹⁷¹.

B. OUTLINE OF THE THESIS

My Ph.D. project focused on the synthesis of boron-containing compounds for two medical applications, such as Boron Neutron Capture Therapy (BNCT) and drug development. This thesis can be divided into four parts: the first three regard the synthesis of potential boron delivery agents for BNCT, while the last one discusses the development of boron-containing drug analogs.

Chapter 1 and Chapter 2 describe the main project of the thesis concerning the synthesis of potential boron-delivery agents for a BNCT guided by Positron Emission Tomography (PET). As presented in the **Introduction – section 3**, pairing the BNCT with a proper imaging technique could greatly increase the efficacy and applicability of the therapy. This goal can be achieved by developing new theranostic agents. In this context, our aim has been the development of glycoconjugates bearing a stable trifluoroborate group (BF_3).

We conceived these molecules as typical theranostic agents: the carbohydrate moiety for the targeting and the BF_3 group as the active part for BNCT and PET.

Chapter 1 details the synthesis and subsequent studies performed on trifluoroborates stabilized by internal ammonium salts. We designed two reliable synthetic routes that granted us twelve compounds in satisfying yield. Then, thanks to the collaboration of many colleagues, we thoroughly investigated their chemical and biological properties. We tested their cytotoxicity in vitro and their stability under pseudo-physiological conditions, discovering a fascinating relationship between the two properties. On a couple of compounds, we performed the radiolabeling procedure through isotope exchange - as described in the **Introduction – section 4** - and eventually, one of them was injected in vivo for a PET imaging acquisition.

In the meanwhile, the second part of this project took place. Chapter 2 describes the synthesis of a second family of glycoconjugates containing sulfonium ions instead of ammonium. From the data collected from the first class of compounds, we decided to move toward molecules bearing the trifluoroborates stabilized by internal sulfonium salts. This time, the synthesis required a thorough and time-consuming optimization because of the lower nucleophilicity of the sulfur atom compared to nitrogen. I carried out part of this project during my stay at the University of Leipzig under the supervision of professor Hey-Hawkins. Eventually, we obtained four compounds from

two different synthetic routes. The stability of these molecules was tested similarly to the ammonium family, and their applications are still under evaluation.

Chapter 3 focuses on a small side project steamed from the collaboration between the University of Milan, the University of Firenze, and the University of Pavia. In this case, we wanted to approach another open issue in the BNCT field, the difficulty of delivering a high amount of boron to cancer cells. Our idea has been the preparation of a nanomaterial decorated with boranes. We performed a straightforward synthesis to obtain the desired borane with a short azido linker suitable for conjugation.

Chapter 4 explains the synthetic efforts made to obtain a carborane analog of naproxen, a well-known non-steroidal anti-inflammatory drug (NSAID). This project has been part of a broader effort ongoing in the Hey-Hawkins's laboratory to perform isosteric substitutions of aromatic rings in common drug scaffolds with inorganic structures, such as carboranes. As described in the **Introduction – section 1.4**, carboranes can be successfully employed to improve some pharmacological properties, like extending the circulation time or enhancing the interaction with the receptors.

C. RESULTS AND DISCUSSION

1. Organotrifluoroborate Sugar Conjugates – part I

1.1 Synthetic project

The first part of the main project of my Ph.D. thesis concerns the synthesis of a small library of twelve organotrifluoroborate sugar conjugates whose generic structure is shown in **Figure 1**.

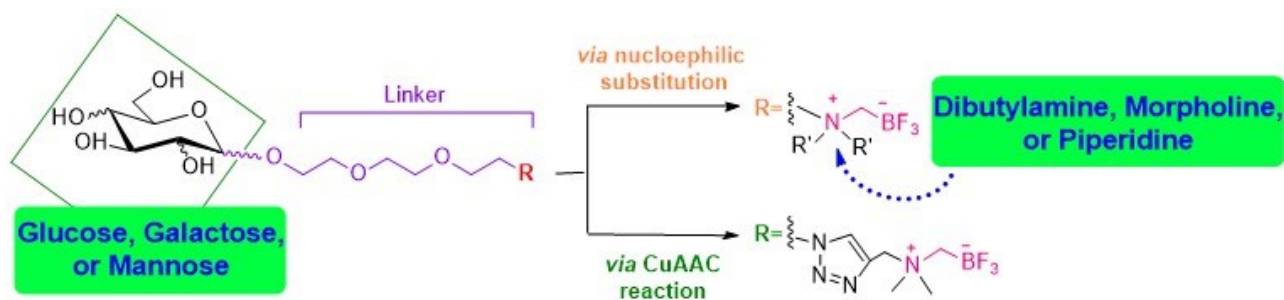


Figure 2 – General structure for the Organotrifluoroborate sugar conjugates containing ammonium salts

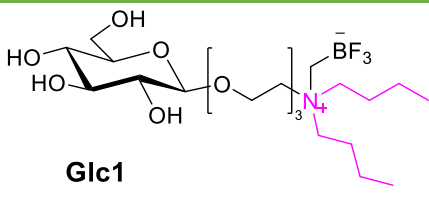
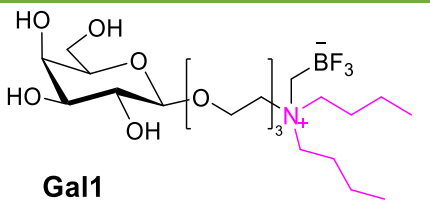
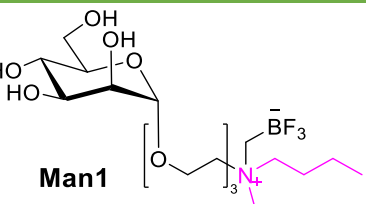
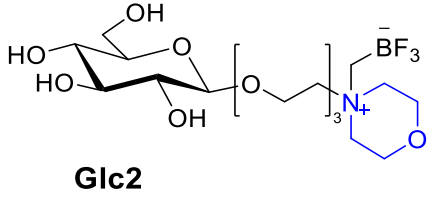
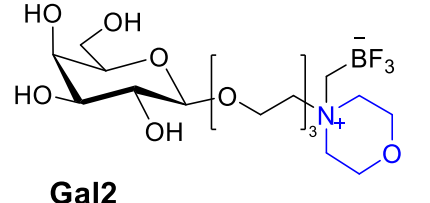
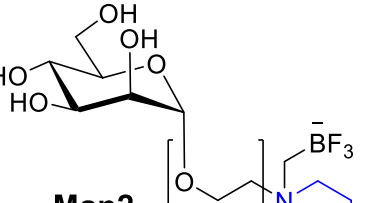
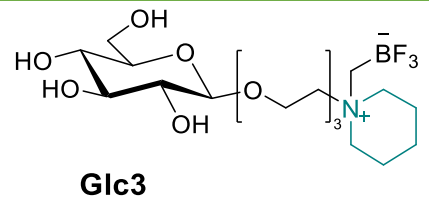
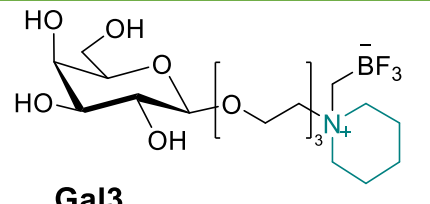
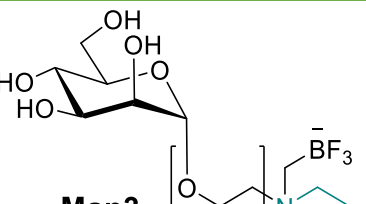
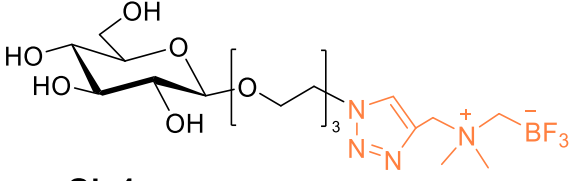
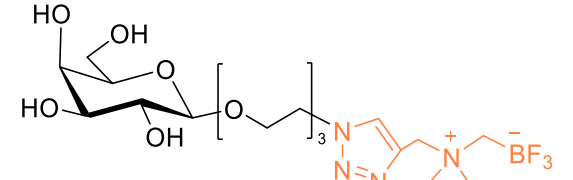
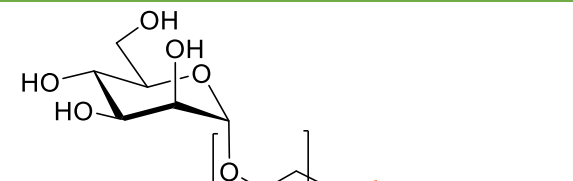
We designed the products as potential theranostic agents for a BNCT guided by PET. They consist of a monosaccharide unit linked to a trifluoroborate group (BF₃) stabilized by an internal ammonium salt. Sugars can act as targeting moieties for cells with enhanced consumption of carbohydrates, a well-known hallmark of cancers and other related pathologies⁸⁸. Instead, as extensively described in the **Introduction -section 4.2.3**, the trifluoroborate group plays the role of the active part of the molecule - when exposed to the neutron flux - and precursor for the PET tracer.

The short triethylene glycol that connects the anomeric position of the sugar to the trifluoroborate also enhances the molecules' biocompatibility. Polyethylene glycol (PEG) is a polymer widely used in various formulations thanks to its biocompatibility¹⁷². PEGylation of proteins, drugs, and bioactive molecules, is known to increase the solubility of hydrophobic compounds in aqueous media, extend the circulation time, reduce the nonspecific uptake, and achieve specific tumor targetability¹⁷³.

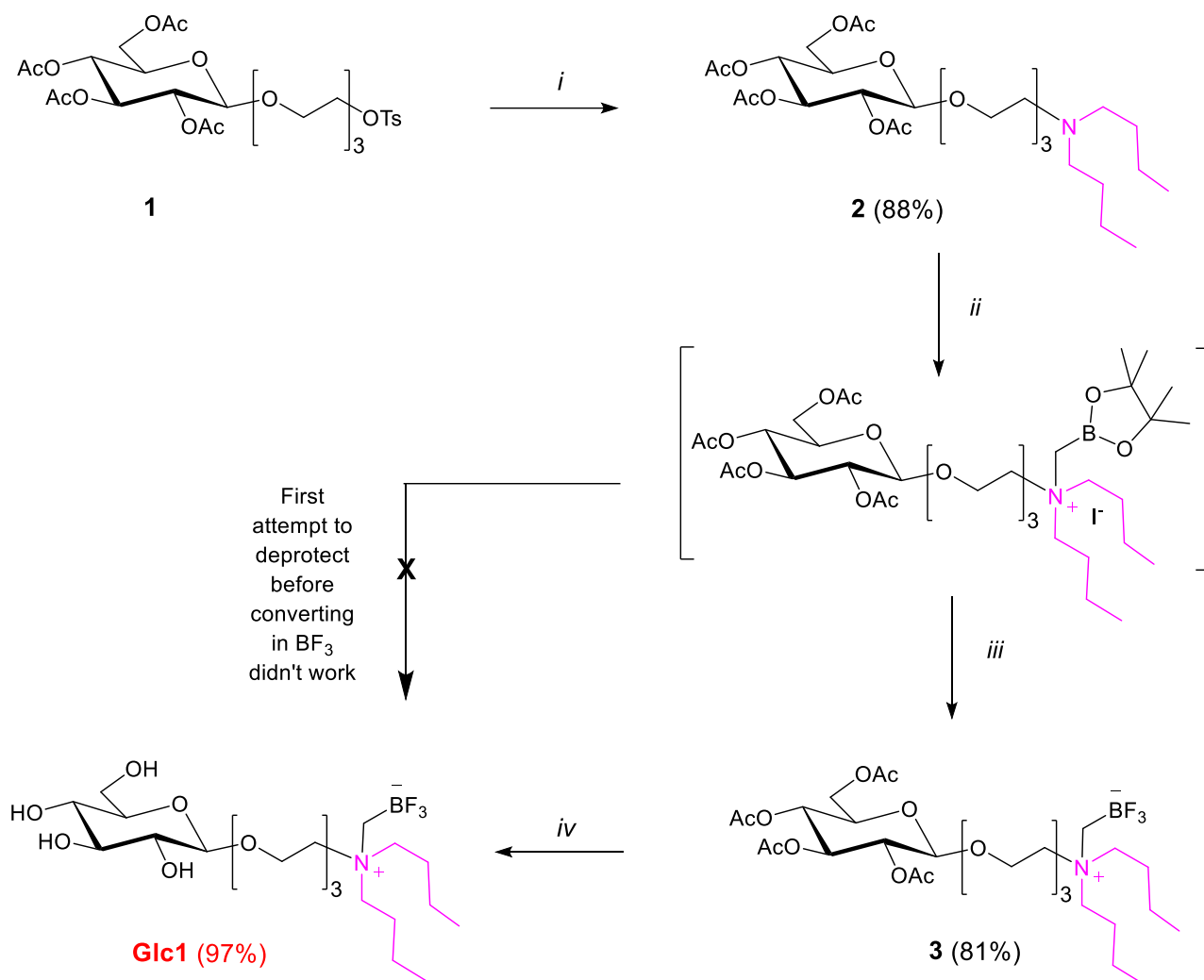
Starting from a common intermediate, we introduced the stabilized trifluoroborate group in two ways: *via* nucleophilic substitution or *via* copper-catalyzed azide-alkyne cycloaddition (CuAAC, click reaction).

Table 1 shows the twelve synthesized products divided into two families based on the synthetic methodology.

Table 1 - Structures of the twelve synthesized products

| Family A | | |
|---|--|---|
|  <p>Glc1</p> |  <p>Gal1</p> |  <p>Man1</p> |
|  <p>Glc2</p> |  <p>Gal2</p> |  <p>Man2</p> |
|  <p>Glc3</p> |  <p>Gal3</p> |  <p>Man3</p> |
| Family B | | |
|  <p>Glc4</p> | | |
|  <p>Gal4</p> | | |
|  <p>Man4</p> | | |

“Family A” was made *via* nucleophilic substitution with three amines – dibutylamine, morpholine, and piperidine – on three different monosaccharides – glucose, galactose, and mannose. **Scheme 1** shows the overall synthetic pathway that was first tested and optimized for the glucose derivative **Glc1**.



Scheme 1 – Overall synthetic pathway for Glc1. i) Dibutylamine, CH_3CN , 82°C , ii) Iodomethylboronyl pinacolate, Et_2O , r.t., iii) KHF_2 , CH_3CN , H_2O , r.t., iv) KOH , MeOH , r.t.

The first step of our work was to carefully plan the synthetic route, especially with regards to the protecting groups for the sugar moiety. Protecting groups are installed in the first synthetic step, but they have to be removed at the end of the synthesis without endangering the structural integrity of the molecule.

Very little is known about the stability of the trifluoroborate group to the deprotection conditions, but our previous studies on this subject evidenced an incompatibility with the hydrogenolysis conditions required to remove the benzyl esters – a routine protective group for carbohydrates. Therefore, we decided to use the acetates as sugar-protecting groups. They allow easy control over the glycosylation stereochemistry outcome and can be easily removed in mild basic conditions. Starting from the known compound **1**¹⁷⁴, the first nucleophilic substitution with an excess of dibutylamine in acetonitrile at reflux gave product **2** in satisfactory yield. The nitrogen atom was then alkylated with iodomethylboronyl pinacolate in diethyl ether at room temperature yielding the intermediate ammonium salt.

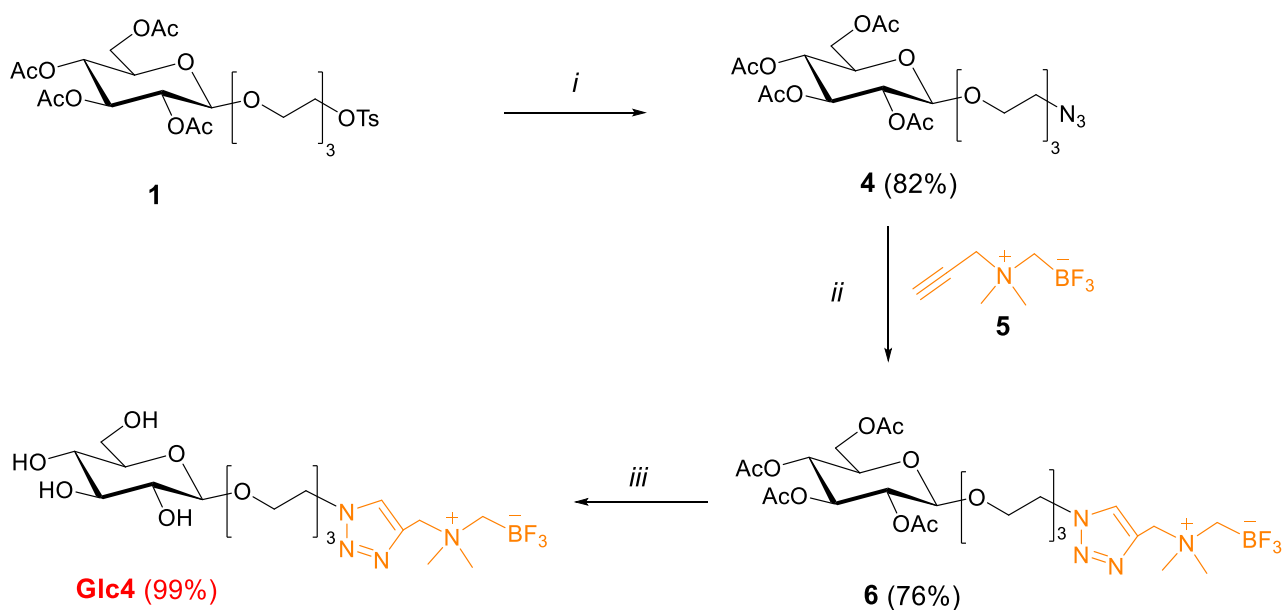
At this point, in a first attempt to obtain the final product, we tried to deprotect the intermediate, fearing that the required basic conditions would have been incompatible with the final BF₃. Unfortunately, this approach did not work; the obtained product was too polar and almost impossible to purify.

So, the protected boronyl pinacolate was first converted into the corresponding trifluoroborate by treatment with an aqueous solution of potassium hydrogen difluoride. The reaction required acetonitrile as a cosolvent due to the limited solubility of the ammonium salt in water. Product **3** was easily purified over silica gel and obtained in good yield. The final deprotection was carried out with a catalytic amount of potassium hydroxide in methanol, avoiding the stronger basic pH from sodium methoxide, typical of Zemplén conditions.

Luckily, the mild basic conditions and the short reaction time allowed the synthesis of the first target compound **Glc1** in satisfactory yield without affecting the molecule integrity. **Glc1** didn't require any purification.

Glc2 and **Glc3** were synthesized with the same reaction scheme using morpholine and piperidine respectively. The remaining product of "Family A" – **Gal1**, **Gal2**, **Gal3**, **Man1**, **Man2**, and **Man3** – were obtained in the same way from the proper common precursors.

"Family B" consists of three products - **Glc4**, **Gal4**, and **Man4** - synthesized through a click reaction. The synthetic scheme was optimized for **Glc4** and then repeated for the other compounds (**Scheme 2**).



Scheme 2 - Overall synthetic pathway for Glc4. i) NaN_3 , DMF, 70°C , ii) Sodium ascorbate, $\text{CuSO}_4 \cdot 5\text{H}_2\text{O}$, *t*-BuOH, H_2O , r.t., iii) KOH, MeOH, r.t.

The key compound **1** was converted into the azido derivative **4** following a literature procedure¹⁷⁴. Then, the click reaction between **4** and the known zwitterionic alkynyl trifluoroborate **5**¹⁶⁸ gave product **6** in satisfactory yield. The reaction was conducted in a mixture of water and *tert*-butanol with sodium ascorbate and catalytic amounts of copper sulfate. The last deprotection, in mild basic conditions, afforded the target compound **Glc4** without the need for further purification.

The same approach was employed for the synthesis of **Gal4** and **Man4** from the corresponding azido derivatives (Detailed reaction schemes, synthetic procedures, and characterizations are reported in the **Experimental Details - section 1.1**).

1.2 Cytotoxicity evaluation

The cytotoxicity of all twelve compounds was tested on human fibroblasts using boronophenylalanine (BPA) as the reference compound. **Figure 2** shows the unexpected results found by our colleague, Silvia Fallarini (Further experimental details in **Experimental Details - section 1.2**).

Although at low concentrations all products are harmless, the compounds of “**Family A**”, minus **Man3**, showed higher toxicity than BPA at the highest concentration tested (1 mM).

“**Family B**” and **Man3** instead showed a behavior like BPA at all the concentrations tested.

This fact slightly altered our plans since further experiments in the BNCT field would have required the use of high concentrations of the compounds, clearly unsafe from the toxicology point of view. For this reason, we moved forward with PET experiments, which required way lower amount of material and could have been performed under safe conditions.

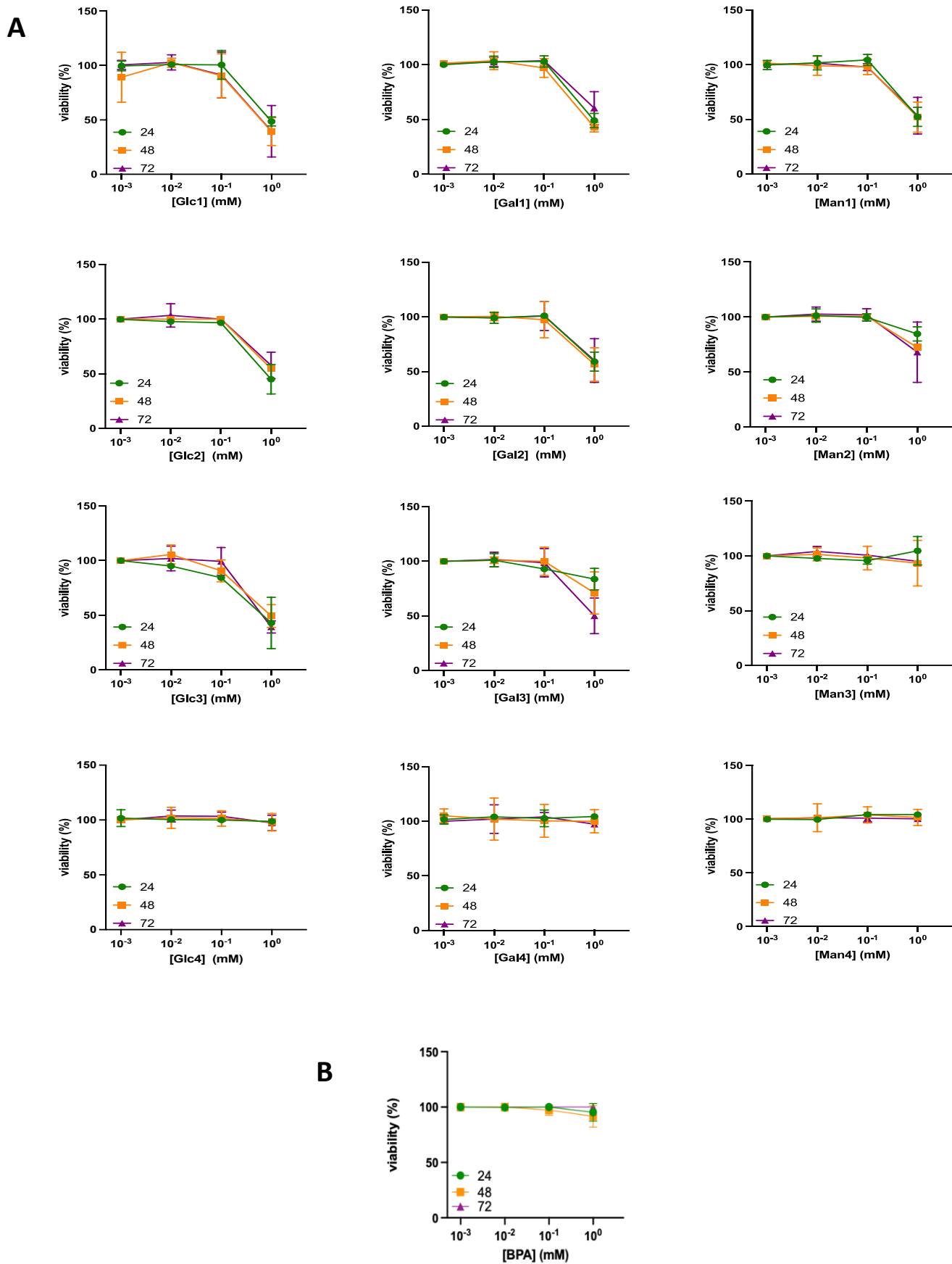


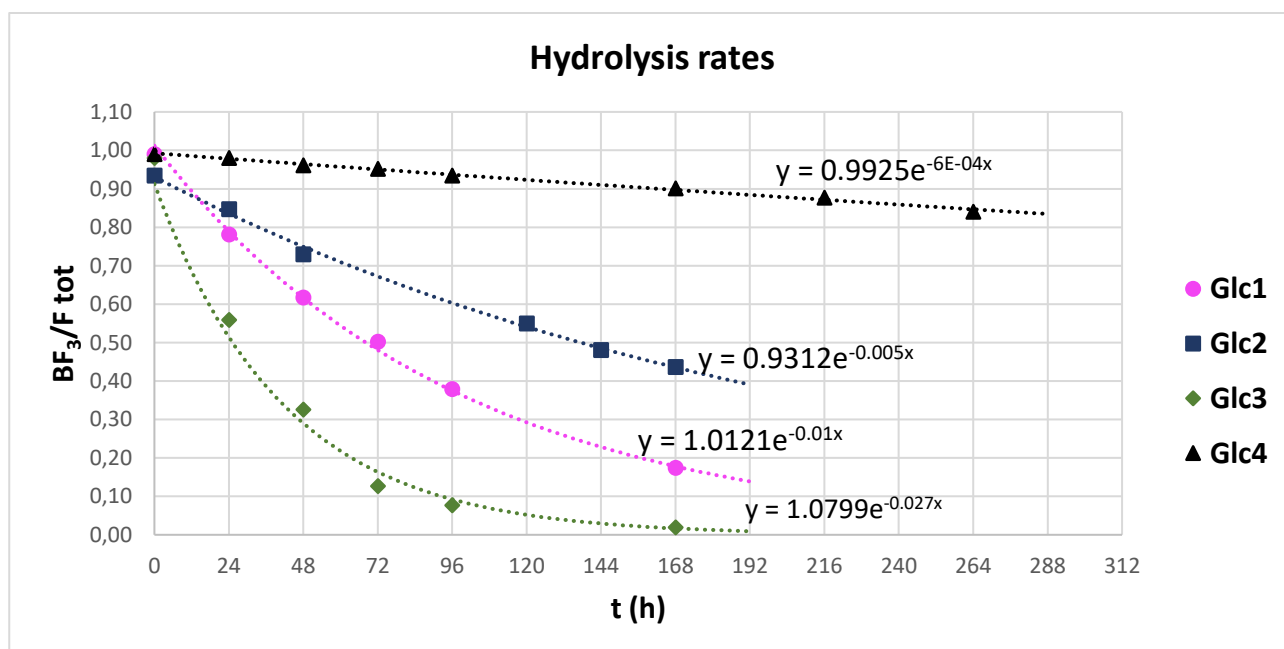
Figure 2 - Effects of (A) tested compounds (Glc1-4, Gal1-4, and Man1-4), and (B) boronophenylalanine (BPA) on cell viability. The effect of tested compounds on human primary fibroblast viability were assessed by MTT assay after 24 h, 48 h, and 72 h of treatment with increasing concentrations (0.001 – 1 mM) of each compound. The concentration-response curves show the percentage of cells. The data represent the mean \pm SD of at least three independent experiments run in triplicate.

1.3 Stability evaluation

First, we monitored the stability of the trifluoroborate group at physiological pH by [¹⁹F] NMR spectroscopy. We chose to test just the glucose-containing compounds (**Glc 1-4**), assuming that all the molecules with the same zwitterionic part share the same stability since the sugar part, being far from the BF₃ group, should exert a negligible influence.

Each compound was dissolved in phosphate buffer (pH 7.5) at a very low concentration (2 mg/mL) to assure a pseudo-first-order kinetic. The [¹⁹F] spectra were acquired at fixed times (320 scans, 298K). The peaks of the starting material (ca. -135 ppm) and of the free fluoride (ca. -120 ppm) were integrated and plotted in the graph showing the fraction of starting material present ($[\text{BF}_3]/([\text{BF}_3] + [\text{F}^-])$) versus time values (t). The results were fit to the equation $([\text{BF}_3]/([\text{BF}_3] + [\text{F}^-]))_t = ([\text{BF}_3]/([\text{BF}_3] + [\text{F}^-]))_0 \cdot e^{-kt}$ to calculate the rate constants (k) and half-life value (t_{1/2}) for each tested compound¹⁶⁸.

Scheme 3 shows the kinetic curves for all the products tested, while **Table 2** resumes the values for k and t_{1/2}. ([¹⁹F] spectra for each compound are reported in **Experimental Details - section 1.3**)



Scheme 3 – Kinetic curves for Glc1, Glc2, Glc3, and Glc4

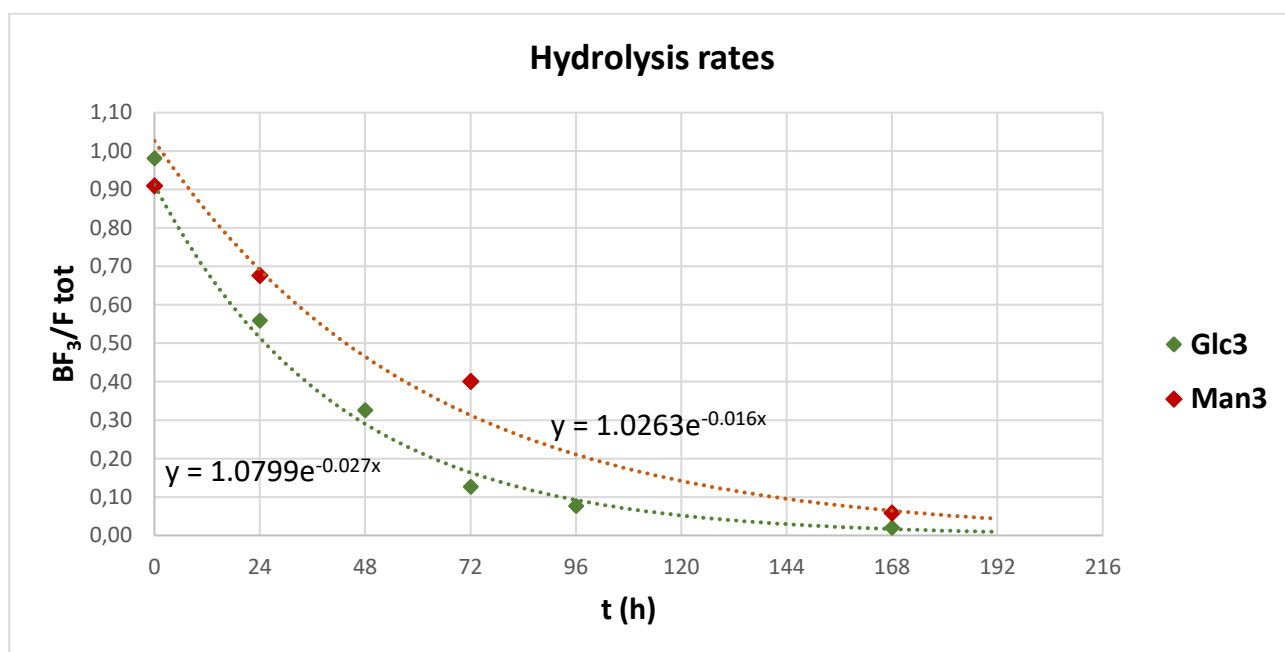
Table 2 – Significant values for Glc1, Glc2, Glc3, and Glc4

| Sample | k | t _½ (h) | t _½ (days) |
|--------|------------------------|--------------------|-----------------------|
| Glc3 | 2.7 * 10 ⁻² | 28 | 1.16 |
| Glc1 | 1.2 * 10 ⁻² | 62 | 2.58 |
| Glc2 | 5.0 * 10 ⁻³ | 124 | 5.15 |
| Glc4 | 6.0 * 10 ⁻⁴ | 1142 | 47.58 |

Glc3 was the less stable compound with a half-life value of 28h. **Glc4** showed the highest stability, with a rate constant two orders of magnitude smaller ($k = 7 \cdot 10^{-4}$) and an extrapolated half-life value of 47 days. **Glc1** and **Glc2** exhibited similar behaviors and were situated in the middle.

Comparing the stability data with the cytotoxicity ones seemed that the more stable compounds were less cytotoxic, while the easily hydrolyzed compounds showed higher toxicity.

Only one cytotoxicity data did not match the trend, **Man3** was far less cytotoxic than the corresponding **Glc3** and **Gal3** derivatives. For this reason, we performed a stability study also on **Man3** (Scheme 4).



Scheme 4 – Comparison between Man3 and Glc3 hydrolysis rates

The results confirm the marginal influence of the carbohydrate moiety on the trifluoroborate stability. **Man3** hydrolyzes similarly to **Glc3**, with a half-life value of 43h.

On the other hand, these results do not justify the **Man3** cytotoxicity profile. In the future, it could be useful to repeat the cytotoxic evaluation on **Man3** to confirm the data obtained.

1.4 Radiolabeling optimization

Then, **Glc1** and **Glc4** were selected to undergo the radiolabeling procedure. This project phase required a deep optimization by Dr. Alvaro Erhard at Centro Nacional de Aceleradores (Spain).

According to the literature procedures^{167,175,176}, the trifluoroborates radiolabeling can be performed at room temperature in an acidic aqueous solution containing [¹⁸F] F⁻. Temperature, pH, and [¹⁸F] form played crucial roles in the procedure optimization. **Table 3** reports part of the conditions tested. Further experimental details are reported in the **Experimental Details - section 1.4**.

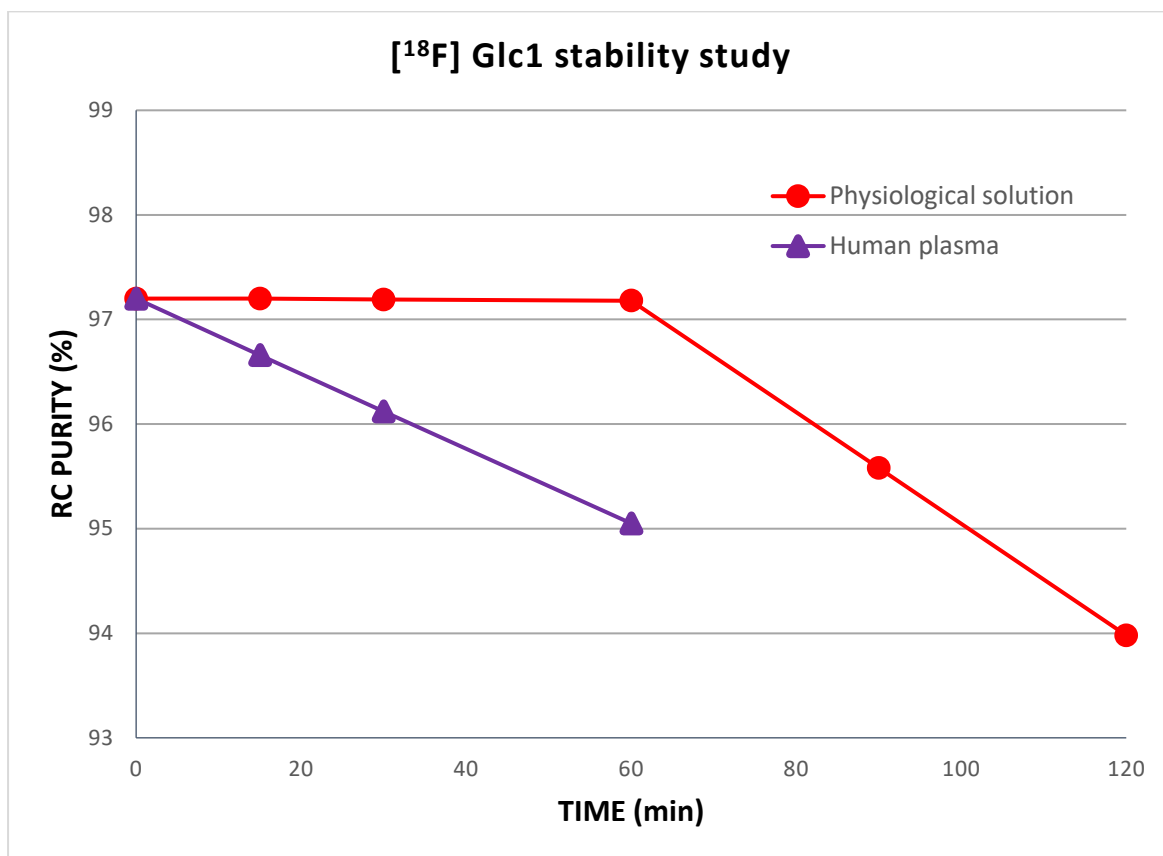
Table 3 – Results of the different radiolabeling methods applied on Glc1. a) the method described as “Direct from cyclo” means that [¹⁸F] F⁻ was used without any further purification and obtained from the liquid [¹⁸O] target (1.85 - 2.22 GBq in 50 mL unfixed target ¹⁸O water). b) the method described as “Dissolved” means that Glc1 was dissolved in a physiological solution, then treated with the [¹⁸F] F⁻ solution. c) the maximum radiochemical yield (RCY) has been obtained by radio-TLC at the time specified. d) the purity of [¹⁸F] Glc1 has been determined after purification over Alumina cartridge.

| [¹⁸ F] F ⁻ source ^a | Glc1 ^b | T (°C) | max RCY (%) ^c | t _{max RCY} (min) | Purity (%) ^d |
|---|-------------------|-----------|--------------------------|----------------------------|-------------------------|
| Direct from cyclo | Solid | 40 | 64.3 | 120 | 96.9 |
| Direct from cyclo | Solid | 85 | 42.4 | 20 | 96.6 |
| Direct from cyclo | Dissolved | 40 | 23.1 | 150 | -- |
| Direct from cyclo | Dissolved | 85 | 41.7 | 60 | -- |
| Acidified [¹⁸F] | solid | 85 | 49.9 | 20 | 97.2 |

[¹⁸F] **Glc1** was obtained with a radiolabeled purity of 97.2% through a reaction with acidified [¹⁸F] at 85°C. Compared to the optimal conditions found in the next section (**Result and Discussion – section 1.5**) the reaction temperature employed is indeed higher. This has been a compromise between the compound stability and the need to operate in a narrow timeframe due to the short half-life of [¹⁸F].

On the other hand, **Glc4** did not respond in the same way, and it was impossible to obtain a radiolabeled equivalent with enough activity to be tested in vivo. This unexpected result may be due to the greater stability of **Glc4** compared to the other glucose-containing compounds, and its lower tendency to exchange fluoride ions.

The in vitro stability of [¹⁸F] **Glc1** was investigated in human plasma and physiological solutions. **Scheme 5** shows that at 37 °C [¹⁸F] **Glc1** is stable for 1 hour in human plasma and 100 min in a physiological solution. The stability limit was set at 95% of the radiochemical (RC) purity, which means a 5% maximum of free [¹⁸F] F⁻, a quantity considered safe for in vivo experiments.



Scheme 5 - Radiolabeling stability for $[^{18}\text{F}]$ Glc1 obtained with the acidified $[^{18}\text{F}]$ method. The study was conducted in physiological solution and human plasma. The stability of $[^{18}\text{F}]$ Glc1 was 60 min in human plasma and 100 min in physiological solution

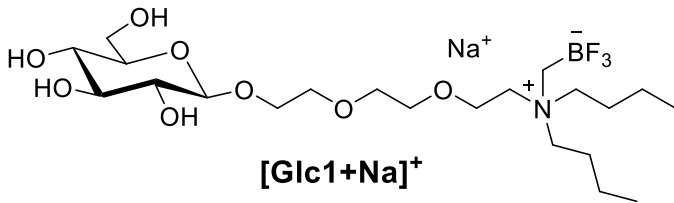
1.5 HR-MS stability studies for the radiolabeling optimization.

To screen the temperature and pH conditions for the optimization of the radiolabeling, together with Dr. Daniela Imperio e Dr. Erika Del Grosso, we performed further stability studies on **Glc1** and **Glc4**. In particular, we tested the effects of temperature and acidic pH on the molecules' integrity, first by TLC (**Table 4**) and then through mass spectrometry (**Figure 3**). **Glc1** and **Glc4** were dissolved in demineralized water, and the pH was adjusted with HCl 1M. This sort of experiment allowed us to collect data about the compounds' stability in different reaction conditions but did not indicate the effectiveness of the radiolabeling.

From the analysis, we confirmed that the main degradation product, as expected, was the boronic acid derivative, which tends to increase at lower pH, higher temperature, and prolonged time. At 40°C, no degradation was recorded, but the temperature was too low to promote a fast radiolabeling (see **Result and Discussion – section 1.4**). 85°C and pH 2 have been a compromise between the need to preserve the compounds integrity and to promote the radiochemical reaction.

Table 4 – Stability experiments carried out on Glc1 and Glc4. 1 mg of compound was dissolved in 0.5 mL of demineralized water and the pH was adjusted with HCl 1M. The samples were heated, and TLC were performed at given times.

| Substrate | pH | T (°C) | t (min) ^a | Result |
|-----------|-----|--------|----------------------|-----------------------|
| Glc1 | 0.5 | 85 | 15 | Extensive degradation |
| Glc4 | 0.5 | 85 | 15 | Extensive degradation |
| Glc1 | 2.0 | 85 | 15 | Partial degradation |
| Glc4 | 2.0 | 85 | 15 | Partial degradation |
| Glc1 | 2.0 | 40 | 15, 30, 60 | No degradation |
| Glc4 | 2.0 | 40 | 15, 30, 60 | No degradation |

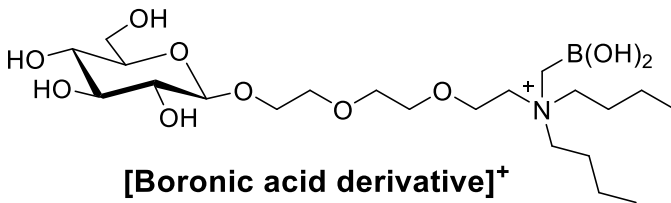


Chemical Formula: $C_{21}H_{43}BF_3NNaO_8^+$

Exact Mass: 528.29260

Molecular Weight: 528.36843

m/z: 528.29260 (100.0%)



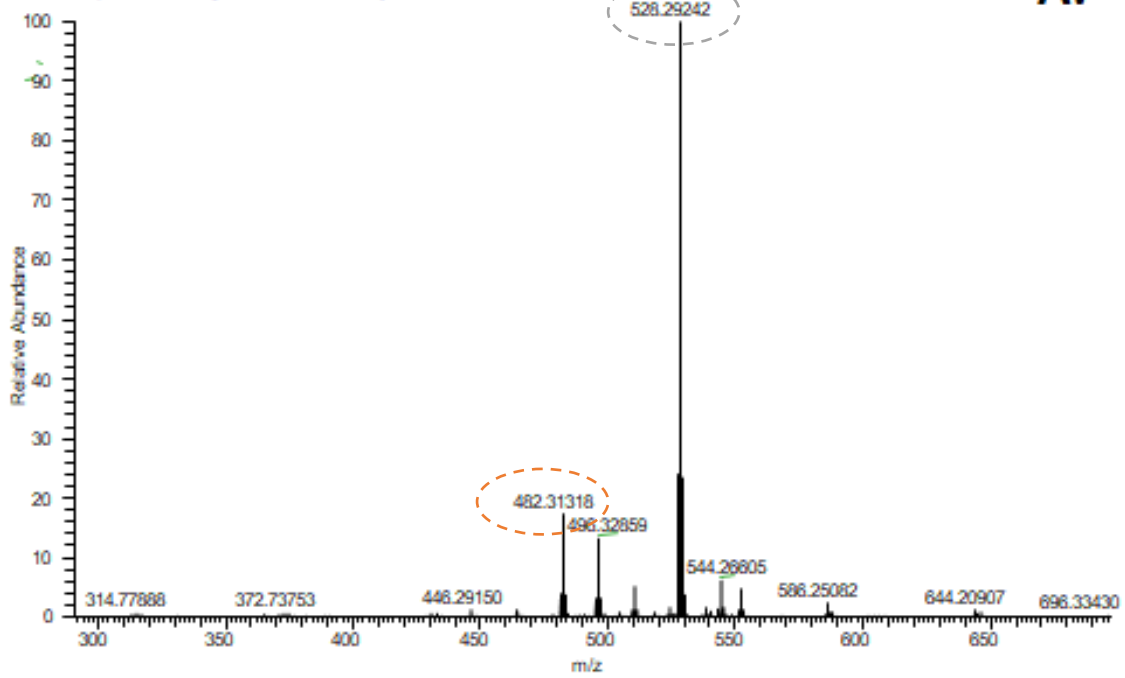
Chemical Formula: $C_{21}H_{45}BNO_{10}^+$

Exact Mass: 482.31310

Molecular Weight: 482.39745

m/z: 482.31310 (100.0%)

SI_T0 #142 RT: 1.44 AV: 1 SB: 52 0.01-1.07 NL: 3.72E9
T: FTMS + p ESI Full ms [100.0000-1500.0000]



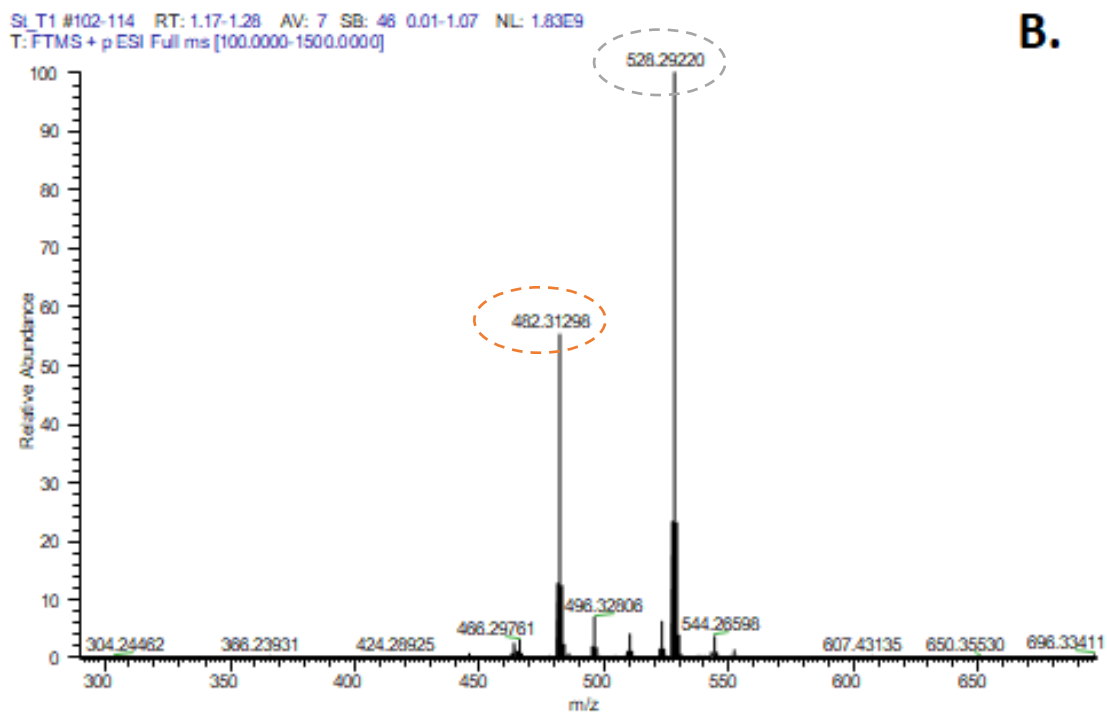


Figure 3A and 3B - HR-MS analysis of Glc1 at pH 2.0. Glc1 was dissolved in 100 μL of a solution of KF ($3.7 \times 10^{-9} \text{ M}$), and the pH was adjusted to 2 with HCl 1N. The mixture was warmed at 85 $^{\circ}\text{C}$, and mass spectrometry analyses were performed at rt at time zero (t_0), and after 20' (t_1), 30' (t_2), 45' (t_3), and 60' (t_4):

A. t_0 at r.t. – found m/z 528.29242 [$\text{Glc1}+\text{Na}$] $^{+}$ (vs calculated 528.29260)

B. t_1 at 85 $^{\circ}\text{C}$ – found m/z 528.29242 [$\text{Glc1}+\text{Na}$] $^{+}$ (vs calculated 528.29260), found m/z 482.31298 [boronic acid derivative] $^{+}$ (vs calculated 482.31299)

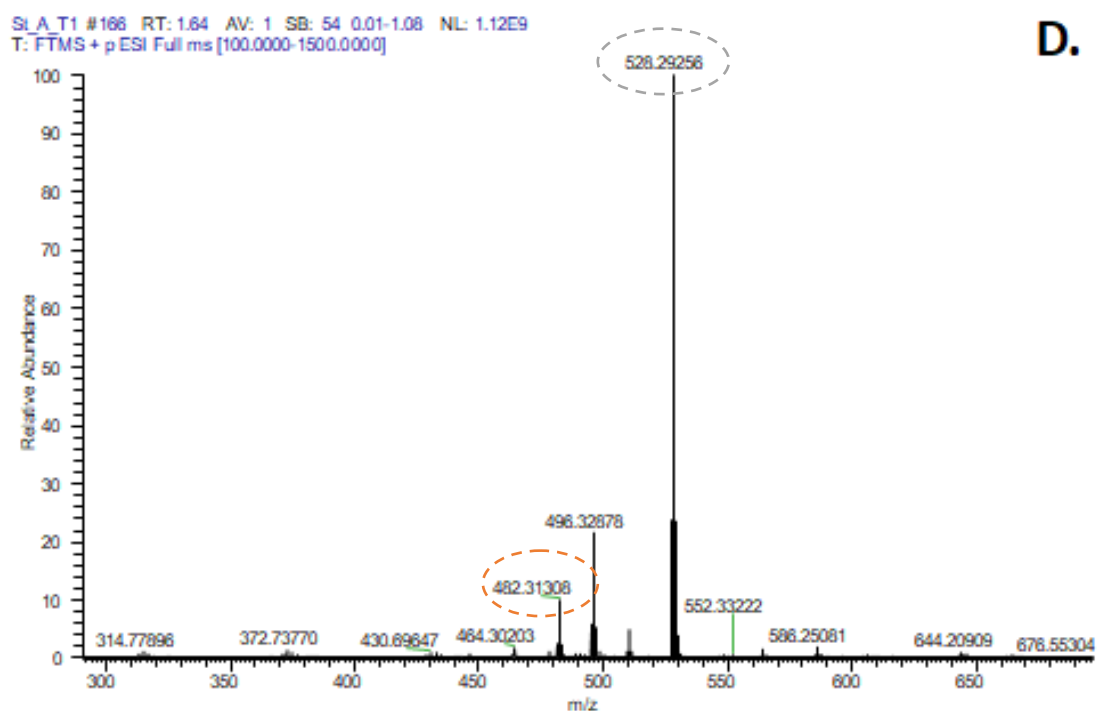
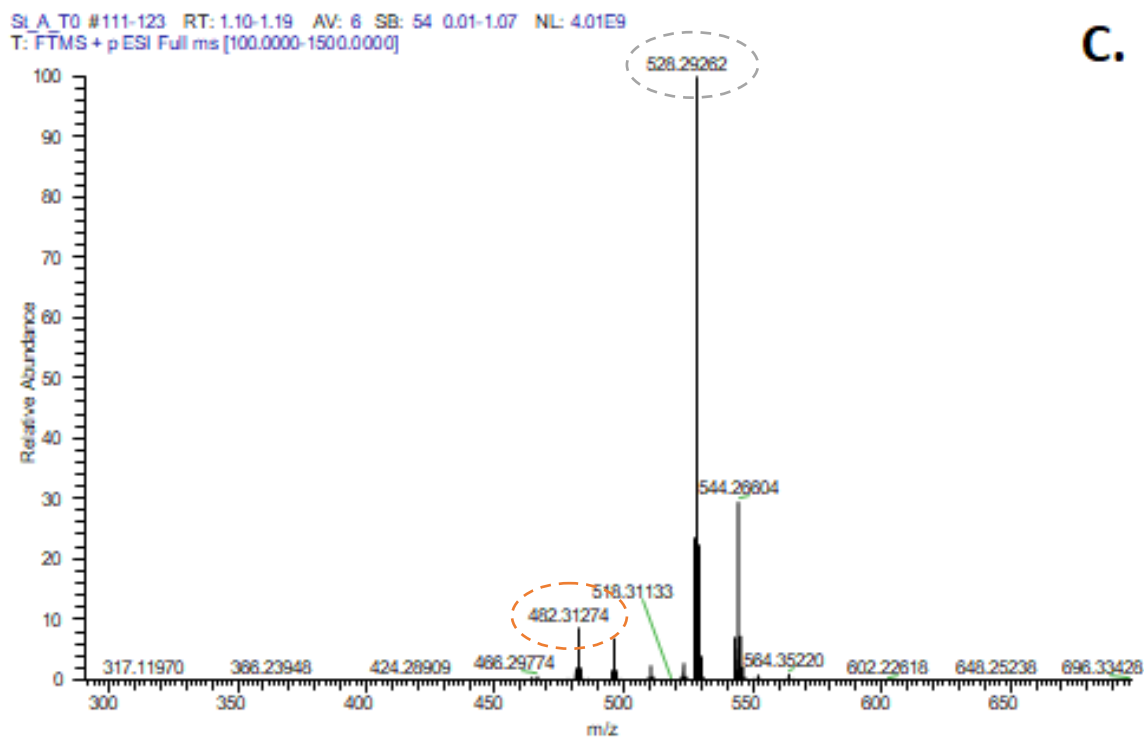


Figure 3C and 3D - HR-MS analysis of Glc1 at pH 2.0. Purification step from boronic acid derivative through an Alumina cartridge (Sep-Pak) after 20' at 85°C:

C. t0 after alumina cartridge purification

D. 20' at 85°C, after alumina cartridge purification.

1.6 In vivo PET imaging

To conclude this first part, Professor Marcin Balcerzyk at Centro Nacional de Aceleradores (Spain) performed an initial in vivo PET experiment using [^{18}F] Glc1.

Figure 4A shows the PET/CT scan performed with [^{18}F] Glc1 on healthy white mice 8-week-old, while **Figure 4B** represents a [^{18}F] FDG scan. (Further experimental details are reported in **Experimental Details - section 1.5**).

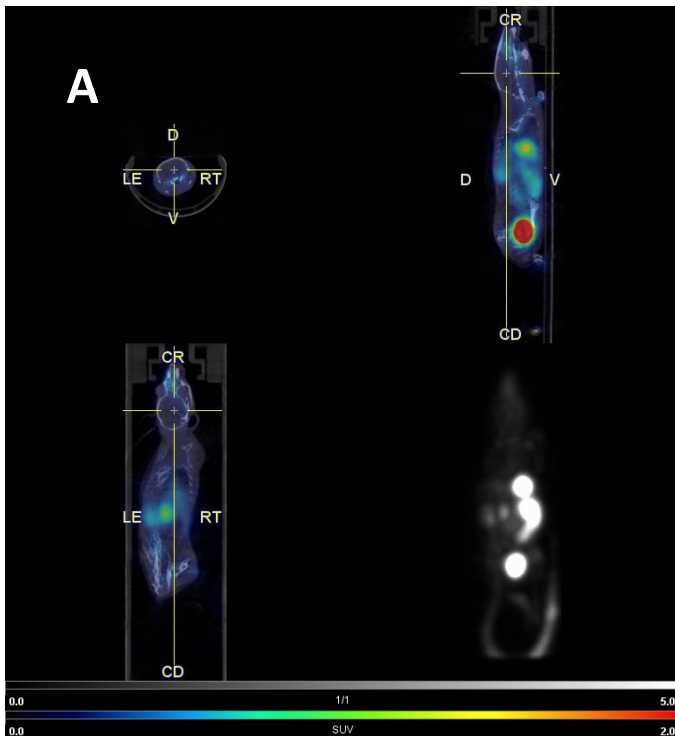
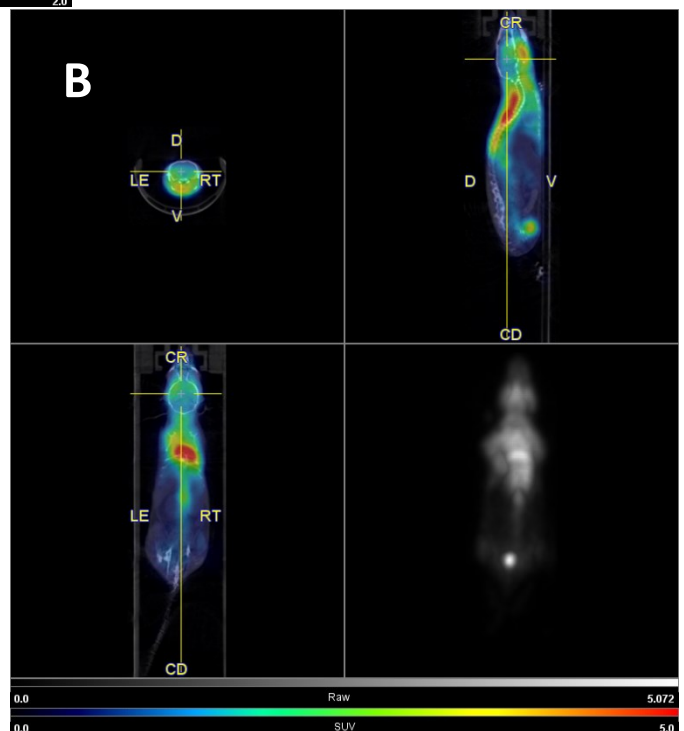


Figure 4A. The PET/CT study of the radiopharmaceutical [^{18}F] Glc1 in healthy mice. Uptake in the liver and elimination through the bladder are observed. No metabolism is observed in the brain or heart.

Figure 4B. The PET/CT study of the radiopharmaceutical [^{18}F] FDG in healthy mouse. Uptake was observed in the brain and heart.



The behavior of the two compounds is remarkably different. In particular, [¹⁸F] **Glc1** localizes in the lower part of the mice – in the liver and the bladder – does not cross the Blood-Brain Barrier and is not metabolized in the heart. [¹⁸F] FDG shows typical metabolism in the heart, brain, and brown fat.

In both scans show no uptake in the bones relative to free fluoride ions, so [¹⁸F] **Glc1** does not hydrolyze in the time frame required for the imaging. These observations suggest the need to optimize the biodistribution but prove the stability of these types of structures.

2. Organotrifluoroborate Sugar Conjugates – part II

2.1 Synthetic project

The second part of this main project started shortly after the [¹⁹F] NMR stability studies on the glucose-containing compounds. We aimed to obtain more stable compounds, with hopefully less cytotoxicity. Our research in the literature showed a possible solution in the trifluoroborates stabilized by a sulfonium salt¹⁶⁸. We opted for synthesizing products with the general structure shown in **Figure 5**. **Table 5** shows a library of compounds obtained either *via* nucleophilic substitution or *via* click reactions.

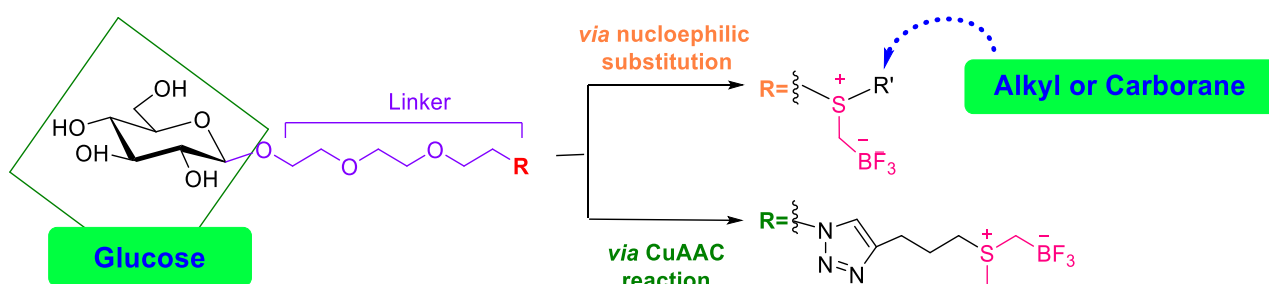
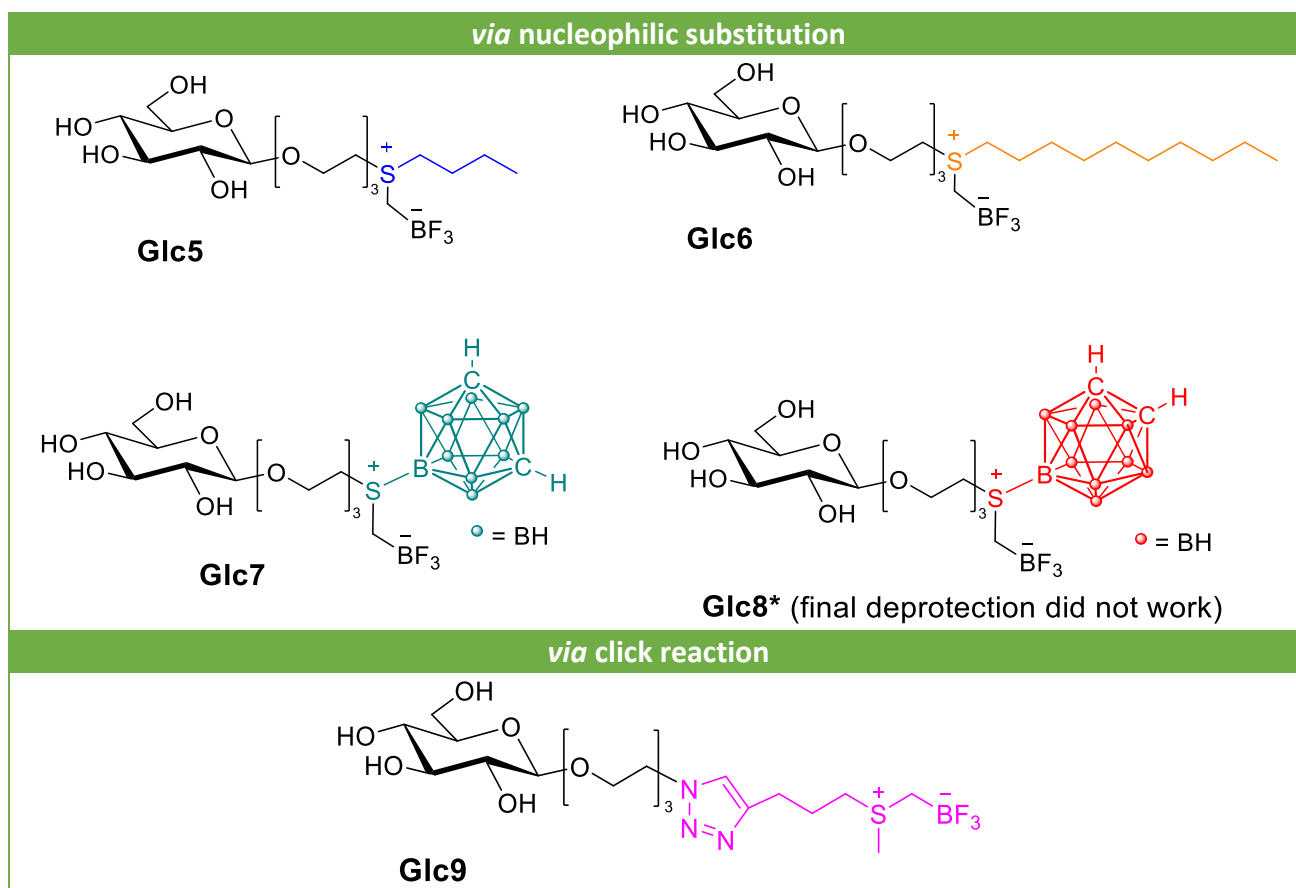


Figure 5 - General structure for the Organotrifluoroborate sugar conjugates containing sulfonium salts

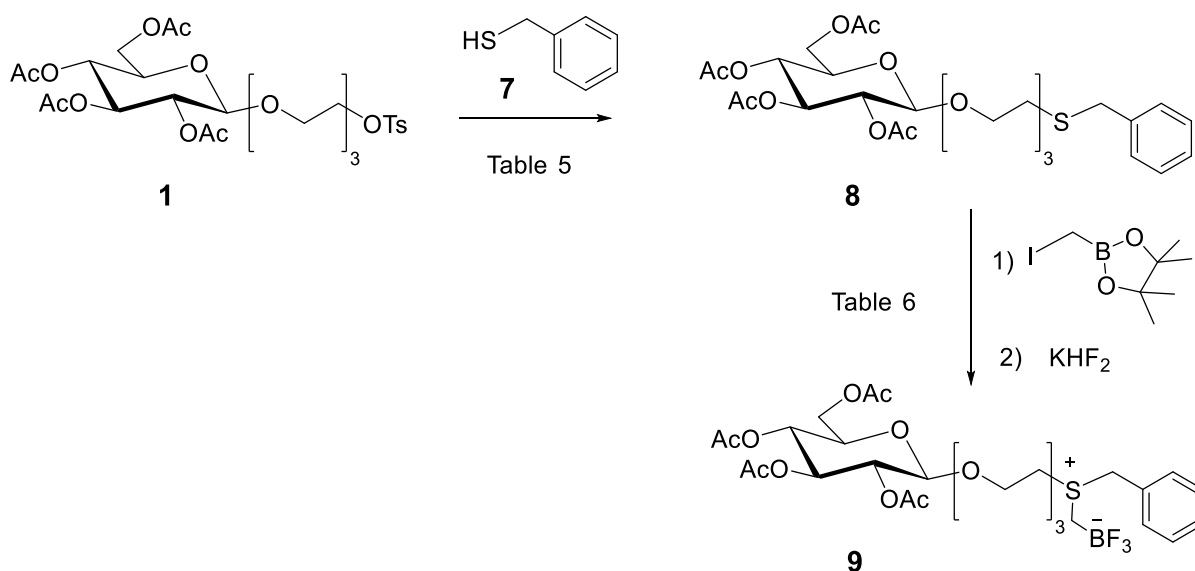
Table 5 - Structures of the synthesized products



The first four compounds were synthesized through nucleophilic substitution with nonaromatic thiols or carborane - containing thiols starting from the key common intermediate **1**. I carried out this part of the project in the laboratory of professor Hey-Hawkins (Universität Leipzig, Leipzig, Germany), where I was able to access their catalog of functionalized carboranes. We decided to add these kinds of moieties to our products to increase the quantity of boron per molecule.

The synthesis, even if very similar to the one already developed for the ammonium salts, required an accurate optimization and much more careful evaluation due to the sulfur atom's lower nucleophilicity.

Scheme 5 illustrates the synthetic pathway developed on the benzylic derivative used just as a model.



Scheme 5 – Synthetic pathway developed for the synthesis of compound 9. Table 5 and Table 6 list the reaction conditions used for both synthetic steps.

The benzyl mercaptan **7** was synthesized from the corresponding benzyl bromide according to literature procedures and used as a crude product^{177,178}. Then, as reported in **Table 6** we screened a few conditions for the first substitution reaction on the key intermediate **1**. We needed to find the right combination of base and solvent to promote the thiol deprotonation without endangering the starting material.

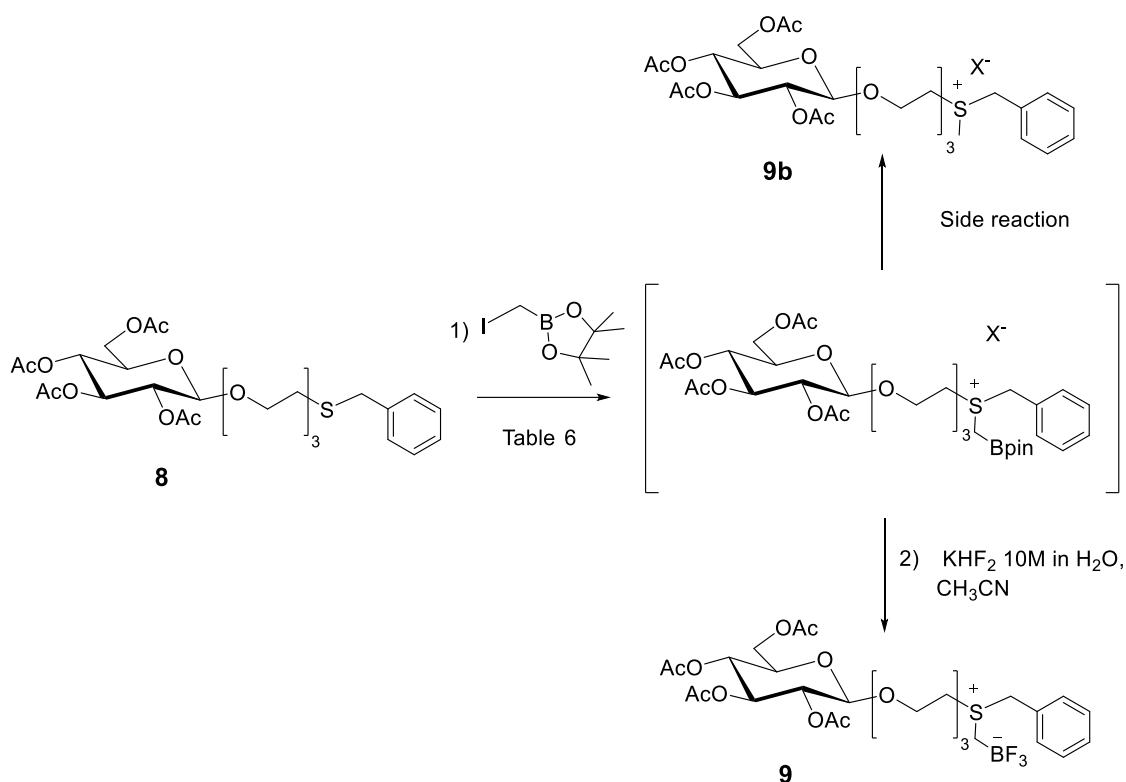
Table 6 – Reaction conditions tested for the nucleophilic substitution with benzyl mercaptan.

| Trial | Base | Solvent | Temperature | Result | yield |
|-------|--------------------------------|--------------------|--------------|--|-------|
| 1 | KOH | MeOH | r.t. | Deacetylated product | |
| 2 | NaH | DMF | r.t. to 80°C | Unreacted starting material and byproducts | |
| 3 | DBU | CH ₃ CN | r.t. to 80°C | Byproducts | |
| 4 | K ₂ CO ₃ | CH ₃ CN | r.t. to 80°C | product (8) | 12% |
| 5 | K ₂ CO ₃ | CH ₃ CN | 80°C | product (8) | 65% |

In the end, the best combination has been K₂CO₃ in CH₃CN at 80°C. In this way, we were able to obtain compound **8** in a quite satisfactory yield. Right after the optimization of this first step, we focused on the synthesis of the trifluoroborate **9**. We started with the same conditions used for the ammonium derivatives, iodomethylboronyl pinacolate in diethyl ether at room temperature, but this time the typical sticky precipitate did not form. As suggested in the literature, in a second attempt we added a silver salt to the reaction to promote the alkylation. Unfortunately, as we discovered during further research in the literature^{179,180}, silver salts also promote molecule deboration giving the byproduct **9b** (Scheme 6). Table 7 resumes some of the conditions used, but despite all attempts made, we were unable to increase the yield above 30%.

The quantity of byproduct **9b** can be reduced by carefully working in anhydrous conditions and removing the silver salts before the second reaction step. In fact, during the first reaction step, silver iodide precipitates from the reaction solution as yellow solid. It is important to completely remove the solid from the reaction before starting the second step; otherwise, the aqueous solution of KHF₂ further promotes the side reaction.

Even if the second step had not an encouraging yield, we decided to move forward and started to work on the synthesis of the remaining sulfonium-containing compounds.

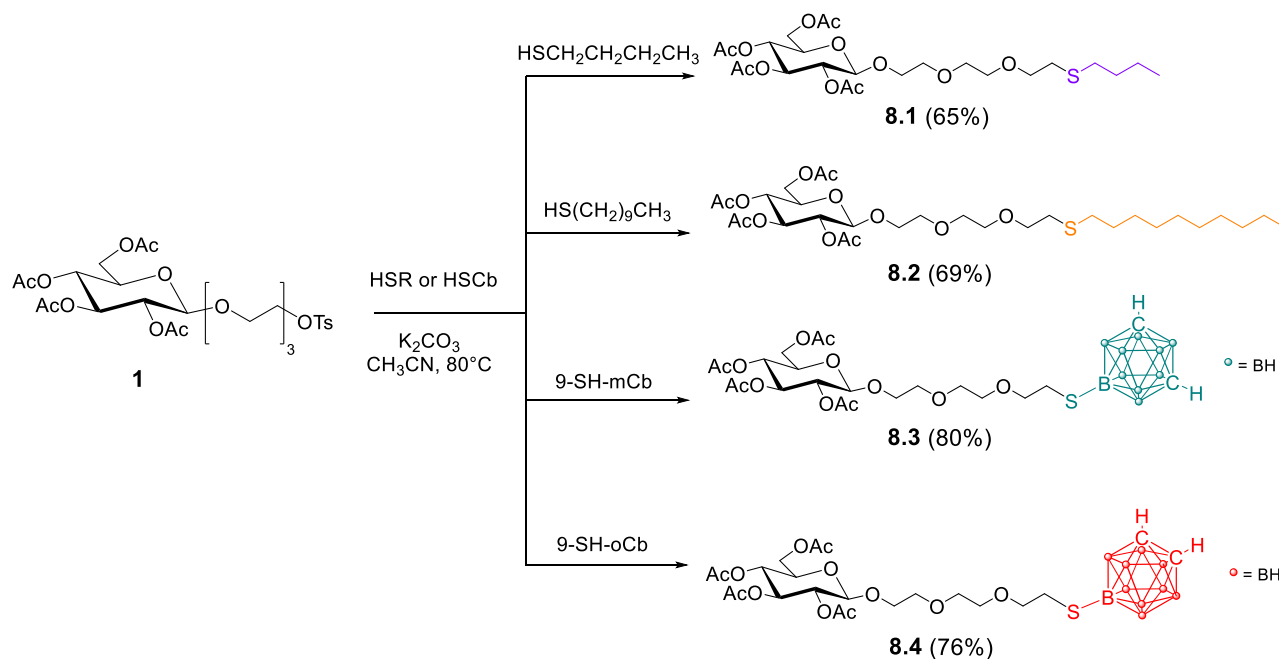


Scheme 6 – Alkylation reaction on compound 8. The byproduct 9b is unavoidable but can be reduced by carefully working in anhydrous conditions and removing the silver iodide from the first step.

| Trial | Silver salt | Solvent | Result | yield |
|-------|-----------------------------|--------------------|-----------------------------|-------|
| 1 | no | Et ₂ O | Unreacted starting material | |
| 2 | AgOTf (1.5 eq) | CH ₃ CN | Deboronated product (9b) | |
| 3 | AgOTf (1.1 eq) | CH ₃ CN | product (9) | 30% |
| 4 | AgOTf (1.1 eq) | THF | Unreacted starting material | |
| 5 | AgClO ₄ (1.3 eq) | CH ₃ CN | product (9) | 28% |

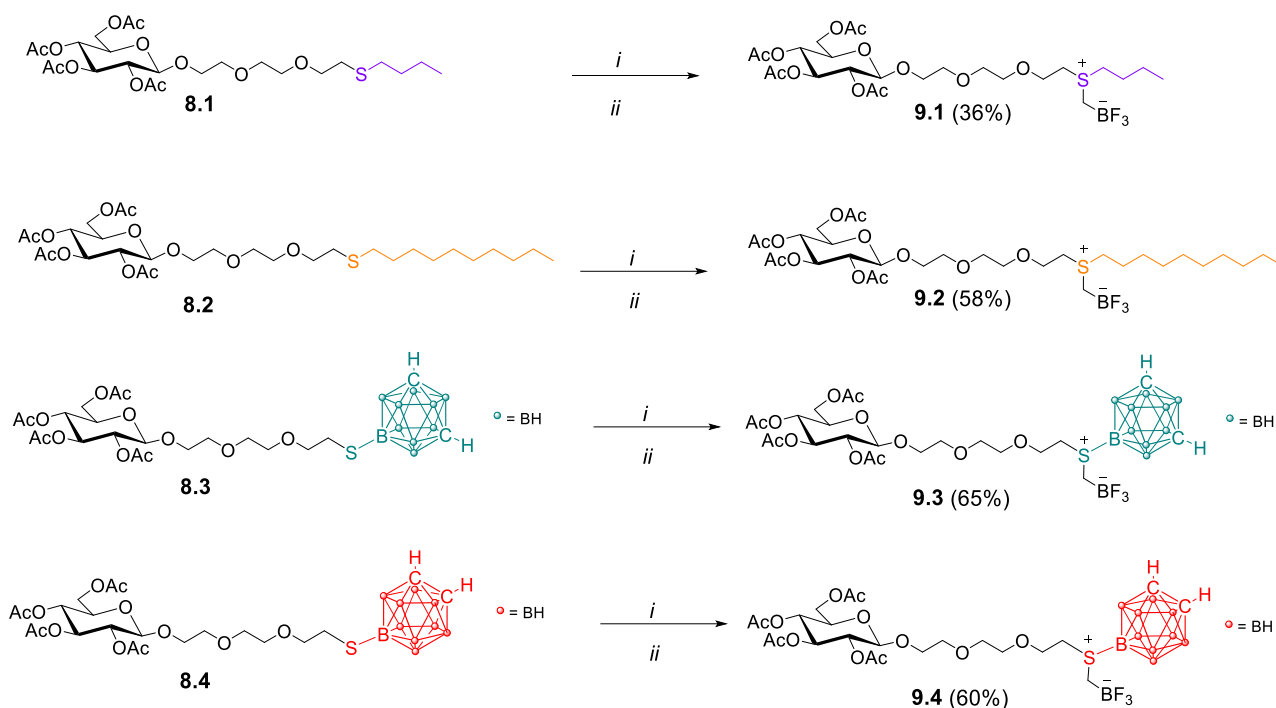
Table 7 – Reaction conditions tested for the alkylation with iodomethylboronyl pinacolate.

The procedure for the first synthetic step was successfully employed for all remaining compounds, using the proper thiol reagents. Surprisingly, the conditions were also compatible with the carborane structures, and all the products were obtained with satisfactory yields as shown in **Scheme 7**.



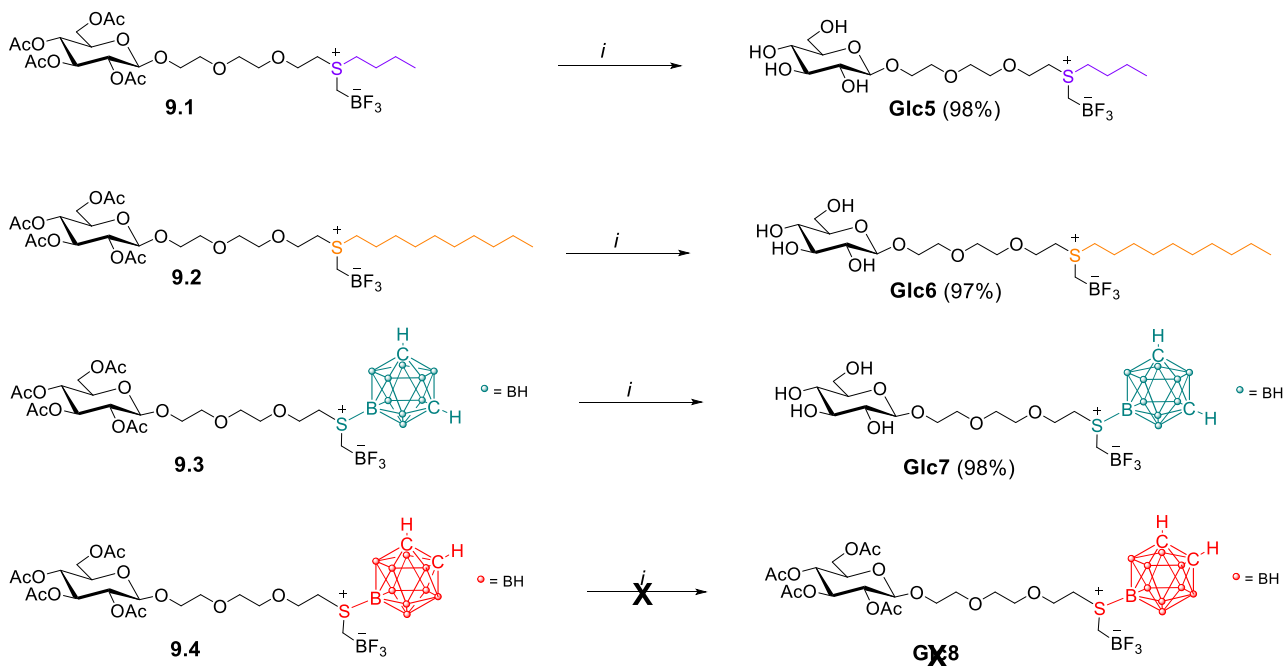
Scheme 7 – Substitution reactions on key intermediate **1**. The reaction conditions optimized for product **8** were successfully employed for the synthesis of the remaining products with the proper thiols.

As shown in **Scheme 8**, the aliphatic thioethers **8.1** and **8.2** underwent the next alkylation step without any further problems, even with a slight improvement in the yield for product **9.2**. Instead, for the carborane-containing products – **8.3** and **8.4** – there was the need to switch the order of the reagents to avoid the direct interaction between the starting materials and the silver salt. For these reactions, AgOTf was premixed with the iodomethylboronyl pinacolate and then added to the solution of starting material. In this way, the reaction yields increased and no traces of the nido-carboranes were detected. The product containing *meta*-carborane – **9.3** – was easier to purify and less prone to degradation compared to the product containing the *ortho*-carborane, **9.4**.



Scheme 8 – Alkylation reactions with iodomethylboronyl pinacolate. i) Iodomethylboronyl pinacolate, AgOTf, CH₃CN, 0°C. ii) KHF₂ 10M in H₂O, CH₃CN, r.t.

In a similar way to the ammonium salts previously reported, we performed the last deprotection step under mild basic conditions with a catalytic amount of potassium hydroxide in methanol. Target products **Glc5**, **Glc6**, and **Glc7** were obtained with excellent yield and did not require any further purification (**Scheme 9**).



Scheme 9 – Deacetylation reactions for the final products synthesis. i) KOH (0.1 eq), MeOH, r.t.

Unfortunately, the deprotection of **9.4** gave some problems and it was not possible to obtain **Glc8**. A possible explanation for this unexpected result is the higher sensitivity of orto-carborane towards the basic environment and the consequent starting material degradation to partially deacetylated *nido*-structures. From the HRMS (+p ESI) spectrum of **Glc8**, **Figure 6A**, is evident the lack of signals corresponding to compound exact mass. Instead, in the HRMS spectrum acquired in negative ionization (-p ESI), **Figure 6B**, it is possible to identify a set of signals corresponding to the partially deacetylated *nido*-structures (**Table 8**).

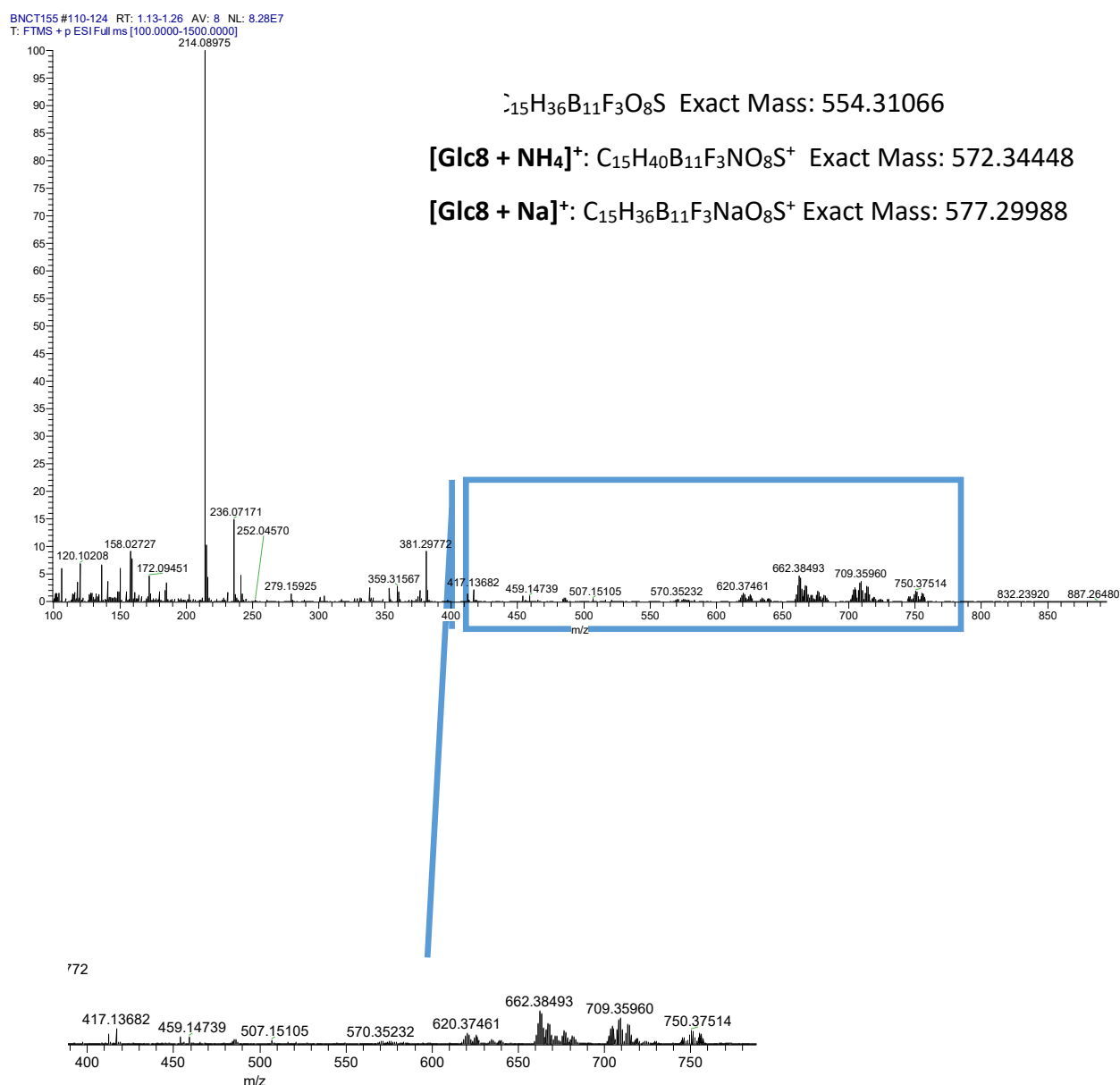


Figure 5A – HR-MS spectrum for **Glc8**. RT: 1.13-1.26 AV: 8 NL: 8.28E7 T: FTMS + p ESI Full ms [100.0000-1500.0000]

BNCT155 #108-126 RT: 1.12-1.27 AV: 9 NL: 4.60E7
T: FTMS - p ESI Full ms [100.0000-1500.0000]

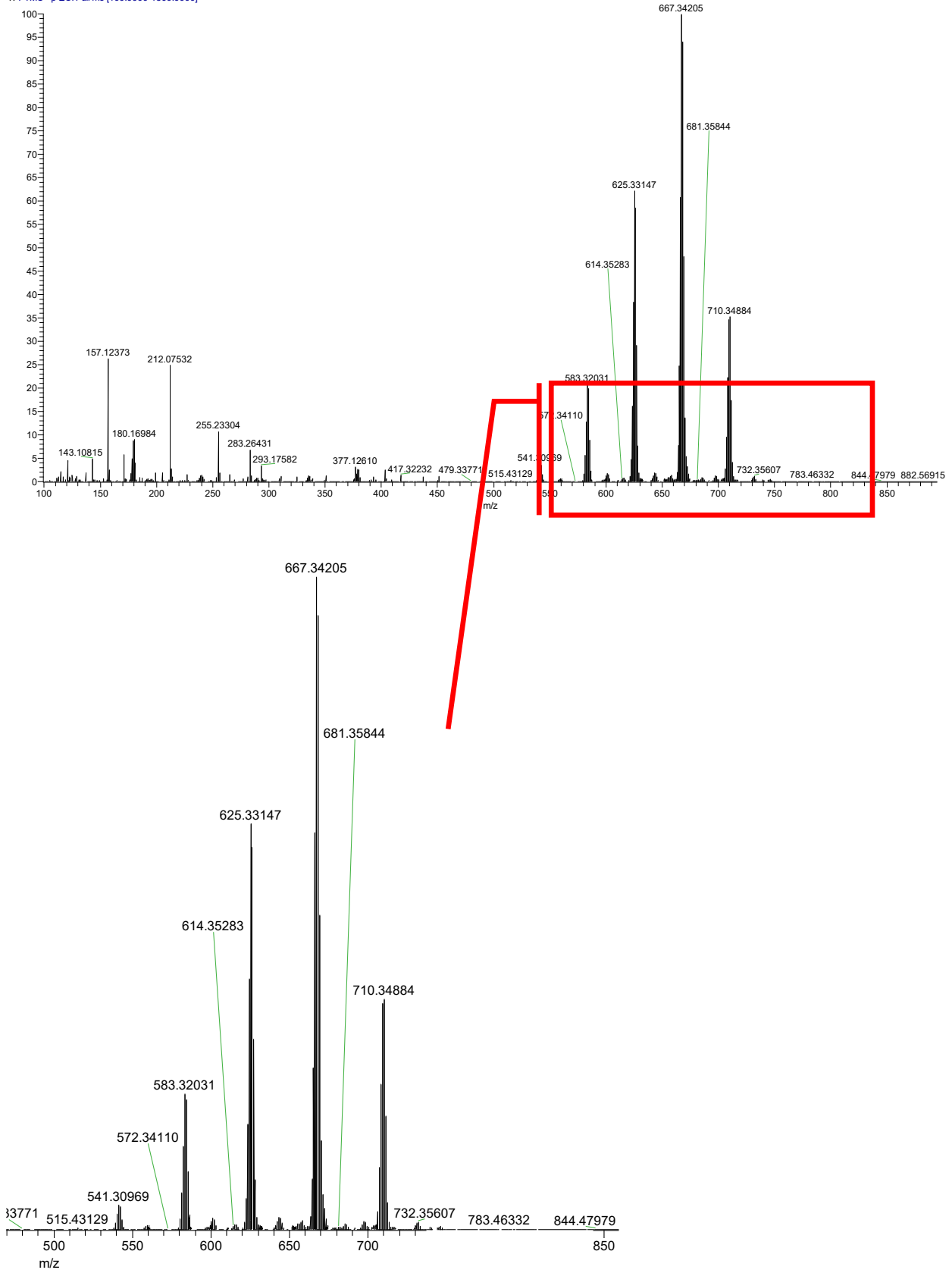
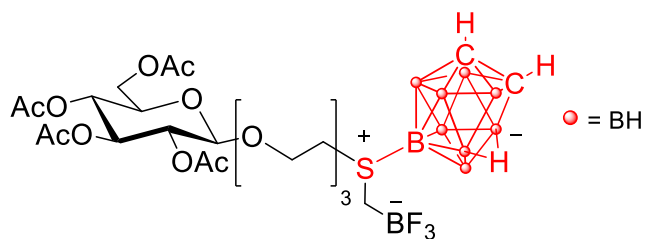
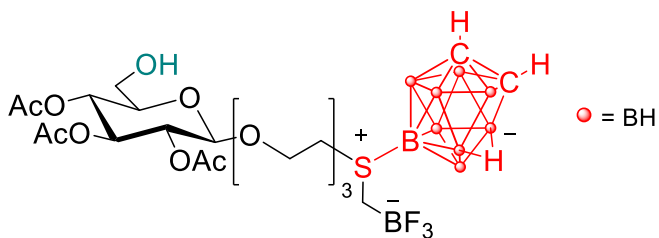


Figure 6B – HR-MS spectrum for Glc8. RT: 1.12-1.27 AV: 9 NL:4.60E7 T: FTMS - p ESI Full ms [100.0000-1500.0000]

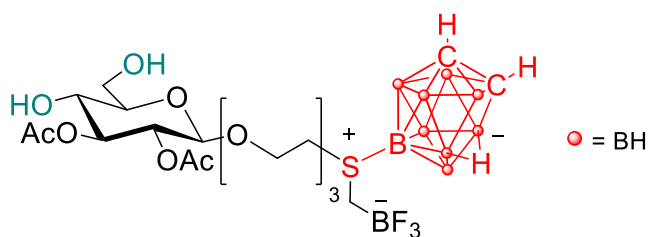
Table 8 – Possible structures explaining the results from the HR-MS



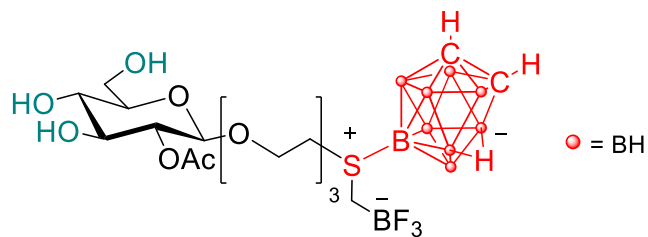
Chemical Formula: $C_{23}H_{44}B_{10}F_3O_{12}S^-$
 Exact Mass: 711.34416
 m/z: 709.35142 (100.0%), **710.34879 (89.4%)**



Chemical Formula: $C_{21}H_{42}B_{10}F_3O_{11}S^-$
 Exact Mass: 669.33360
 m/z: **667.34256 (100.0%)**, 668.33723 (89.4%)

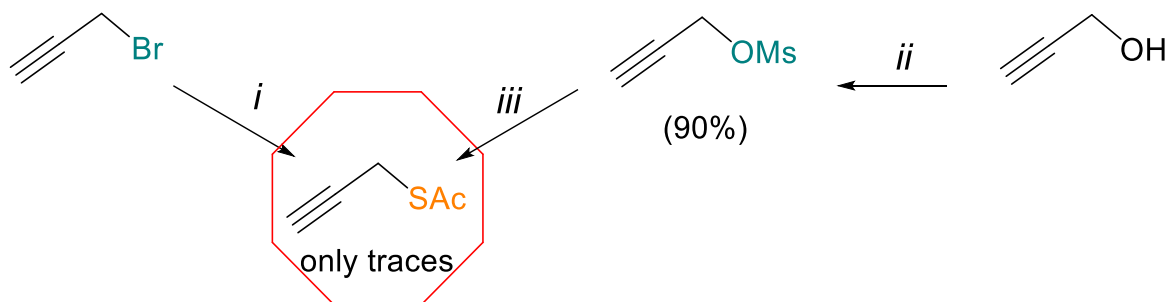


Chemical Formula: $C_{19}H_{40}B_{10}F_3O_{10}S^-$
 Exact Mass: 627.32303
 m/z: 626.32666 (100.0%), **625.33029 (89.4%)**



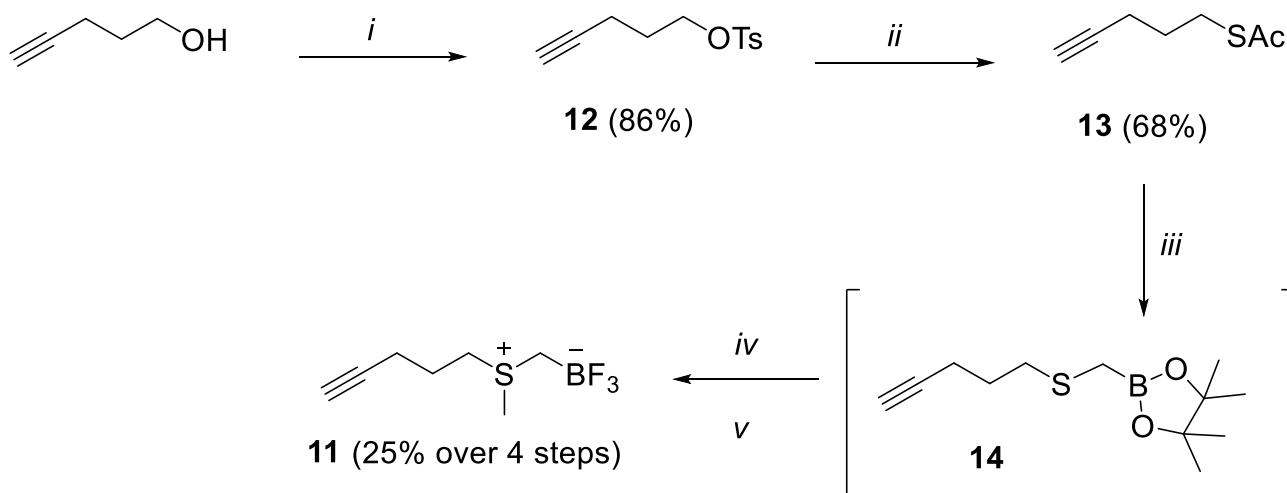
Chemical Formula: $C_{17}H_{38}B_{10}F_3O_9S^-$
 Exact Mass: 585.31247
 m/z: 584.31610 (100.0%), **583.32073 (89.4%)**

We started this synthesis from either propargyl bromide or propargyl alcohol - activated as mesyl derivative - but both approaches were quite difficult, mainly because of the volatile nature of the intermediates (**Scheme 11B**).



Scheme 11B – Synthetic approaches to propargyl thioacetate. i) KSAc, DMF, 0°C to r.t. ii) MsCl, Et₃N, DCM, -10°C iii) KSAc, K₂CO₃, H₂O

Therefore, we applied what we had learned to a slightly longer carbon chain and realized the synthetic path described in **Scheme 12** to obtain the functionalized alkyne **11**.



Scheme 12 – Synthetic scheme for alkyne **11**. i) TsCl, Et₃N, DCM, 0°C to r.t. ii) KSAc, DMF, 60°C iii) KOH, iodomethylboronyl pinacolate, MeOH, 0°C to r.t. iv) MeOTf, Et₂O, r.t. v) KHF₂ 10M in H₂O, CH₃CN, r.t.

We activated the commercially available 4-pentyn-1-ol as tosyl derivative **12**, obtaining a really pure product after column purification with a satisfactory yield¹⁸¹. Then, substitution with potassium thioacetate in DMF at 60°C gave the intermediate **13** without any complications¹⁸². **13** was deacetylated with a solution of potassium hydroxide in methanol and alkylated in situ with iodomethylboronyl pinacolate. The intermediate **14** was used as crude in the following step, alkylated with methyl triflate, and then converted into the trifluoroborate **11**. The overall yield over four steps was 25%.

In a first attempt to obtain **11**, we purified compound **14** over silica gel, but the combined yield over the four steps was only 16% because **14** was difficult to purify. The completely characterized alkyne **11** reacted with the azido derivative **4** in the click reaction to give the intermediate product **15**, as shown in **Scheme 10**. Upon deacetylation, the final product **Glc9** was obtained in good yield with a reliable synthetic pathway (Detailed synthetic procedures and characterizations are reported in the **Experimental Details - section 2.1**).

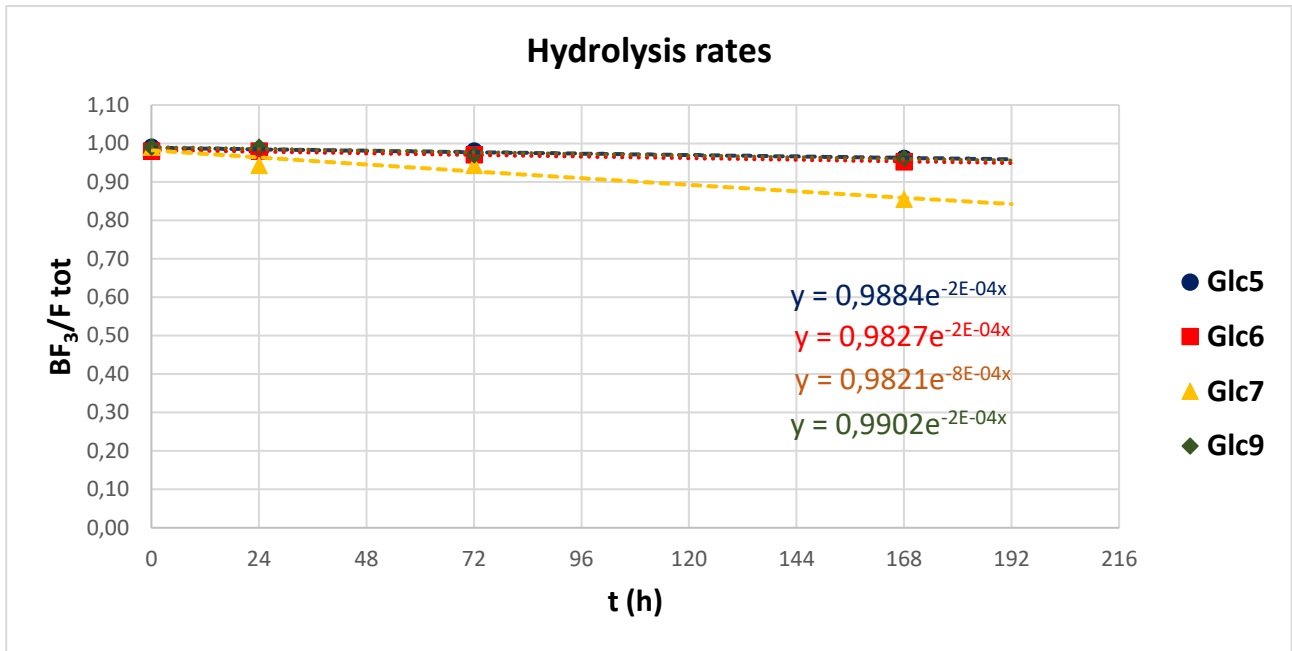
2.2 Stability evaluation

In the same fashion as the ammonium-containing compounds, we tested the stability of **Glc5**, **Glc6**, **Glc7**, and **Glc9** in pseudo-physiological conditions.

Each compound was dissolved in phosphate buffer (pH 7.5) at a very low concentration (2 mg/mL) to assure a pseudo-first-order kinetic. The [¹⁹F] spectra were acquired at fixed times (320 scans, 298K). The peaks of the starting material (ca. -135 ppm) and of the free fluoride (ca. -120 ppm) were integrated and plotted in the graph showing the fraction of starting material present ($\frac{[BF_3]}{[BF_3] + [F^-]}$) versus time values (t). The results were fit to the equation $\left(\frac{[BF_3]}{[BF_3] + [F^-]}\right)_t = \left(\frac{[BF_3]}{[BF_3] + [F^-]}\right)_0 \cdot e^{-kt}$ to calculate the rate constants (k) and half-life value ($t_{1/2}$) for each tested compound¹⁶⁸.

Scheme 13 shows the kinetic curves for all the products tested, while **Table 9** resumes the values for k and $t_{1/2}$. ([¹⁹F] spectra for each compound are reported in **Experimental Details - section 2.2**)

This time, all compounds were significantly stable. The rate constants (k) were all in the same order of magnitude, and the half-life values ranged from 35 to over 140 days. If these encouraging results are going to be backed up by the cytotoxicity results, these compounds should be evaluated for further biological applications as potential theranostic agents for BNCT guided by PET or ¹⁹F-MRI.



Scheme 14 – Kinetic curves for Glc5, Glc6, Glc7, and Glc9

Table 9 – Significant values for Glc5, Glc6, Glc7, and Glc9

| Sample | k | t _½ (h) | t _½ (days) |
|--------|----------------------|--------------------|-----------------------|
| Glc5 | 2 * 10 ⁻⁴ | 3407 | 142 |
| Glc6 | 2 * 10 ⁻⁴ | 3375 | 140 |
| Glc7 | 8 * 10 ⁻⁴ | 843 | 35 |
| Glc9 | 2 * 10 ⁻⁴ | 3415 | 142 |

3. Nanomaterial decorated with borane structures.

This project stems from a collaboration between the University of Milan, the University of Piemonte Orientale, the University of Firenze, and the University of Pavia.

The aim of the project is the synthesis, characterization, and biological evaluation of a functionalized nanomaterial for potential BNCT applications. Our contribution has been the synthesis of a specific borane structure **1** that has been conjugated to the nanomaterial.

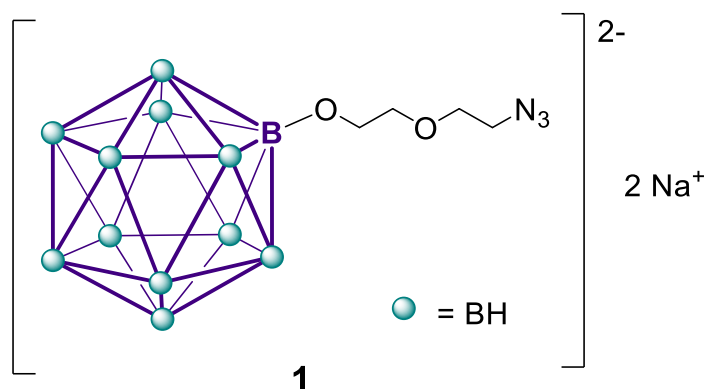
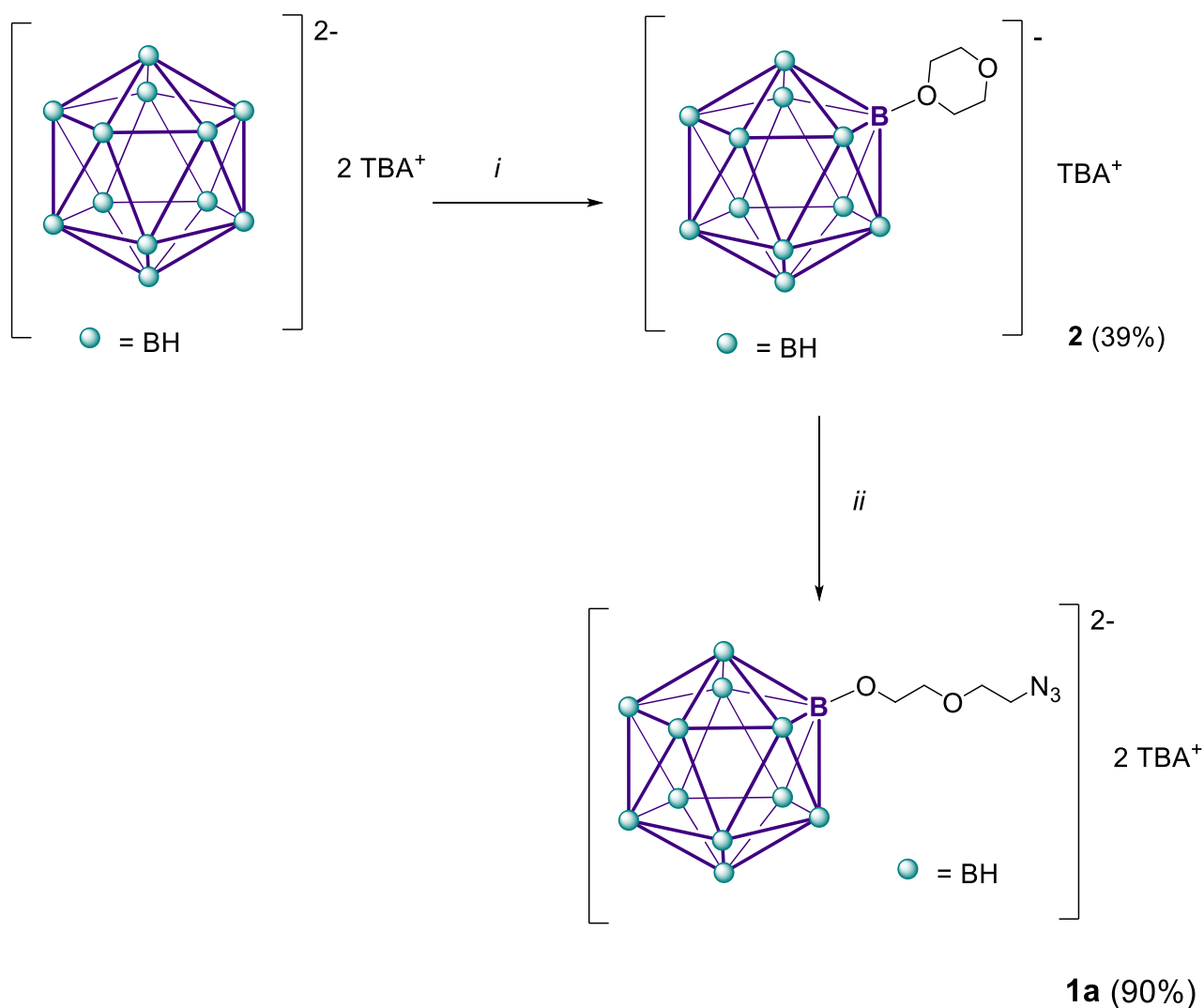


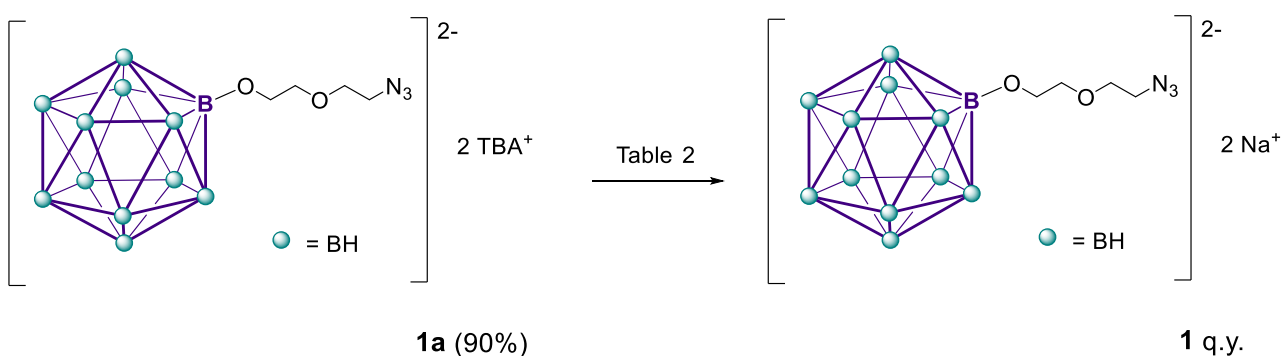
Figure 1 – Borane structure 1

The borane structure **1a** was synthesized as shown in **Scheme 1** following the literature procedures. Starting from the *closo*-dodecaborate ion, as tetrabutylammonium salt, by treatment with a proton source is possible to obtain the high unstable $[B_{12}H_{13}]^-$ ion. This molecule eliminates molecular hydrogen and gives $[B_{12}H_{11}]^-$ that is subjected to the attack of 1,4-dioxane. Compound **2** was obtained in 39% yield without the need of further purification⁶. Compound **2** reacted with freshly prepared tetrabutylammonium azide to give the product as tetrabutylammonium salt **1a**. The reaction lasted 24 hours and gave the product in a satisfying 90% yield¹⁸³.



Scheme 1 – Synthesis of product 1a. i) NaBF_4 , HCl 2M in Et_2O , 1,4-dioxane, r.t. to reflux. ii) $\text{N}_3\text{Bu}_4\text{N}$, dichloromethane, r.t.

The last step of the synthesis consisted of the counter ion exchange between tetrabutylammonium (TBA) and sodium (**Scheme 2**). The former counter ion was not suitable for the subsequent characterization of the nanomaterial. In fact, our colleagues in Firenze evaluate the efficacy of the click reaction through elemental analysis of nitrogen. A counter ion like the tetrabutylammonium would have impaired the results.



Scheme 2 – Counter ion exchange between TBA^+ and Na^+

We tried all the conditions for the counter ion exchange listed in **Table 1**, but none of them worked.

Table 1 – Conditions used for the counter ion exchange. Method A consists in stirring a solution of **1a** with the proper resin or salt. Method B consists in pouring a solution of **1a** over a column packed with the resin. (*) Sodium resin freshly activated with NaOH.

| Trial | Reagent | Solvent | Method | Result |
|-------|--|-----------------------------|--------|--------|
| 1 | Amberlite Na ⁺ | CHCl ₃ | A | None |
| 2 | Amberlite Na ⁺ | MeOH: CHCl ₃ 1:1 | A | None |
| 3 | CsF | MeOH | A | None |
| 4 | CaCO ₃ and Amberlite H ⁺ | MeOH | A | None |
| 5 | Amberlite Na ⁺ (*) | MeOH | B | None |

From the ¹H-NMR spectra was easy to determine the presence of the TBA⁺ ion after each trial.

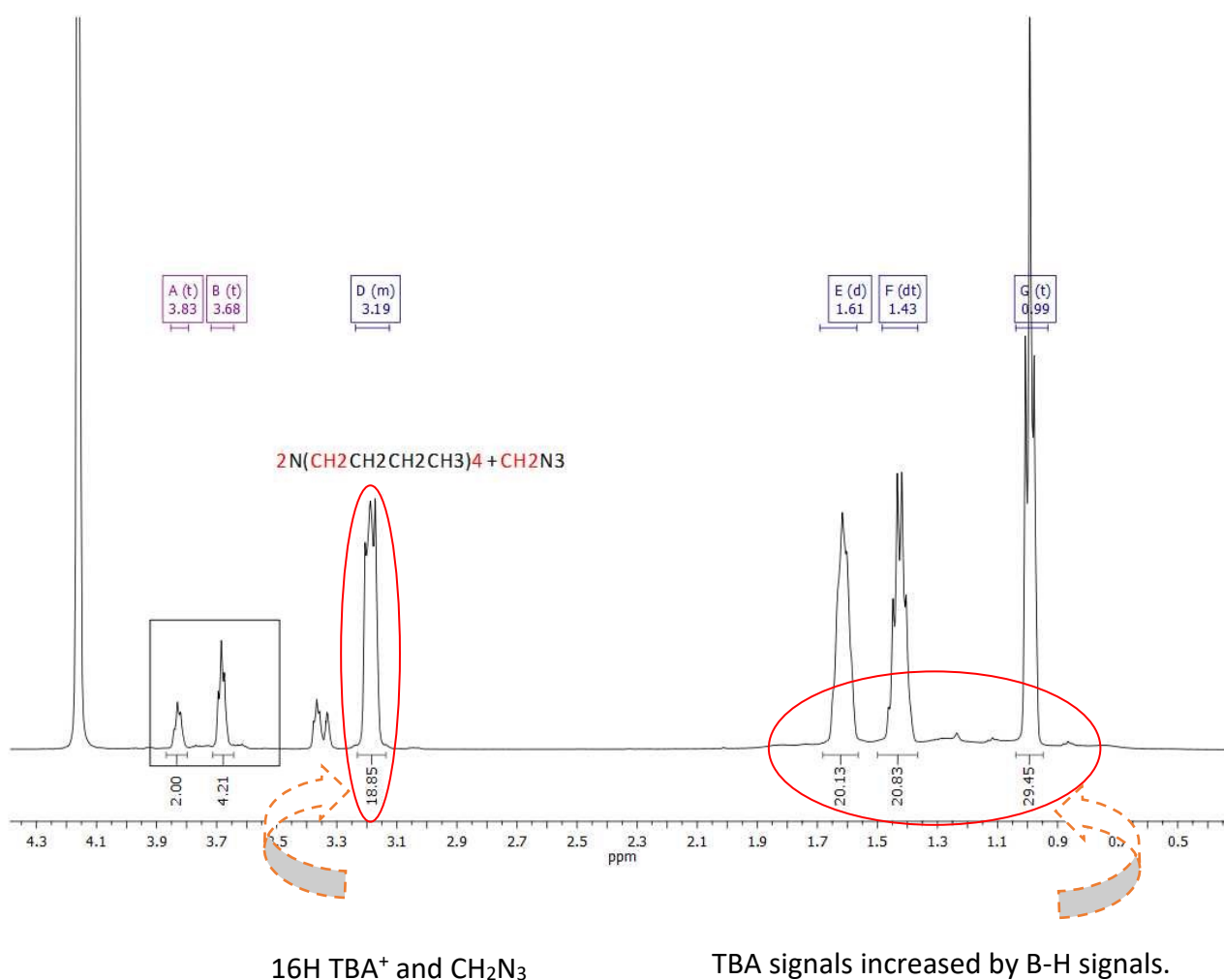


Figure 3 – ¹H-NMR recorded in CD₃OD.

After further research in the literature¹⁸⁴, we found a promising method involving the sodium tetraphenyl borate salt (BPh₄Na). In this case the exchange was made in a heterogeneous system, product **1** as TBA salt was dissolved in dichloromethane, while the sodium tetraphenyl borate was dissolved in water. The two solutions were mixed and vigorously stirred for 3 hours. Over time, the aqueous solution became less clear, then the two phases were divided. The water phase containing the product as sodium salt was concentrated to dryness under reduced pressure. **Table 2** resumes all the attempts made using this procedure and the results obtained.

*Table 2 – Experimental conditions used for the cation exchange between compound **1a** and BPh₄Na.*

| Trials | Equivalents of BPh ₄ Na | [BPh ₄ Na] (g/L) | Results |
|----------|------------------------------------|-----------------------------|--|
| 1 | 2 | 13 | Product + traces of BPh ₄ Na and BPh ₄ TBA |
| 2 | 2 | 5 | Product + lower quantities of BPh ₄ Na and BPh ₄ TBA |
| 3 | 1.92 | 5 | Product + traces of BPh ₄ TBA* |

*The last traces of BPh₄TBA were successfully removed through extraction with dichloromethane

Analyzing the ¹H-NMR spectra it was possible to track the progress made. It can be observed that the signals above 7 ppm corresponding to the aromatic rings are progressively less present, as well as the diagnostic signal of the TBA at 3.2 ppm. Moreover, the ratio between these two sets of signals allowed us to roughly estimate the presence of residual traces of BPh₄Na. If the aromatic part exceeded the quantity of TBA present, there was some BPh₄Na left.

1° Trial

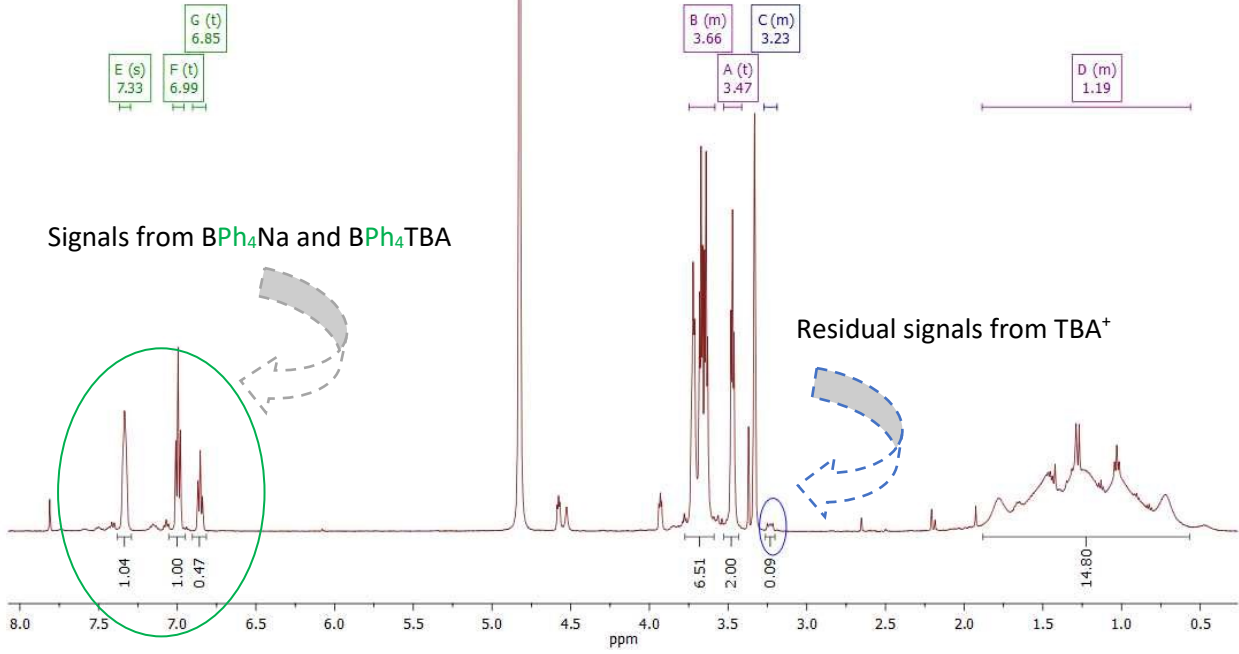


Figure 3 – 1H -NMR recorded in $500\mu L$ of CD_3OD + $100\mu L$ CD_3Cl .

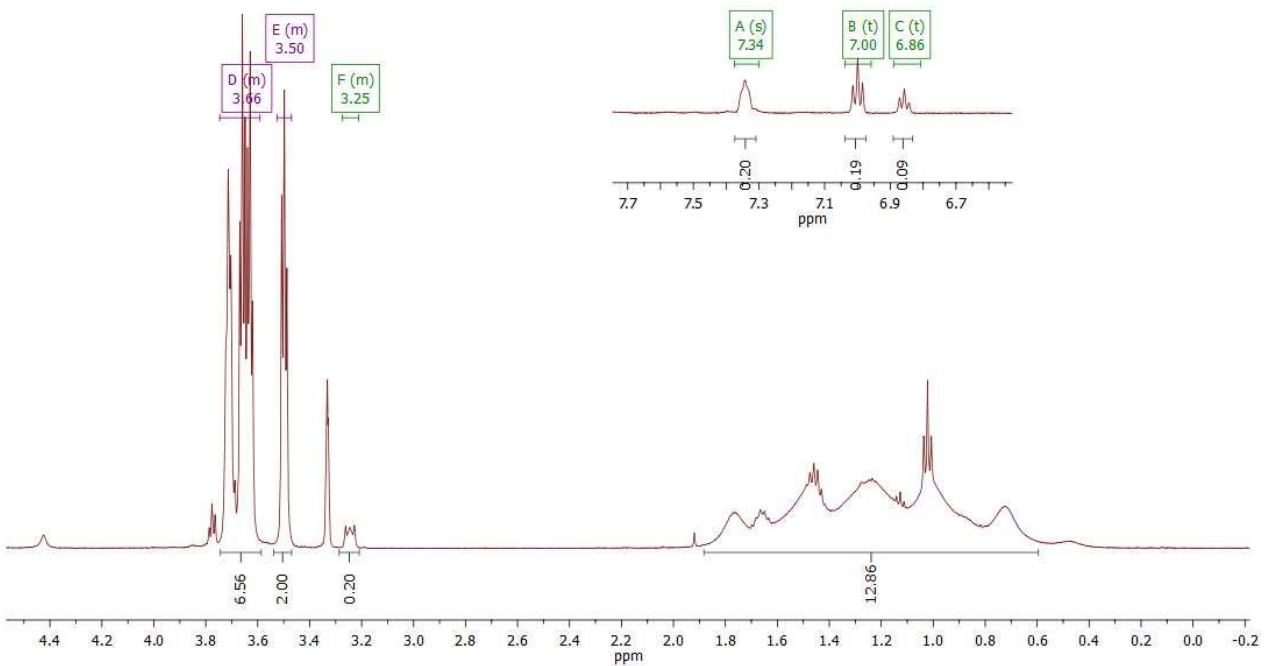


Figure 4 - 1H -NMR recorded in $500\mu L$ of CD_3OD + $100\mu L$ CD_3Cl .

3° Trial – After extraction with dichloromethane

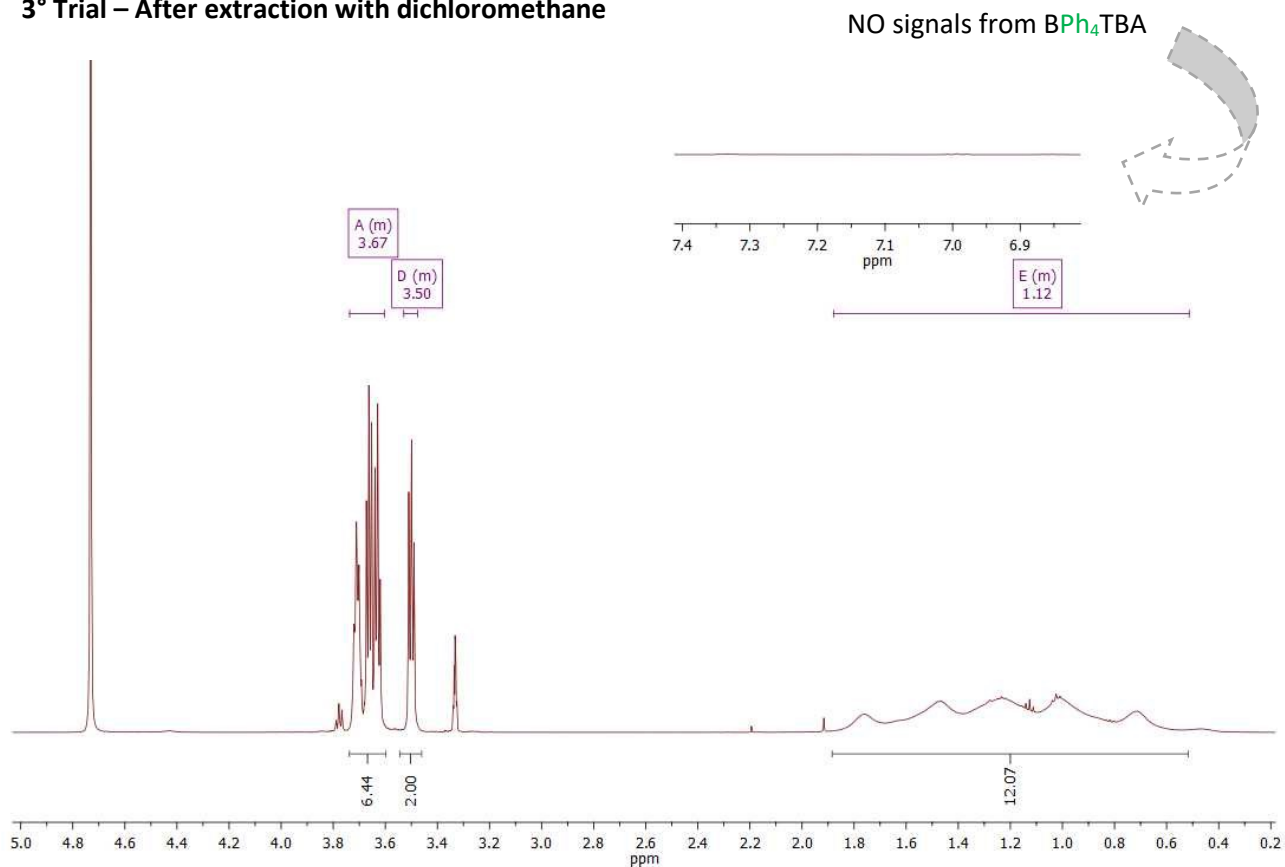


Figure 5 - ¹H-NMR recorded in 500μL of CD₃OD + 100μL CD₃Cl.

Eventually, we obtained 75 mg of compound **1** as sodium salt. It was sent to our colleagues in Firenze for the conjugation with the nanomaterial and further biological tests.

4. Carborane-containing drug analogs.

During my stay at the University of Leipzig, I took part in a broad project ongoing in Professor Hey-Hawkins' laboratories about the synthesis of carborane-containing drug analogs. As described in the **Introduction - section 1.4**, carboranes can replace part of the organic molecules used as drugs to improve some pharmacological aspects¹⁸⁵.

In this case, the project focused on the synthesis of two carborane-containing molecules having a structure like Diclofenac or Naproxen (**Figure 1**), two well-known non-steroidal anti-inflammatory drugs (NSAIDs). These kinds of medications are non-selective inhibitors of both cyclooxygenase (COX) isozymes. Since the active site of COX-2 is slightly larger than that of COX-1 – approximately 25% larger – a size-extension of classical NSAIDs can lead to inhibitors with COX-2 selectivity¹⁹.

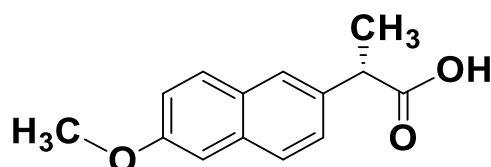


Figure 1 – Naproxen structure

I took care of the synthesis of the Naproxen analog, starting from a bis-carborane (bis-mCb) already present in the Hey-Hawkins' laboratory. The molecule consists of two meta-carborane joined together through a C-C bond (**Figure 2A**). This bond disposition leaves two C-H positions, with identical reactivity, free and twenty B-H groups. We wanted to use the bis-carborane as backbone for the analog and attached the methoxy and carboxylic group as substituents. The two substituents and the two types of atoms present in the carborane structure – boron or carbon – give rise to four different regioisomers listed in **Figure 2B**. Isomers **A** and **B** have both the substituents linked to the same kind of atom, both carbon or boron. Instead, in isomers **C** and **D** the substituents are joined to different atoms.

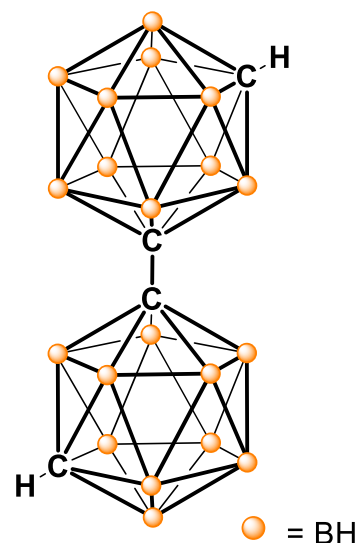


Figure 2A - bis-meta-carborane structure (bis-mCb)

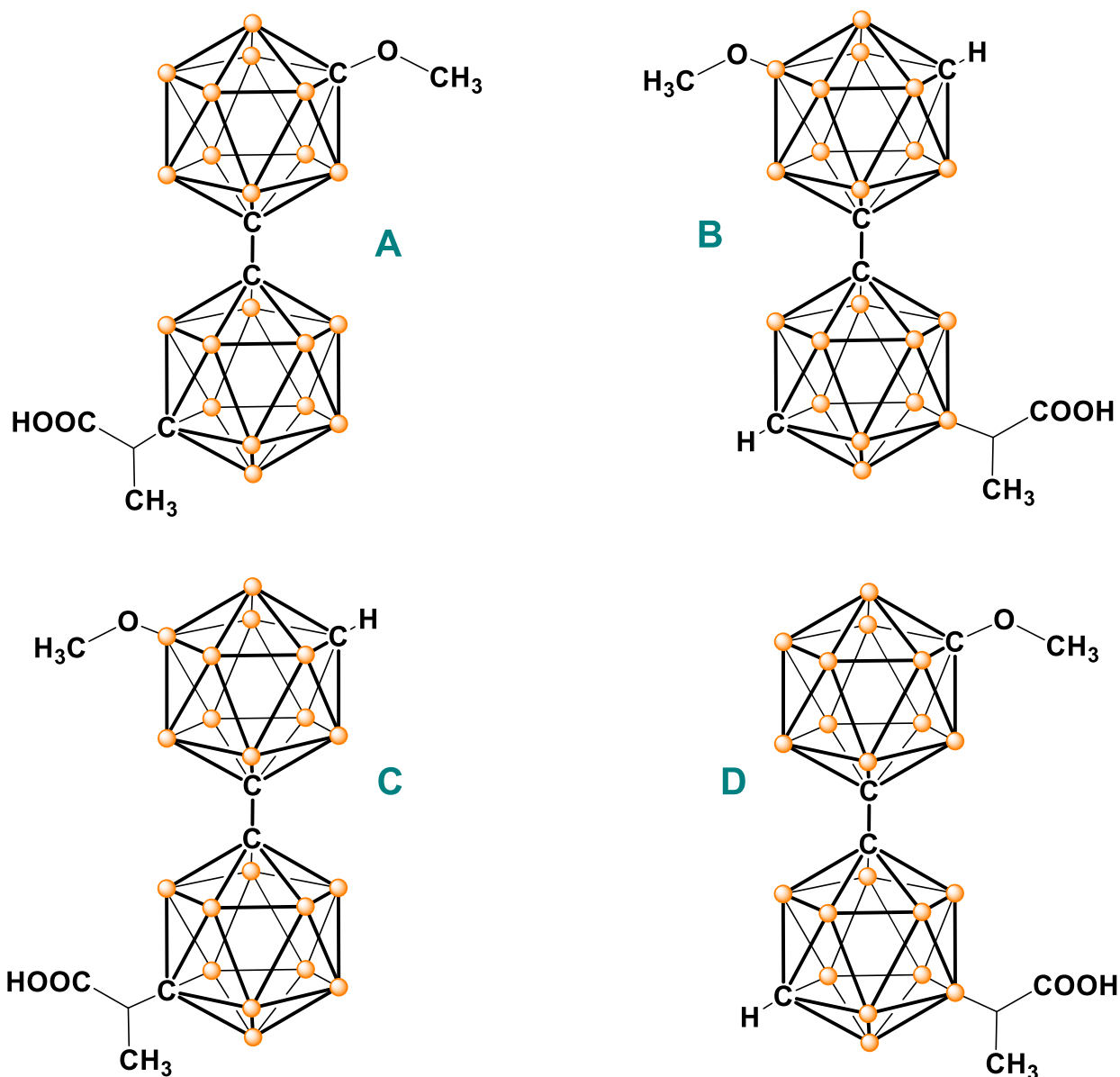
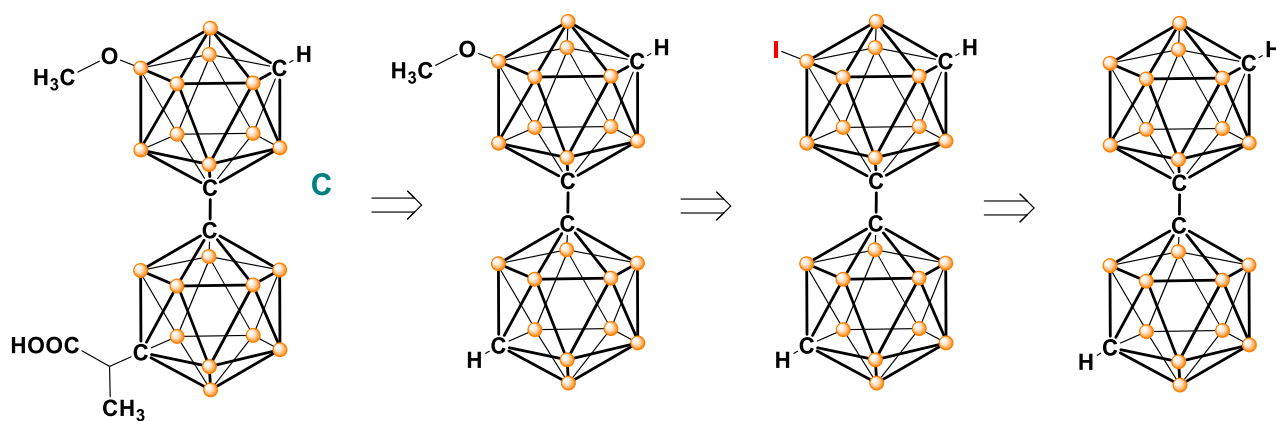


Figure 2B – The four possible regioisomers for our target molecule. Isomers **A** and **B** have both the substituents linked to the same kind of atom, both carbon or boron. Instead, in isomers **C** and **D** the substituents are joined to different atoms.

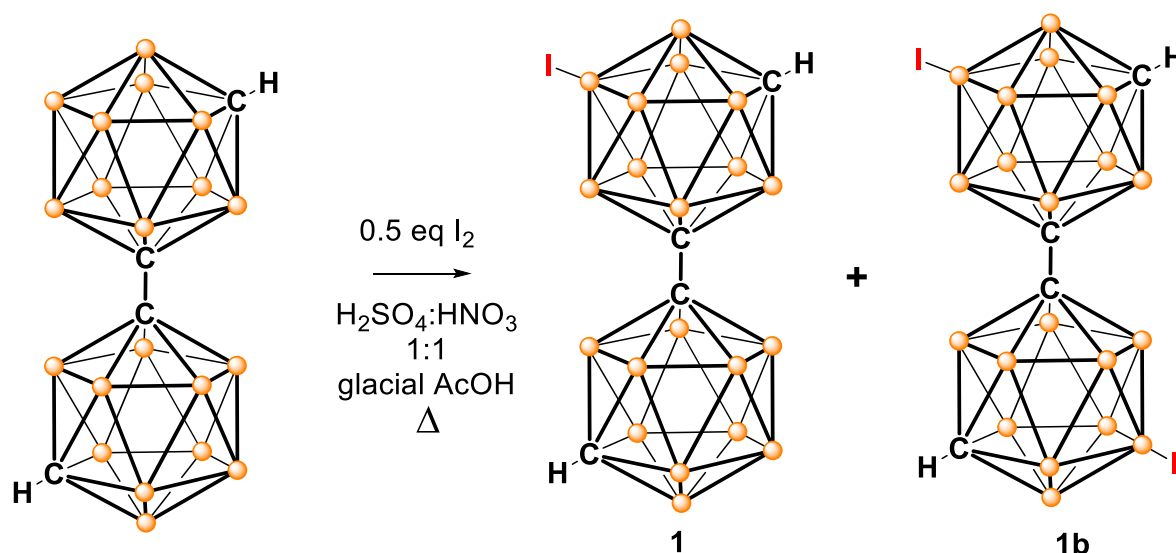
Among the four regioisomers we decided to start with **C**, the one that has the methoxy group attached to a boron atom and the carboxylic group to a carbon atom. We thought of the retrosynthetic **Scheme 1**. First, the methoxy group would have been introduced through a palladium mediated cross-coupling reaction between the bis-mCb iodine derivative and sodium methoxide. Then, the carboxylic group would have been linked to the C-metallated derivative.



Scheme 1 – Retrosynthetic approach to compound **C**.

The first step consisted in the synthesis of the mono iodinate derivative **1**, which required a careful optimization to avoid the formation of the bis iodinate derivative **1b** (**Scheme 2**).

The course of the electrophilic halogenation on a simple m-carborane is dictated by charge distribution in the carborane framework. The halogen substitution occurs preferentially at the most electronegative BH vertexes, which in m-carborane are B(9,10) (the only borons not adjacent to carbon) followed by B(4,6,8,11) and then B(5,12). When conducted under less than forcing conditions, halogenation of m-carborane does not usually proceed beyond B(9,10) substitution, which parallels the action of o-carborane in that only those boron atoms not adjacent to carbon [B(8,9,10,12)] are attacked⁷.



On a bis-mCb structure, there are four boron atoms susceptible to halogenations; B(9,10) on each cage. The reaction can be facilitated by aluminum (III) or iron (III) salts or protonic acid.

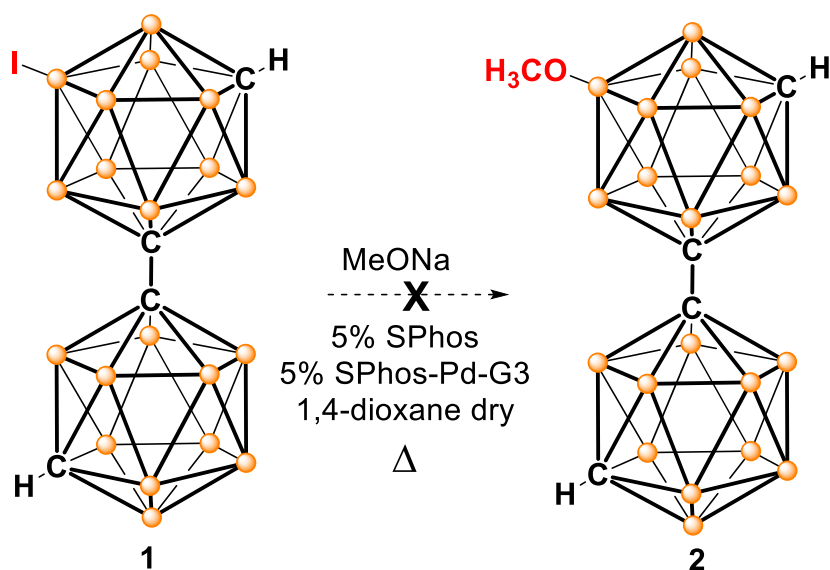
Table 1 shows the reaction conditions tried for optimizing the electrophilic halogenation. The reactions were performed using 0.5 eq of Iodine (I_2) respect to the bis-mCb, and glacial acetic acid

as solvent¹⁸⁶. Heating the reaction mixture from the beginning and for a brief period of time resulted the best way to promote the product formation and minimized the byproduct. Compounds **1**, **1b**, and the unreacted starting material were easily separated by silica gel chromatography.

Table 1 – Reaction conditions for the electrophilic halogenation. a) Amount of acid mixture (H₂SO₄:HNO₃ 1:1) express in mL for mg of bis-mCb. b) Yields were calculated after purification on column chromatography.

| Trials | T (°C) | Amount of acid ^a | Time (h) | Unreacted starting material | Byproduct (1b) | Yield ^b |
|----------|-----------|-----------------------------|----------|-----------------------------|----------------|--------------------|
| 1 | r.t. → 60 | 0.01 (mL/mg) | 6 | 45% | 7% | 25% |
| 2 | 60 → 80 | 0.01 (mL/mg) | 3 | 37% | 17% | 44% |
| 3 | 60 → 80 | 0.02 (mL/mg) | 1.5 | n.d. | 30% | 54% |
| 4 | 60 → 80 | 0.01 (mL/mg) | 2 | 18% | 19% | 46% |

The second step of the synthesis consisted in the formation of the B-O bond *via* Palladium-Catalyzed Cross-Coupling (**Scheme 3a**). Starting from a literature procedure¹⁸⁷, we tried different combination of temperatures, sodium methoxide equivalents, and reaction times. Unfortunately, too harsh conditions lead to the cage degradation, while blander combinations just afforded unreacted starting material or de-iodinated product (**Table 2**).

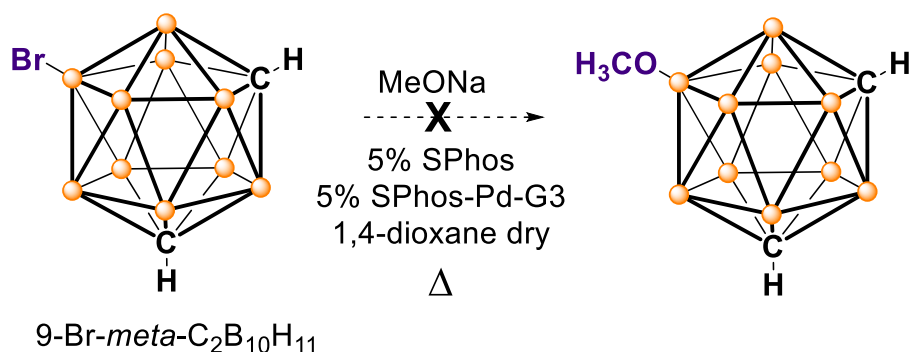


Scheme 3a – Formation of the B-O bond through a Palladium-catalyzed cross-coupling reaction.

Table 2 – Reaction conditions for the Palladium catalyzed cross-coupling reaction.

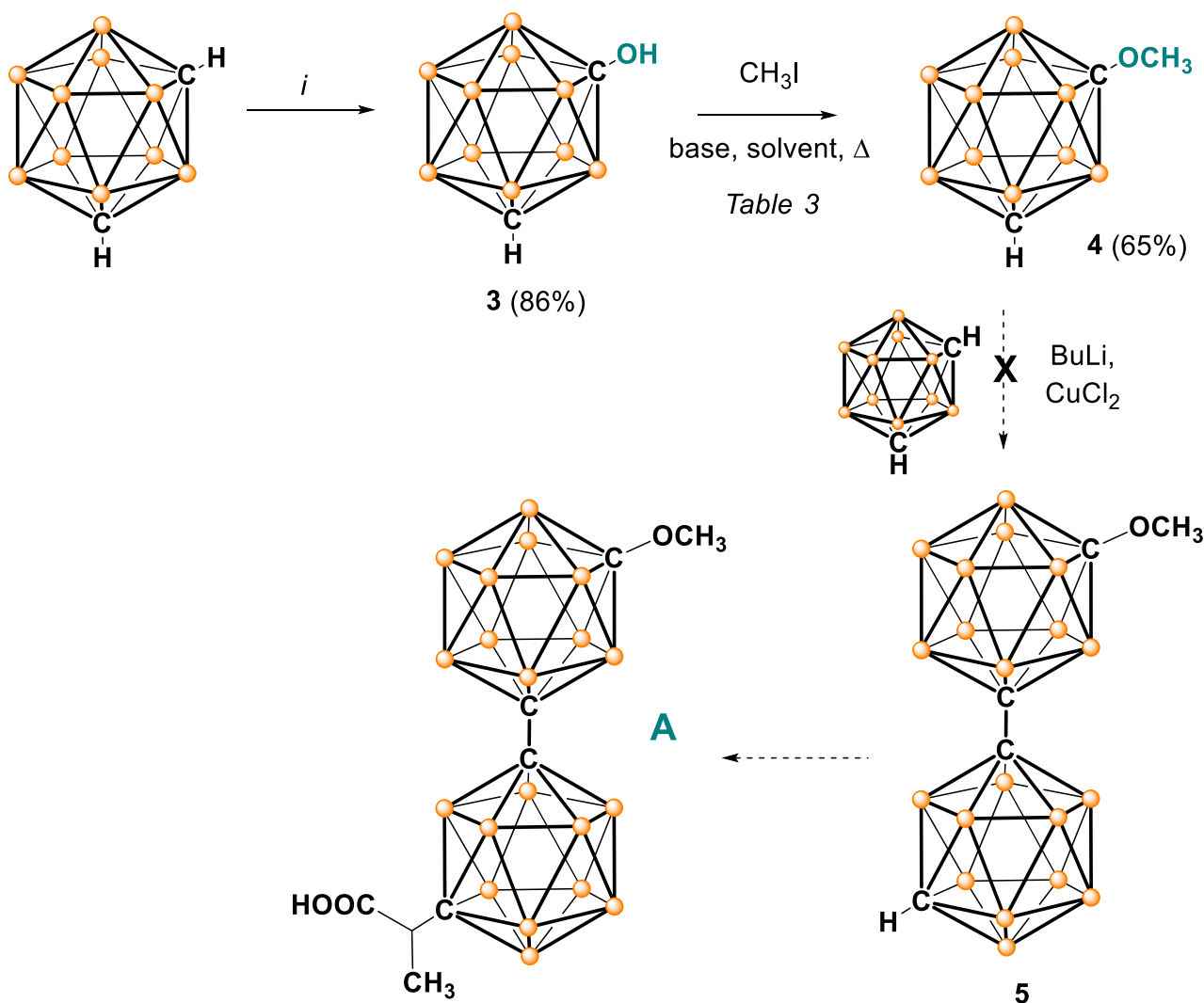
| Trials | Solid NaOCH ₃ (eq) | T (°C) | Time (h) | Results |
|--------|-------------------------------|-----------|----------------|--|
| 1 | 8 | 70 | 1 | cage degradation |
| 2 | 4 | r.t. | 1 | only starting material |
| 3 | 4 | r.t. → 50 | overnight + 3h | starting material + de-iodinated product |
| 4 | 4 | r.t. → 70 | 3h | starting material + de-iodinated product |

To better understand the reaction, we tried the condition of the first trial on the 9-Br-*meta*-C₂B₁₀H₁₁ described in the article (**Scheme 3b**). Also in this case, the reaction didn't work. A possible explanation could have been the difficulties encountered in obtaining a reproducible solid sodium methoxide.



Scheme 3b – Palladium-catalyzed cross-coupling reaction on 9-Br-*meta*-C₂B₁₀H₁₁

At this point, we choose to change our target compound and moved on with the synthesis of the regioisomers **A**, which has both substituents linked to the C atoms (**Figure 2B**). **Scheme 4** shows our first approach to the synthesis of **A**. We decided to start from the commercially available *meta*-carborane, adding the methoxy group to one carbon, and then create the bis-mCb structure. Compound **3** was synthesized with a satisfying yield following a literature procedure with a slight variation¹⁸⁸. In the described procedure, the authors employed H₂O₂ and an acidic additive to promote the oxidative rearrangement of the intermediate carboranyl boron ester. The additive is considered to activate H₂O₂ by forming the peracetic acid *in situ*¹⁸⁹. Our variation consisted in using directly the peracetic acid, avoiding the unstable H₂O₂. Then, compound **3** was converted into compound **4**, but the reaction condition required some adjustment. **Table 3** summarized all the conditions tried, starting from the ones described in the literature¹⁹⁰.



Scheme 4 – First synthetic approach to the synthesis of compound A. i) *n*BuLi 1.6M in Hexane, Et₂O dry, 0°C to r.t.; B(OMe)₃, -30°C to r.t.; CH₃COOH 35% w/w, 0°C to r.t.; NaOH 10%, NaHSO₄

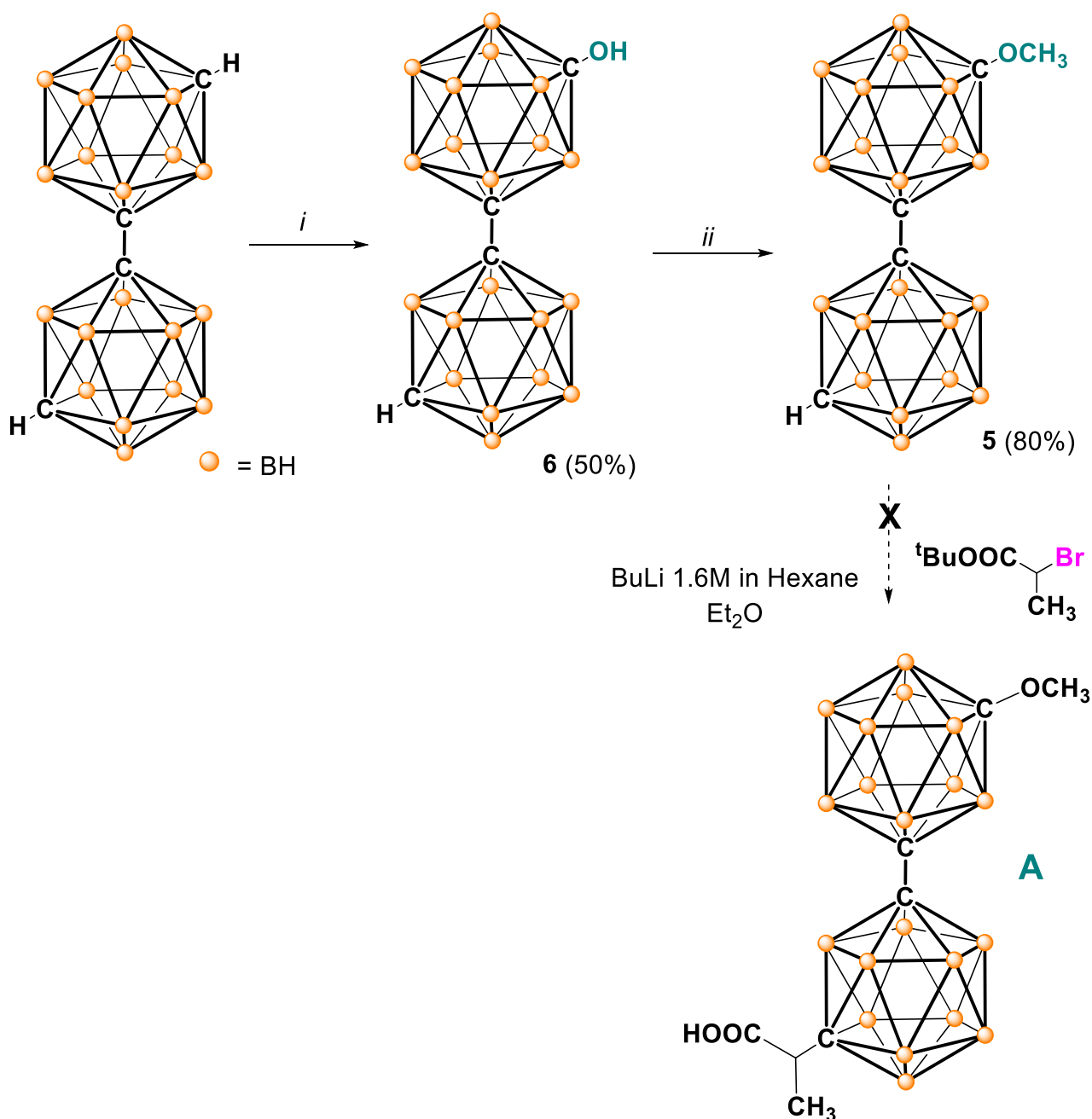
Table 3 – Reaction conditions used for the synthesis of compound 4. The first trial was carried out with the parameters described in the literature, but they were too harsh. Milder conditions gave better results.

| Trial | Base | Solvent | Temperature | t (h) | Yield product 4 |
|-------|--------------------------------|---------|-------------|-----------|----------------------------|
| 1 | NaH (60%) | DME | reflux | 1 | 35% + degradation products |
| 2 | K ₂ CO ₃ | DMF | r.t. | 1 | only traces |
| 3 | K ₂ CO ₃ | DME | r.t. | overnight | 65% |

The optimal conditions were a weaker base, potassium carbonate instead of sodium hydride, and a longer reaction time at lower temperature. Then, we approached the synthesis of the asymmetrical bis-mCb structure **5**. In the literature, there are few articles about this kind of synthesis, and the reaction is usually performed on unfunctionalized carboranes^{191,192}. The coupling takes place on the mono lithiated m-carborane, and it is mediated by copper (II) chloride. In our case, the possibility of having more than one product due to homocoupling reactions was

far than remote. Indeed, the reaction yielded a rather complex mixture of products and unreacted materials difficult to separate.

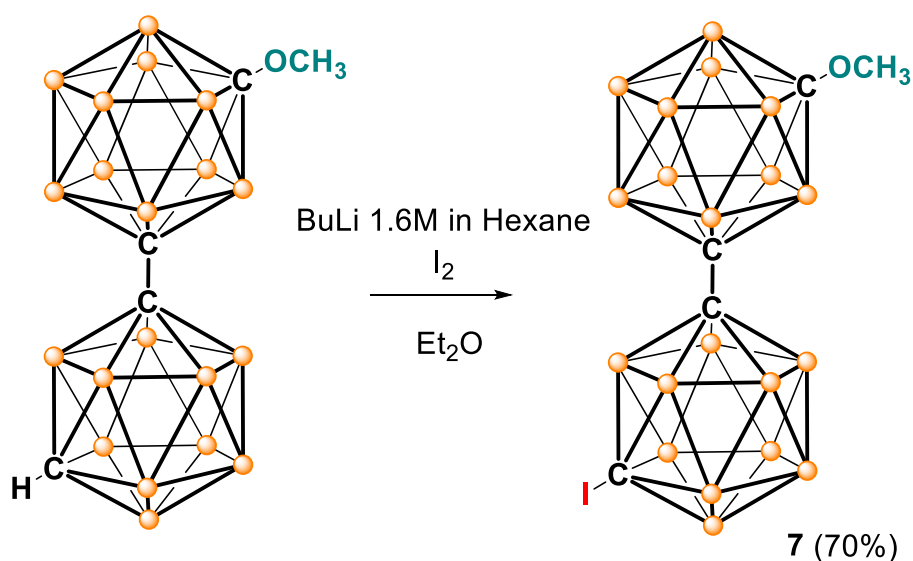
Since the first approach did not work, we thought to a new synthetic route shown in **Scheme 5**. We applied what we have learnt on the mCb to the bis-mCb cage. The first two steps went quite smoothly, and we were able to obtain compound **5** in a quite satisfying yield.



Scheme 5 – Second synthetic approach to the synthesis of compound A. i) *n*BuLi 1.6M in Hexane, 0°C to r.t.; B(OMe)₃, -30°C to r.t.; CH₃COOOH 35% w/w, 0°C to r.t.; NaOH 10%, NaHSO₄. ii) CH₃I, K₂CO₃, DME, r.t.

Then, we focused on the last step for the synthesis of the target compound **A**, the formation of the C-metallated intermediate and the following reaction with the acid 2-bromo-propanoic protected as terz-butanoic ester. We performed this reaction several times changing the conditions, but we only obtained starting material.

To better understand the formation of the C-metallated intermediate, we performed the reaction shown in **scheme 6**. The reaction worked well, confirming that the problem in our approach regarded the propanoic derivative.



Scheme 6 – Iodination reaction on the C-metallated intermediate. This reaction was performed to better understand the mechanism of the first reaction step.

A possible explanation for the difficulties encountered in this reaction step could have been the presence of an acidic proton in the protected propanoic acid that impaired the reaction result. Unfortunately, due to the end of my stay at the University of Leipzig, I was not able to complete the last step of the synthesis.

D. LIST OF PUBLICATIONS

- (1) Laura Confalonieri, Daniela Imperio, Alvaro Erhard, Silvia Fallarini, Federica Compostella, Erika Del Grosso, Marcin Balcerzyk, Luigi Panza
Organotrifluoroborate Sugar Conjugates for a Guided Boron Neutron Capture Therapy: from Synthesis to Positron Emission Tomography
ACS Omega, 51, **2022**, 48340,
<https://doi.org/10.1021/acsomega.2c06551>
- (2) Barbara Muz, Abdel Kareem Azab, Laura Confalonieri, Erika Del Grosso, Silvia Fallarini, Daniela Imperio, Luigi Panza
Synthesis, equilibrium, and biological study of a C-7 glucose boronic acid derivative as a potential candidate for boron neutron capture therapy
Bioorganic & Medicinal Chemistry, 59, **2022**, 116659,
<https://doi.org/10.1016/j.bmc.2022.116659>.
- (3) Laura Morelli, Laura Legnani, Silvia Ronchi, Laura Confalonieri, Daniela Imperio, Lucio Toma, Federica Compostella.
2,3-Carbamate mannosamine glycosyl donors in glycosylation reactions of diacetone-d-glucose. An experimental and theoretical study
Carbohydrate Research, 509, **2021**, 108421,
<https://doi.org/10.1016/j.carres.2021.108421>

E. EXPERIMENTAL DETAILS

1. Organotrifluoroborate Sugar Conjugates – part I

1.1 Chemistry

1.1.1 General

The products of the glycosylation reactions **1**¹⁷⁴, **1a**^{193,194}, and **1b**¹⁹⁴ were synthesized as reported in the literature. As well as the corresponding azido derivatives **4**¹⁷⁴, **4a**¹⁹⁴, and **4b**¹⁹⁴, and the alkyne **5**¹⁶⁸ synthesized by Perrin and coworkers.

All reagents and solvents were purchased from Sigma-Aldrich (Milan) and used as supplied without further purification unless otherwise stated. Thin-layer chromatography was performed on silica gel plates with a fluorescent indicator (Merck, Milan) and visualized at the UV light (254 nm) and/or by staining in ceric ammonium molybdate or sulfuric acid solution (5% in methanol). Anhydrous solvents were obtained using activated molecular sieves (0.3 or 0.4 nm based on the type of solvent).

All reactions (if not specifically containing water as reactant, solvent, or co-solvent) were performed under a nitrogen atmosphere. Flash column chromatography was performed with 230–400 mesh silica gel (Merck, Milan).

NMR spectra were recorded using a Bruker Avance Neo 400 MHz spectrometer (Bruker, Italy). Singlets are presented as parts per million (ppm), and the resonance multiplicities are identified as “s” (singlet), “d” (doublet), “t” (triplet), “q” (quartet), or “m” (multiplet). Broad resonances are indicated as “br”. ¹³C, ¹¹B, and ¹⁹F experiments were recorded with proton NMR decoupling. The carbon atoms bound to boron are usually not detectable.

The ¹¹B-¹⁹F coupling constant varies remarkably with the concentration, the ligands bound to the boron nuclei, the symmetry of the molecule, and the type of solvent. It can be well appreciated in small and symmetric molecules, while it is negligible in larger compounds^{195,196}.

¹¹B nuclear spin is 3/2, so, if the coupling constant is visible, the ¹⁹F spectra show one resonance signal with four peaks. Instead, ¹⁹F nuclear spin is 1/2, so the ¹¹B spectra show one resonance signal with four peaks due to the presence of three fluorine atoms¹⁹⁹.

Mass spectrometry analysis was recorded on a Thermo Scientific Q-Exactive Plus; data were acquired and processed using Xcalibur® software. Optical rotations were measured on a JASCO P1010 polarimeter at 20 °C. Infrared Spectroscopy was performed using a Bruker Alpha II FTIR.

1.1.1 Abbreviations

DCM = Dicloromethane

H = Hexane

EA = Etyl Acetate

TEA = Triethylamine

cHex = Ciclohexane

1.1.2 General Procedures

General procedure A: Nucleophilic substitution with morpholine, piperidine, or dibutylamine to obtain compounds **2**.

The amine of choice (from 3 to 8 eq.) was added dropwise to a solution of **1** (1 eq.) in dry acetonitrile (0.1 M). The reaction was heated at 82°C until the disappearance of starting material in TLC. The solvent was then removed under reduced pressure. The crude was dissolved in 30 mL of DCM and washed with NaHCO₃ aq. The aqueous phase was extracted 2 x 20 mL of DCM. The combined organic extracts were washed with 2 x 20 mL of water, and brine, and dried over anhydrous Na₂SO₄. The evaporation of the solvent gave the crude product that was purified through silica gel column chromatography.

General procedure B: Synthesis of the stable trifluoroborate group in compounds **3**.

The iodomethylboronyl pinacolate (2.5 eq.) was added dropwise to a solution of **2** (1eq.) in dry diethyl ether (0.2M). The reaction was allowed to stir at room temperature until the disappearance of the starting material in TLC. Over time, the formation of a sticky precipitate was observed. At the end of the reaction, the supernatant was taken off, and the solid triturated twice with fresh diethyl ether to remove the excess of the reagent. The crude was dissolved in acetonitrile and a solution of KHF₂ (5.0 M, 10 eq.) was added to the reaction. The reaction was stirred at room temperature and monitored with TLC until the disappearance of the starting material. After the reaction ended, the solvent was removed under reduced pressure and the solid was dissolved in 20 mL of CHCl₃ and 20 mL of water. The aqueous phase was extracted five times with 20mL of fresh CHCl₃. The combined organic phases were washed with water, and brine, and dried over anhydrous Na₂SO₄. The evaporation of the solvent gave the crude product that was purified through silica gel column chromatography.

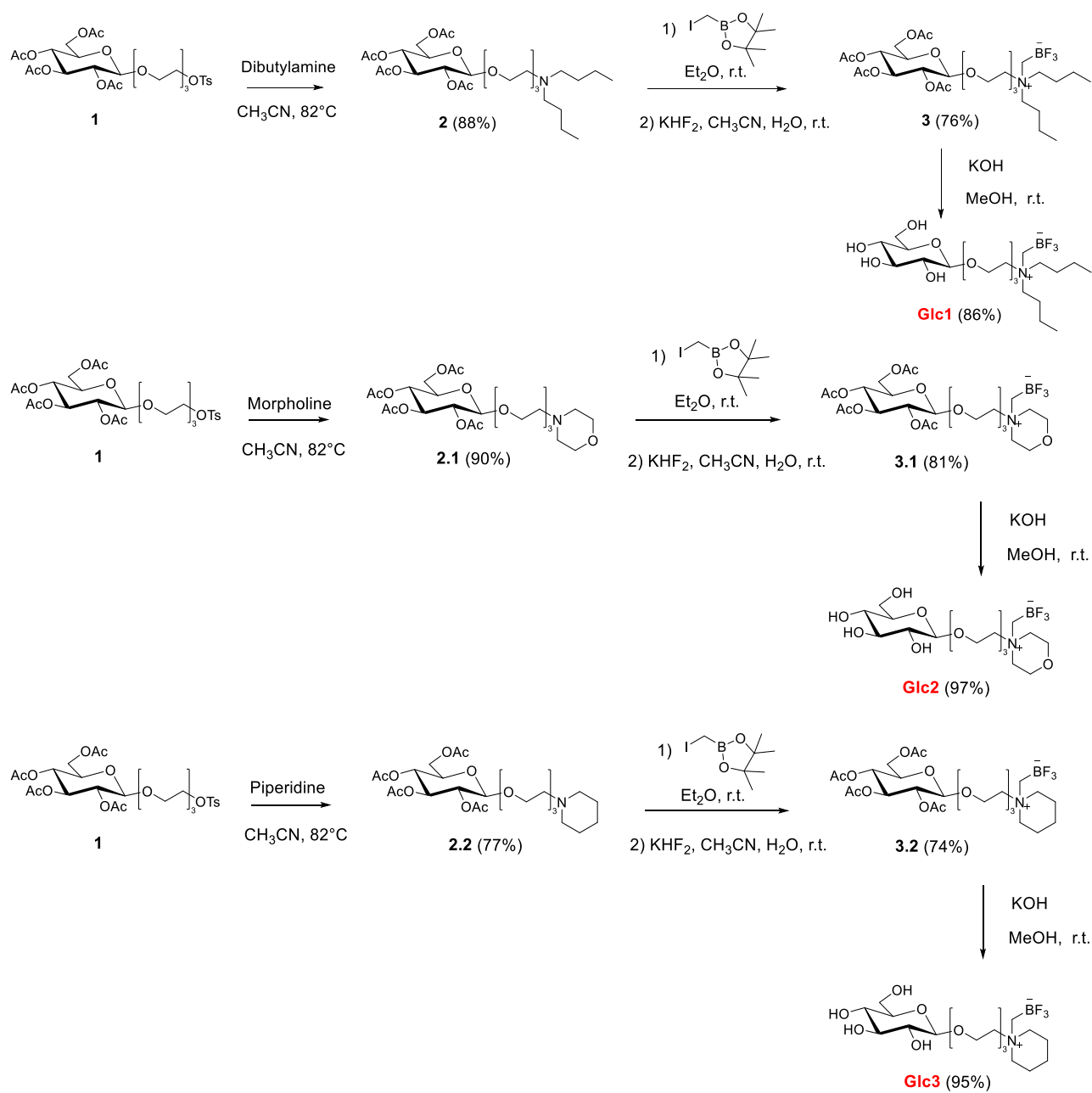
General procedure C: Base catalyzed deprotection to obtain **Glc1-4**, **Gal1-4**, and **Man1-4**.

A solution of potassium hydroxide in methanol (0.27 M, 0.1 eq.) was added to a solution of **3** or **6** (1 eq.) in methanol (0.03M). The reaction was stirred at room temperature for 12h. The solution was then neutralized with Dowex® hydrogen form, filtered, and concentrated.

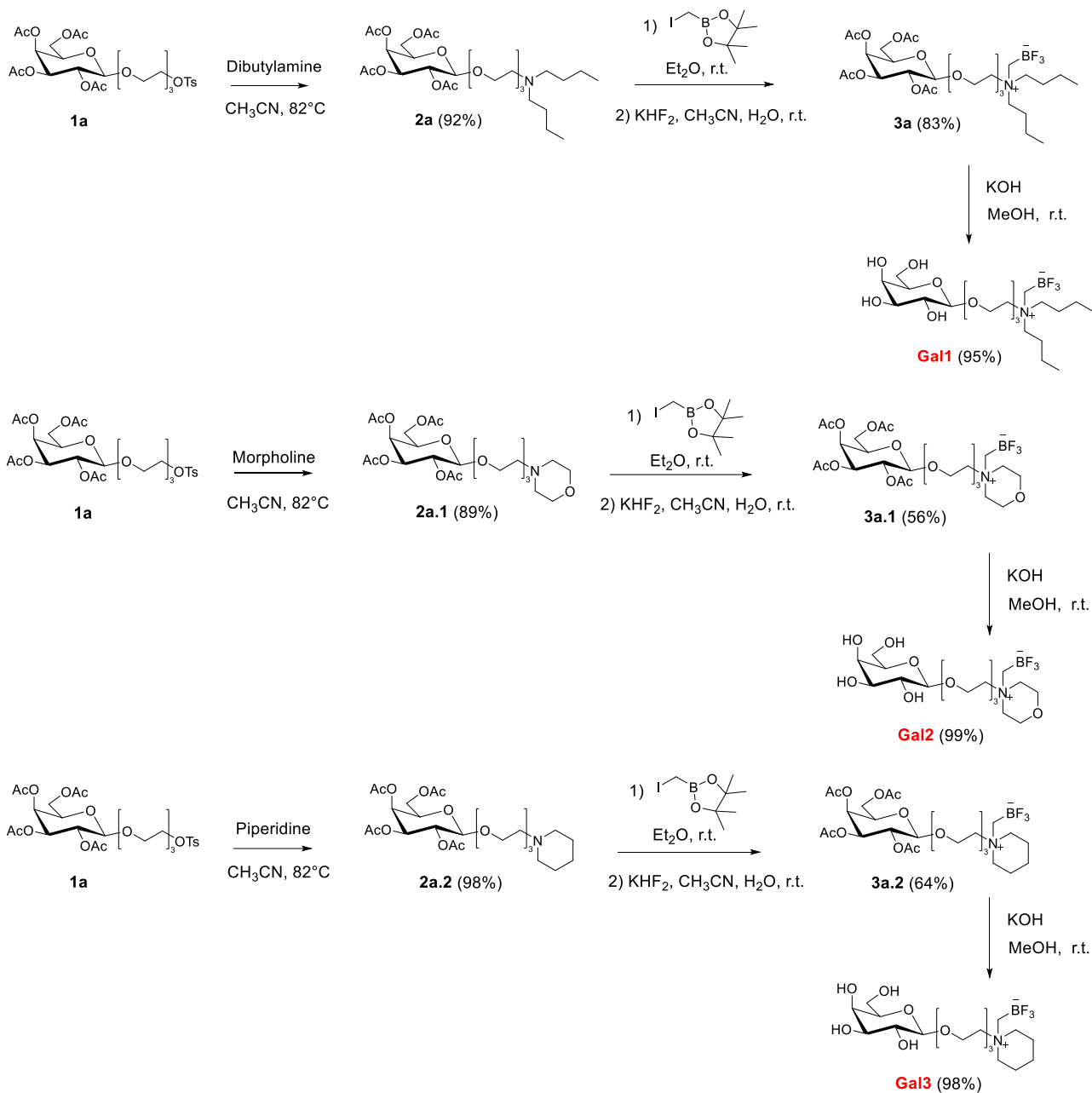
General procedure D: Copper-catalyzed azide-alkyne cycloaddition (CuAAC) to obtain compound **6**.

An aqueous solution of sodium ascorbate (0.6 M, 0.8 eq.) was added to a suspension of **4** (1 eq.) and alkyne **5** (1 eq.) in tert-Butyl alcohol (0.3 M). Then, a solution of copper (II) sulfate pentahydrate (0.3 M, 0.4 eq.) was added under high stirring conditions at room temperature. After the reaction ended, it was diluted with water and the mixture was extracted with CHCl₃. The combined extracts were dried over anhydrous Na₂SO₄ and concentrated to dryness. The crude product was purified through silica gel column chromatography using DCM: MeOH 95:5.

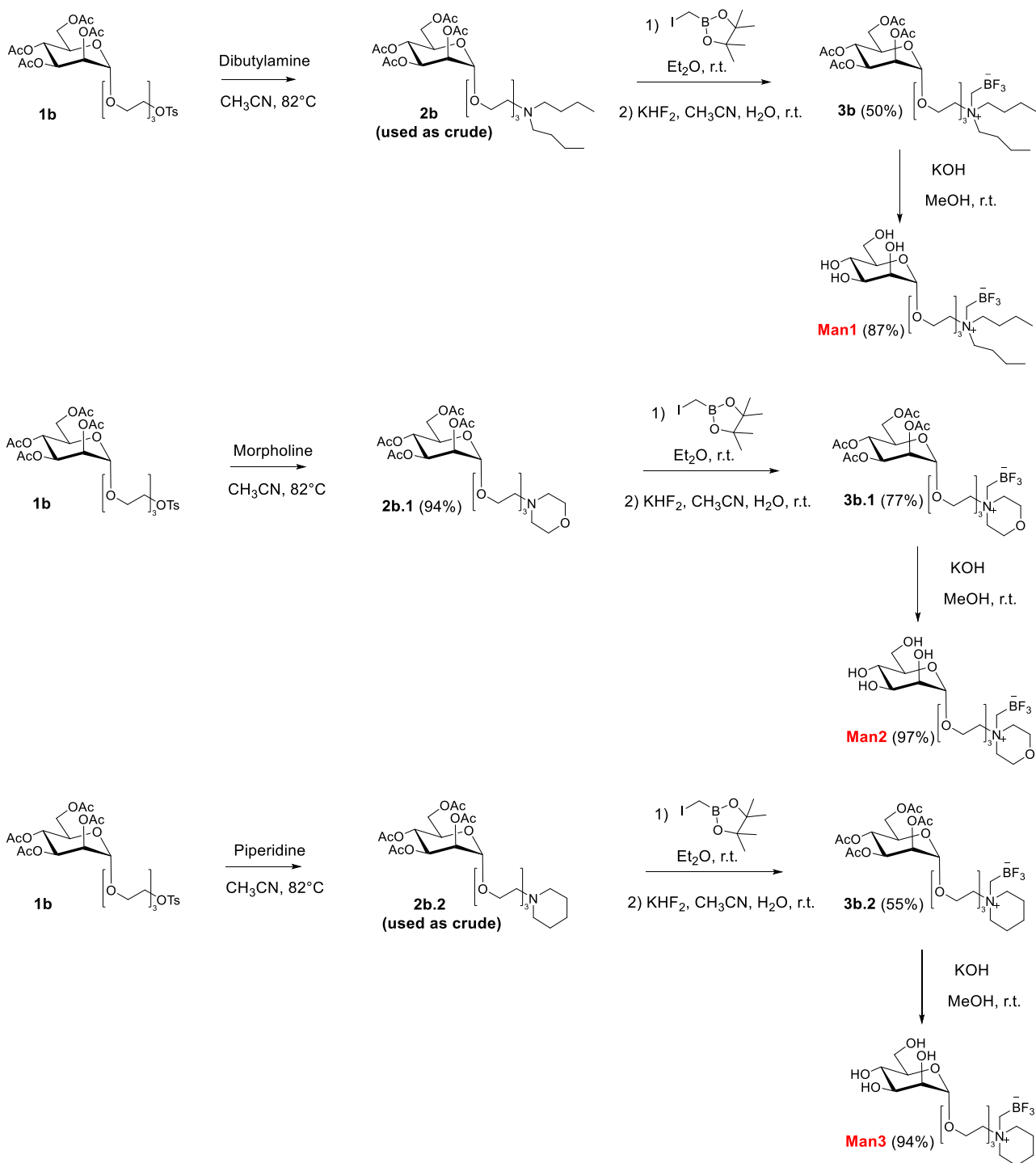
1.1.3 Synthetic Schemes



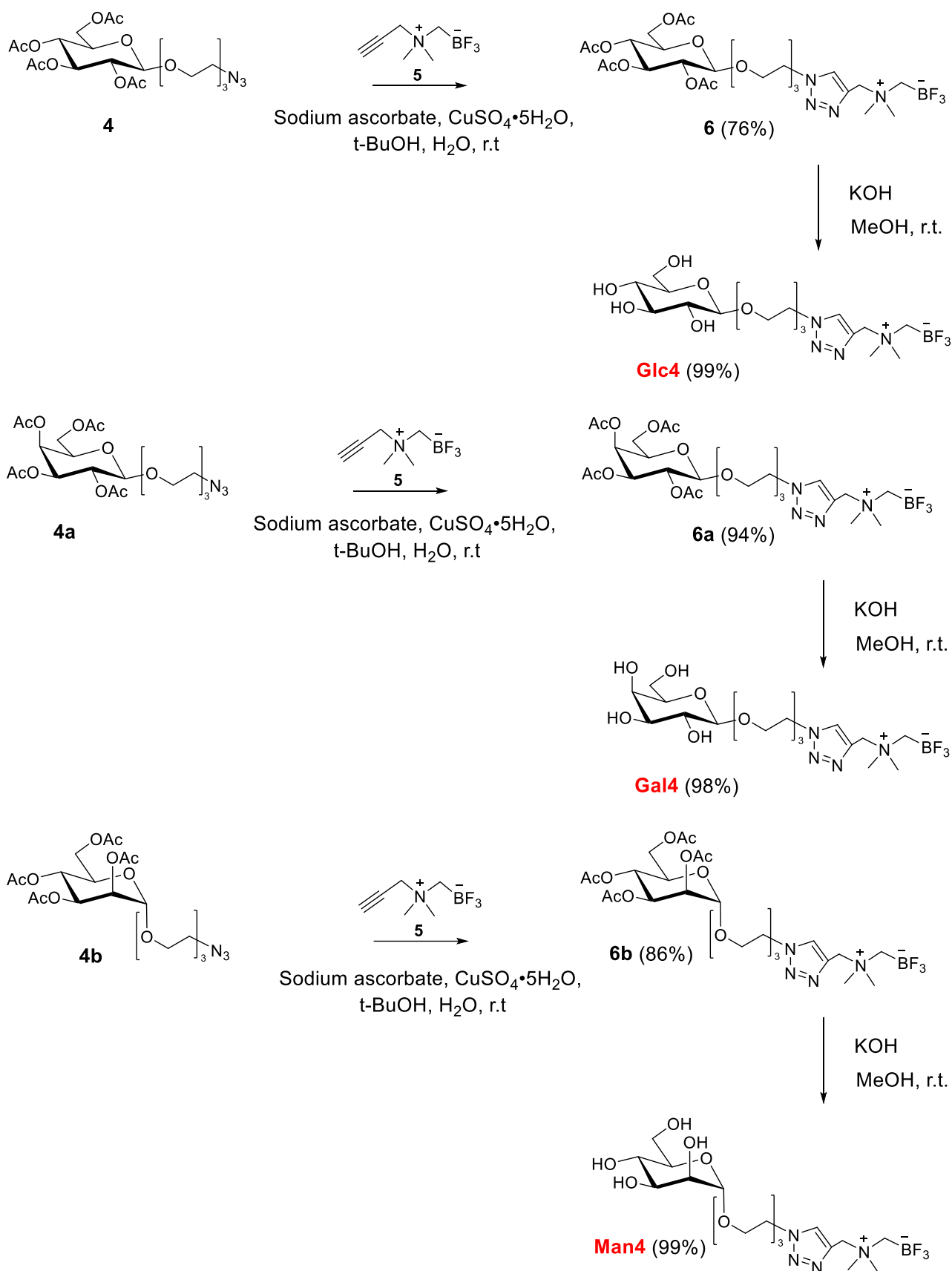
Scheme 1 – Synthesis of Glc1, Glc2, and Glc3 (Substrates named *.1 contain Morpholine, *.2 contain Piperidine)



Scheme 2 – Synthesis of Gal1, Gal2, and Gal3 (Substrates named **a* contain Galactose, **.1* contain Morpholine, **.2* contain Piperidine)



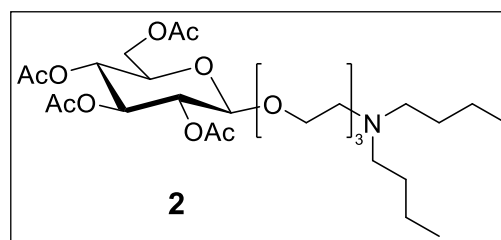
Scheme 3 – Synthesis of Man1, Man2, and Man3 (Substrates named **b* contains Mannose, **.1* contain Morpholine, **.2* contain Piperidine)



Scheme 4 – Synthesis of Glc4, Gal4, and Man4 (Substrates named *a contains Galactose, *b contains Mannose)

1.1.4 Products characterizations

Synthesis of **2**

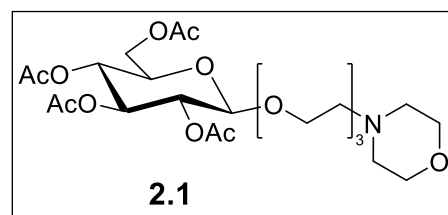


1 (300 mg, 0.47 mmol) reacted with dibutylamine (3 eq.) according to the general procedure **A**. Purification over silica gel (DCM: MeOH from 95:5 to 8:2) gave **2** (R_f product 0.5 in DCM: MeOH 95:5 + 1% TEA) as a yellowish amorphous solid (208 mg, 88%).

$[\alpha]_D^{20}$: -11.6 ($c = 1.0$ g/100 mL, chloroform).

$^1\text{H NMR}$ (400 MHz, CDCl_3) δ 5.20 (t, $J = 9.5$ Hz, 1H, H3), 5.08 (t, $J = 9.7$ Hz, 1H, H4), 4.99 (dd, $J = 9.6, 8.0$ Hz, 1H, H2), 4.60 (d, $J = 8.0$ Hz, 1H, H1), 4.26 (dd, $J = 12.3, 4.7$ Hz, 1H, H6a), 4.14 (dd, $J = 12.3, 2.4$ Hz, 1H, H6b), 3.99 - 3.90 (m, 1H, H1'a linker), 3.78 - 3.56 (m, 10H, H5, H1'b linker, 4CH₂ linker), 2.80 (br s, 2H, 2H6' linker), 2.62 (br s, 4H, 2 NCH₂CH₂CH₂CH₃ dibutylamine), 2.09, 2.04, 2.02, 2.00 (4s, 3H each, CH₃), 1.58 - 1.45 (m, 4H, 2 NCH₂CH₂CH₂CH₃ dibutylamine), 1.38 - 1.24 (m, 4H, 2 NCH₂CH₂CH₂CH₃ dibutylamine), 0.92 (t, $J = 7.3$ Hz, 6H, 2 NCH₂CH₂CH₂CH₃ dibutylamine). **$^{13}\text{C}\{^1\text{H}\}$ NMR (101 MHz, $\text{CDCl}_3/\text{MeOD}$ 3:2, 50°)** δ 174.90 (C, C=O), 174.33 (C, C=O), 173.74 (C, C=O), 173.66 (C, C=O), 104.67 (CH, C1), 81.47 (CH, C3), 76.95 (CH, C-5), 75.66 (CH, C2), 75.50 (CH₂, C linker), 74.38 (CH₂, C linker), 74.23 (CH₂, C linker), 74.07 (CH₂, C linker), 72.93 (CH₂, C1' linker), 72.60 (CH, C4), 71.82 (CH₂, C6), 65.98 (CH₂, 2C, 2 NCH₂CH₂CH₂CH₃ dibutylamine), 58.05 (CH₂, C6' linker), 56.88 (CH₂, 2C, 2 NCH₂CH₂CH₂CH₃ dibutylamine), 33.40 (CH₃), 31.52 (CH₃), 24.23 (CH₃), 24.07 (CH₃), 23.95 (CH₂, 2C, NCH₂CH₂CH₂CH₃ dibutylamine), 17.34 (CH₃, 2C, 2 NCH₂CH₂CH₂CH₃ dibutylamine). **IR** (neat, cm^{-1}): 3600, 3402, 2956, 2934, 2872, 1753, 1457, 1366, 1220, 1172, 1118, 1037, 908, 803, 741, 697. **HRMS** ($\text{C}_{28}\text{H}_{49}\text{NO}_{12}$, MW 591.32); found m/z 592.33911 $[\text{M}+\text{H}]^+$ (vs 592.32883 calculated).

Synthesis of 2.1

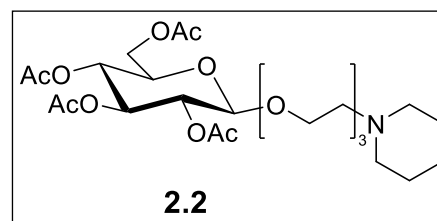


1 (200 mg, 0.32 mmol) reacted with morpholine (3 eq.) according to the general procedure **A**. Purification over silica gel (DCM: MeOH 95:5) gave **2.1** (Rf product 0.5) as a yellowish amorphous solid (158 mg, 90%).

$[\alpha]_D^{20} = -13.0^\circ$ ($c = 1.0$ g/100 mL, chloroform).

$^1\text{H NMR}$ (400 MHz, CDCl_3) δ 5.19 (t, $J = 9.5$ Hz, 1H, H3), 5.07 (t, $J = 9.7$ Hz, 1H, H4), 4.98 (dd, $J = 9.6, 8.0$ Hz, 1H, H2), 4.59 (d, $J = 8.0$ Hz, 1H, H1), 4.25 (dd, $J = 12.3, 4.7$ Hz, 1H, H6a), 4.12 (dd, $J = 12.3, 2.4$ Hz, 1H, H6b), 3.98 - 3.88 (m, 1H, H1'a linker), 3.77 - 3.66 (m, 6H, H5, H1'b linker, 2 $\text{NCH}_2\text{CH}_2\text{O}$ morpholine), 3.65 - 3.53 (m, 8H, 4 CH_2 linker), 2.59 (t, $J = 5.8$ Hz, 2H, 2H6' linker), 2.55 - 2.47 (m, 4H, 2 $\text{NCH}_2\text{CH}_2\text{O}$ morpholine), 2.07, 2.03, 2.01, 1.99 (4s, 3H each, CH_3). **$^{13}\text{C}\{^1\text{H}\}$ NMR (101 MHz, CDCl_3)** δ 170.63 (C, C=O), 170.24 (C, C=O), 169.39 (C, C=O), 169.32 (C, C=O), 100.83 (CH, C1), 72.80 (CH, C3), 71.77 (CH, C5), 71.25 (CH, C2), 70.66 (CH_2 , C linker), 70.36 (CH_2 , C linker), 70.26 (CH_2 , C linker), 69.08 (CH_2 , C1' linker), 68.59 (CH_2 , C linker), 68.40 (CH, C4), 66.79 (CH_2 , 2C, $\text{NCH}_2\text{CH}_2\text{O}$ morpholine), 61.93 (CH_2 , C6), 58.16 (CH_2 , C6' linker), 54.02 (CH_2 , 2C, $\text{NCH}_2\text{CH}_2\text{O}$ morpholine), 20.71 (CH_3), 20.65 (CH_3), 20.59 (CH_3), 20.57 (CH_3). **IR** (neat, cm^{-1}): 2918, 2858, 2312, 2110, 1745, 1434, 1365, 1325, 1215, 1173, 1115, 1034, 946, 909, 858, 771. **HRMS** ($\text{C}_{24}\text{H}_{39}\text{NO}_{13}$, MW 549.24); found m/z 550.24891 [$\text{M}+\text{H}$] $^+$ (vs 550.24550 calculated).

Synthesis of 2.2

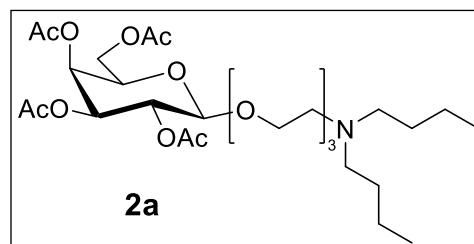


1 (300 mg, 0.47 mmol) reacted with piperidine (2 eq.) according to the general procedure **A**. Purification over silica gel (DCM: MeOH 95:5 + 1% TEA) gave **2.2** (R_f product 0.3) as a yellowish amorphous solid (198 mg, 77%).

$[\alpha]_D^{20}$: -12.1 ($c = 1.0$ g/100 mL, chloroform).

$^1\text{H NMR}$ (400 MHz, CDCl_3) δ 5.21 (t, $J = 9.5$ Hz, 1H, H3), 5.09 (t, $J = 9.7$ Hz, 1H, H4), 5.00 (dd, $J = 9.6, 8.0$ Hz, 1H, H2), 4.61 (d, $J = 8.0$ Hz, 1H, H1), 4.27 (dd, $J = 12.3, 4.7$ Hz, 1H, H6a), 4.14 (dd, $J = 12.3, 2.4$ Hz, 1H, H6b), 3.95 (dt, $J = 11.0, 4.3$ Hz, 1H, H1'a linker), 3.79 – 3.57 (m, 10H, H5, H1'b linker, 4CH₂ linker), 2.62 (t, $J = 6.0$ Hz, 2H, 2H6' linker), 2.51 (br s, 4H, 2 NCH₂CH₂CH₂ piperidine), 2.10, 2.05, 2.03, 2.01 (4s, 3H each, CH₃), 1.64 (dt, $J = 11.1, 5.6$ Hz, 4H, 2 NCH₂CH₂CH₂ piperidine), 1.50 – 1.41 (m, 2H, NCH₂CH₂CH₂ piperidine). **$^{13}\text{C}\{^1\text{H}\}$ NMR (101 MHz, CDCl_3)** δ 170.69 (C, C=O), 170.28 (C, C=O), 169.42 (C, C=O), 169.38 (C, C=O), 100.86 (CH, C1), 72.85 (CH, C3), 71.78 (CH, C5), 71.27 (CH, C2), 70.66 (CH₂, C linker), 70.34 (CH₂, C linker), 70.28 (CH₂, C linker), 69.11 (CH₂, C1' linker), 68.70 (CH₂, C linker), 68.42 (CH, C4), 61.95 (CH₂, C6), 58.33 (CH₂, C6' linker), 54.95 (CH₂, 2C, NCH₂CH₂CH₂ piperidine), 25.55 (CH₂, 2C, NCH₂CH₂CH₂ piperidine), 24.02 (CH₂, NCH₂CH₂CH₂ piperidine), 20.75 (CH₃), 20.68 (CH₃), 20.62 (CH₃), 20.60 (CH₃). **IR** (neat, cm^{-1}): 2935, 2859, 2105, 1746, 1639, 1438, 1365, 1213, 1172, 1033, 907, 805, 780, 759. **HRMS** ($\text{C}_{25}\text{H}_{41}\text{NO}_{12}$, MW 547.26); found m/z 548.26951 $[\text{M}+\text{H}]^+$ (vs 548.26623 calculated).

Synthesis of 2a

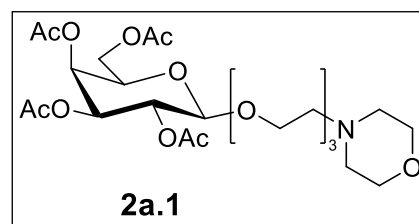


1a (250 mg, 0.40 mmol) reacted with dibutylamine (8 eq.) according to the general procedure **A**. Purification over silica gel (DCM: MeOH 9:1) gave **2a** (Rf product 0.3 cHex: EA 3:7) as a yellowish amorphous solid (215 mg, 92%).

$[\alpha]_D^{20}$: -12.75 (c = 1.0 g/100 mL, chloroform).

$^1\text{H NMR}$ (400 MHz, CDCl_3) δ 5.39 (dt, J = 5.9, 2.9 Hz, 1H, H4), 5.21 (dd, J = 10.5, 8.0 Hz, 1H, H2), 5.02 (dd, J = 10.5, 3.4 Hz, 1H, H3), 4.56 (d, J = 8.0 Hz, 1H, H1), 4.23 – 4.09 (m, 2H, 2H6), 4.01 – 3.89 (m, 2H, H5, H1'a linker), 3.81 – 3.70 (m, 3H, H1'b linker, 2H5' linker), 3.68 – 3.58 (m, 6H, 3CH₂ linker), 2.93 (br s, 2H, 2H6' linker), 2.76 (br s, 4H, 2 NCH₂CH₂CH₂CH₃ dibutylamine), 2.15 (s, 3H, CH₃), 2.06 (s, 3H, CH₃), 2.05 (s, 3H, CH₃) 1.99 (s, 3H, CH₃), 1.60 (br s, 4H, 2 NCH₂CH₂CH₂CH₃ dibutylamine), 1.41 – 1.28 (m, 4H, 2 NCH₂CH₂CH₂CH₃ dibutylamine), 0.94 (t, J = 7.4 Hz, 6H, 2 NCH₂CH₂CH₂CH₃ dibutylamine). **$^{13}\text{C}\{^1\text{H}\}$ NMR (101 MHz, CDCl_3)** δ 170.19 (C, C=O), 170.06 (C, C=O), 169.93 (C, C=O), 169.25 (C, C=O), 101.42 (CH, C1), 70.96 (CH, C3), 70.82 (CH, C5), 70.58 (CH₂, C linker), 70.50 (CH₂, C linker), 70.23 (CH₂, C linker), 68.97 (2C, C1' linker and C2), 67.74 (CH₂, C5' linker), 67.18 (CH, C4), 61.27 (C6), 53.85 (CH₂, 2C, 2 NCH₂CH₂CH₂CH₃ dibutylamine), 52.91 (CH₂, C6' linker), 27.04 (CH₂, 2C, 2 NCH₂CH₂CH₂CH₃ dibutylamine), 20.62 (CH₃), 20.48 (2C, CH₃), 20.40 (CH₃), 20.32 (CH₂, 2C, NCH₂CH₂CH₂CH₃ dibutylamine), 13.65 (CH₃, 2C, 2 NCH₂CH₂CH₂CH₃ dibutylamine). **IR** (neat, cm^{-1}): 3367, 2932, 2958, 2873, 2373, 2120, 1988, 2015, 1746, 1646, 1457, 1368, 1217, 1174, 1043, 955, 917, 900, 800, 737, 706. **HRMS** ($\text{C}_{28}\text{H}_{49}\text{NO}_{12}$, MW 591.32); found m/z 592.33000 $[\text{M}+\text{H}]^+$ (vs 592.32883 calculated).

Synthesis of 2a.1

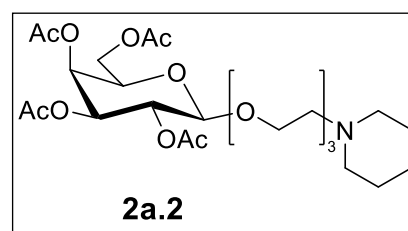


1a (200 mg, 0.32 mmol) reacted with morpholine (3 eq.) according to the general procedure **A**. Purification over silica gel (DCM: MeOH 95:5) gave **2a.1** (Rf product 0.5) as a yellowish amorphous solid (181 mg, 89%).

$[\alpha]_D^{20} = -9.55^\circ$ ($c = 1.0$ g/100 mL, chloroform).

$^1\text{H NMR}$ (400 MHz, CDCl_3) δ 5.40 (d, $J = 3.3$ Hz, 1H, H4), 5.22 (dd, $J = 10.4, 8.0$ Hz, 1H, H2), 5.03 (dd, $J = 10.5, 3.4$ Hz, 1H, H3), 4.57 (d, $J = 8.0$ Hz, 1H, H1), 4.16 (qd, $J = 11.2, 6.7$ Hz, 2H, 2H6), 4.01 – 3.89 (m, 2H, H5, H1'a linker), 3.82 – 3.71 (m, 5H, H1'b linker, 2 $\text{NCH}_2\text{CH}_2\text{O}$ morpholine), 3.71 – 3.58 (m, 8H, 4 CH_2 linker), 2.63 (br s, 2H, 2H6' linker), 2.55 (br s, 4H, 2 $\text{NCH}_2\text{CH}_2\text{O}$ morpholine), 2.16, 2.07, 2.06, 2.00 (4s, 3H each, CH_3). **$^{13}\text{C}\{^1\text{H}\}$ NMR (101 MHz, CDCl_3)** δ 170.40 (C, C=O), 170.27 (C, C=O), 170.17 (C, C=O), 169.46 (C, C=O), 101.39 (CH, C1), 70.91 (CH, C3), 70.69 (CH_2 , C linker), 70.67 (CH, C5), 70.40 (CH_2 , C linker), 70.27 (CH_2 , C linker), 70.11 (CH_2 , C linker), 69.11 (CH_2 , C1' linker), 68.81 (CH, C2), 68.58 (CH_2 , $\text{NCH}_2\text{CH}_2\text{O}$), 67.06 (CH, C4), 66.75 (CH_2 , $\text{NCH}_2\text{CH}_2\text{O}$), 61.28 (CH_2 , C6), 58.16 (CH_2 , C6' linker), 54.02 (CH_2 , 2C, $\text{NCH}_2\text{CH}_2\text{O}$), 20.79 (CH_3), 20.67 (CH_3), 20.59 (CH_3), 1.01 (CH_3). **IR** (neat, cm^{-1}): 2860, 2316, 2106, 1744, 1436, 1454, 1368, 1217, 1175, 1115, 1045, 954, 915, 900, 859, 803, 772, 738, 710. **HRMS** ($\text{C}_{24}\text{H}_{39}\text{NO}_{13}$, MW 549.24); found m/z 550.24951 [$\text{M}+\text{H}$] $^+$ (vs 550.24550 calculated).

Synthesis of 2a.2



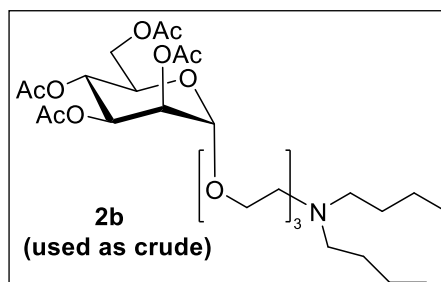
1a (200 mg, 0.32 mmol) reacted with piperidine (3 eq.) according to the general procedure **A**. Purification over silica gel (DCM: MeOH 9:1 + 1% TEA) gave **2a.2** (Rf product 0.3 in DCM: MeOH 95:5 + 1% TEA) as a yellowish amorphous solid (177 mg, 98%).

$[\alpha]^{20}_D$: -9.25 (c = 1.0 g/100 mL, chloroform).

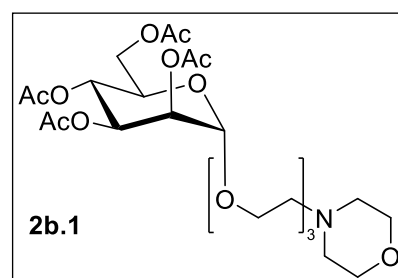
$^1\text{H NMR}$ (400 MHz, CDCl_3) δ 5.40 (dd, J = 0.9 Hz, 3.4, 1H, H4), 5.21 (dd, J = 8.0 Hz, 10.5, 1H, H2), 5.02 (dd, J = 3.4 Hz, 10.5, 1H, H3), 4.57 (d, J = 8.0 Hz, 1H, H1), 4.21 – 4.11 (m, 2H, 2H6), 4.01 – 3.88 (m, 2H, H5, H1'a linker), 3.76 (ddd, J = 4.0, 7.1, 11.0 Hz, 1H, H1'b linker), 3.69 – 3.56 (m, 8H, 4CH₂ linker), 2.59 (t, J = 6.1 Hz, 2H, 2H6' linker), 2.47 (br s, 4H, 2 NCH₂CH₂CH₂ piperidine), 2.16 (s, 3H, CH₃), 2.06 (2s, 3H each, CH₃), 1.99 (s, 3H, CH₃), 1.62 (dt, J = 5.6, 11.1 Hz, 4H, 2 NCH₂CH₂CH₂ piperidine), 1.49 – 1.40 (m, 2H, NCH₂CH₂CH₂ piperidine). **$^{13}\text{C}\{^1\text{H}\}$ NMR (101 MHz, CDCl_3)** δ 170.40 (C, C=O), 170.28 (C, C=O), 170.17 (C, C=O), 169.50 (C, C=O), 101.40 (CH, C1), 70.93 (CH, C3), 70.69 (CH, C5), 70.66 (CH₂, C linker), 70.33 (CH₂, C linker), 70.27 (CH₂, C linker), 69.12 (CH₂, C1' linker), 68.83 (CH₂, C linker), 68.82 (CH, C2), 67.07 (CH, C4), 61.30 (CH₂, C6), 58.41 (CH₂, C6' linker), 54.98 (CH₂, 2C, NCH₂CH₂CH₂ piperidine), 25.69 (CH₂, 2C, NCH₂CH₂CH₂ piperidine), 24.13 (CH₂, NCH₂CH₂CH₂ piperidine), 20.78 (CH₃), 20.67 (2C, CH₃), 20.59 (CH₃). **IR** (neat, cm^{-1}): 3301, 2933, 2119, 1746, 1651, 1435, 1368, 1216, 1174, 1074, 1041, 955, 918, 899, 863, 758, 779, 737, 708. **HRMS** ($\text{C}_{25}\text{H}_{41}\text{NO}_{12}$, MW 547.26); found m/z 548.26998 $[\text{M}+\text{H}]^+$ (vs 548.26623 calculated).

Synthesis of 2b

1b (450 mg, 0.71 mmol) reacted with dibutylamine (8 eq.) according to the general procedure **A** giving **2b** (Rf product 0.3 cHex: EA 3:7) as a crude product.



Synthesis of 2b.1



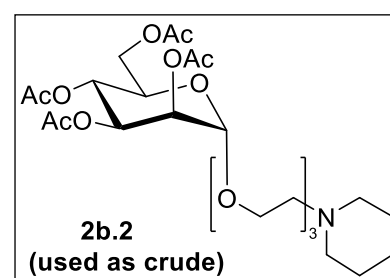
1b (300 mg, 0.47 mmol) reacted with morpholine (3 eq.) according to the general procedure **A**. Purification over silica gel (DCM: MeOH 9:1) gave **2b.1** (Rf product 0.5) as a yellowish amorphous solid (245 mg, 94%).

$[\alpha]^{20}_{\text{D}} = +31.88^\circ$ ($c = 1.0$ g/100 mL, chloroform).

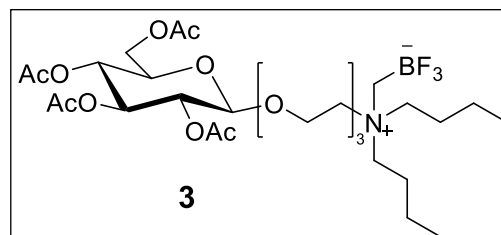
$^1\text{H NMR}$ (400 MHz, CDCl_3) δ 5.40 – 5.26 (m, 3H, H2, H3, H4), 4.88 (d, $J = 1.6$ Hz, 1H, H1), 4.31 (dd, $J = 12.1, 4.9$ Hz, 1H, H6a), 4.15 – 4.04 (m, 2H, H5, H6b), 3.82 (ddd, $J = 13.7, 7.4, 4.8$ Hz, 1H, H1'a linker), 3.78 – 3.72 (m, 4H, 2 $\text{NCH}_2\text{CH}_2\text{O}$ morpholine), 3.71 – 3.60 (m, 9H, H1'b linker, 4 CH_2 PEG), 2.63 (t, $J = 5.6$ Hz, 2H, 2H6' linker), 2.55 (s, 4H, 2 $\text{NCH}_2\text{CH}_2\text{O}$ morpholine), 2.17 (s, 3H, CH_3), 2.12 (s, 3H, CH_3), 2.05 (s, 3H, CH_3), 2.00 (s, 3H, CH_3). **$^{13}\text{C}\{^1\text{H}\}$ NMR (101 MHz, CDCl_3)** δ 170.68 (C, C=O), 170.04 (C, C=O), 169.91 (C, C=O), 169.72 (C, C=O), 97.74 (CH, C1), 70.71 (CH_2 , C linker), 70.39 (CH_2 , C linker), 70.00 (CH_2 , C linker), 69.57 (CH, C2), 69.08 (CH, C3), 68.56 (CH_2 , C linker), 68.43 (CH, C5), 67.41 (CH_2 , C1' linker), 66.76 (2 CH_2 , $\text{NCH}_2\text{CH}_2\text{O}$), 66.14 (C4), 62.40 (C6), 58.17 (CH_2 , C6' linker), 54.01 (2 CH_2 , $\text{NCH}_2\text{CH}_2\text{O}$), 20.90 (CH_3), 20.76 (CH_3), 20.72 (CH_3), 20.69 (CH_3). **IR** (neat, cm^{-1}): 2860, 2125, 1742, 1653, 1541, 1558, 1507, 1454, 1368, 1217, 1116, 1134, 1081, 1044, 978, 915, 937, 859, 772, 792. **HRMS** ($\text{C}_{24}\text{H}_{39}\text{NO}_{13}$, MW 549.24); found m/z 550.24913 $[\text{M}+\text{H}]^+$ (vs 550.24550 calculated).

Synthesis of 2b.2

1b (400 mg, 0.63 mmol) reacted with piperidine (3 eq.) according to the general procedure **A** giving **2b.2** (Rf product 0.3 in DCM: MeOH 95:5 + 1% TEA) as a crude product.



Synthesis of 3

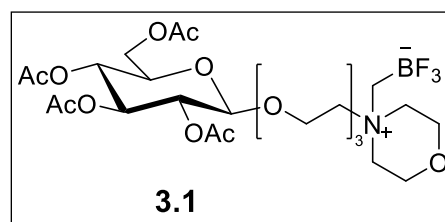


2 (200 mg, 0.34 mmol) reacted according to the general procedure **B**. Purification over silica gel (DCM: MeOH 98:2) gave **3** (Rf product 0.8) as a yellowish amorphous solid (174 mg, 76%).

$[\alpha]_D^{20} = -8.8^\circ$ ($c = 1.0$ g/100 mL, chloroform).

$^1\text{H NMR}$ (400 MHz, CDCl_3) δ 5.21 (t, $J = 9.5$ Hz, 1H, H3), 5.08 (t, $J = 9.7$ Hz, 1H, H4), 4.99 (dd, $J = 9.5, 8.0$ Hz, 1H, H2), 4.58 (d, $J = 7.9$ Hz, 1H, H1), 4.27 (dd, $J = 12.3, 4.7$ Hz, 1H, H6a), 4.15 (dd, $J = 12.3, 2.4$ Hz, 1H, H6b), 3.99 – 3.86 (m, 3H, H1'a linker, 2H5' linker), 3.76 – 3.66 (m, 2H, H5, H1'b linker), 3.65 – 3.56 (m, 6H, 3CH₂ linker), 3.51 – 3.44 (m, 2H, 2H6' linker), 3.36 – 3.16 (m, 4H, 2 NCH₂CH₂CH₂CH₃ dibutylamine), 2.47 (q, $J = 4.4$ Hz, 2H, NCH₂B), 2.09, 2.04, 2.03, 2.01 (4s, 3H each, CH₃), 1.71 – 1.56 (m, 4H, 2 NCH₂CH₂CH₂CH₃ dibutylamine), 1.43 – 1.30 (m, 4H, 2 NCH₂CH₂CH₂CH₃ dibutylamine), 0.99 (t, $J = 7.3$ Hz, 6H, 2 NCH₂CH₂CH₂CH₃ dibutylamine). **$^{13}\text{C}\{^1\text{H}\}$ NMR (101 MHz, CDCl_3)** δ 170.62 (C, C=O), 170.22 (C, C=O), 169.45 (C, C=O), 169.29 (C, C=O), 100.86 (CH, C1), 72.77 (CH, C3), 71.82 (CH, C5), 71.23 (CH, C2), 70.50 (CH₂, C linker), 70.43 (CH₂, C linker), 70.16 (CH₂, C linker), 69.10 (CH₂, C1' linker), 68.39 (CH, C4), 65.28 (CH₂, C5' linker), 61.94 (CH₂, C6), 61.71 (CH₂, 2C, 2 NCH₂CH₂CH₂CH₃ dibutylamine), 60.22 (CH₂, C6' linker), 24.21 (CH₂, 2C, 2 NCH₂CH₂CH₂CH₃ dibutylamine), 20.73 (CH₃), 20.68 (CH₃), 20.60 (2C, 2CH₃), 19.72 (CH₂, 2C, 2 NCH₂CH₂CH₂CH₃ dibutylamine), 13.68 (CH₃, 2C, 2 NCH₂CH₂CH₂CH₃ dibutylamine). **$^{11}\text{B}\{^1\text{H}\}$ NMR (128 MHz, CDCl_3)** δ 1.62 (br s). **$^{19}\text{F}\{^1\text{H}\}$ NMR (376 MHz, CDCl_3)** δ -140.16 (s). **IR** (neat, cm^{-1}): 3625, 2962, 2876, 2116, 1746, 1637, 1459, 1366, 1215, 1172, 1117, 1031, 895, 832, 806, 752. **HRMS** ($\text{C}_{29}\text{H}_{51}\text{BF}_3\text{NO}_{12}$, MW 673.51); found m/z 696.33451 $[\text{M}+\text{Na}]^+$ (vs 696.33486 calculated).

Synthesis of 3.1

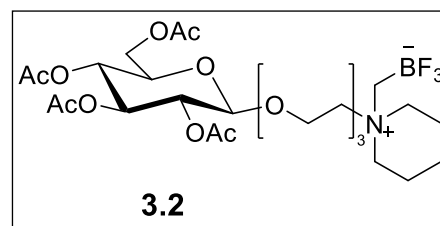


2.1 (150 mg, 0.27 mmol) reacted according to the general procedure **B**. Purification over silica gel (DCM: MeOH 95:5) gave **3.1** (Rf product 0.5) as a yellowish amorphous solid (139 mg, 81%).

$[\alpha]_D^{20} = -8.9^\circ$ ($c = 1.0$ g/100 mL, chloroform).

$^1\text{H NMR}$ (400 MHz, CDCl_3) δ 5.21 (t, $J = 9.5$ Hz, 1H, H3), 5.08 (t, $J = 9.7$ Hz, 1H, H4), 4.99 (dd, $J = 9.6, 8.0$ Hz, 1H, H2), 4.56 (d, $J = 8.0$ Hz, 1H, H1), 4.28 (dd, $J = 12.3, 4.7$ Hz, 1H, H6a), 4.14 (dd, $J = 12.3, 2.4$ Hz, 1H, H6b), 4.09 – 3.90 (m, 7H, H1'a linker + 6H), 3.76 – 3.43 (m, 14H, H5, H1'b linker + 12H), 2.76 – 2.65 (m, 2H, NCH_2B), 2.09, 2.05, 2.03, 2.01 (4s, 3H each, CH_3). **$^{13}\text{C}\{^1\text{H}\}$ NMR (101 MHz, CDCl_3)** δ 170.64 (C, C=O), 170.24 (C, C=O), 169.45 (C, C=O), 169.40 (C, C=O), 100.95 (CH, C1), 72.68 (CH, C3), 71.87 (CH, C5), 71.16 (CH, C2), 70.32 (CH_2), 70.18 (CH_2), 70.14 (CH_2), 69.33 (CH_2 , C1' linker), 68.35 (CH, C4), 65.15 (CH_2), 62.74 (CH_2), 62.10 (CH_2), 61.88 (CH_2 , 2C, C6), 60.92 (CH_2), 60.85 (CH_2), 20.72 (CH_3), 20.70 (CH_3), 20.60 (CH_3), 20.59 (CH_3). **$^{11}\text{B}\{^1\text{H}\}$ NMR (128 MHz, CDCl_3)** δ 1.85 (br s). **$^{19}\text{F}\{^1\text{H}\}$ NMR (376 MHz, CDCl_3)** δ -139.05 (s). **IR** (neat, cm^{-1}): 2881, 2110, 1745, 1639, 1438, 1366, 1216, 1170, 1124, 1030, 952, 900, 806, 751. **HRMS** ($\text{C}_{25}\text{H}_{41}\text{BF}_3\text{NO}_{13}$, MW 631.41); found m/z 654.25171 [$\text{M}+\text{Na}$] $^+$ (vs 654,25153 calculated).

Synthesis of 3.2

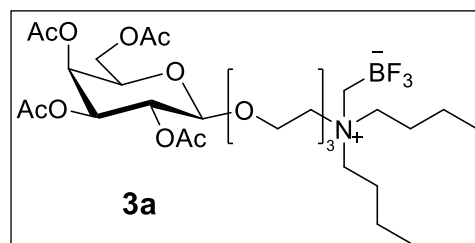


2.2 (170 mg, 0.31 mmol) reacted according to the general procedure **B**. Purification over silica gel (DCM: MeOH 95:5) gave **3.2** (Rf product 0.5) as a yellowish amorphous solid (144 mg, 74%).

$[\alpha]_D^{20} = -15.3^\circ$ ($c = 1.0$ g/100 mL, chloroform).

$^1\text{H NMR}$ (400 MHz, CDCl_3) δ 5.20 (t, $J = 9.5$ Hz, 1H, H3), 5.08 (t, $J = 9.7$ Hz, 1H, H4), 4.97 (dd, $J = 9.6, 8.0$ Hz, 1H, H2), 4.57 (d, $J = 8.0$ Hz, 1H, H1), 4.27 (dd, $J = 12.3, 4.7$ Hz, 1H, H6a), 4.14 (dd, $J = 12.3, 2.4$ Hz, 1H, H6b), 3.99 – 3.91 (m, 3H, H1'a linker, CH_2 linker), 3.76 – 3.67 (m, 2H, H5, H1'b linker), 3.65 – 3.55 (m, 8H, 4 CH_2 linker), 3.49 – 3.30 (m, 4H, 2 $\text{NCH}_2\text{CH}_2\text{CH}_2$ piperidine), 2.54 (q, $J = 4.4$ Hz, 2H, NCH_2B), 2.09, 2.04, 2.03, 2.01 (4s, 3H each, CH_3), 1.97 – 1.77 (m, 4H, 2 $\text{NCH}_2\text{CH}_2\text{CH}_2$ piperidine), 1.74 – 1.55 (m, 2H, $\text{NCH}_2\text{CH}_2\text{CH}_2$ piperidine). **$^{13}\text{C}\{^1\text{H}\}$ NMR (101 MHz, CDCl_3)** δ 170.62 (C, C=O), 170.21 (C, C=O), 169.46 (C, C=O), 169.34 (C, C=O), 100.88 (CH, C1), 72.75 (CH, C3), 71.81 (CH, C5), 71.23 (CH, C2), 70.37 (CH_2 , C linker), 70.32 (CH_2 , C linker), 70.15 (CH_2 , C linker), 69.22 (CH_2 , C1' linker), 68.38 (CH, C4), 65.27 (CH_2 , C linker), 63.22 (CH_2 , 2C, $\text{NCH}_2\text{CH}_2\text{CH}_2$ piperidine), 61.93 (CH_2 , C6), 61.26 (CH_2 , C6' linker), 21.40 (CH_2 , $\text{NCH}_2\text{CH}_2\text{CH}_2$ piperidine), 20.74 (CH_3), 20.69 (CH_3), 20.60 (2C, CH_3), 20.21 (CH_2 , 2C, $\text{NCH}_2\text{CH}_2\text{CH}_2$ piperidine). **$^{11}\text{B}\{^1\text{H}\}$ NMR (128 MHz, CDCl_3)** δ 1.84 (s). **$^{19}\text{F}\{^1\text{H}\}$ NMR (376 MHz, CDCl_3)** δ -139.38 (s). **IR** (neat, cm^{-1}): 2944, 2875, 2113, 1744, 1638, 1436, 1366, 1325, 1215, 1172, 1031, 941, 907, 891, 837, 804, 752. **HRMS** ($\text{C}_{26}\text{H}_{43}\text{BF}_3\text{NO}_{12}$, MW 629.41); found m/z 652.27192 [$\text{M}+\text{Na}$] $^+$ (vs 652.27226 calculated).

Synthesis of 3a

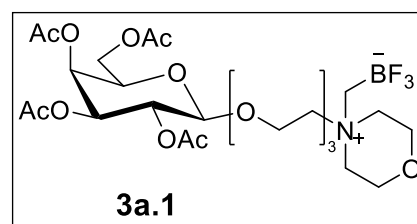


2a (200 mg, 0.34 mmol) reacted according to the general procedure **B**. Purification over silica gel (DCM: MeOH 97:3) gave **3a** (Rf product 0.5) as a colorless amorphous solid (191 mg, 83%).

$[\alpha]_D^{20} = -8.36^\circ$ ($c = 1.0$ g/100 mL, chloroform).

^1H NMR (400 MHz, CDCl_3) δ 5.40 (dd, $J = 6.5, 3.8$ Hz, 1H, H4), 5.20 (dd, $J = 10.5, 8.0$ Hz, 1H, H2), 5.03 (dd, $J = 10.5, 3.4$ Hz, 1H, H3), 4.54 (d, $J = 8.0$ Hz, 1H, H1), 4.23 – 4.10 (m, 2H, 2H6), 4.01 – 3.88 (m, 4H, H5, H1'a linker, 2H5' linker), 3.75 – 3.68 (m, 1H, H1'b linker), 3.67 – 3.58 (m, 6H, 3CH₂ linker), 3.52 – 3.46 (m, 2H, 2H6' linker), 3.35 – 3.16 (m, 4H, 2 NCH₂CH₂CH₂CH₃ dibutylamine), 2.48 (d, $J = 4.4$ Hz, 2H, NCH₂B), 2.16 (s, 3H, CH₃), 2.06 (2s, 3H each, CH₃), 2.00 (s, 3H, CH₃), 1.76 – 1.59 (m, 4H, 2 NCH₂CH₂CH₂CH₃ dibutylamine), 1.45 – 1.31 (m, 4H, 2 NCH₂CH₂CH₂CH₃ dibutylamine), 1.00 (t, $J = 7.3$ Hz, 6H, 2 NCH₂CH₂CH₂CH₃ dibutylamine). **$^{13}\text{C}\{^1\text{H}\}$ NMR (101 MHz, CDCl_3)** δ 170.42 (C, C=O), 170.22 (C, C=O), 170.13 (C, C=O), 169.40 (C, C=O), 101.41 (CH, C1), 70.85 (CH, C3), 70.71 (CH, C5), 70.51 (CH₂, C linker), 70.44 (CH₂, C linker), 70.18 (CH₂, C linker), 69.12 (CH₂, C1' linker), 68.77 (CH, C2), 67.02 (CH, C4), 65.30 (CH₂, C5' linker), 61.70 (CH₂, 2C, 2 NCH₂CH₂CH₂CH₃ dibutylamine), 61.18 (CH₂, C6), 60.22 (CH₂, C6' linker), 24.22 (CH₂, 2C, 2 NCH₂CH₂CH₂CH₃ dibutylamine), 20.79 (CH₃), 20.68 (CH₃), 20.65 (CH₃), 20.58 (CH₃), 19.72 (CH₂, 2C, 2 NCH₂CH₂CH₂CH₃ dibutylamine), 13.69 (CH₃, 2C, 2 NCH₂CH₂CH₂CH₃ dibutylamine). **$^{11}\text{B}\{^1\text{H}\}$ NMR (128 MHz, CDCl_3)** δ 1.77 (br s). **$^{19}\text{F}\{^1\text{H}\}$ NMR (376 MHz, CDCl_3)** δ -140.20 (s). **IR** (neat, cm^{-1}): 3648, 2962, 2875, 2119, 1743, 1459, 1368, 1217, 1175, 1042, 896, 835, 806, 738. **HRMS** ($\text{C}_{29}\text{H}_{51}\text{BF}_3\text{NO}_{12}$, MW 673.51); found m/z 696.33441 [$\text{M}+\text{Na}$]⁺ (vs 696.33486 calculated).

Synthesis of 3a.1

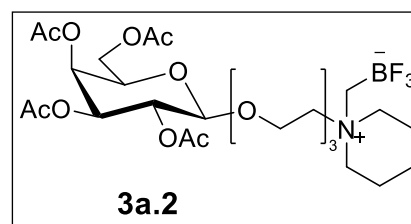


2a.1 (180 mg, 0.32 mmol) reacted according to the general procedure **B**. Purification over silica gel (DCM: MeOH 95:5) gave **3a.1** (Rf product 0.5) as a yellowish amorphous solid (116 mg, 56%).

$[\alpha]_D^{20} = -7.42^\circ$ ($c = 1.0$ g/100 mL, chloroform).

^1H NMR (400 MHz, CDCl_3) δ 5.40 (dd, $J = 3.4, 0.9$ Hz, 1H, H4), 5.17 (dd, $J = 10.5, 7.9$ Hz, 1H, H2), 5.03 (dd, $J = 10.5, 3.4$ Hz, 1H, H3), 4.51 (d, $J = 8.0$ Hz, 1H, H1), 4.20 (dd, $J = 11.2, 6.5$ Hz, 1H, H6a), 4.12 (dd, $J = 11.3, 6.8$ Hz, 1H, H6b), 4.09 – 3.90 (m, 8H, H5, H1'a linker, 3CH₂), 3.74 – 3.64 (m, 3H), 3.64 – 3.44 (m, 11H, H1'b linker, 3CH₂ linker, 2CH₂), 2.71 (q, $J = 4.4$ Hz, 2H, NCH₂B), 2.17, 2.063, 2.057, 2.00 (4s, 3H each, CH₃). **$^{13}\text{C}\{^1\text{H}\}$ NMR (101 MHz, CDCl_3)** δ 170.43 (C, C=O), 170.24 (C, C=O), 170.13 (C, C=O), 169.46 (C, C=O), 101.51 (CH, C1), 70.77 (CH, 2C, C3 and C5), 70.32 (CH₂, C linker), 70.15 (CH₂, C linker), 70.14 (CH₂, C linker), 69.44 (CH₂, C1' linker), 68.71 (CH, C2), 67.02 (CH, C4), 65.16, 62.52, 62.12, 62.07, 61.22 (CH₂, C6), 60.93, 60.91, 20.79 (CH₃), 20.68 (CH₃), 20.60 (CH₃), 20.59 (CH₃). **$^{11}\text{B}\{^1\text{H}\}$ NMR (128 MHz, CDCl_3)** δ 1.65 (s). **$^{19}\text{F}\{^1\text{H}\}$ NMR (376 MHz, CDCl_3)** δ -139.15 (s). **IR** (neat, cm^{-1}): 3622, 2881, 2116, 1741, 1644, 1437, 1368, 1216, 1174, 1126, 1032, 952, 898, 917, 751. **HRMS** ($\text{C}_{25}\text{H}_{41}\text{BF}_3\text{NO}_{13}$, MW 631.41); found m/z 654.25161 [$\text{M}+\text{Na}$]⁺ (vs 654.25153 calculated).

Synthesis of 3a.2

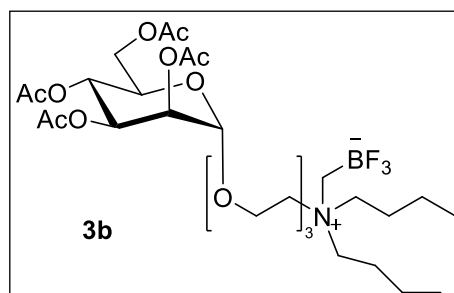


2a.2 (140 mg, 0.26 mmol) reacted according to the general procedure **B**. Purification over silica gel (DCM: MeOH 98:2) gave **3a.2** (Rf product 0.5) as a yellowish amorphous solid (104 mg, 64%).

$[\alpha]_D^{20} = -8.46^\circ$ ($c = 1.0$ g/100 mL, chloroform).

^1H NMR (400 MHz, CDCl_3) δ 5.40 (dt, $J = 6.4, 3.2$ Hz, 1H, H4), 5.19 (dd, $J = 10.5, 7.9$ Hz, 1H, H2), 5.03 (dd, $J = 10.5, 3.4$ Hz, 1H, H3), 4.54 (d, $J = 8.0$ Hz, 1H, H1), 4.16 (ddd, $J = 27.4, 11.2, 6.7$ Hz, 2H, H6), 4.00 – 3.90 (m, 4H, H5, H1'a linker, 2H6' linker), 3.75 – 3.68 (m, 1H, H1'b linker), 3.66 – 3.56 (m, 8H, 4CH₂ linker), 3.51 – 3.41 (m, 2H, NCH₂CH₂CH₂ piperidine), 3.36 (dd, $J = 10.3, 6.8$ Hz, 2H, NCH₂CH₂CH₂ piperidine), 2.56 (d, $J = 4.4$ Hz, 2H, NCH₂B), 2.16 (s, 3H, CH₃), 2.07 (2s, 3H each, CH₃), 2.00 (s, 3H, CH₃), 1.97 – 1.80 (m, 4H, 2xNCH₂CH₂CH₂), 1.77 – 1.56 (m, 2H, NCH₂CH₂CH₂). **$^{13}\text{C}\{^1\text{H}\}$ NMR (101 MHz, CDCl_3)** δ 170.43 (C, C=O), 170.20 (C, C=O), 170.13 (C, C=O), 169.45 (C, C=O), 101.43 (CH, C1), 70.83 (CH, C5), 70.71 (CH₂, C linker), 70.36 (CH₂, C linker), 70.17 (CH₂, C linker), 69.26 (CH₂, C1' linker), 68.76 (CH, C2), 67.03 (CH, C4), 65.30 (CH₂, C6' linker), 63.31 (CH₂, 2C, NCH₂CH₂CH₂ piperidine), 61.19 (CH₂, 2C, C6, C linker), 21.44 (CH₂, NCH₂CH₂CH₂ piperidine), 20.80 (CH₃), 20.69 (CH₃), 20.66 (CH₃), 20.59 (CH₃), 20.22 (CH₂, 2C, NCH₂CH₂CH₂ piperidine). **$^{11}\text{B}\{^1\text{H}\}$ NMR (128 MHz, CDCl_3)** δ 1.95 (d, $J = 28.1$ Hz). **$^{19}\text{F}\{^1\text{H}\}$ NMR (376 MHz, CDCl_3)** δ -139.50 (s). **IR** (neat, cm^{-1}): 3854, 3649, 3287, 2921, 2325, 2213, 2234, 2166, 2116, 1990, 2015, 1952, 1966, 1743, 1652, 1434, 1368, 1298, 1218, 1075, 1018, 941, 893, 864, 797, 704, 729. **HRMS** ($\text{C}_{26}\text{H}_{43}\text{BF}_3\text{NO}_{12}$, MW 629.41); found m/z 652.27161 $[\text{M}+\text{Na}]^+$ (vs 652.27226 calculated).

Synthesis of 3b

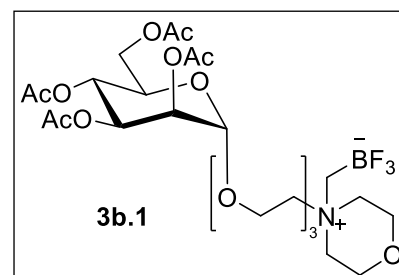


2b (250 mg crude product, 0.42 mmol) reacted according to the general procedure **B**. Purification over silica gel (DCM: MeOH 97:3) gave **3b** (Rf product 0.5) as a yellowish amorphous solid (235 mg, 50% over three steps).

$[\alpha]_D^{20} = +30.64^\circ$ ($c = 1.0$ g/100 mL, chloroform).

^1H NMR (400 MHz, CDCl_3) δ 5.36 – 5.24 (m, 3H, H2, H3, H4), 4.87 (d, $J = 1.4$ Hz, 1H, H1), 4.29 (dd, $J = 12.2, 5.1$ Hz, 1H, H6a), 4.12 (dd, $J = 12.3, 2.4$ Hz, 1H, H6b), 4.07 – 3.99 (m, 1H, H5), 3.95 – 3.88 (m, 2H, 2H5' linker), 3.81 (ddd, $J = 12.5, 7.6, 2.8$ Hz, 1H, H1'a linker), 3.70 – 3.59 (m, 7H, H1'b linker, 3CH₂ linker), 3.54 – 3.47 (m, 2H, 2H6' linker), 3.34 – 3.18 (m, 4H, 2 NCH₂CH₂CH₂CH₃ dibutylamine), 2.48 (d, $J = 4.4$ Hz, 2H, NCH₂B), 2.17 (s, 3H, CH₃), 2.11 (s, 3H, CH₃), 2.06 (s, 3H, CH₃), 2.00 (s, 3H, CH₃), 1.66 (dt, $J = 15.7, 8.0$ Hz, 4H, 2 NCH₂CH₂CH₂CH₃ dibutylamine), 1.44 – 1.30 (m, 4H, 2 NCH₂CH₂CH₂CH₃ dibutylamine), 0.99 (t, $J = 7.3$ Hz, 6H, 2 NCH₂CH₂CH₂CH₃ dibutylamine). **$^{13}\text{C}\{^1\text{H}\}$ NMR (101 MHz, CDCl_3)** δ 170.64 (C, C=O), 170.10 (C, C=O), 169.98 (C, C=O), 169.73 (C, C=O), 97.75 (CH, C1), 70.50 (PEG), 70.42 (CH₂, C linker), 69.99 (CH₂, C linker), 69.47 (CH, C2), 69.06 (CH, C3), 68.51 (CH, C5), 67.34 (CH₂, C1' linker), 66.09 (CH, C4), 65.29 (CH₂, C5' linker), 62.43 (CH₂, C6), 61.72 (CH₂, 2C, 2 NCH₂CH₂CH₂CH₃ dibutylamine), 60.19 (CH₂, C6' linker), 24.21 (CH₂, 2C, 2 NCH₂CH₂CH₂CH₃ dibutylamine), 20.88 (CH₃), 20.75 (CH₃), 20.70 (CH₃), 20.69 (CH₃), 19.72 (CH₂, 2C, 2 NCH₂CH₂CH₂CH₃ dibutylamine), 13.69 (CH₃, 2C, 2 NCH₂CH₂CH₂CH₃ dibutylamine). **$^{11}\text{B}\{^1\text{H}\}$ NMR (128 MHz, CDCl_3)** δ 1.75 (br s). **$^{19}\text{F}\{^1\text{H}\}$ NMR (376 MHz, CDCl_3)** δ -140.25 (s). **IR** (neat, cm^{-1}): 2962, 2876, 2377, 2126 1742, 1653, 1541, 1558, 1507, 1457, 1368, 1218, 1134, 1042, 978, 1003, 936, 895, 831, 793, 753. **HRMS** ($\text{C}_{29}\text{H}_{51}\text{BF}_3\text{NO}_{12}$, MW 673.51); found m/z 696.33411 $[\text{M}+\text{Na}]^+$ (vs 696.33486 calculated).

Synthesis of 3b.1

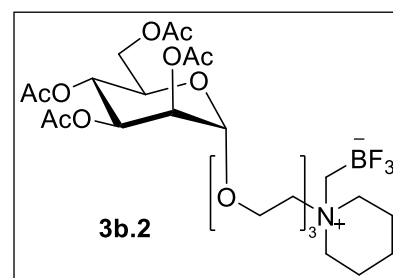


2b.1 (200 mg, 0.39 mmol) reacted according to the general procedure **B**. Purification over silica gel (DCM: MeOH 95:5) gave **3b.1** (R_f product 0.5) as a yellowish amorphous solid (190 mg, 77%).

$[\alpha]_D^{20} = +24.24^\circ$ ($c = 1.0$ g/100 mL, chloroform).

$^1\text{H NMR}$ (400 MHz, CDCl_3) δ 5.34 – 5.29 (m, 2H, H3, H4), 5.25 (dd, $J = 2.9, 1.8$ Hz, 1H, H2), 4.88 (d, $J = 1.7$ Hz, 1H, H1), 4.28 (dd, $J = 12.2, 5.2$ Hz, 1H, H6a), 4.13 (dd, $J = 12.2, 2.6$ Hz, 1H, H6b), 4.09 – 3.99 (m, 5H, H5, 2H5' linker, $\text{NCH}_2\text{CH}_2\text{O}$ morpholine), 3.94 (br d, $J = 13.8$ Hz, 2H, $\text{NCH}_2\text{CH}_2\text{O}$ morpholine), 3.86 – 3.77 (m, 1H, H1'a linker), 3.77 – 3.71 (m, 2H, 2H6' linker), 3.71 – 3.61 (m, 7H, H1'b linker, 3 CH_2 linker), 3.61 – 3.45 (m, 4H, 2 $\text{NCH}_2\text{CH}_2\text{O}$ morpholine), 2.71 (dd, $J = 8.8, 4.3$ Hz, 2H, NCH_2B), 2.17 (s, 3H, CH_3), 2.11 (s, 3H, CH_3), 2.07 (s, 3H, CH_3), 2.01 (s, 3H, CH_3). **$^{13}\text{C}\{^1\text{H}\}$ NMR (101 MHz, CDCl_3)** δ 170.66 (C, C=O), 170.19 (C, C=O), 170.14 (C, C=O), 169.72 (C, C=O), 97.66 (CH, C1), 70.30 (CH_2 , 2C linker), 69.95 (CH_2 , C linker), 69.47 (CH, C2), 69.07 (CH, C3), 68.57 (CH, C5), 67.37 (CH_2 , C1' linker), 66.05 (CH, C4), 65.18 (CH_2 , C5' linker), 62.58 (CH_2 , C6' linker), 62.44 (CH_2 , C6), 61.97 (CH_2 , 2C, $\text{NCH}_2\text{CH}_2\text{O}$), 60.91 (CH_2 , 2C, $\text{NCH}_2\text{CH}_2\text{O}$), 20.89 (CH_3), 20.75 (CH_3), 20.71 (2C, CH_3). **$^{11}\text{B}\{^1\text{H}\}$ NMR (128 MHz, CDCl_3)** δ 1.90 (s). **$^{19}\text{F}\{^1\text{H}\}$ NMR (376 MHz, CDCl_3)** δ -139.21 (s). **IR** (neat, cm^{-1}): 2881, 1844, 1869, 1829, 1792, 1739, 1670, 1684, 1636, 1653, 1541, 1558, 1507, 1521, 1472, 1488, 1457, 1437, 1368, 1289, 1218, 1130, 1038, 899, 917, 791, 731. **HRMS** ($\text{C}_{25}\text{H}_{41}\text{BF}_3\text{NO}_{13}$, MW 631.41); found m/z 654.25051 [$\text{M}+\text{Na}$] $^+$ (vs 654.25153 calculated).

Synthesis of 3b.2

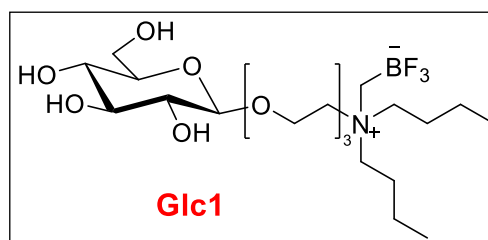


2b.2 (300 mg crude product, 0.54 mmol) reacted according to the general **B**. Purification over silica gel (DCM: MeOH 95:5) gave **3b.2** (Rf product 0.5) as a yellowish amorphous solid (189 mg, 55% over three steps).

$[\alpha]_D^{20} = +36.04^\circ$ ($c = 1.0$ g/100 mL, chloroform).

^1H NMR (400 MHz, CDCl_3) δ 5.36 – 5.22 (m, 3H, H2, H3, H4), 4.87 (d, $J = 1.4$ Hz, 1H, H1), 4.28 (dd, $J = 12.2, 5.1$ Hz, 1H, H6a), 4.16 – 4.09 (m, 1H, H6b), 4.06 – 3.94 (m, 3H, H5, 2H5'linker), 3.85 – 3.76 (m, 1H, H1'a linker), 3.71 – 3.57 (m, 9H, H1'b linker, 4CH₂ linker), 3.40 (ddd, $J = 21.4, 16.2, 11.9$ Hz, 4H, 2 NCH₂CH₂CH₂ piperidine), 2.55 (d, $J = 4.3$ Hz, 2H, NCH₂B), 2.17 (s, 3H, CH₃), 2.11 (s, 3H, CH₃), 2.06 (s, 3H, CH₃), 2.00 (s, 3H, CH₃), 1.97 – 1.76 (m, 4H, 2 NCH₂CH₂CH₂ piperidine), 1.74 – 1.57 (m, 2H, NCH₂CH₂CH₂ piperidine). **$^{13}\text{C}\{^1\text{H}\}$ NMR (101 MHz, CDCl_3)** δ 170.66 (C, C=O), 170.14 (C, C=O), 170.03 (C, C=O), 169.73 (C, C=O), 97.70 (CH, C1), 70.34 (CH₂, C linker), 70.28 (CH₂, C linker), 69.95 (CH₂, C linker), 69.45 (CH, C2), 69.09 (CH, C3), 68.51 (CH, C5), 67.38 (CH₂, C1' linker), 66.06 (CH, C4), 65.27 (CH₂, C5' linker), 63.21 (CH₂, 2C, NCH₂CH₂CH₂ piperidine), 62.43 (CH₂, C6), 60.99 (CH₂, C6' linker), 21.36 (CH₂, NCH₂CH₂CH₂ piperidine), 20.89 (CH₃), 20.76 (CH₃), 20.71 (2C, CH₃), 20.24 (CH₂, 2C, NCH₂CH₂CH₂ piperidine). **$^{11}\text{B}\{^1\text{H}\}$ NMR (128 MHz, CDCl_3)** δ 1.94 (s). **$^{19}\text{F}\{^1\text{H}\}$ NMR (376 MHz, CDCl_3)** δ -139.53 (s). **IR** (neat, cm^{-1}): 2943, 2877, 2376, 2318, 2126, 1740, 1636, 1653, 1541, 1558, 1507, 1521, 1436, 1456, 1368, 1218, 1171, 1134, 1041, 940, 892, 837, 792, 754. **HRMS** ($\text{C}_{26}\text{H}_{43}\text{BF}_3\text{NO}_{12}$, MW 629.41); found m/z 652.27051 [$\text{M}+\text{Na}$]⁺ (vs 652.27226 calculated).

Synthesis of Glc1

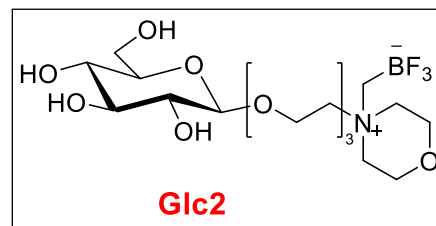


3 (120 mg, 0.18 mmol) reacted according to the general procedure **C** to give **Glc1** (77 mg, 86%) as a white foam.

$[\alpha]_D^{20} = -11.0^\circ$ ($c = 1.0$ g/100 mL, methanol).

¹H NMR (400 MHz, CD₃OD) δ 4.32 (d, $J = 7.8$ Hz, 1H, H1), 4.04 (dt, $J = 8.5, 3.8$ Hz, 1H, H1'a linker), 3.89 (dd, $J = 7.5, 2.8$ Hz, 3H, H6a, CH₂ liker), 3.80 – 3.62 (m, 8H, H6b, H1'b linker, 3CH₂ liker), 3.56 – 3.47 (m, 2H, 2H6' linker), 3.37 (t, $J = 4.5$ Hz, 1H, H3), 3.34 – 3.25 (m, 6H, H4, H5, 2 NCH₂CH₂CH₂CH₃ dibutylamine), 3.22 (dd, $J = 9.0, 8.98$ Hz, 1H, H2), 2.44 (q, $J = 4.9$ Hz, 2H, NCH₂B), 1.82 – 1.61 (m, 4H, 2 NCH₂CH₂CH₂CH₃ dibutylamine), 1.46 – 1.34 (m, 4H, 2 NCH₂CH₂CH₂CH₃ dibutylamine), 1.02 (t, $J = 7.4$ Hz, 6H, 2 NCH₂CH₂CH₂CH₃ dibutylamine). **¹³C{¹H} NMR (101 MHz, CD₃OD)** δ 103.13 (CH, C1), 76.61 (CH, 2C, C3, C5*), 73.68 (CH, C2), 70.25 (CH, C4*), 70.08 (CH₂, 2C, C linker), 70.00 (CH₂, C linker), 68.33 (CH₂, C1' linker), 64.73 (CH₂, C linker), 61.40 (CH₂, 3C, C6, 2 NCH₂CH₂CH₂CH₃ dibutylamine), 59.77 (CH₂, C6' linker), 23.86 (CH₂, 2C, 2 NCH₂CH₂CH₂CH₃ dibutylamine), 19.39 (CH₂, 2C, 2 NCH₂CH₂CH₂CH₃ dibutylamine), 12.69 (CH₃, 2C, 2 NCH₂CH₂CH₂CH₃ dibutylamine) *may be interchanged. **¹¹B{¹H} NMR (128 MHz, CD₃OD)** δ 2.00 (s). **¹⁹F{¹H} NMR (376 MHz, CD₃OD)** δ -140.32 (s). **IR** (neat, cm⁻¹): 3393, 2961, 2932, 2875, 2105, 1638, 1460, 1352, 1301, 1254, 1162, 1033, 896, 805, 737, 717. **HRMS** (C₂₁H₄₃BF₃NO₈, MW 505.31); found m/z 528.29361 [M+Na]⁺ (vs 528.29261 calculated).

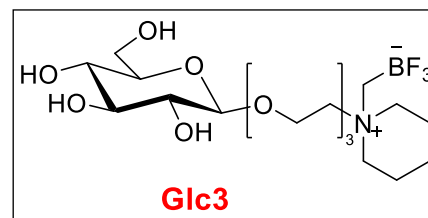
Synthesis of Glc2



3.1 (120 mg, 0.19 mmol) reacted according to the general procedure **C** to give **Glc2** (85 mg, 97%) as a white foam. $[\alpha]^{20}_D = -9.8^\circ$ ($c = 1.0$ g/100 mL, methanol).

^1H NMR (400 MHz, CD_3OD) δ 4.32 (d, $J = 7.8$ Hz, 1H, H1), 4.07 – 3.93 (m, 7H, H1'a linker, 6H), 3.89 (dd, $J = 11.9, 1.5$ Hz, 1H, H6a), 3.78 – 3.64 (m, 10H, H6b, H5, H1'b linker, 7H), 3.61 – 3.48 (m, 4H), 3.41 – 3.38 (m, 1H, H3), 3.31 – 3.27 (m, 2H, H4), 3.21 (dd, $J = 7.8, 9.0$ Hz, 1H, H2), 2.68 (q, $J = 9.1, 4.4$ Hz, 2H, NCH_2B). **$^{13}\text{C}\{^1\text{H}\}$ NMR (101 MHz, CD_3OD)** δ 103.11 (CH, C1), 76.62 (CH, C3)*, 76.61 (CH, C4)*, 73.66 (CH, C2), 70.22 (CH, C5), 70.01 (CH₂), 69.86 (CH₂), 69.79 (CH₂), 68.46 (CH₂, C1' linker), 64.62 (CH₂), 61.37 (CH₂, 3C, C6), 60.59 (CH₂, 2C). *may be interchanged. **$^{11}\text{B}\{^1\text{H}\}$ NMR (128 MHz, CD_3OD)** δ 1.86 (s). **$^{19}\text{F}\{^1\text{H}\}$ NMR (376 MHz, CD_3OD)** δ -139.07 (s). **IR** (neat, cm^{-1}): 3387, 2880, 2083, 1639, 1460, 1352, 1299, 1254, 1222, 1197, 1163, 1065, 1029, 952, 918, 899, 849, 818, 779. **HRMS** ($\text{C}_{17}\text{H}_{33}\text{BF}_3\text{NO}_9$, MW 463.21); found m/z 486.20911 $[\text{M}+\text{Na}]^+$ (vs 486.20927 calculated).

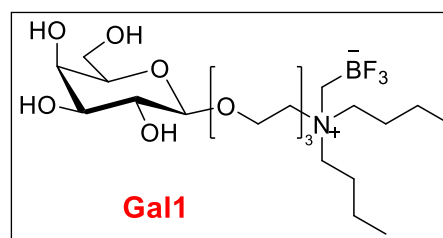
Synthesis of Glc3



3.2 (115 mg, 0.18 mmol) reacted according to the general procedure **C** to give **Glc3** (81 mg, 95%) as a white foam. $[\alpha]^{20}_D = -11.3^\circ$ ($c = 1.0$ g/100 mL, methanol).

^1H NMR (400 MHz, CD_3OD) δ 4.32 (d, $J_{1,2} = 7.8$ Hz, 1H, H1), 4.09 – 4.00 (m, $J = 7.7, 4.3$ Hz, 1H, H1'a linker), 3.99 – 3.93 (m, 2H, CH₂ liker), 3.89 (d, $J = 11.4$ Hz, 1H, H6a), 3.80 – 3.64 (m, 8H, H6b, H1'b linker, 3CH₂ liker), 3.64 – 3.59 (m, 2H, 2H6' linker), 3.44 (t, $J = 5.4$ Hz, 4H, 2 $\text{NCH}_2\text{CH}_2\text{CH}_2$ piperidine), 3.40 – 3.26 (m, 3H, H3, H4, H5), 3.21 (dd, $J = 8.9, 7.9$ Hz, 1H, H2), 2.53 (q, $J = 4.6$ Hz, 2H, NCH_2B), 2.00 – 1.82 (m, 4H, 2 $\text{NCH}_2\text{CH}_2\text{CH}_2$), 1.72 – 1.60 (m, 2H, $\text{NCH}_2\text{CH}_2\text{CH}_2$). **$^{13}\text{C}\{^1\text{H}\}$ NMR (101 MHz, CD_3OD)** δ 103.11 (CH, C1), 76.60 (CH, 2C, C3, C5), 73.69 (CH, C2), 70.25 (CH, C4), 70.05 (CH₂, C linker), 69.96 (CH₂, C linker), 69.84 (CH₂, C linker), 68.38 (CH₂, C1' linker), 64.74 (CH₂, C linker), 62.46 (CH₂, 2C, $\text{NCH}_2\text{CH}_2\text{CH}_2$ piperidine), 61.40 (CH₂, C6), 60.71 (CH₂, C6' linker), 21.00 (CH₂, $\text{NCH}_2\text{CH}_2\text{CH}_2$ piperidine), 19.91 (CH₂, 2C, $\text{NCH}_2\text{CH}_2\text{CH}_2$ piperidine). **$^{11}\text{B}\{^1\text{H}\}$ NMR (128 MHz, CD_3OD)** δ 2.00 (d, $J = 45.0$ Hz). **$^{19}\text{F}\{^1\text{H}\}$ NMR (376 MHz, CD_3OD)** δ -139.55 (s). **IR** (neat, cm^{-1}): 3385, 2876, 2094, 1638, 1462, 1351, 1326, 1300, 1250, 1195, 1165, 1029, 1008, 989, 940, 89, 837, 793. **HRMS** ($\text{C}_{18}\text{H}_{35}\text{BF}_3\text{NO}_8$, MW 461.21); found m/z 484.2091 $[\text{M}+\text{Na}]^+$ (vs 484.20331 calculated).

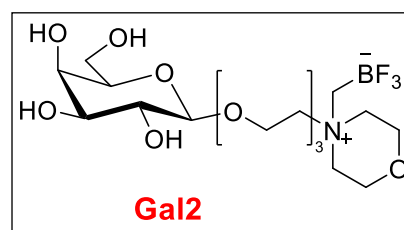
Synthesis of Gal1



3a (120 mg, 0.17 mmol) reacted according to the general procedure **C** to give **Gal1** (85 mg, 95%) as a white foam. $[\alpha]^{20}_D = -15.18^\circ$ ($c = 1.0$ g/100 mL, methanol).

^1H NMR (400 MHz, CD_3OD) δ 4.27 (d, $J = 7.4$ Hz, 1H, H1), 4.07 – 4.01 (m, 1H, H1'a linker), 3.91 – 3.84 (m, 3H, H4, 2H5' linker), 3.79 – 3.62 (m, 9H, H1'b linker, 3CH₂ liker, 2H6), 3.56 – 3.47 (m, 5H, H2, H3, H5, 2H6' linker), 3.35 – 3.30 (m, 4H, 2 NCH₂CH₂CH₂CH₃ dibutylamine), 2.44 (dd, $J = 9.1, 4.4$ Hz, 2H, NCH₂B), 1.80 – 1.60 (m, 4H, 2 NCH₂CH₂CH₂CH₃ dibutylamine), 1.45 – 1.33 (m, 4H, 2 NCH₂CH₂CH₂CH₃ dibutylamine), 1.01 (t, $J = 7.4$ Hz, 6H, 2 NCH₂CH₂CH₂CH₃ dibutylamine). **$^{13}\text{C}\{^1\text{H}\}$ NMR (101 MHz, CD_3OD)** δ 103.75 (CH, C1), 75.31 (CH, C5), 73.55 (CH, C3), 71.11 (CH, C2), 70.09 (CH₂, 2C, C linker), 69.99 (CH₂, C linker), 68.87 (CH, C4), 68.24 (CH₂, C1' linker), 64.73 (CH₂, C5' linker), 61.37 (CH₂, 2C, 2 NCH₂CH₂CH₂CH₃ dibutylamine), 61.12 (CH₂, C6), 59.77 (CH₂, C6' linker), 23.86 (CH₂, 2C, 2 NCH₂CH₂CH₂CH₃ dibutylamine), 19.39 (CH₂, 2C, 2 NCH₂CH₂CH₂CH₃ dibutylamine), 12.69 (CH₃, 2C, 2 NCH₂CH₂CH₂CH₃ dibutylamine). **$^{11}\text{B}\{^1\text{H}\}$ NMR (128 MHz, CD_3OD)** δ 1.88 (br s). **$^{19}\text{F}\{^1\text{H}\}$ NMR (376 MHz, CD_3OD)** δ -140.31 (s). **IR** (neat, cm^{-1}): 3396, 2934, 2960, 2875, 2107, 1989, 1652, 1541, 1558, 1507, 1463, 1352, 1378, 1300, 1254, 1045, 894, 757, 781, 738, 702. **HRMS** ($\text{C}_{21}\text{H}_{43}\text{BF}_3\text{NO}_8$, MW 505.51); found m/z 523.33749 [$\text{M}+\text{NH}_4$]⁺ (vs 523.33776 calculated).

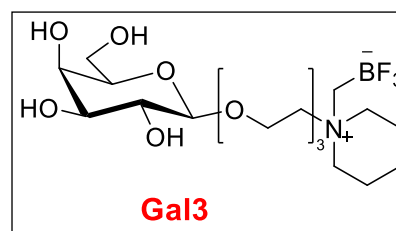
Synthesis of Gal2



3a.1 (120 mg, 0.19 mmol) reacted according to the general procedure **C** to give **Gal2** (88 mg, 99%) as a white foam. $[\alpha]^{20}_D = -4.65^\circ$ ($c = 1.0$ g/100 mL, methanol).

^1H NMR (400 MHz, CD_3OD) δ 4.27 (d, $J = 7.4$ Hz, 1H, H1), 4.09 – 3.92 (m, 7H, H1'a linker, 2H5' linker, 2 NCH₂CH₂O morpholine), 3.85 (d, $J = 2.5$ Hz, 1H, H4), 3.81 – 3.64 (m, 11H, 2H6, H1'b linker, 2H6' linker, 3CH₂ liker), 3.61 – 3.46 (m, 7H, H2, H3, H5, 2 NCH₂CH₂O morpholine), 2.68 (q, $J = 4.6$ Hz, 2H, NCH₂B). **$^{13}\text{C}\{^1\text{H}\}$ NMR (101 MHz, CD_3OD)** δ 103.77 (CH, C1), 75.33 (CH, C5), 73.56 (CH, C3), 71.11 (CH, C2), 70.05 (CH₂, C linker), 69.86 (CH₂, C linker), 69.80 (CH₂, C linker), 68.90 (CH, C4), 68.39 (CH₂, C1' linker), 64.67 (CH₂, C5' linker), 61.40 (CH₂, 2C, NCH₂CH₂O), 61.17 (CH₂, C6), 60.59 (CH₂, 2C, NCH₂CH₂O). **$^{11}\text{B}\{^1\text{H}\}$ NMR (128 MHz, CD_3OD)** δ 1.94 (d, $J = 43.4$ Hz). **$^{19}\text{F}\{^1\text{H}\}$ NMR (376 MHz, CD_3OD)** δ -139.45 (br s). **IR** (neat, cm^{-1}): 3387, 2921, 2883, 2118, 1638, 1461, 1329, 1352, 1298, 1254, 1222, 1120, 1020, 947, 896, 918, 849, 758, 778, 701. **HRMS** ($\text{C}_{17}\text{H}_{33}\text{BF}_3\text{NO}_9$, MW 463.41); found m/z 486.20902 [$\text{M}+\text{Na}$]⁺ (vs 486.20927 calculated).

Synthesis of Gal3

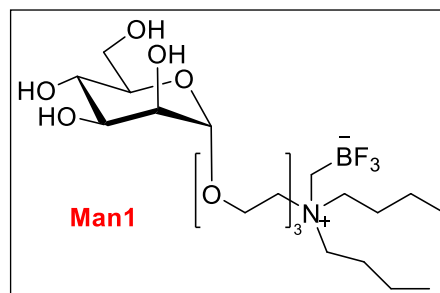


3a.2 (120 mg, 0.19 mmol) reacted according to the general procedure **C** to give **Gal3** (85 mg, 98%) as a white foam.

$[\alpha]^{20}_{\text{D}} = -3.09^{\circ}$ ($c = 1.0$ g/100 mL, methanol).

¹H NMR (400 MHz, CD₃OD) δ 4.27 (d, $J = 7.3$ Hz, 1H, H1), 4.04 (ddd, $J = 9.4, 5.0, 2.7$ Hz, 1H, H1'a linker), 3.96 (dd, $J = 8.9, 4.3$ Hz, 2H, 2H5' linker), 3.85 (dd, $J = 3.1, 0.7$ Hz, 1H, H4), 3.81 – 3.74 (m, 3H, 2H6, H1'b linker), 3.74 – 3.64 (m, 6H, 3CH₂ linker), 3.62 (dd, $J = 9.5, 4.8$ Hz, 2H, 2H6' linker), 3.51 (ddt, $J = 13.5, 7.0, 2.8$ Hz, 3H, H2, H3, H5), 3.43 (t, $J = 5.7$ Hz, 4H, 2 NCH₂CH₂CH₂ piperidine), 2.53 (d, $J = 4.8$ Hz, 2H, NCH₂B), 1.98 – 1.82 (m, 4H, 2 NCH₂CH₂CH₂ piperidine), 1.74 – 1.57 (m, 2H, NCH₂CH₂CH₂ piperidine). **¹³C{¹H} NMR (101 MHz, CD₃OD)** δ 103.73 (CH, C1), 75.30 (CH, C5), 73.53 (CH, C3), 71.12 (CH, C2), 70.08 (CH₂, C linker), 69.96 (CH₂, C linker), 69.84 (CH₂, C linker), 68.88 (CH, C4), 68.32 (CH₂, C1' linker), 64.76 (CH₂, C5' linker), 62.47 (CH₂, 2C, NCH₂CH₂CH₂ piperidine), 61.16 (CH, C6), 60.65 (CH₂, C6' linker), 21.00 (CH₂, NCH₂CH₂CH₂ piperidine), 19.90 (CH₂, 2C, NCH₂CH₂CH₂ piperidine). **¹¹B{¹H} NMR (128 MHz, CD₃OD)** δ 2.02 (d, $J = 42.9$ Hz). **¹⁹F{¹H} NMR (376 MHz, CD₃OD)** δ -139.50 (s). **IR** (neat, cm⁻¹): 3401, 2928, 2878, 2372, 2216, 2168, 2119, 2015, 2037, 1993, 1919, 1747, 1637, 1457, 1367, 1327, 1300, 1229, 1029, 940, 891, 839, 862, 757, 778, 700. **HRMS** (C₁₈H₃₅BF₃NO₈, MW 461.41); found m/z 484.22980 [M+Na]⁺ (vs 484.22331 calculated).

Synthesis of Man1

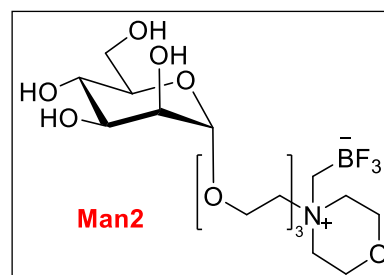


3b (120 mg, 0.17 mmol) reacted according to the general procedure **C** to give **Man1** (74 mg, 87%) as a yellowish solid.

$[\alpha]^{20}_D = +27.88^\circ$ ($c = 1.0$ g/100 mL, methanol).

$^1\text{H NMR}$ (400 MHz, CD_3OD) δ 4.81 (d, $J = 1.6$ Hz, 1H, H1), 3.92 – 3.80 (m, 5H, H2, H6a, H1'a linker, 2H5' linker), 3.76 – 3.55 (m, 11H, H3, H4, H5, H6b, H1'b linker, 3CH₂ liker), 3.54 – 3.48 (m, 2H, 2H6' linker), 3.35 – 3.26 (m, 4H, 2 NCH₂CH₂CH₂CH₃ dibutylamine), 2.44 (dd, $J = 9.2, 4.5$ Hz, 2H, NCH₂B), 1.79 – 1.63 (m, 4H, 2 NCH₂CH₂CH₂CH₃ dibutylamine), 1.45 – 1.33 (m, 4H, 2 NCH₂CH₂CH₂CH₃ dibutylamine), 1.02 (t, $J = 7.4$ Hz, 6H, 2 NCH₂CH₂CH₂CH₃ dibutylamine). **$^{13}\text{C}\{^1\text{H}\}$ NMR (101 MHz, CD_3OD)** δ 100.34 (CH, C1), 73.22 (CH, C5), 71.20 (CH, C3), 70.72 (CH, C2), 70.17 (CH₂, C linker), 70.11 (CH₂, C linker), 70.01 (CH₂, C linker), 67.19 (CH, C4), 66.35 (CH₂, C1' linker), 64.77 (CH₂, C5' linker), 61.56 (CH₂, C6), 61.39 (CH₂, C6' linker), 59.78 (CH₂, 2C, 2 NCH₂CH₂CH₂CH₃ dibutylamine), 23.86 (CH₂, 2C, 2 NCH₂CH₂CH₂CH₃ dibutylamine), 19.38 (CH₂, 2C, 2 NCH₂CH₂CH₂CH₃ dibutylamine), 12.68 (CH₃, 2C, 2 NCH₂CH₂CH₂CH₃ dibutylamine). **$^{11}\text{B}\{^1\text{H}\}$ NMR (128 MHz, CD_3OD)** δ 1.76 (br s). **$^{19}\text{F}\{^1\text{H}\}$ NMR (376 MHz, CD_3OD)** δ -140.35 (s). **IR** (neat, cm^{-1}): 3394, 2960, 2932, 2875, 2107, 1749, 1652, 1541, 1558, 1507, 1459, 1353, 1380, 1302, 1252, 1050, 976, 1003, 883, 806, 719, 737. **HRMS** ($\text{C}_{21}\text{H}_{43}\text{BF}_3\text{NO}_8$, MW 505.41); found m/z 528.2922 [$\text{M}+\text{Na}$]⁺ (vs 528.29261 calculated).

Synthesis of Man2



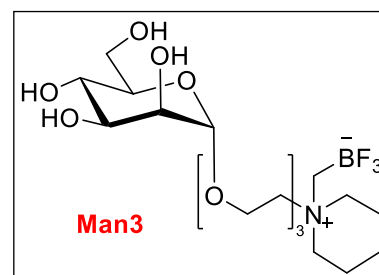
3b.1 (120 mg, 0.19 mmol) reacted according to the general procedure **C** to give **Man2** (85 mg, 97%) as a colorless solid.

$[\alpha]^{20}_D = +29.31^\circ$ ($c = 1.0$ g/100 mL, methanol).

$^1\text{H NMR}$ (400 MHz, CD_3OD) δ 4.83 (d, $J = 1.1$ Hz, 1H, H1), 4.07 – 3.94 (m, 6H, 2H5' linker, 2 NCH₂CH₂O morpholine), 3.84 (m, 3H, H2, H6a, H1'a linker), 3.77 – 3.64 (m, 10H, H3, H6b, 2H6' linker, 3CH₂ liker), 3.65 – 3.60 (m, 3H, H4, H5, H1'b linker), 3.58 – 3.47 (m, 4H, 2 NCH₂CH₂O morpholine), 2.68 (d, $J = 4.6$ Hz, 2H, NCH₂B). **$^{13}\text{C}\{^1\text{H}\}$ NMR (101 MHz, CD_3OD)** δ 100.31 (CH, C1),

73.25 (CH, C5), 71.20 (CH, C3), 70.71 (CH, C2), 70.01 (CH₂, C linker), 70.00 (CH₂, C linker), 69.92 (CH₂, C linker), 67.20 (CH, C4), 66.31 (CH₂, C1' linker), 64.67 (CH₂, C5' linker), 61.53 (CH₂, 2C, C6 and C6' linker), 61.31 (CH₂, 2C, NCH₂CH₂O), 60.56 (CH₂, 2C, NCH₂CH₂O). **¹¹B{¹H} NMR (128 MHz, CD₃OD)** δ 1.92 (d, J = 50.5 Hz). **¹⁹F NMR{¹H} (376 MHz, CD₃OD)** δ -139.42 (s). IR (neat, cm⁻¹): 3383, 2921, 2882, 2108, 1734, 1647, 1559, 1459, 1352, 1300, 1254, 1223, 1125, 1022, 897, 917, 848, 807, 679. HRMS (C₁₇H₃₃BF₃NO₉, MW 463.41); found *m/z* 481.25386 [M+NH₄]⁺ (vs 481.25387 calculated).

Synthesis of Man3

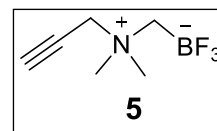


3b.2 (120 mg, 0.19 mmol) reacted according to the general procedure **C** to give **Man3** (83 mg, 94%) as a yellowish solid.

[α]²⁰_D = +16.82° (c = 1.0 g/100 mL, methanol).

¹H NMR (400 MHz, CD₃OD) δ 4.82 (d, J = 1.6 Hz, 1H, H1), 4.00 – 3.92 (m, 2H, 2H5' linker), 3.89 – 3.81 (m, 3H, H2, H6a, H1'a linker), 3.77 – 3.53 (m, 13H, H3, H4, H5, H6b, H1'b linker, 4CH₂ liker), 3.48 – 3.39 (m, 4H, 2 NCH₂CH₂CH₂ piperidine), 2.53 (d, J = 4.7 Hz, 2H, NCH₂B), 1.97 – 1.82 (m, 4H, 2 NCH₂CH₂CH₂ piperidine), 1.73 – 1.59 (m, 2H, NCH₂CH₂CH₂ piperidine). **¹³C{¹H} NMR (101 MHz, CD₃OD)** δ 100.33 (CH, C1), 73.25 (CH, C5), 71.20 (CH, C3), 70.72 (CH, C2), 70.06 (CH₂, C linker), 70.01 (CH₂, C linker), 69.96 (CH₂, C linker), 67.21 (CH, C4), 66.35 (CH₂, C1' linker), 64.79 (CH₂, C5' linker), 62.44 (CH₂, 2C, NCH₂CH₂CH₂ piperidine), 61.57 (CH₂, C6), 60.69 (CH₂, C6' linker), 20.99 (CH₂, NCH₂CH₂CH₂ piperidine), 19.91 (CH₂, 2C, NCH₂CH₂CH₂ piperidine). **¹¹B{¹H} NMR (128 MHz, CD₃OD)** δ 1.99 (d, J = 44.4 Hz). **¹⁹F{¹H} NMR (376 MHz, CD₃OD)** δ -139.57 (s). IR (neat, cm⁻¹): 3383, 2925, 2879, 2106, 1733, 1702, 1652, 1541, 1558, 1507, 1457, 1353, 1301, 1249, 1128, 1026, 941, 891, 834, 807, 678. HRMS (C₁₈H₃₅BF₃NO₈, MW 461.41); found *m/z* 484.2296 [M+Na]⁺ (vs 484. 22331 calculated).

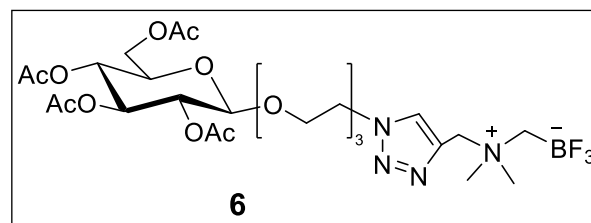
Synthesis of 5



According to the literature procedure, **5** was synthesized starting from the N,N-dimethylpropargylamine (2 mmol, 230 μ L) dissolved in dry diethylether (8 mL, 0.3 M). The iodomethylboronyl pinacolate (2 mmol, 390 μ L) was added dropwise to the solution at room temperature. Almost instantaneously, the alkylated product precipitated from the solution as a yellow solid, and it was isolated through filtration. The crude product was dissolved in an aqueous solution of KHF_2 (10 mmol, 3M, 3,5 mL). The reaction was monitored through TLC (R_f product 0.9 in DCM: MeOH 8:2 – stain KMnO_4) until the complete disappearance of the starting material. The solvent was removed under reduced pressure, and the remaining solid was dissolved in boiling acetone to remove the inorganic salts. The suspension was filtered in a round bottom flask, and the acetone was removed under reduced pressure. The crude product was purified over silica gel (DCM: MeOH 9:1) and gave **5** (280 mg, 80%).

^1H NMR (400 MHz, CD_3OD) δ 4.23 (d, $J = 2.4$ Hz, 2H, CH_2N), 3.39 (t, $J = 2.6$ Hz, 1H, HCC), 3.15 (s, 6H, 2 CH_3), 2.54 (b s, 2H, NCH_2B). **$^{13}\text{C}\{^1\text{H}\}$ NMR (101 MHz, CD_3OD)** δ 80.10 (HCC), 72.38 (HCC), 56.33 (CH_2N), 51.73(2C, CH_3). **$^{11}\text{B}\{^1\text{H}\}$ NMR (128 MHz, CD_3OD)** δ 1.87 (q, $J = 50.6$ Hz). **$^{19}\text{F}\{^1\text{H}\}$ NMR (376 MHz, CD_3OD)** δ -140.65 (q, $J = 98.5, 46.7$ Hz). **IR** (neat, cm^{-1}): 3268, 2991, 2924, 2851, 2130, 1474, 1380, 1349, 1318, 1254, 1233, 1057, 967, 885, 801, 720, 671, 631, 557. **HRMS** ($\text{C}_6\text{H}_{11}\text{BF}_3\text{N}$, MW 164.96); found m/z 188.08299 [$\text{M}+\text{Na}$] $^+$ (vs 188.08289 calculated).

Synthesis of 6

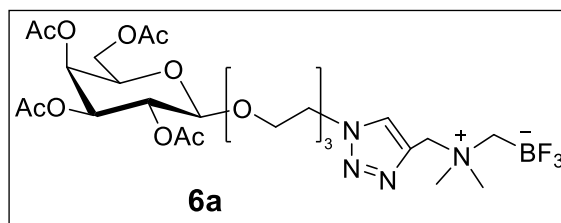


4 (250 mg, 0.49 mmol) reacted with **5** (81 mg, 0.49 mmol) according to the general procedure **D**. Purification over silica gel gave **6** (Rf product 0.6 in DCM: MeOH 95:5) as a white foam (249 mg, 76%).

$[\alpha]^{20}_{\text{D}} = -12.8^{\circ}$ ($c = 1.0$ g/100 mL, chloroform).

^1H NMR (400 MHz, CDCl_3) δ 8.28 (s, 1H, H triazole), 5.23 (t, $J = 9.5$ Hz, 1H, H4), 5.09 (t, $J = 9.7$ Hz, 1H, H3), 4.97 (dd, $J = 9.6, 8.0$ Hz, 1H, H2), 4.68 – 4.54 (m, 5H, H1, 2H6' linker, Triazole $\text{CH}_2\text{N}(\text{CH}_3)_2$), 4.28 (dd, $J = 12.3, 4.6$ Hz, 1H, H6a), 4.15 (dd, $J = 12.3, 2.3$ Hz, 1H, H6b), 3.96 (ddd, $J = 16.4, 8.2, 4.2$ Hz, 1H, H1'a linker), 3.89 (td, $J = 5.3, 2.9$ Hz, 2H, 2H5' linker), 3.80 – 3.69 (m, 2H, H1'b linker, H5), 3.66 – 3.57 (m, 6H, 3 CH_2 linker), 3.15 and 3.13 (2s, 3H each, $\text{N}(\text{CH}_3)_2$), 2.38 (br q, $J = 4.2$ Hz, 2H, NCH_2B), 2.09, 2.03, 2.01, 2.007 (4s, 3H each, CH_3). **$^{13}\text{C}\{^1\text{H}\}$ NMR (101 MHz, CDCl_3)** δ 170.72 (C, C=O), 170.30 (C, C=O), 169.49 (C, C=O), 169.46 (C, C=O), 136.20 (C, C triazole), 129.02 (CH triazole), 100.81 (CH, C-1), 72.80 (CH, C-4), 71.73 (CH, C-5), 71.33 (CH, C-2), 70.67 (CH_2 , C linker), 70.51 (CH_2 , C linker), 70.13 (CH_2 , C linker), 69.39 (CH_2 , C1' linker), 69.09 (CH_2 , C5' linker), 68.39 (CH, C-3), 61.92 (CH_2 , C6), 59.85 (CH_2 , C6' linker), 54.44 (CH_3 , 2C, $\text{N}(\text{CH}_3)_2$), 50.55 (CH_2 , Triazole CH_2N), 20.76 (CH_3), 20.65 (2C, CH_3), 20.61 (CH_3). **$^{11}\text{B}\{^1\text{H}\}$ NMR (128 MHz, CDCl_3)** δ 1.84 (br s). **$^{19}\text{F}\{^1\text{H}\}$ NMR (376 MHz, CDCl_3)** δ -138.71 (s). **IR** (neat, cm^{-1}): 2942, 2941, 1743, 1217, 1031. **HRMS** ($\text{C}_{26}\text{H}_{42}\text{BF}_3\text{N}_4\text{O}_{12}$, MW 670.44); found m/z 693.27295 [$\text{M}+\text{Na}$] $^+$ (vs calculated 693.27366).

Synthesis of 6a

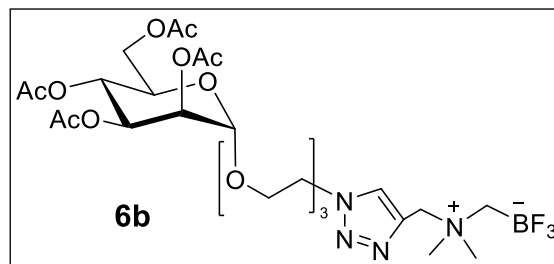


4a (249 mg, 0.49 mmol) reacted with **5** (81 mg, 0.49 mmol) according to the general procedure **D**. Purification over silica gel gave **6a** (Rf product 0.6 in DCM: MeOH 95:5) as a white foam (309 mg, 94%).

$[\alpha]_D^{20} = -9.57^\circ$ ($c = 1.0$ g/100 mL, chloroform).

$^1\text{H NMR}$ (400 MHz, CDCl_3) δ 8.29 (s, 1H, H triazole), 5.40 (d, $J = 2.7$ Hz, 1H, H4), 5.17 (dd, $J = 10.5, 7.9$ Hz, 1H, H2), 5.06 (dd, $J = 10.4, 3.4$ Hz, 1H, H3), 4.63 (t, $J = 5.0$ Hz, 2H, 2H6' linker), 4.61 – 4.57 (m, 3H, H1, Triazole $\text{CH}_2\text{N}(\text{CH}_3)_2$), 4.16 (ddd, $J = 25.7, 11.2, 6.7$ Hz, 2H, 2H6), 4.00 – 3.94 (m, 2H, H5, H1'a linker), 3.90 (td, $J = 5.4, 2.6$ Hz, 2H, 2H5' linker), 3.78 – 3.71 (m, 1H, H1'b linker), 3.66 – 3.58 (m, 6H, 3 CH_2 linker), 3.14 and 3.13 (2s, 3H each, $\text{N}(\text{CH}_3)_2$), 2.38 (br q, $J = 4.2$ Hz, 2H, NCH_2B), 2.14 (s, 3H, CH_3), 2.05 (s, 3H, CH_3), 2.03 (s, 3H, CH_3), 1.99 (s, 3H, CH_3). **$^{13}\text{C}\{^1\text{H}\}$ NMR (101 MHz, CDCl_3)** δ 170.46 (C, C=O), 170.26 (C, C=O), 170.15 (C, C=O), 169.57 (C, C=O), 136.19 (C, C triazole), 129.02 (CH, CH triazole), 101.34 (CH, C1), 70.82 (CH, C3), 70.66 (CH_2 , C linker), 70.64 (CH, C5), 70.52 (CH_2 , C linker), 70.15 (CH_2 , C linker), 69.36 (CH_2 , C1' linker), 69.11 (CH_2 , C5' linker), 68.93 (CH, C2), 67.12 (CH, C4), 61.22 (CH_2 , C6), 59.93 (CH_2 , Triazole CH_2N), 54.37 (CH_3 , 2C, $\text{N}(\text{CH}_3)_2$), 50.56 (CH_2 , C6' linker), 20.76 (CH_3), 20.70 (CH_3), 20.65 (CH_3), 20.60 (CH_3). **$^{11}\text{B}\{^1\text{H}\}$ NMR (128 MHz, CDCl_3)** δ 1.87 (br s). **$^{19}\text{F}\{^1\text{H}\}$ NMR (376 MHz, CDCl_3)** δ -138.93 (s). **IR** (neat, cm^{-1}): 2929, 1742, 1218, 1038. **HRMS** ($\text{C}_{26}\text{H}_{42}\text{BF}_3\text{N}_4\text{O}_{12}$, MW 670.44); found m/z 693.27342 [$\text{M}+\text{Na}$] $^+$ (vs calculated 693.27366).

Synthesis of 6b

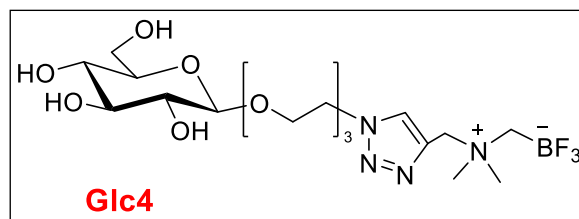


4b (220 mg, 0.44 mmol) reacted with **5** (73 mg, 0.44 mmol) according to the general procedure **D**. Purification over silica gel gave **6b** (Rf product 0.6 in DCM: MeOH 95:5) as a white foam (253 mg, 86%).

$[\alpha]_D^{20} = +24.8^\circ$ ($c = 1.0$ g/100 mL, chloroform).

$^1\text{H NMR}$ (400 MHz, CDCl_3) δ 8.24 (s, 1H, H Triazole), 5.33-5.26 (m, 2H, H4, H3), 5.23 (m, 1H, H2), 4.87 (d, $J = 1.3$ Hz, 1H, H1), 4.62 (t, $J = 4.8$ Hz, 2H, 2H6' linker), 4.57 (s, 2H, Triazole- $\text{CH}_2\text{N}(\text{CH}_3)_2$), 4.26 (dd, $J = 12.2, 5.0$ Hz, 1H, H6a), 4.10 (dd, $J = 12.3, 2.3$ Hz, 1H, H6b), 4.06 – 4.00 (m, 1H, H5), 3.91 (t, $J = 4.8$ Hz, 2H, 2H5' linker), 3.83 – 3.75 (m, 1H, H1'a linker), 3.70 - 3.65 (m, $J = 8.9, 4.5$ Hz, 1H, H1'b linker), 3.65 – 3.58 (m, 6H, 3 CH_2 linker), 3.11 (s, 6H, $\text{N}(\text{CH}_3)_2$), 2.36 (br q, $J = 4.4$ Hz, 2H, NCH_2B), 2.14 (s, 3H, CH_3), 2.09 (s, 3H, CH_3), 2.03 (s, 3H, CH_3), 1.97 (s, 3H, CH_3). **$^{13}\text{C}\{^1\text{H}\}$ NMR (101 MHz, CDCl_3)** δ 170.73 (C, C=O), 170.16 (C, C=O), 170.10 (C, C=O), 169.73 (C, C=O), 136.16 (C, C triazole), 128.96 (CH, CH triazole), 97.62 (CH, C1), 70.67 (CH_2 , C linker), 70.61 (CH_2 , C linker), 69.95 (CH_2 , C linker), 69.49 (CH, C2), 69.18 (CH, C4)*, 69.17 (CH_2 , C5' linker), 68.45 (CH, C5), 67.29 (CH_2 , C1' linker), 66.08 (CH, C3)*, 62.42 (CH_2 , C6), 59.90 (CH_2 , Triazole CH_2N), 54.40 (CH_3 , 2C, $\text{N}(\text{CH}_3)_2$), 50.61 (CH_2 , C6' linker), 20.91 (CH_3), 20.77 (CH_3), 20.72 (2C, CH_3). *May be interchanged. **$^{11}\text{B}\{^1\text{H}\}$ NMR (128 MHz, CDCl_3)** δ 1.79 (s). **$^{19}\text{F}\{^1\text{H}\}$ NMR (376 MHz, CDCl_3)** δ -138.74 (s). **IR** (neat, cm^{-1}): 2916, 1740, 1220, 1036. **HRMS** ($\text{C}_{26}\text{H}_{42}\text{BF}_3\text{N}_4\text{O}_{12}$, MW 670.44); found m/z 693.27318 $[\text{M}+\text{Na}]^+$ (vs calculated 693,27366).

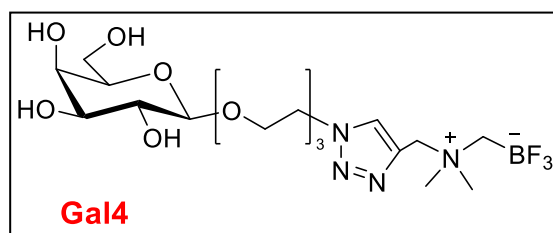
Synthesis of Glc4



Compound **6** (249 mg, 0.37 mmol) reacted according to the general procedure **C** to give **Glc4** (185 mg, 99%) as a white foam. $[\alpha]^{20}_D = -9.6^\circ$ ($c = 1.0$ g/100 mL, methanol).

^1H NMR (400 MHz, CD_3OD) δ 8.36 (s, 1H, H triazole), 4.68 (br t, $J = 5.0$ Hz, 2H, 2H6' linker), 4.60 (s, 2H, Triazole $\text{CH}_2\text{N}(\text{CH}_3)_2$), 4.33 (d, $J = 7.8$ Hz, 1H, H1), 4.04 – 3.97 (m, 1H, H1'a linker), 3.94 (b t, $J = 5.0$ Hz, 2H, 2H5' linker), 3.89 (br d, $J = 11.8$ Hz, 1H, H6a), 3.76 – 3.62 (m, 9H, H1'b linker, H6b, H5, 3 CH_2 linker), 3.41 – 3.36 (m, 1H, H3), 3.32 – 3.28 (m, 1H, H4), 3.20 (dd, $J = 9.0, 7.8$ Hz, 1H, H2), 3.08 (s, 6H, $\text{N}(\text{CH}_3)_2$), 2.39 (q, $J = 4.7$ Hz, 2H, NCH_2B). **$^{13}\text{C}\{^1\text{H}\}$ NMR (101 MHz, CD_3OD)** δ 136.41 (C, C triazole), 128.84 (CH, CH triazole), 103.04 (CH, C1), 76.57 (CH, 2C, C4, C3), 73.70 (CH, C2), 70.24 (CH, C5), 70.02 (CH_2 , 2C, C linker), 69.98 (CH_2 , C linker), 68.81 (CH_2 , C5' linker), 68.29 (CH_2 , C1' linker), 61.36 (CH_2 , C6), 60.10 (CH_2 , Triazole CH_2N), 52.25 (CH_3 , 2C, $\text{N}(\text{CH}_3)_2$), 50.22 (CH_2 , C6' linker). **$^{11}\text{B}\{^1\text{H}\}$ NMR (128 MHz, CD_3OD)** δ 2.09 (s). **$^{19}\text{F}\{^1\text{H}\}$ NMR (376 MHz, CD_3OD)** δ -139.31 (s). **IR** (neat, cm^{-1}): 3387, 2879, 1639, 1030, 969. **HRMS** ($\text{C}_{18}\text{H}_{34}\text{BF}_3\text{N}_4\text{O}_8$, MW 502.29); found m/z 525.23151 [$\text{M}+\text{Na}$] $^+$ (vs calculated 525.23140).

Synthesis of Gal4

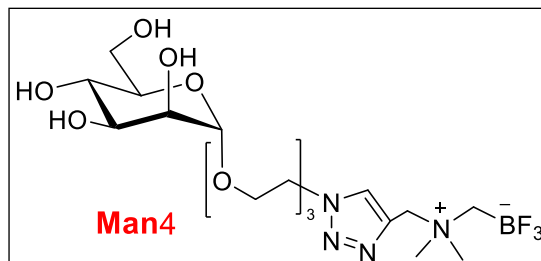


6a (309 mg, 0.46 mmol) reacted according to the general procedure for **C** to give **Gal4** (231 mg, 98%) as a white foam. $[\alpha]^{20}_D = -4.7^\circ$ ($c = 1.0$ g/100 mL, methanol).

^1H NMR (400 MHz, CD_3OD) δ 8.37 (s, 1H, H triazole), 4.71 – 4.65 (br t, $J = 5.0$ Hz, 2H, 2H6'), 4.61 (s, 2H, Triazole $\text{CH}_2\text{N}(\text{CH}_3)_2$), 4.28 (d, $J = 7.3$ Hz, 1H, H1), 4.05 – 3.98 (m, 1H, H1'a linker), 3.96 – 3.92 (br t, $J = 5.0$ Hz, 2H, 2H5' linker), 3.85 (dd, $J = 2.8, 0.8$ Hz, 1H, H4), 3.81 – 3.61 (m, 9H, 2H6, H1'b linker, 3 CH_2 linker), 3.53 (m, 3H, H2, H3, H5), 3.08 (s, 6H, $\text{N}(\text{CH}_3)_2$), 2.40 (br q, 4.5 Hz, 2H, NCH_2B). **$^{13}\text{C}\{^1\text{H}\}$ NMR (101 MHz, CD_3OD)** δ 136.40 (C, C triazole), 128.88 (CH, CH triazole), 103.71 (CH, C1), 75.49, 73.32, 71.16 (CH, 3C, C2, C3, C5), 70.01 (CH_2 , 2C, C linker), 69.95 (CH_2 , C linker), 68.90 (CH, C4), 68.79 (CH_2 , C5' linker), 68.28 (CH_2 , C1' linker), 61.18 (CH_2 , C6), 60.22 (CH_2 , Triazole CH_2N), 52.20 (CH_3 , 2C, $\text{N}(\text{CH}_3)_2$), 50.22 (CH_2 , C6' linker). **^{11}B NMR $\{^1\text{H}\}$ (128 MHz, CD_3OD)** δ 2.25 (s). **$^{19}\text{F}\{^1\text{H}\}$**

NMR (376 MHz, CD₃OD) δ -139.52 (s). **IR** (neat, cm⁻¹): 3378, 2918, 1331, 1027, 970. **HRMS** (C₁₈H₃₄BF₃N₄O₈, MW 502.29); found m/z 525.23166 [M+Na]⁺ (vs calculated 525.23140).

Synthesis of Man4



6b (250 mg, 0.37 mmol) reacted according to the general procedure **C** to give **Man4** (187 mg, 99%) as a white foam.

$[\alpha]_D^{20} = +24.68^\circ$ ($c = 1.0$ g/100 mL, methanol).

¹H NMR (400 MHz, CD₃OD) δ 8.34 (s, 1H, H Triazole), 4.82 (d, $J = 1.6$ Hz, 1H, H1), 4.68 (t, $J = 4.9$ Hz, 2H, 2H6' linker), 4.60 (s, 2H, TriazoleCH₂N(CH₃)₂), 3.94 (t, $J = 5.0$ Hz, 2H, 2H5' linker), 3.87 – 3.79 (m, 3H, H2, H6a, H1'a linker), 3.75 – 3.68 (m, 2H, H6b, H3), 3.66 – 3.55 (m, 9H, H2, H5, 3CH₂ linker, H1'b linker), 3.08 (s, 6H, N(CH₃)₂), 2.38 (q, $J = 4.6$ Hz, 2H, NCH₂B). **¹³C{¹H} NMR (101 MHz, CD₃OD)** δ 137.93 (C, C Triazole), 130.28 (CH, CH Triazole), 101.82 (CH, C1), 74.76 (CH, C5), 72.71 (CH, C3), 72.24 (CH, C2), 71.68 (CH₂, C linker), 71.64 (CH₂, C linker), 71.51 (CH₂, C linker), 70.43 (CH₂, C5' linker), 68.76 (CH, C4), 67.81 (CH₂, C1' linker), 63.08 (CH₂, C6), 61.56 (CH₂, triazoleCH₂N), 53.79 (CH₃, 2C, N(CH₃)₂), 51.77 (CH₂, C6' linker) **¹¹B{¹H} NMR (128 MHz, CD₃OD)** δ 1.86 (s). **¹⁹F{¹H} NMR (376 MHz, CD₃OD)** δ -139.41 (s). **IR** (neat, cm⁻¹): 3365, 2923, 1331, 1021, 927. **HRMS** (C₁₈H₃₄BF₃N₄O₈, MW 502.29); found m/z 525.23170 [M+Na]⁺ (vs calculated 525.23140).

1.2 Biology

1.2.1 Cell culture

The human primary fibroblasts (ATCC; American Type Culture Collection, Manassas, VA, USA) were isolated from abdominal skin biopsy of a healthy 52 years-old woman. Fibroblasts were cultured in fibroblast basal medium supplemented with 2% fetal bovine serum (FBS), 5 ng/mL recombinant human (rh) fibroblast growth factor (FGF) b, 7.5 mM L-glutamine, 50 µg/mL ascorbic acid, 1 µg/mL hydrocortisone hemisuccinate, 5 µg/mL rh insulin, and cultured in a humidified incubator (5% CO₂, 37 °C).

1.2.2 Cell viability assay

Cell viability was measured by the 3-(4,5-dimethylthiazol-2-yl)-2,5- diphenyl-tetrazolium bromide (MTT) assay, as previously described.¹⁹⁷ Fibroblasts were seeded (5 x 10³ cells/ well) in 96-well plates in complete medium. After 24 h, fibroblasts were treated with increasing concentrations (0.001–1 mM) of test compounds (**Glc1-4**, **Gal1-4**, and **Man1-4**) for 24-72 h at 37 °C in a 5% CO₂ humidified incubator. The percentage of cell viability was calculated as $[100 (x-y) / (z-y)]$, where x, y, and z were the absorbance read in compound-treated, resting, and compound-untreated cells, respectively. Results are expressed as mean ± SD of at least three experiments run in triplicate.

1.3 Stability evaluation

2 mg of the compound was dissolved in 900 μL of phosphate buffer 0.2M, then 100 μL of D_2O was added. The sample was transferred into an NMR test tube, and the ^{19}F NMR spectra were acquired at the given times (320 scans, 295 K). Between the acquisitions, the samples were stored at room temperature.

1.3.1 ^{19}F NMR kinetic analysis for Glc1

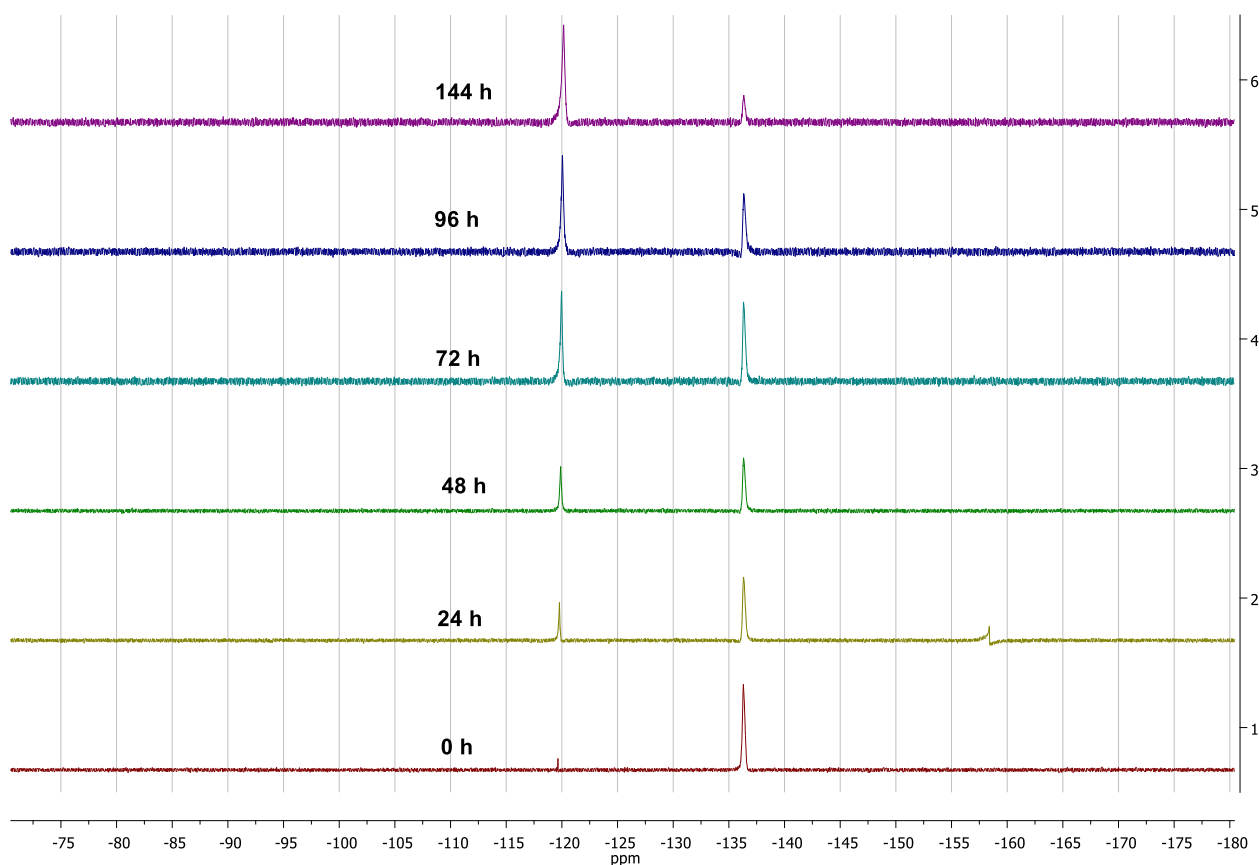
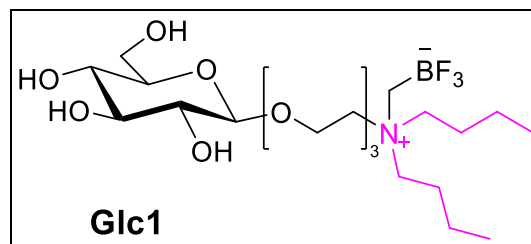


Figure 1 – ^{19}F -NMR spectra (^{19}F :- 121 ppm, Glc1: -136 ppm)

1.3.2 ^{19}F NMR kinetic analysis for Glc2

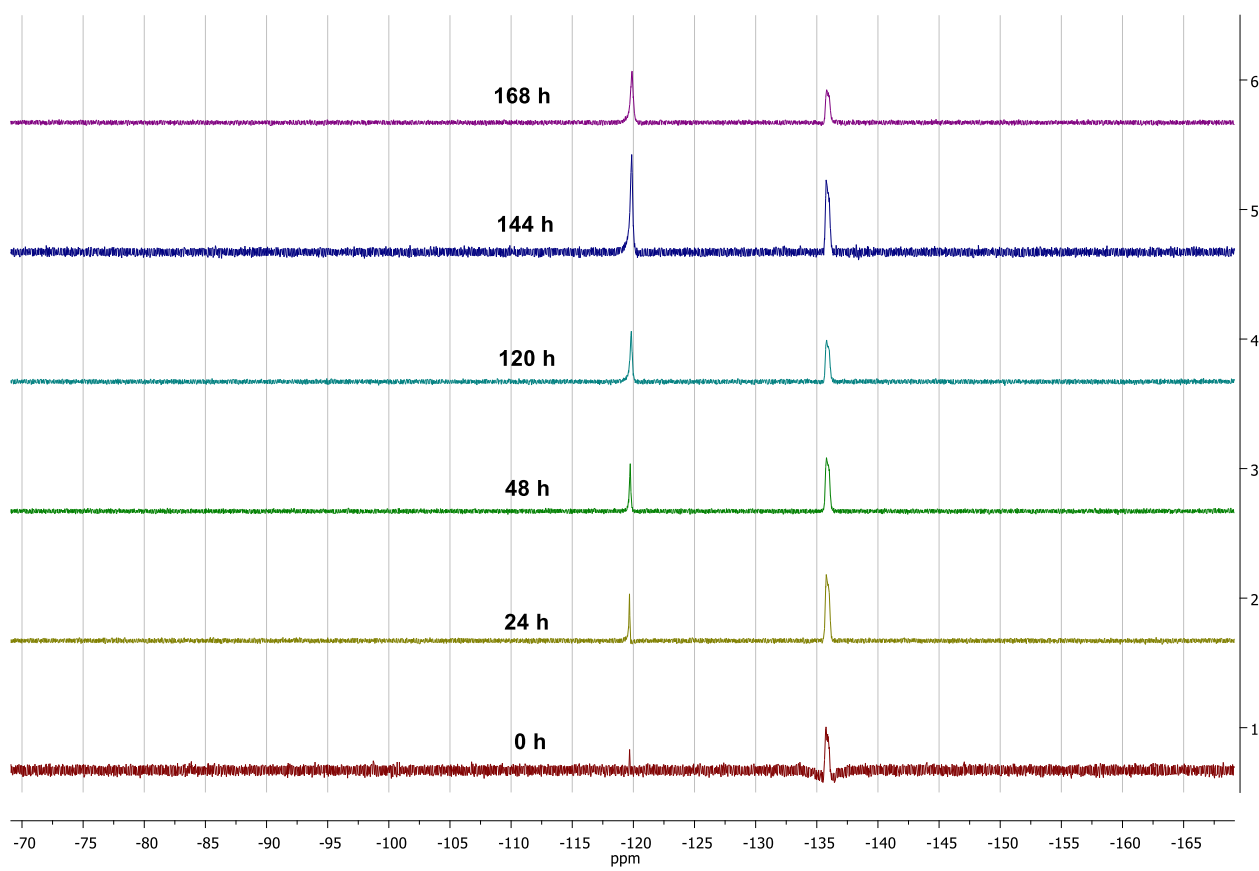
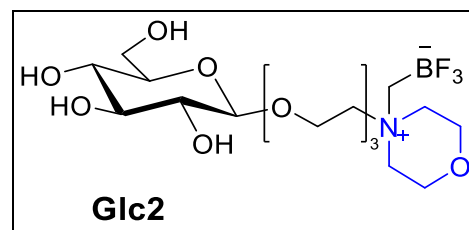


Figure 2 – ^{19}F -NMR spectra (^{19}F :-121 ppm, Glc2: -136 ppm)

1.3.3 ^{19}F NMR kinetic analysis for Glc3

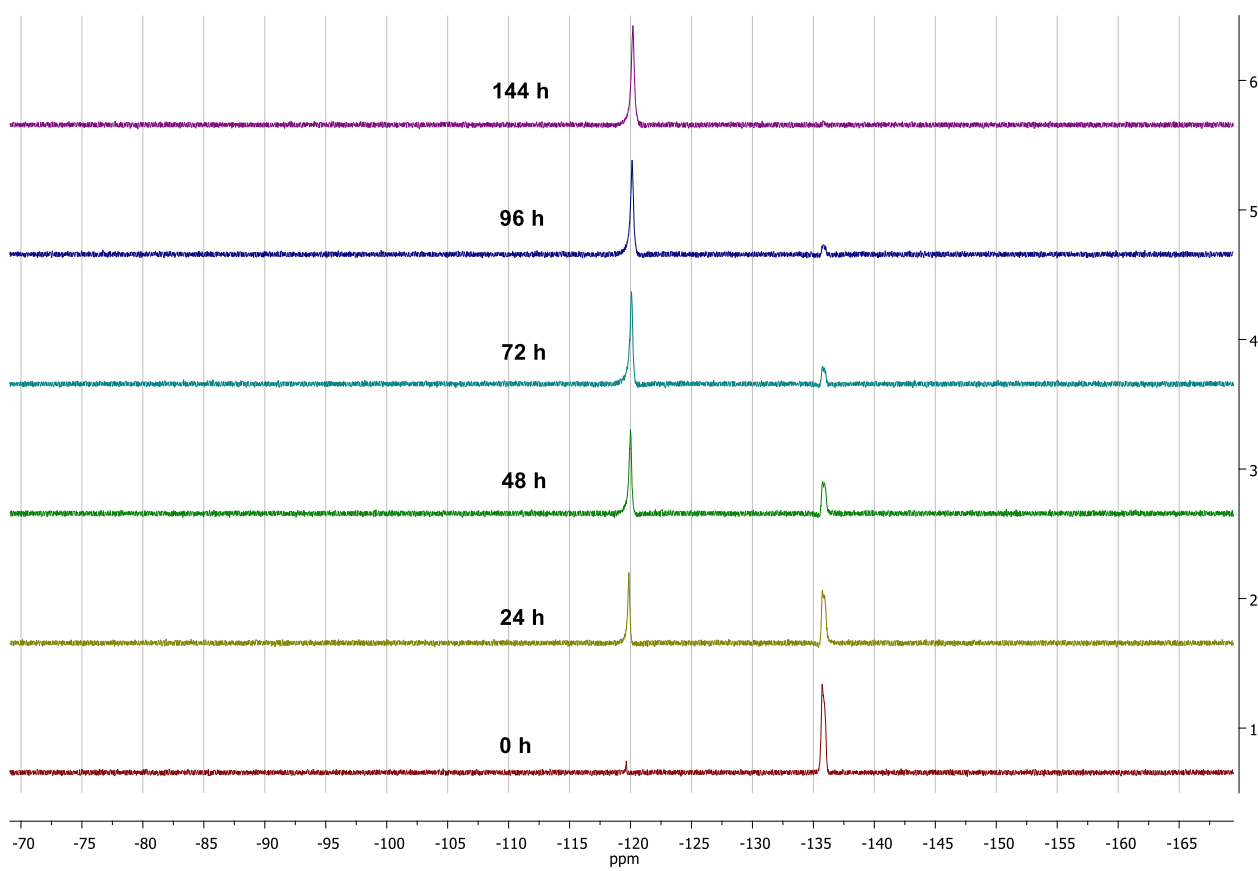
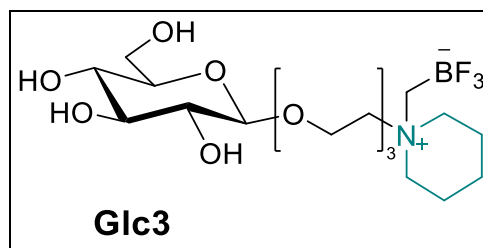


Figure 3 - ^{19}F -NMR spectra (^{19}F :-121 ppm, Glc3: -136 ppm)

1.3.4 ^{19}F NMR kinetic analysis for Glc4

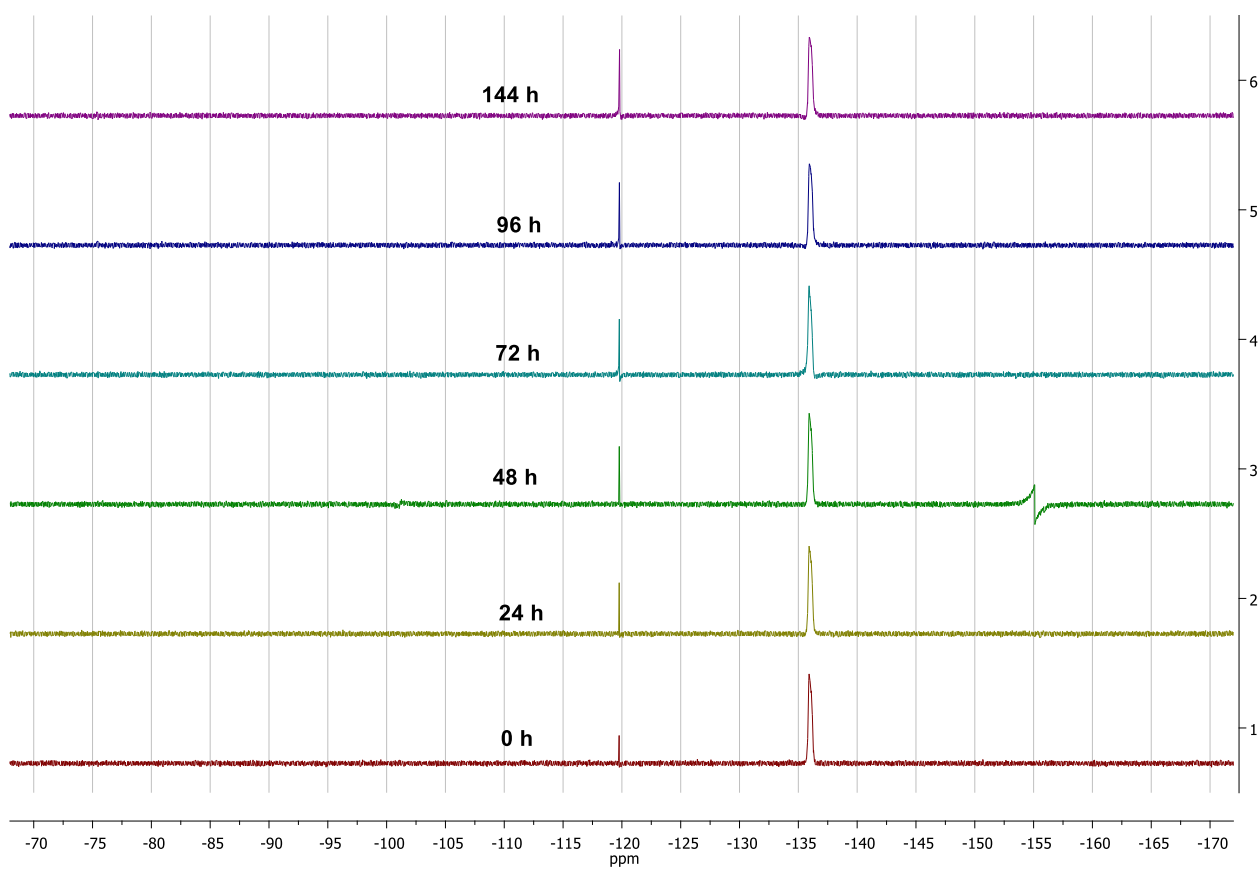
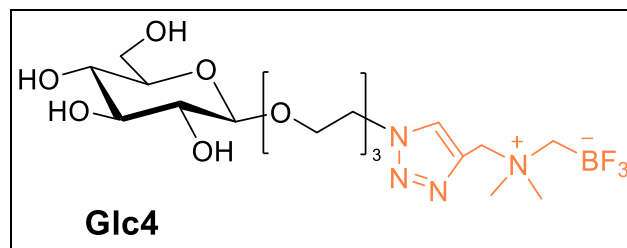


Figure 4 - ^{19}F -NMR spectra (^{19}F :-121 ppm, Glc4: -136 ppm)

1.3.5 ^{19}F NMR Kinetic analysis for Man3

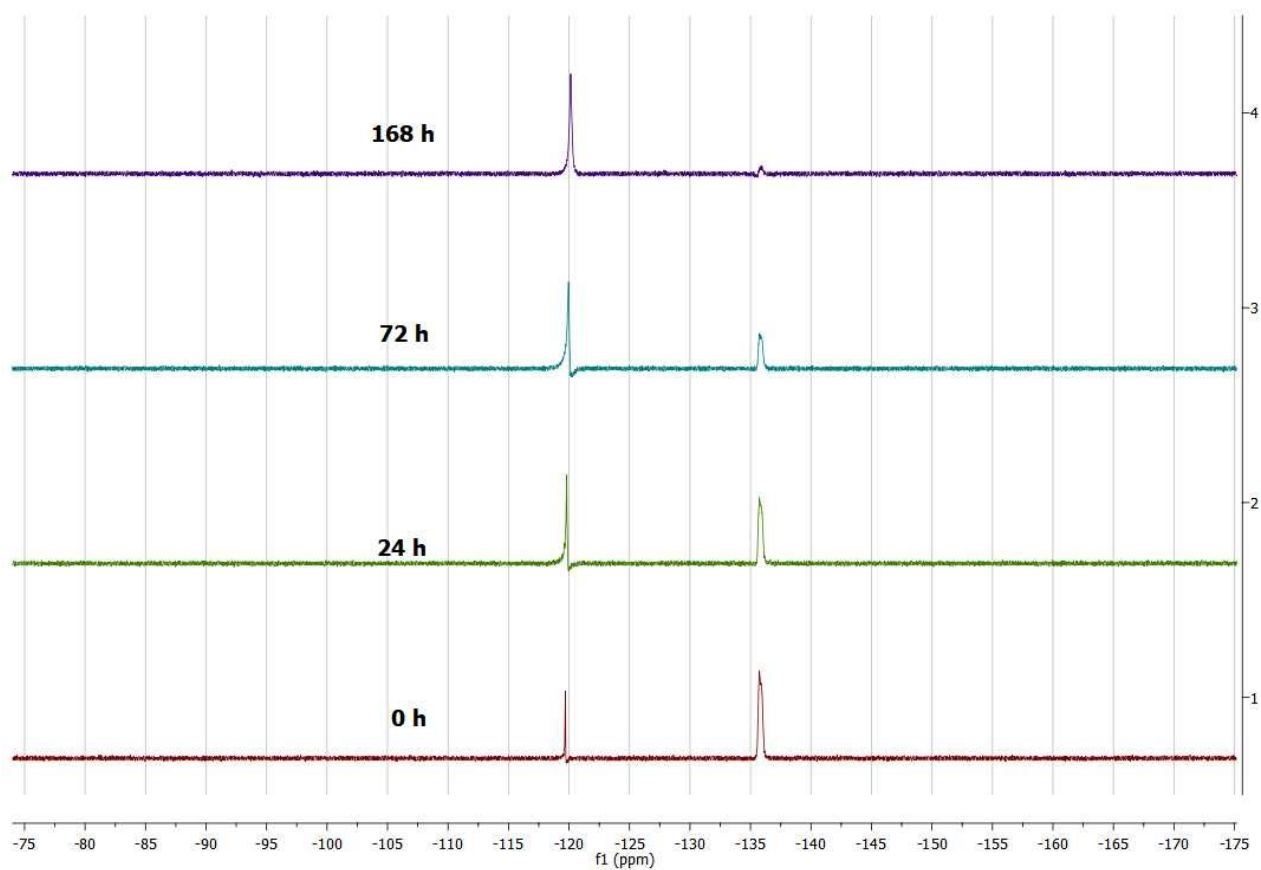
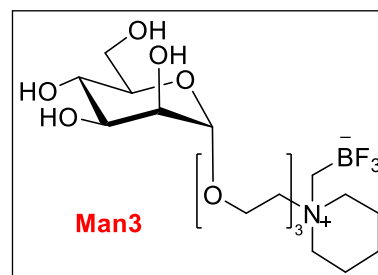


Figure 5 - ^{19}F -NMR spectra (^{19}F :-: -121 ppm, Man3: -136 ppm)

1.4 ¹⁸F radiolabeling and stability studies

1.4.1 General

[¹⁸F]F⁻ was produced in a Cyclone 18/18 MeV cyclotron (IBA, Belgium) by the nuclear reaction ¹⁸O (p,n)¹⁸F. For radiolabeling procedure, [¹⁸F]F⁻ was used directly as obtained from cyclotron or was retained in a QMA 130 mg sorbent cartridge (Waters, USA) preconditioned with NaHCO₃ (5 ml, 0.5 M) and water for injection (5 ml) or in a PS-HCO₃ Chromafix small cartridge (Macherey-Nagel, Germany), previously preconditioned absolute ethanol (1 ml) followed by water for injection (1 ml). When retention of [¹⁸F]F⁻ was applied in the QMA cartridge, elution was made with 0.1 ml of saline and when using the Chromafix cartridge, elution was made with 0.5 ml of a saline and 10% HCl 0.5M to obtain an acidified [¹⁸F] solution with a pH of 2.0 in the radiolabeling reaction mixture and a radioactive concentration of 37 MBq/μL.

1.4.2 Radiolabeling with [¹⁸F]⁻ and solid precursor.

For radiolabeling, 50 μL of [¹⁸F]⁻ (1.85 – 2.22 GBq) was added to 500 nmol of the solid precursor placed on a spatula tip, and pH was adjusted to 2.0 using HCl 0.5M in a 1.5 ml Eppendorf tube. A water-bath with a magnetic stirrer at the bottom, was used for incubation at 40 and 85 °C with the Eppendorf tube closed and placed in a vertical manner inside the bath. At defined period of times, different 1.5 μL aliquots were taken with a micropipette for evaluation of the radiolabeling efficiency and radiolabeling kinetics. These aliquots were analyzed using a radio-TLC method (SilicaGel60 F254 (Merck, Spain) as stationary phase and acetonitrile/water 95:5 as mobile phase) in an appropriate qualified radio-TLC equipment (miniGITA Single, Elysia Raytest, Germany). The reaction time and temperature were optimized using the radiolabeling kinetics data.

After reaction time, quenching and dilution was made by adding 0.5 ml of saline to the reaction mixture. The mixture was passed through a preconditioned Alumina N cartridge (Sep-Pak Alumina N Plus Light Cartridge 280mg sorbent, Waters, USA) with water for injection (10 ml), for purification of the radiolabeled molecule from free [¹⁸F]⁻. Radiolabeling purity was analyzed using the radio-TLC method described previously and pH was measured using pH-strips.

1.4.3 Radiolabeling with [¹⁸F]⁻ and solid precursor

We investigated the suitability of the radiolabeling reaction using the precursor dissolved in saline, so we may be able to reproduce it using a semi-automated module. We dissolved 500 nmol of each precursor in 30 μ L of saline and we mixed it with a solution of [¹⁸F] F⁻ obtained from cyclotron (1.85 - 2.22 GBq, previously trapped in a preconditioned QMA cartridge and eluted with 0.1 ml of saline). HCl 0.5M was added to reduce pH and the mixture was heated to 40 or 85 °C, taking different aliquots for radio-TLC analysis at different times. No purification was made when the manually procedure was applied. For semi-automatic procedure, we used a TracerLAB FX-FN synthesis module (GE, USA), and we purified our product using a preconditioned Alumina N cartridge.

1.4.4 Radiolabeling with acidified [¹⁸F]⁻ and solid precursor

For radiolabeling, 50 μ L of acidified [¹⁸F]⁻ solution (1.85 - 2.22 GBq) was added to 500 nmol of the solid precursor placed on a spatula tip in a 1.5 ml Eppendorf tube, and pH was measured to assure that pH was 2.0. Incubation was made at 85 °C in a similar water-bath that was used when radiolabeling was made with [¹⁸F] obtained from cyclotron. Different aliquots were taken with a micropipette for evaluation of the radiolabeling efficiency and kinetics. These aliquots were analyzed using the same radio-TLC method as used for [¹⁸F]⁻ (**Figure 6**). Dilution and purification were made in the same way as used for [¹⁸F]⁻ and pH was measured with pH-strips, prior to injection.

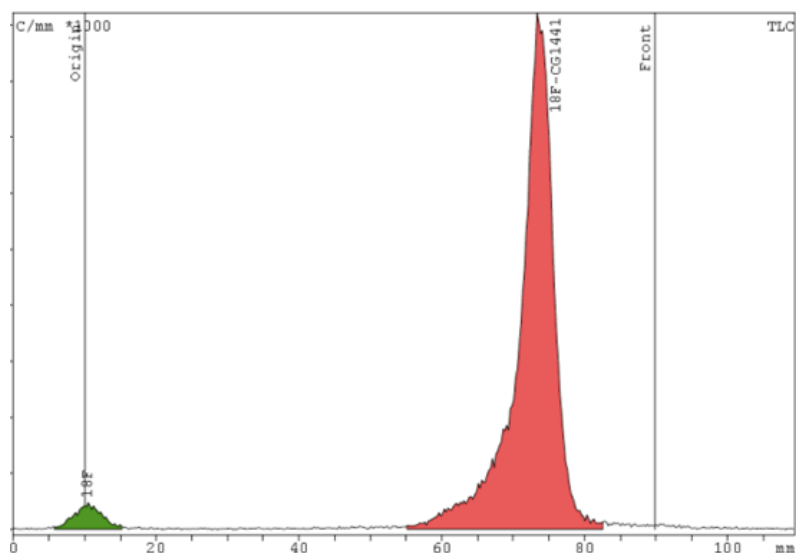


Figure 6 – Example of $[^{18}\text{F}]$ Glc1 radio-TLC after Alumina N purification. The radiolabeling was performed using acidified $[^{18}\text{F}]$ -fluorine method. In the origin of the strip, $[^{18}\text{F}]$ -fluorine appeared with $R_f=0$, while $[^{18}\text{F}]$ Glc1 appeared with $R_f=0.8$.

1.4.5 Stability in vitro studies

Radiolabeling stability studies were performed in saline and human plasma, in a water bath under agitation at 37 °C. An aliquot of 60 μL of the recently purified radiolabeled compound was diluted in 100 μL of saline or human plasma in a 1.5 ml Eppendorf tube, placed in a vertical manner inside the water bath. At defined period of times, an aliquot of this incubation was extracted with a micropipette for analysis, using the radio-TLC method described previously, and stability was studied for up to 120 minutes.

1.5 In vivo PET imaging

All animal experiments were conducted according to a local Ethical Committee of University of Seville (permit number CEEA-US2022-02). 8 weeks old BalbC female mice were not put to fast before PET experiments, as we specifically wanted to obtain [¹⁸F]FDG related signal in the heart and in the brain together. They were maintained in 12/12 hours dark/light cycle and given water and standardized food ad libitum. Mice weighting 18-22 g were anesthetized with 2% isoflurane in medicinal oxygen. They were introduced the 30G catheter in the tail vein and injected with radiotracer for static PET experiments. For dynamic experiments, the injection was done in the PET scanner (Mosaic, Philips, Eindhoven, Netherlands). The animals for static experiments were awakened and maintained on the heated pad in the cage for 45 min. Then they were anesthetized again and placed on a bed heated to 32 °C (Minerve, Esternay, France) for a 10 min static scan. For dynamic 2-hour scan, the animals were injected into the PET scanner.

The PET acquisition was done to receive 1x1x1 mm images of 100 mm length and 128 mm diameter. After PET scan, the bed was transferred without moving the animal to NanoCT system (Mediso, Budapest, Hungary) for anatomical image. The scans were done at 45 kVp voltage with 240 projections and 500 ms exposition per projection. The images were reconstructed with filtered back projection method at 0.2 mm pixel resolution. The PET images were fused in PMOD software version 4.3 (PMOD Technologies LLC, Zurich, Switzerland, subsidiary of Bruker Preclinical Imaging). PET and CT images were analyzed in the same PMOD 4.3.

2. Organotrifluoroborate Sugar Conjugates – part II

2.1 Chemistry

2.1.1 General

Compounds **7**^{177,178}, **12**¹⁸¹, and **13**¹⁸² were obtained following literature procedures, and their characterizations matched what reported in the literature. All reagents and solvents were purchased from Sigma-Aldrich (Milan) and used as supplied without further purification unless otherwise stated. Thin-layer chromatography was performed on silica gel plates with a fluorescent indicator (Merck, Milan) and visualized at the UV light (254 nm) and/or by staining in ceric ammonium molybdate or sulfuric acid solution (5% in methanol). Anhydrous dimethylformamide (DMF), methanol (MeOH), and acetonitrile (CH₃CN) were obtained using activated molecular sieves 0.3 nm. Diethyl ether (Et₂O) and tetrahydrofuran (THF) were purchased as anhydrous solvents and used as supplied. Dichloromethane (DCM) was refluxed with calcium hydride, then distilled.

All reactions (if not specifically containing water as reactant, solvent, or co-solvent) were performed under a nitrogen or argon atmosphere. Flash column chromatography was performed with 230–400 mesh silica gel (Merck, Milan).

NMR spectra were recorded using a Bruker Avance Neo 400 MHz spectrometer (Bruker, Italy) or Bruker FT-NMR AVANCE DRX500 (Bruker, Italy). Singlets are presented as parts per million (ppm), and the resonance multiplicities are identified as “s” (singlet), “d” (doublet), “t” (triplet), “q” (quartet), or “m” (multiplet). Broad resonances are indicated as “br”. ¹³C and ¹⁹F experiments were recorded with proton NMR decoupling. The carbon atoms bound to boron are usually not detectable.

The ¹¹B-¹⁹F coupling constant varies remarkably with the concentration, the ligands bound to the boron nuclei, the symmetry of the molecule, and the type of solvent. It can be well appreciated in small and symmetric molecules, while it is negligible in larger compounds^{195,196}.

¹¹B nuclear spin is 3/2, so the ¹⁹F spectrum shows one resonance signal with four peaks. Instead, ¹⁹F nuclear spin is 1/2, so the ¹¹B spectrum shows one resonance signal with four peaks due to the three fluorine atoms¹⁹⁹.

Mass spectrometry analysis was recorded on a Thermo Scientific Q-Exactive Plus; data were acquired and processed using Xcalibur® software. Optical rotations were measured on a JASCO P1010 polarimeter at 20 °C or on Anton Paar Polarimeter at 25°C. Infrared Spectroscopy was performed using a Bruker Alpha II FTIR.

2.1.2 Abbreviations

DCM = Dichloromethane

H = Hexane

EA = Ethyl Acetate

TEA = Triethylamine

AgOTf = silver triflate

DMF = dimethylformamide

2.1.3 General Procedures

General procedure E: Nucleophilic substitution with thiols to obtain compounds **8.**

Potassium carbonate (0.9 eq respect to the thiol) was added to a solution of the thiol of choice (from 2 to 8 eq.) in dry acetonitrile (0.8 M) and stirred for 2h at r.t. Then, a solution of **1** (1eq) in dry acetonitrile (0.1M) was added to the suspension and the reaction was heated 80°C until the disappearance of starting material in TLC. Eventually, the reaction was diluted with CH₃CN and filtered over a Hirsh funnel to remove the solid. The evaporation of the solvent gave the crude product that was purified through silica gel column chromatography.

General procedure F: Synthesis of the stable trifluoroborate group in compounds **9.**

The iodomethylboronyl pinacolate (from 1.2 to 1.8 eq.) was added dropwise to a solution of AgOTf (from 1.1 to 1.5 eq.) in dry acetonitrile (0.15M) and stirred for 20 minutes. Then, this solution was added dropwise to a solution of **8** (1 eq.) in dry acetonitrile (0.1 M) cooled at 0°C. The reaction was stirred at 0°C until the disappearance of the starting material in TLC. Almost instantaneously, the formation of a yellow precipitate was observed. At the end of the reaction, the solid was removed through centrifugation and the supernatant was transferred into a new round bottom flask.

A solution of KHF₂ (5.0 M, 10 eq.) was added to the reaction. The reaction was stirred at room temperature and monitored with TLC until the disappearance of the starting material. Over the time, the reaction became cloudier and more yellowish. After the reaction ended, the solution was filtered, and the solvent was removed under reduced pressure. The remaining solid was dissolved in 20 mL of CHCl₃ and 20 mL of water. The aqueous phase was extracted five times with 20mL of fresh CHCl₃. The combined organic phases were washed with water, and brine, and dried over anhydrous Na₂SO₄. The evaporation of the solvent gave the crude product that was purified through silica gel column chromatography.

General procedure G: Base catalyzed deprotection to obtain **Glc5, **Glc6**, and **Glc7**.**

A solution of potassium hydroxide in methanol (0.2 M, 0.1 eq.) was added to a solution of **9** or **15** (1 eq.) in methanol (0.03M). The reaction was stirred at room temperature until the disappearance of the starting material in TLC. The solution was then neutralized with Dowex[®] hydrogen form, filtered, and concentrated.

General procedure H: Copper-catalyzed azide-alkyne cycloaddition (CuAAC) to obtain compound **15.**

An aqueous solution of sodium ascorbate (0.6 M, 0.8 eq.) was added to a suspension of **4** (1 eq.) and alkyne **11** (1 eq.) in tert-Butyl alcohol (0.3 M). Then, a solution of copper (II) sulfate pentahydrate (0.3 M, 0.4 eq.) was added under high stirring conditions at room temperature. After the reaction ended, it was diluted with water and the mixture was extracted with CHCl₃. The

combined extracts were dried over anhydrous Na_2SO_4 and concentrated to dryness. The crude product was purified through silica gel column chromatography using DCM: MeOH 95:5.

2.1.4 Synthesis and characterization of alkyne 11

Synthesis of 12

To a solution of 4-pentyn-1-ol (840 mg, 10 mmol) and TEA (2.8 mL, 20 mmol) in CH_2Cl_2 (60 mL) at 0°C were added tosyl chloride (2.9 g, 15.2 mmol). After 30 minutes, the mixture was allowed to warm slowly to room temperature, then stirred for 24 h. The reaction was diluted with CH_2Cl_2 , washed with brine, then water, dried with Na_2SO_4 , and concentrated under reduced pressure. The crude product was purified by column chromatography (H: EA 8:2) to give **12** (2g, 86%) as a colorless oil.

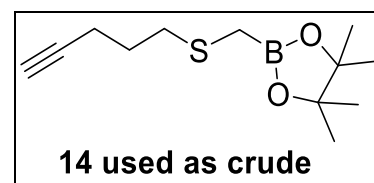
Characterization as described in the literature¹⁹⁸

Synthesis of 13

To a solution of **12** (2 g, 8.4 mmol) in DMF (60 mL) was added potassium thioacetate (2.2 g, 19 mmol). The mixture was heated at 60°C and stirred for 1 h. The reaction was diluted with CH_2Cl_2 and washed with brine. The aqueous phase was extracted with fresh CH_2Cl_2 . The combined organic phases were washed with water 5 times, dried with MgSO_4 , and concentrated under reduced pressure. The crude product was purified by column chromatography (H: EA 95:5) to give **13** (770 mg, 68%) as a colorless oil.

Characterization as described in the literature¹⁸²

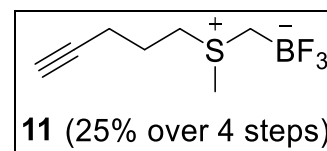
Synthesis of 14



A freshly prepared solution of potassium hydroxide in dry MeOH (0.4M, 20 mL) was purged with nitrogen for 30 minutes. Then, 15 mL of this solution (2.2 eq) were added dropwise to a solution of **13** (1 eq, 3.4 mmol) in dry MeOH (0.7M, 5 mL) cooled to 0°C . The solution was stirred at the same temperature for 10 minutes, and then the iodomethylboronyl pinacolate (1.2 eq, 770 μL) was slowly added. The reaction was stirred at room temperature and monitored with TLC until the disappearance of the starting material. After the reaction ended, the solvent was removed under reduced pressure. The remaining solid was dissolved in 50 mL of water and the pH was neutralized

with HCl 1M. The aqueous phase was extracted two times with fresh DCM. The combined organic phases were washed with brine and dried over anhydrous Na₂SO₄. The evaporation of the solvent gave the crude product that was used in the following step.

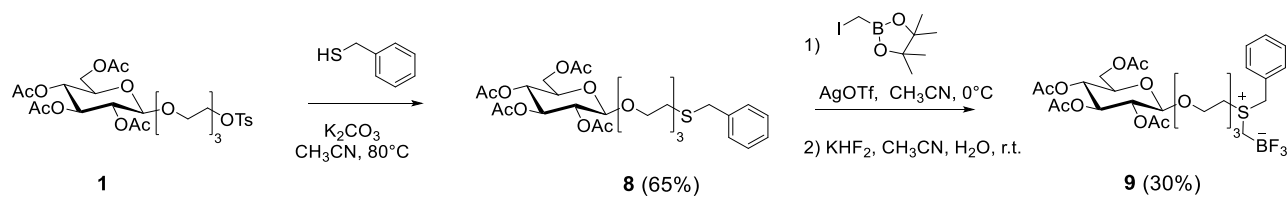
Synthesis of **11**



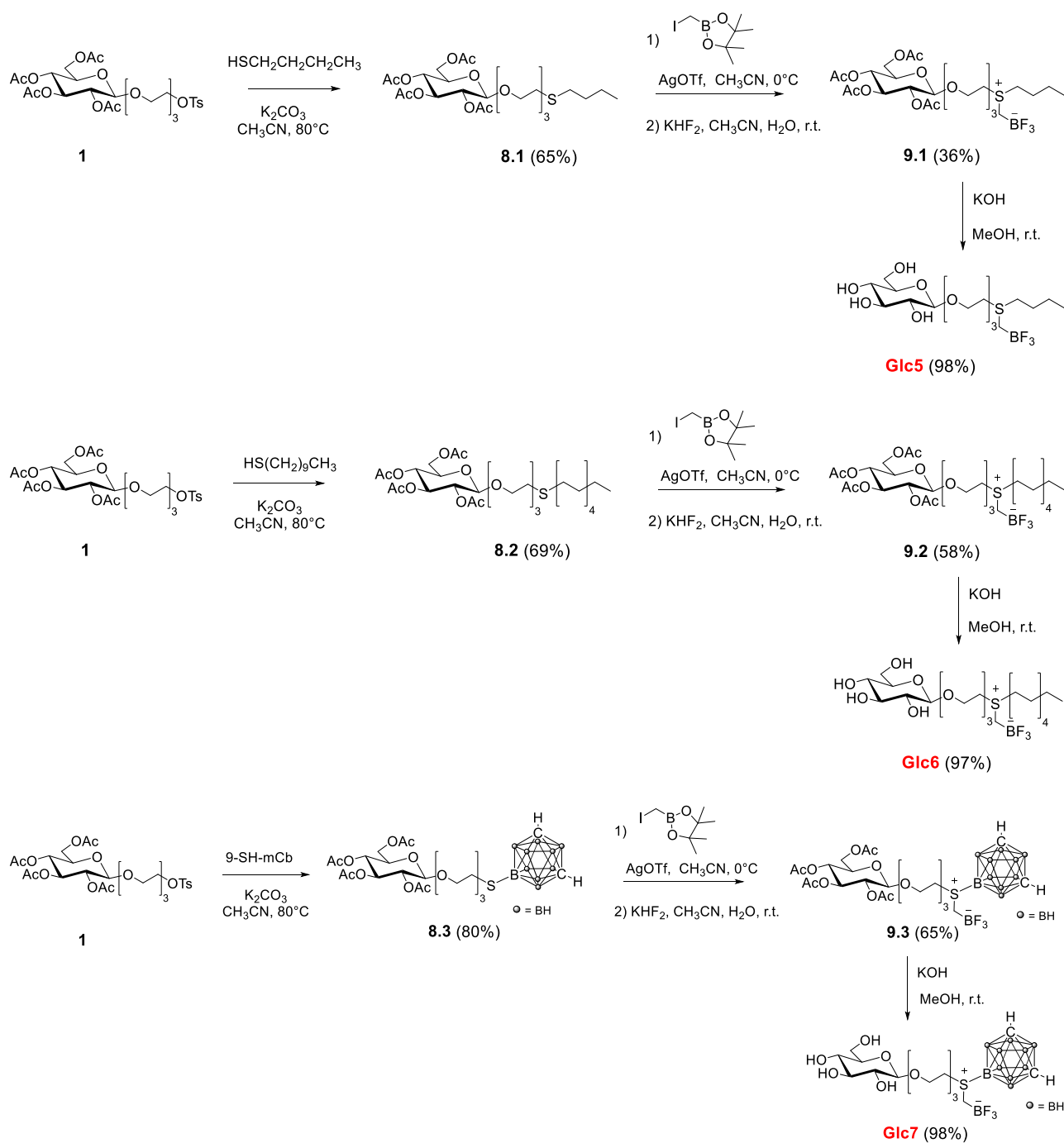
Methyl triflate (1.6 eq, 2,09 mmol) was added dropwise to a solution of **14** (1 eq, 1,35 mmol), as crude product, in dry Et₂O (0.15M, 10 mL). The reaction was stirred at room temperature and monitored with TLC until the disappearance of the starting material. Over the time, a yellow liquid precipitate formed at the flask's bottom. At the end of the first step, the solvent was removed under reduced pressure and the remaining liquid was diluted in acetonitrile (0.2 M, 6 mL). A solution of KHF₂ (5.0 M, 10 eq.) was added to the reaction and stirred upon disappearance of the starting material. After the reaction ended, the solvent was removed under reduced pressure, and the remaining solid was dissolved in 30 mL of DCM and 30 mL of water. The aqueous phase was extracted three times with 30 mL of fresh DCM. The combined organic phases were washed with water, and brine, and dried over anhydrous Na₂SO₄. The evaporation of the solvent gave the crude product that was purified through silica gel column chromatography.

¹H NMR (500 MHz, CDCl₃) δ 3.33 (dt, J = 13.3, 7.6 Hz, 1H, H1a), 3.21 (dt, J = 13.2, 7.6 Hz, 1H, H1b), 2.83 (s, 3H, CH₃), 2.45 (td, J = 6.6, 2.6 Hz, 2H, H3), 2.19 (br s, 1H, 1H SCH₂B), 2.12 (t, J = 2.6 Hz, 1H, H5 alkyne), 2.08 (br s, 1H, 1H SCH₂B), 2.06 – 1.97 (m, 2H, H2). **¹³C{¹H} NMR (101 MHz, CD₃OD + CDCl₃)** δ 80.97 (C, alkyne), 71.08 (CH, alkyne), 42.66 (CH₂, C1), 28.87 (very low signal, very broad, SCH₂B) 24.78 (CH₃), 22.83 (CH₂, C2), 17.15 (CH₂, C3). **¹¹B{¹H} NMR (128 MHz, CD₃OD+ CDCl₃)** δ 1.89 (q, J = 47.4 Hz). **¹⁹F{¹H} NMR (377 MHz, CD₃OD + CDCl₃)** δ -137.99 (q, J = 92.2, 43.4 Hz). **IR** (neat, cm⁻¹): 3270, 2357, 1419, 1271, 1200, 1151, 1020, 1004, 954, 675. **HRMS** (C₇H₁₂BF₃S, MW 196.04); found *m/z* 219.05940 [M+Na]⁺ (vs 219.05971 calculated), found *m/z* 415.12981 [2M+Na]⁺ (vs 415.12919 calculated).

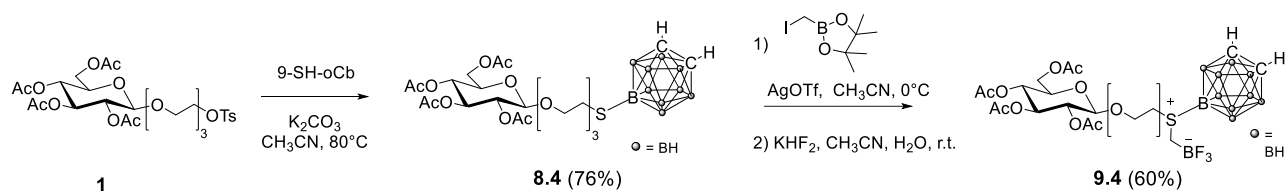
2.1.5 Synthetic Schemes



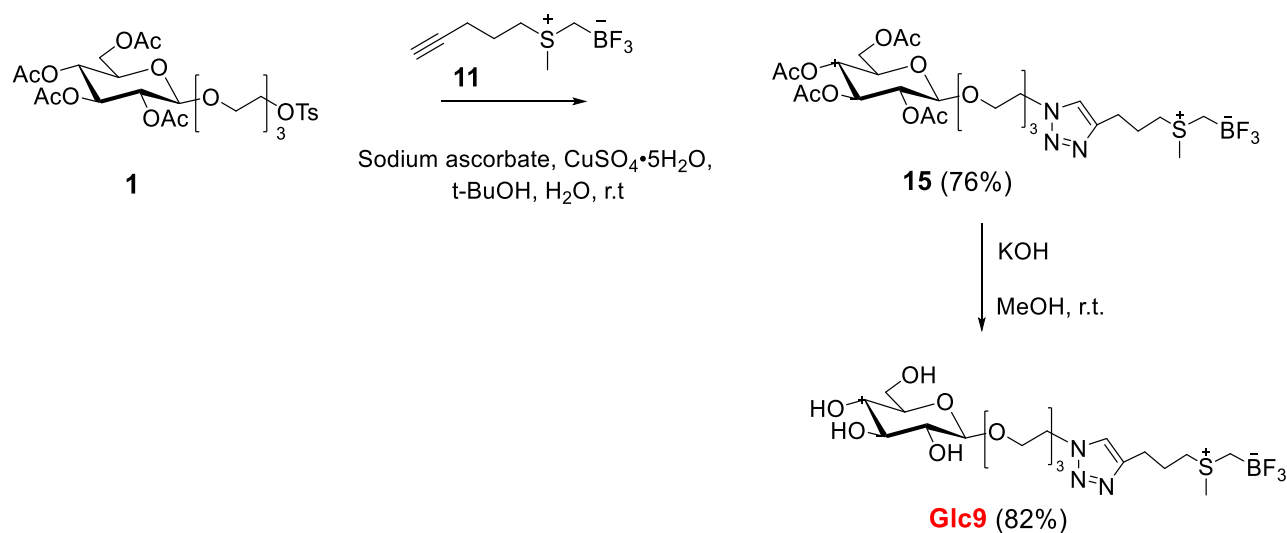
Scheme 5 – Synthesis of compounds 8 and 9.



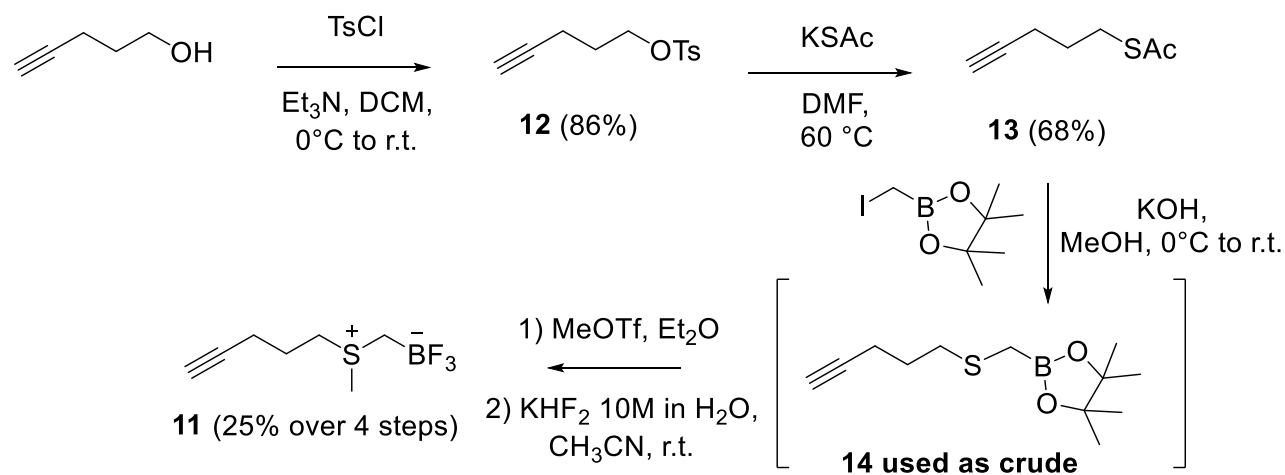
Scheme 6 – Synthesis of Glc5, Glc6, and Glc7



Scheme 7 – Synthesis of compounds 9.4



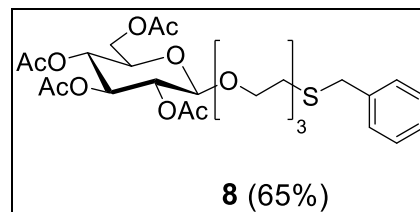
Scheme 8 – Synthesis of Glc9



Scheme 9 – Synthesis of alkyne 11

2.1.6 Products characterizations

Synthesis of **8**

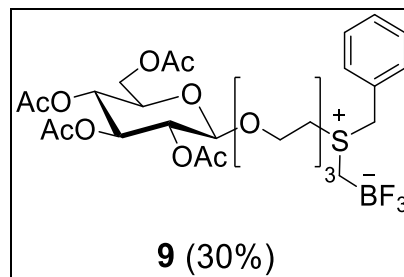


1 (500 mg, 0.80 mmol) reacted with benzyl mercaptan (5 eq.) and potassium carbonate (0.9 eq respect to the thiol) according to the general procedure **E**. Purification over silica gel (H: EA 1:1) gave **8** (Rf product 0.3 in H:EA 4:6) as an amorphous solid (300 mg, 65%).

$[\alpha]_D^{20}$: -17.1 (c = 1.0 g/100 mL, chloroform).

¹H NMR (500 MHz, CDCl₃) δ 7.37 – 7.24 (m, 5H, Ar), 5.23 (t, *J* = 9.5 Hz, 1H, H3), 5.10 (t, *J* = 9.7 Hz, 1H, H4), 5.01 (dd, *J* = 9.6, 8.0 Hz, 1H, H2), 4.62 (d, *J* = 8.0 Hz, 1H, H1), 4.27 (dd, *J* = 12.3, 4.7 Hz, 1H, H6a), 4.15 (dd, *J* = 12.2, 2.2 Hz, 1H, H6b), 3.96 (ddd, *J* = 14.7, 9.7, 5.0 Hz, 1H, H1'a linker), 3.81 – 3.56 (m, 12H, H5, H1'b linker, 4CH₂ linker, CH₂Bn), 2.65 (t, *J* = 6.7 Hz, 2H, 2H6' linker), 2.10 (s, 3H, CH₃), 2.06 (s, 3H, CH₃), 2.04 (s, 3H, CH₃), 2.03 (s, 3H, CH₃). **¹³C{¹H} NMR (126 MHz, CDCl₃)** δ 170.66 (C, C=O), 170.27 (C, C=O), 169.40 (C, C=O), 169.34 (C, C=O), 138.26 (C, Ar), 128.92 (CH, 2C, Ar), 128.50 (CH, 2C, Ar), 127.03 (CH, Ar), 100.86 (CH, C1), 72.86 (CH, C3), 71.81 (CH, C-5), 71.30 (CH, C2), 70.82 (CH₂, C linker), 70.69 (CH₂, C linker), 70.34 (CH₂, C linker), 70.30 (CH₂, C linker), 69.08 (CH₂, C1' linker), 68.46 (CH, C4), 61.98 (CH₂, C6), 36.64 (CH₂, CH₂Bn), 30.64 (CH₂, C6' linker), 20.73 (CH₃), 20.67 (CH₃), 20.61 (CH₃), 20.59 (CH₃). **IR** (neat, cm⁻¹): 2921, 2870, 1745, 1494, 1430, 1365, 1215, 1034, 908, 770, 703. **HRMS** (C₂₇H₃₈O₁₂S, MW 586.64); found *m/z* 609.19751 [M+Na]⁺ (vs 609.19762 calculated).

Synthesis of 9

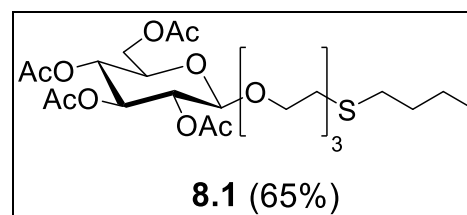


8 (100 mg, 0.17 mmol) reacted according to the general procedure **F** with 1.2 eq of IBpin and 1.1 eq of AgOTf. Purification over silica gel (DCM: MeOH 95:5) gave **9** (Rf product 0.5 in DCM: MeOH 95:5) as an amorphous solid (35 mg, 30%).

$[\alpha]_D^{20} = -12.4^\circ$ ($c = 0.5$ g/100 mL, chloroform).

$^1\text{H NMR}$ (500 MHz, CDCl_3) δ 7.52 – 7.39 (m, 5H, Ar), 5.19 (td, $J = 9.5, 2.0$ Hz, 1H, H3), 5.03 (td, $J = 9.7, 5.1$ Hz, 1H, H4), 4.96 – 4.87 (m, 1H, H2), 4.62 – 4.47 (m, 3H, H1, CH_2Bn), 4.30 – 4.21 (m, 1H, H6a), 4.13 (dd, $J = 12.3, 2.2$ Hz, 1H, H6b), 4.04 – 3.99 (m, 1H, H5'a linker), 3.98 – 3.91 (m, 2H, H1'a linker, H5'b linker), 3.76 – 3.61 (m, 8H, H5, H1'b linker, 3 CH_2 linker), 3.38 – 3.28 (m, 1H, H6'a linker), 3.19 (ddd, $J = 18.0, 12.0, 3.8$ Hz, 1H, H6'b linker), 2.09 (s, 3H, CH_3), 2.06 – 1.99 (m, 11H, SCH_2B , 3 CH_3). **$^{13}\text{C}\{^1\text{H}\}$ NMR (126 MHz, CDCl_3)** δ 170.58 (C, C=O), 170.20 (C, C=O), 169.42 (C, C=O), 169.35 & 169.33 (C, C=O), 131.17 & 131.09 (2CH, Ar), 129.92 (CH, Ar), 129.49 & 129.47 (2CH, Ar), 127.66 & 127.56 (C, Ar), 100.89 (CH, C1), 72.74 (CH, C3), 71.82 (CH, C5), 71.24 (CH, C2), 70.62 (CH_2 , C linker), 70.45 & 70.40 (CH_2 , C linker), 70.19 (CH_2 , C linker), 69.21 & 69.17 (CH_2 , C1' linker), 68.42 (CH, C4), 65.89 & 65.84 (CH_2 , C5' linker), 61.96 (CH_2 , C6), 46.87 & 46.80 (CH_2 , CH_2Bn), 39.63 & 39.33 (CH_2 , C6' linker), 25.77 (br s, SCH_2B), 20.72 (CH_3), 20.66 (CH_3), 20.58 (2C, CH_3). **$^{11}\text{B}\{^1\text{H}\}$ NMR (128 MHz, CDCl_3)** δ 2.02 (d, $J = 38.1$ Hz). **$^{19}\text{F}\{^1\text{H}\}$ NMR (376 MHz, CDCl_3)** δ -137.00 (br s). **IR** (neat, cm^{-1}) 3628, 2923, 1742, 1456, 1366, 1214, 1119, 1029, 978, 908, 702. **HRMS** ($\text{C}_{28}\text{H}_{40}\text{BF}_3\text{O}_{12}\text{S}$, MW 668.48); found m/z 691.21744 [$\text{M}+\text{Na}$] $^+$ (vs 691.21778 calculated).

Synthesis of 8.1

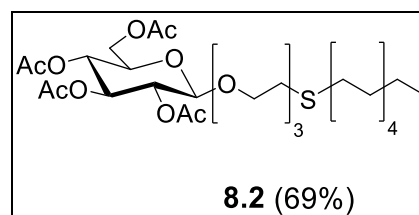


1 (400 mg, 0.60 mmol) reacted with 1-butanethiol (8 eq.) and potassium carbonate (0.9 eq respect to the thiol) according to the general procedure **E**. Purification over silica gel (H: EA 1:1) gave **8.1** (Rf product 0.3 in H:EA 1:1) as a yellowish amorphous solid (225 mg, 65%).

$[\alpha]_{\text{D}}^{20}$: -19.6 ($c = 1.0$ g/100 mL, chloroform).

$^1\text{H NMR}$ (400 MHz, CDCl_3) δ 5.21 (t, $J = 9.5$ Hz, 1H, H3), 5.08 (t, $J = 9.7$ Hz, 1H, H4), 4.99 (dd, $J = 9.5, 8.0$ Hz, 1H, H2), 4.61 (d, $J = 8.0$ Hz, 1H, H1), 4.26 (dd, $J = 12.3, 4.7$ Hz, 1H, H6a), 4.14 (dd, $J = 12.3, 2.3$ Hz, 1H, H6b), 3.95 (dt, $J = 11.0, 4.2$ Hz, 1H, H1'a linker), 3.80 – 3.56 (m, 10H, H5, H1'b linker, 4CH₂ linker), 2.71 (dd, $J = 9.0, 5.2$ Hz, 2H, 2H6' linker), 2.59 – 2.50 (m, 2H, SCH₂CH₂CH₂CH₃ butanethiol), 2.09 (s, 3H, CH₃), 2.05 (s, 3H, CH₃), 2.02 (s, 3H, CH₃), 2.00 (s, 3H, CH₃), 1.57 (dt, $J = 15.1, 5.3$ Hz, 2H, SCH₂CH₂CH₂CH₃ butanethiol), 1.40 (dq, $J = 14.4, 7.2$ Hz, 2H, SCH₂CH₂CH₂CH₃ butanethiol), 0.91 (t, $J = 7.3$ Hz, 3H, SCH₂CH₂CH₂CH₃ butanethiol). **$^{13}\text{C}\{^1\text{H}\}$ NMR (101 MHz, CDCl_3)** δ 170.66 (C, C=O), 170.27 (C, C=O), 169.40 (C, C=O), 169.34 (C, C=O), 100.85 (CH, C1), 72.84 (CH, C3), 71.79 (CH, C5), 71.28 (CH, C2), 71.01 (CH₂, C linker), 70.70 (CH₂, C linker), 70.35 (CH₂, C linker), 70.31 (CH₂, C linker), 69.08 (CH₂, C1' linker), 68.43 (CH, C4), 61.96 (CH₂, C6), 32.25 (CH₂, SCH₂CH₂CH₂CH₃ butanethiol), 31.87 (CH₂, SCH₂CH₂CH₂CH₃ butanethiol), 31.38 (CH₂, C6' linker), 21.95 (CH₂, SCH₂CH₂CH₂CH₃ butanethiol), 20.74 (CH₃), 20.68 (CH₃), 20.61 (CH₃), 20.59 (CH₃), 13.67 (SCH₂CH₂CH₂CH₃ butanethiol). **IR** (neat, cm^{-1}): 2955, 2929, 2871, 1748, 1433, 1365, 1215, 1035, 908. **HRMS** ($\text{C}_{24}\text{H}_{40}\text{O}_{12}\text{S}$, MW 552.63); found m/z 575.21305 $[\text{M}+\text{Na}]^+$ (vs 575.21327 calculated).

Synthesis of 8.2

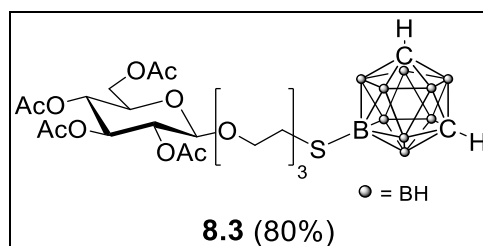


1 (600 mg, 1.02 mmol) reacted with 1-decanethiol (5 eq.) and potassium carbonate (0.9 eq respect to the thiol) according to the general procedure **E**. Purification over silica gel (H: EA 6:4) gave **8.2** (Rf product 0.5 in H:EA 1:1) as a yellowish amorphous solid (448 mg, 69%).

$[\alpha]_D^{20}$: -11.2 (c = 1.0 g/100 mL, chloroform).

$^1\text{H NMR}$ (400 MHz, CDCl_3) δ 5.21 (t, J = 9.5 Hz, 1H, H3), 5.08 (t, J = 9.7 Hz, 1H, H4), 4.99 (dd, J = 9.5, 8.0 Hz, 1H, H2), 4.61 (d, J = 8.0 Hz, 1H, H1, H1), 4.26 (dd, J = 12.3, 4.7 Hz, 1H, H6a), 4.14 (dd, J = 12.3, 2.3 Hz, 1H, H6b), 3.95 (dt, J = 11.0, 4.2 Hz, 1H, H1'a linker), 3.82 – 3.56 (m, 10H, H5, H1'b linker, 4CH₂ linker), 2.71 (t, J = 7.1 Hz, 2H, 2H6' linker), 2.57 – 2.50 (m, 2H, SCH₂(CH₂)₈CH₃ decanethiol), 2.09 (s, 3H, CH₃), 2.05 (s, 3H, CH₃), 2.02 (s, 3H, CH₃), 2.00 (s, 3H, CH₃), 1.63 – 1.51 (m, 2H, SCH₂CH₂(CH₂)₇CH₃ decanethiol), 1.41 – 1.21 (m, 14H, SCH₂CH₂(CH₂)₇CH₃ decanethiol), 0.88 (t, J = 6.8 Hz, 3H, SCH₂CH₂(CH₂)₇CH₃ decanethiol). **$^{13}\text{C}\{^1\text{H}\}$ NMR (101 MHz, CDCl_3)** δ 170.66 (C, C=O), 170.26 (C, C=O), 169.40 (C, C=O), 169.34 (C, C=O), 100.84 (CH, C1), 72.84 (CH, C3), 71.79 (CH, C5), 71.27 (CH, C2), 70.98 (CH₂, C linker), 70.69 (CH₂, C linker), 70.34 (CH₂, C linker), 70.30 (CH₂, C linker), 69.08 (CH₂, C1' linker), 68.42 (CH, C4), 61.96 (CH₂, C6), 32.59 (CH₂, SCH₂(CH₂)₈CH₃ decanethiol), 31.88 (CH₂, SCH₂CH₂(CH₂)₇CH₃ decanethiol), 31.37 (CH₂, C6' linker), 29.80 (CH₂, SCH₂CH₂(CH₂)₇CH₃ decanethiol), 29.54 (CH₂, SCH₂CH₂(CH₂)₇CH₃ decanethiol), 29.52 (CH₂, SCH₂CH₂(CH₂)₇CH₃ decanethiol), 29.29 (CH₂, SCH₂CH₂(CH₂)₇CH₃ decanethiol), 29.24 (CH₂, SCH₂CH₂(CH₂)₇CH₃ decanethiol), 28.88 (CH₂, SCH₂CH₂(CH₂)₇CH₃ decanethiol), 22.66 (CH₂, SCH₂CH₂(CH₂)₇CH₃ decanethiol), 20.74 (CH₃), 20.67 (CH₃), 20.61 (CH₃), 20.59 (CH₃), 14.10 (CH₃, SCH₂CH₂(CH₂)₇CH₃ decanethiol). **IR** (neat, cm^{-1}): 2923, 2853, 1750, 1456, 1434, 1365, 1216, 1036, 907. **HRMS** ($\text{C}_{30}\text{H}_{52}\text{O}_{12}\text{S}$, MW 636.79); found m/z 659.30636 $[\text{M}+\text{Na}]^+$ (vs 659.30717 calculated).

Synthesis of 8.3

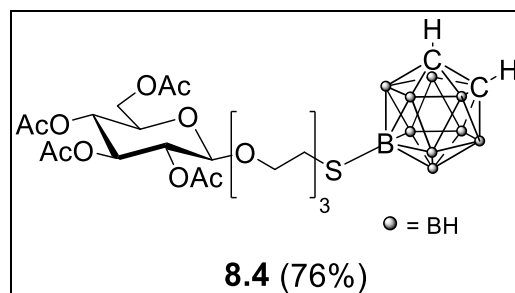


1 (500 mg, 0.78 mmol) reacted with 9-SH-mCb (2 eq.) and potassium carbonate (0.9 eq respect to the thiol) according to the general procedure **E**. Purification over silica gel (H: EA 1:1 to 2:8) gave **8.3** (Rf product 0.3 in H:EA 1:1) as a yellowish amorphous solid (398 mg, 80%).

$[\alpha]_D^{20}$: -5.1 (c = 1.0 g/100 mL, chloroform).

^1H NMR (400 MHz, CDCl_3) δ 5.20 (t, J = 9.5 Hz, 1H, H3), 5.08 (t, J = 9.7 Hz, 1H, H4), 4.99 (dd, J = 9.6, 8.0 Hz, 1H, H2), 4.61 (d, J = 8.0 Hz, 1H, H1), 4.26 (dd, J = 12.3, 4.7 Hz, 1H, H6a), 4.14 (dd, J = 12.3, 2.3 Hz, 1H, H6b), 3.95 (dt, J = 11.0, 4.3 Hz, 1H, H1'a linker), 3.82 – 3.56 (m, 10H, H5, H1'b linker, 4CH₂ linker), 2.98 (s, 2H, C-H mCb), 2.77 (d, J = 5.2 Hz, 2H, 2H6' linker), 2.09 (s, 3H, CH₃), 2.05 (s, 3H, CH₃), 2.02 (s, 3H, CH₃), 2.00 (s, 3H, CH₃) + between 3.3 and 1.5 all signals are increased due to the presence of 9 B-H protons that appear as uneven base line. **$^{13}\text{C}\{^1\text{H}\}$ NMR (101 MHz, CDCl_3)** δ 170.68 (C, C=O), 170.26 (C, C=O), 169.41 (C, C=O), 169.39 (C, C=O), 100.86 (CH, C1), 72.86 (CH, C3), 71.78* (CH, C5), 71.65* (CH₂, C linker), 71.28 (CH, C2), 70.68 (CH₂, C linker), 70.33 (CH₂, C linker), 70.26 (CH₂, C linker), 69.11 (CH₂, C1' linker), 68.42 (CH, C4), 61.95 (CH₂, C6), 54.05 (2CH, mCb), 31.61 (CH₂, C6' linker), 20.75 (CH₃), 20.69 (CH₃), 20.62 (CH₃), 20.60 (CH₃). * may be interchanged. **$^{11}\text{B}\{^1\text{H}\}$ NMR (128 MHz, CDCl_3)** δ 0.34 (s, 1B, B-S), -6.53 (s, 2B), -9.82 (s, 2B), -13.12 (s, 1B), -13.94 (s, 2B), -17.61 (s, 1B), -20.54 (s, 1B). **^{11}B NMR (128 MHz, CDCl_3)** δ 0.33 (s, 1B, B-S), -6.52 (d, J = 161.4 Hz, 2B), -9.82 (d, J = 152.2 Hz, 2B), -11.51 – -15.76 (m, 3B), -17.61 (d, J = 182.2 Hz, 1B), -20.53 (d, J = 177.1 Hz, 1B). **IR** (neat, cm^{-1}): 3056, 2928, 2871, 2600, 1747, 1433, 1365, 1216, 1035, 952, 908, 867. **HRMS** ($\text{C}_{22}\text{H}_{42}\text{B}_{10}\text{O}_{12}\text{S}$, MW 638.72); found m/z 657.37145 [$\text{M}+\text{NH}_4$]⁺ (vs 657.37021 calculated) found m/z 662.32624 [$\text{M}+\text{Na}$]⁺ (vs 662.32561 calculated).

Synthesis of 8.4

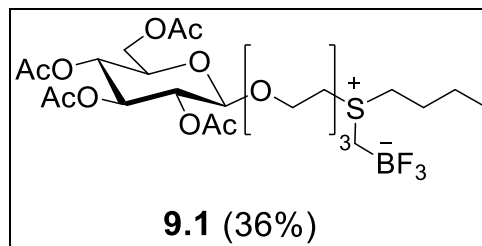


1 (500 mg, 0.78 mmol) reacted with 9-SH-oCb (2 eq.) and potassium carbonate (0.9 eq respect to the thiol) according to the general procedure **E**. Purification over silica gel (H: EA 4:6 to 3:7) gave **8.3** (Rf product 0.2 in H:EA 1:1) as a yellowish amorphous solid (378 mg, 76%).

$[\alpha]_D^{20}$: -8.2 (c = 1.0 g/100 mL, chloroform).

^1H NMR (400 MHz, CDCl_3) δ 5.20 (t, J = 9.5 Hz, 1H, H3), 5.08 (t, J = 9.7 Hz, 1H, H4), 4.99 (dd, J = 9.5, 8.0 Hz, 1H, H2), 4.61 (d, J = 8.0 Hz, 1H, H1), 4.26 (dd, J = 12.3, 4.7 Hz, 1H, H6a), 4.13 (dd, J = 12.3, 2.3 Hz, 1H, H6b), 3.94 (dt, J = 11.0, 4.3 Hz, 1H, H1'a linker), 3.82 – 3.51 (m, 11H, H5, H1'b linker, 4CH₂ linker, 1CH oCb), 3.47 (s, 1H, 1CH oCb), 2.67 (d, J = 5.1 Hz, 2H, 2H6' linker), 2.09 (s, 3H, CH₃), 2.05 (s, 3H, CH₃), 2.02 (s, 3H, CH₃), 2.00 (s, 3H, CH₃) + between 3.3 and 1.5 all signals are increased due to the presence of 9 B-H protons that appear as uneven base line. **$^{13}\text{C}\{^1\text{H}\}$ NMR (101 MHz, CDCl_3)** δ 170.70 (C, C=O), 170.26 (C, C=O), 169.42 (C, C=O), 169.41 (C, C=O), 100.86 (CH, C1), 72.87 (CH, C3), 71.76* (CH, C5), 71.67* (CH₂, C linker), 71.27 (CH, C2), 70.68 (CH₂, C linker), 70.32 (CH₂, C linker), 70.20 (CH₂, C linker), 69.11 (CH₂, C1' linker), 68.43 (CH, C4), 61.95 (CH₂, C6), 52.78 (CH, oCb), 47.39 (CH, oCb), 31.23 (CH₂, C6' linker), 20.75 (CH₃), 20.69 (CH₃), 20.62 (CH₃), 20.60 (CH₃). * may be interchanged. **$^{11}\text{B}\{^1\text{H}\}$ NMR (128 MHz, CDCl_3)** δ 7.30 (s, 1B, B-S), -2.39 (s, 2B), -8.64 (s, 2B), -13.90 (s, 1B), -14.50 (s, 2B), -15.47 (s, 2B). **^{11}B NMR (128 MHz, CDCl_3)** δ 7.27 (s, 1B, B-S), -2.43 (d, J = 145.7 Hz, 2B), -8.66 (d, J = 148.5 Hz, 2B), -14.63 (dd, J = 267.9, 115.6 Hz, 5B). **IR** (neat, cm^{-1}): 3063, 2938, 2870, 2597, 1743, 1431, 1365, 1212, 1032, 879. **HRMS** ($\text{C}_{22}\text{H}_{42}\text{B}_{10}\text{O}_{12}\text{S}$, MW 638.72); found m/z 662.32627 $[\text{M}+\text{Na}]^+$ (vs 662.32561 calculated) found m/z 656.37469 $[\text{M}+\text{NH}_4]^+$ (vs 656.37384 calculated).

Synthesis of 9.1

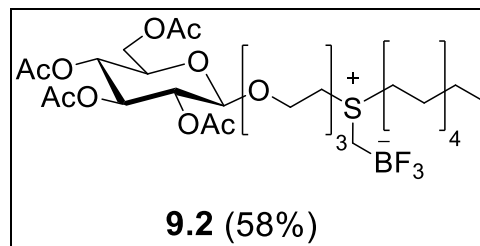


8.1 (150 mg, 0.28 mmol) reacted according to the general procedure **F** with 1.2 eq of IBpin and 1.4 eq of AgOTf. Purification over silica gel (DCM:MeOH 98:2) gave **9.1** (R_f product 0.5 in DCM:MeOH 98:2) as an amorphous solid (63 mg, 36%).

$[\alpha]_D^{20}$: -7.8 ($c = 0.5$ g/100 mL, chloroform).

$^1\text{H NMR}$ (400 MHz, CDCl_3) δ 5.20 (t, $J = 9.5$ Hz, 1H, H3), 5.08 (t, $J = 9.7$ Hz, 1H, H4), 5.01 – 4.93 (m, 1H, H2), 4.57 (dd, $J = 7.9, 1.8$ Hz, 1H, H1), 4.27 (dd, $J = 12.3, 4.7$ Hz, 1H, H6a), 4.15 (dd, $J = 12.3, 1.3$ Hz, 1H, H6b), 4.03 – 3.88 (m, 3H, H1'a linker, 2H5' linker), 3.71 (ddd, $J = 9.9, 6.3, 3.5$ Hz, 2H, H1'b linker, H5), 3.63 (dd, $J = 11.1, 5.5$ Hz, 6H, 3CH₂ linker), 3.56 – 3.45 (m, 1H, H6'a linker), 3.33 – 3.19 (m, 3H, H6'b linker, SCH₂CH₂CH₂CH₃ butanethiol), 2.20 – 1.94 (m, 14H, 4 CH₃, SCH₂B), 1.81 – 1.71 (m, 2H, SCH₂CH₂CH₂CH₃ butanethiol), 1.50 (dq, $J = 14.9, 7.4$ Hz, 2H, SCH₂CH₂CH₂CH₃ butanethiol), 0.99 (t, $J = 7.3$ Hz, 3H, SCH₂CH₂CH₂CH₃ butanethiol). **$^{13}\text{C}\{^1\text{H}\}$ NMR (101 MHz, CDCl_3)** δ 170.63 (C, C=O), 170.24 (C, C=O), 169.45 (C, C=O), 169.35 (C, C=O), 100.89 (CH, C1), 72.76 (CH, C3), 71.86 (CH, C5), 71.27 (CH, C2), 70.63 (CH₂, C linker), 70.60 (CH₂, C linker), 70.56 (CH₂, C linker), 70.21, 69.15 (CH₂, C1' linker), 68.41 (CH, C4), 65.53 (CH₂, C5' linker), 61.95 (CH₂, C6), 42.24 (CH₂, SCH₂CH₂CH₂CH₃ butanethiol), 41.27 & 41.08 (CH₂, C6' linker), 26.08 (CH₂, SCH₂CH₂CH₂CH₃ butanethiol), 21.59 (CH₂, SCH₂CH₂CH₂CH₃ butanethiol), 20.75 (CH₃), 20.71 (CH₃), 20.61 (2 CH₃), 13.40 (SCH₂CH₂CH₂CH₃ butanethiol). **$^{11}\text{B}\{^1\text{H}\}$ NMR (128 MHz, CDCl_3)** δ 1.93 (dd, $J = 94.3, 47.1$ Hz). **$^{19}\text{F}\{^1\text{H}\}$ NMR (377 MHz, CDCl_3)** δ -137.67 (q, $J = 88.0, 29.7$ Hz). **IR** (neat, cm^{-1}): 2959, 2934, 2874, 1743, 1432, 1366, 1215, 1030, 980, 908. **HRMS** ($\text{C}_{25}\text{H}_{42}\text{BF}_3\text{O}_{12}\text{S}$, MW 634.46); found m/z 657.23280 $[\text{M}+\text{Na}]^+$ (vs 657.23243 calculated).

Synthesis of 9.2

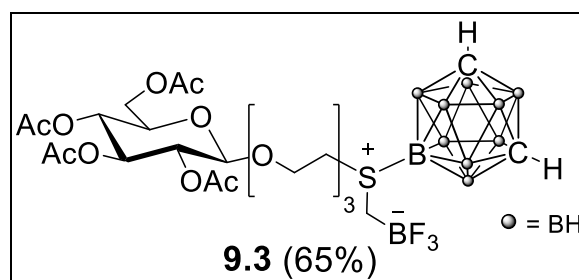


8.2 (125 mg, 0.20 mmol) reacted according to the general procedure **F** with 1.8 eq of IBpin and 1.5 eq of AgOTf. Purification over silica gel (H: EA 1:9) gave **9.2** (Rf product 0.3 in H: EA 5:95) as an amorphous solid (84 mg, 58%).

$[\alpha]_D^{20}$: -10.8 (c = 0.5 g/100 mL, chloroform).

^1H NMR (400 MHz, CDCl_3) δ 5.22 (t, J = 9.5 Hz, 1H, H3), 5.10 (t, J = 9.4 Hz, 1H, H4), 4.99 (ddd, J = 9.4, 8.0, 1.2 Hz, 1H, H2), 4.59 (dd, J = 7.9, 1.6 Hz, 1H, H1), 4.28 (dd, J = 12.3, 4.7 Hz, 1H, H6a), 4.16 (dd, J = 12.3, 1.3 Hz, 1H, H6b), 4.04 – 3.89 (m, 3H, H1'a linker, 2H5' linker), 3.77 – 3.69 (m, 2H, H1'b linker, H5), 3.68 – 3.58 (m, 6H, 3CH₂ linker), 3.52 (dtd, J = 14.5, 5.6, 3.4 Hz, 1H, H6'a linker), 3.30 (ddd, J = 9.8, 6.3, 2.2 Hz, 1H, H6'b linker), 3.26 – 3.19 (m, 2H, SCH₂(CH₂)₈CH₃ decanethiol), 2.15 – 2.00 (m, 14H, 4 CH₃, SCH₂B), 1.83 – 1.73 (m, 2H, SCH₂CH₂(CH₂)₇CH₃ decanethiol), 1.46 (dt, J = 14.5, 7.3 Hz, 2H, SCH₂CH₂(CH₂)₇CH₃ decanethiol), 1.40 – 1.23 (m, 12H, SCH₂CH₂(CH₂)₇CH₃ decanethiol), 0.90 (t, J = 6.9 Hz, 3H, SCH₂CH₂(CH₂)₇CH₃ decanethiol). **$^{13}\text{C}\{^1\text{H}\}$ NMR (101 MHz, CDCl_3)** δ 170.63 (C, C=O), 170.24 (C, C=O), 169.45 (C, C=O), 169.35 (C, C=O), 100.88 (CH, C1), 72.76 (CH, C3), 71.84 (CH, C5), 71.27 (CH, C2), 70.60 (CH₂, C linker), 70.57 (CH₂, C linker), 70.19 (CH₂, C linker), 69.16 (CH₂, C1' linker), 68.40 (CH, C4), 65.50 & 65.48 (CH₂, C5' linker), 61.94 (CH₂, C6), 42.47 & 42.43 (CH₂, SCH₂(CH₂)₈CH₃ decanethiol), 41.25 & 41.24, 41.04 (CH₂, C6' linker), 31.83 (CH₂, SCH₂CH₂(CH₂)₇CH₃ decanethiol), 29.69 (CH₂, SCH₂CH₂(CH₂)₇CH₃ decanethiol), 29.42 (CH₂, SCH₂CH₂(CH₂)₇CH₃ decanethiol), 29.28 (CH₂, SCH₂CH₂(CH₂)₇CH₃ decanethiol), 29.22 (CH₂, SCH₂CH₂(CH₂)₇CH₃ decanethiol), 28.94 (CH₂, SCH₂CH₂(CH₂)₇CH₃ decanethiol), 28.36 (CH₂, SCH₂CH₂(CH₂)₇CH₃ decanethiol), 24.19 & 24.17 (CH₂, SCH₂CH₂(CH₂)₇CH₃ decanethiol), 22.64 (CH₂, SCH₂CH₂(CH₂)₇CH₃ decanethiol), 20.75 (CH₃), 20.70 (CH₃), 20.60 (2 CH₃), 14.09 (CH₃, SCH₂CH₂(CH₂)₇CH₃ decanethiol). **$^{11}\text{B}\{^1\text{H}\}$ NMR (128 MHz, CDCl_3)** δ 1.90 (br s). **$^{19}\text{F}\{^1\text{H}\}$ NMR (377 MHz, CDCl_3)** δ -136.93 (br s). **IR** (neat, cm^{-1}): 2925, 2855, 1747, 1457, 1431, 1365, 1216, 1032, 981. **HRMS** ($\text{C}_{31}\text{H}_{54}\text{BF}_3\text{O}_{12}\text{S}$, MW 718.62); found m/z 741.32660 $[\text{M}+\text{Na}]^+$ (vs 741.32733 calculated).

Synthesis of 9.3

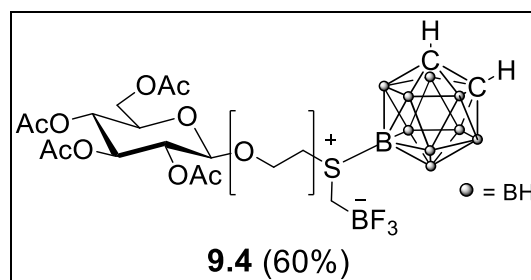


8.3 (125 mg, 0.20 mmol) reacted according to the general procedure **F** with 1.8 eq of IBpin and 1.5 eq of AgOTf. Purification over silica gel (H: EA 1:9 to 100% EA) gave **9.3** (Rf product 0.3 in 100% EA) as an amorphous solid (94 mg, 65%).

$[\alpha]_D^{20}$: -11.6 (c = 0.5 g/100 mL, chloroform).

^1H NMR (400 MHz, CDCl_3) δ 5.21 (t, J = 9.5 Hz, 1H, H3), 5.09 (t, J = 9.7 Hz, 1H, H4), 4.99 (t, J = 8.8 Hz, 1H, H2), 4.60 (dd, J = 8.0, 1.4 Hz, 1H, H1), 4.28 (dd, J = 12.3, 4.6 Hz, 1H, H6a), 4.15 (dd, J = 12.3, 2.2 Hz, 1H, H6b), 4.00 – 3.90 (m, 3H, H1'a linker, 2H5' linker), 3.79 – 3.71 (m, 2H, H1'b linker, H5), 3.71 – 3.58 (m, 7H, 3CH₂ linker, H6'a linker), 3.34 (s, 2H, C-H mCb), 3.27 – 3.17 (m, 1H, H6'b linker), 2.13 (br s, 2H, SCH₂B), 2.10 (s, 3H, CH₃), 2.06 (s, 3H, CH₃), 2.04 (s, 3H, CH₃), 2.01 (s, 3H, CH₃). + between 3.3 and 1.5 all signals are increased due to the presence of 9 B-H protons that appear as uneven base line. **$^{13}\text{C}\{^1\text{H}\}$ NMR (101 MHz, CDCl_3)** δ 170.64 (C, C=O), 170.19 (C, C=O), 169.45 (C, C=O), 169.38 (C, C=O), 100.89 (CH, C1), 72.84 (CH, C3), 71.79 (CH, C5), 71.30 (CH, C2), 70.67 (CH₂, C linker), 70.56 (CH₂, C linker), 70.23 & 70.21 (CH₂, C linker), 69.19 (CH₂, C1' linker), 68.46 (CH, C4), 66.46 (CH₂, C5' linker), 61.99 (CH₂, C6), 55.90 (2CH, mCb), 42.81 & 42.71 (CH₂, C6' linker), 29.67 (very low signal, quite broad SCH₂B), 20.75 (CH₃), 20.69 (CH₃), 20.59 (2C, CH₃). **$^{11}\text{B}\{^1\text{H}\}$ NMR (128 MHz, CDCl_3)** δ 1.98 (d, J = 39.5 Hz, 1B, SCH₂BF₃), -3.10 (s, 1B, mCb), -6.67 (s, 2B, mCb), -10.44 (s, 1B, mCb), -12.74 (s, 4B, mCb), -16.42 (s, 2B, mCb). **$^{19}\text{F}\{^1\text{H}\}$ NMR (376 MHz, CDCl_3)** δ -139.15 (br s). **IR** (neat, cm^{-1}): 3061, 2941, 2873, 2614, 1744, 1636, 1431, 1366, 1216, 1030, 982. **HRMS** ($\text{C}_{23}\text{H}_{44}\text{B}_{11}\text{F}_3\text{O}_{12}\text{S}$, MW 720.56); found m/z 738.39454 [$\text{M}+\text{NH}_4$]⁺ (vs 738.39401 calculated) found m/z 743.34967 [$\text{M}+\text{Na}$]⁺ (vs 743.34940 calculated).

Synthesis of 9.4



8.4 (120 mg, 0.19 mmol) reacted according to the general procedure **F** with 1.8 eq of IBpin and 1.5 eq of AgOTf. Purification over silica gel (H: EA 1:9 to 100% EA) gave **9.4** (Rf product 0.3 in 100% EA) as an amorphous solid (82 mg, 60%).

$[\alpha]_D^{20}$: -12.4 (c = 0.5 g/100 mL, chloroform).

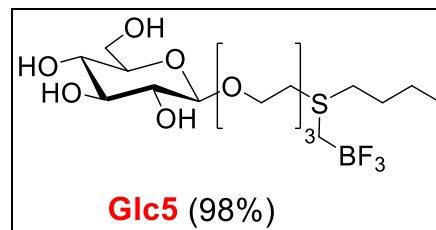
^1H NMR (400 MHz, CDCl_3) 5.21 (t, J = 9.5 Hz, 1H, H3), 5.08 (t, J = 9.7 Hz, 1H, H4), 4.98 (dd, J = 9.4, 8.2 Hz, 1H, H2), 4.60 (d, J = 7.9 Hz, 1H, H1), 4.31 – 4.21 (m, 2H, H6a, 1CH oCb), 4.18 – 4.11 (m, 2H, H6b, 1CH oCb), 3.95 (dt, J = 10.9, 4.3 Hz, 1H, H1'a linker), 3.85 (t, J = 5.7 Hz, 2H, 2H5' linker), 3.74 (ddd, J = 10.8, 6.6, 4.1 Hz, 2H, H1'b linker, H5), 3.69 – 3.59 (m, 6H, 3CH₂ linker), 3.46 (dt, J = 9.0, 4.4 Hz, 1H, H6'a linker), 3.08 (dt, J = 13.2, 6.5 Hz, 1H, H6'b linker), 2.10 (s, 3H, CH₃), 2.05 (s, 3H, CH₃), 2.04 (s, 3H, CH₃), 2.01 (s, 3H, CH₃), 1.93 (dt, J = 16.1, 7.9 Hz, 2H, SCH₂B). + between 3.3 and 1.5 all signals are increased due to the presence of 9 B-H protons that appear as uneven base line.

$^{13}\text{C}\{^1\text{H}\}$ NMR (101 MHz, CDCl_3) δ 170.71 (C, C=O), 170.21 (C, C=O), 169.49 (2C, C=O), 100.91 (CH, C1), 72.80 (CH, C3), 71.79 (CH, C5), 71.26 (CH, C2), 70.62 (CH₂, C linker), 70.52 (CH₂, C linker), 70.24 (CH₂, C linker), 69.28 (CH₂, C1' linker), 68.42 (CH, C4), 66.33 (CH₂, C5' linker), 61.97 (CH₂, C6), 55.29 CH, oCb), 54.67 CH, oCb), 41.87 & 41.82 (CH₂, C6' linker), 29.69 (very low signal, quite broad SCH₂B), 20.77 (CH₃), 20.71 (CH₃), 20.62 (2C, CH₃).

$^{11}\text{B}\{^1\text{H}\}$ NMR (128 MHz, CDCl_3) δ 2.49 (s, 2B, oCb), -3.31 (d, J = 149.0 Hz, 1B, SCH₂BF₃), -9.39 (s, 1B, oCb), -10.54 (s, 1B, oCb), -14.26 (s, 6B, oCb).

$^{19}\text{F}\{^1\text{H}\}$ NMR (376 MHz, CDCl_3) δ -138.91 (s). **IR** (neat, cm^{-1}): 3064, 2924, 2609, 1744, 1366, 1215, 1031, 984. **HRMS** ($\text{C}_{23}\text{H}_{44}\text{B}_{11}\text{F}_3\text{O}_{12}\text{S}$, MW 720.56); found m/z 738.39451 [$\text{M}+\text{NH}_4$]⁺ (vs 738.39401 calculated), found m/z 743.34994 [$\text{M}+\text{Na}$]⁺ (vs 743.34940 calculated).

Synthesis of Glc5

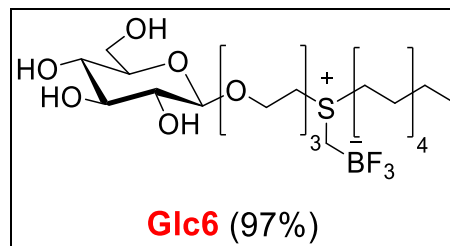


Compound **9.1** (31 mg, 0.05 mmol) reacted according to the general procedure **G** to give **Glc5** (22 mg, 98%) as a white foam.

$[\alpha]_{\text{D}}^{20}$: -15.4 ($c = 0.5$ g/100 mL, methanol).

¹H NMR (400 MHz, CD₃OD) δ 4.36 – 4.27 (m, 3H, H1, SCH₂CH₂CH₂CH₃ butanethiol), 4.08 – 4.01 (m, 1H, H1'a linker), 4.00 – 3.93 (m, 2H, 2H5' linker), 3.89 (dd, $J = 11.9, 1.5$ Hz, 1H, H6a), 3.80 – 3.65 (m, 8H, H6b, H1'b linker, 3CH₂ linker), 3.51 – 3.35 (m, 3H, H6'a linker, H3, H4), 3.30 – 3.18 (m, 3H, H6'b linker, H5, H2), 2.11 (s, $J = 12.1$ Hz, 2H, SCH₂B), 1.79 (tt, $J = 10.9, 5.5$ Hz, 2H, SCH₂CH₂CH₂CH₃ butanethiol), 1.58 – 1.48 (m, 2H, SCH₂CH₂CH₂CH₃ butanethiol), 1.02 (t, $J = 7.4$ Hz, 3H, SCH₂CH₂CH₂CH₃ butanethiol). **¹³C{¹H} NMR (101 MHz, CD₃OD)** δ 103.09 (CH, C1), 76.60 (2CH, C3, C4 or C5), 73.70 (CH, C2), 70.24, 70.07 (2C), 70.02 & 70.03 (3CH₂ linker, C4 or C5), 68.35 (CH₂, C1' linker), 65.88 & 65.58 (CH₂, SCH₂CH₂CH₂CH₃ butanethiol), 65.01 (CH₂, C5' linker), 61.38 (CH₂, C6), 41.19 (CH₂, C6' linker), 25.50 (CH₂, SCH₂CH₂CH₂CH₃ butanethiol), 21.25 (CH₂, SCH₂CH₂CH₂CH₃ butanethiol), 12.37 (CH₃, SCH₂CH₂CH₂CH₃ butanethiol). **¹¹B{¹H} NMR (128 MHz, CD₃OD)** δ 2.09 (dd, $J = 92.9, 45.7$ Hz). **¹⁹F{¹H} NMR (377 MHz, CD₃OD)** δ -139.05 (q, $J = 90.4, 34.4$ Hz). **IR** (neat, cm⁻¹): 3362, 2922, 2874, 1713, 1596, 1460, 1353, 1291, 1247, 1013, 982. **HRMS** (C₁₇H₃₄BF₃O₈S, MW 466,32); found m/z 489.19139 [M+Na]⁺ (vs 489.19153 calculated)

Synthesis of Glc6

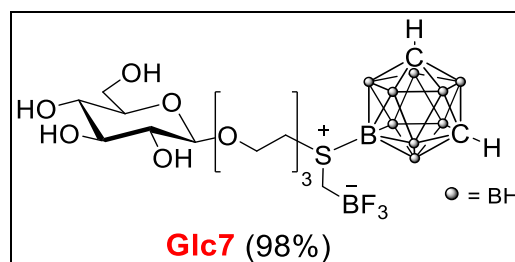


Compound **9.2** (60 mg, 0.08 mmol) reacted according to the general procedure **G** to give **Glc6** (42 mg, 97%) as a white foam.

$[\alpha]^{25}_{\text{D}}$: -7.8 ($c = 1.0$ g/100 mL, methanol).

¹H NMR (400 MHz, CD₃OD) δ 4.33 (d, $J = 7.7$ Hz, 1H, H1), 4.04 (dt, $J = 8.5, 3.8$ Hz, 1H, H1'a linker), 4.01 – 3.93 (m, 2H, 2H5' linker), 3.89 (d, $J = 12.0$ Hz, 1H, H6a), 3.80 – 3.66 (m, 8H, H1'b linker, H6b, 3CH₂ linker), 3.51 – 3.41 (m, 2H, 2H6' linker), 3.38 (dd, $J = 11.2, 5.7$ Hz, 1H, H3), 3.30 – 3.18 (m, 5H, H2, H4, H5, SCH₂(CH₂)₈CH₃ decanethiol), 2.10 (br s, 2H, SCH₂B), 1.82 (dt, $J = 15.4, 7.7$ Hz, 2H, SCH₂CH₂(CH₂)₇CH₃ decanethiol), 1.56 – 1.24 (m, 14H, SCH₂CH₂(CH₂)₇CH₃ decanethiol), 0.92 (t, $J = 6.7$ Hz, 3H, SCH₂CH₂(CH₂)₇CH₃ decanethiol). **¹³C{¹H} NMR (101 MHz, CD₃OD)** δ 103.08 (CH, C1), 76.60 (2CH, C3, C4 or C5), 73.69 (CH, C2), 70.24, 70.07 (2C), 70.03 (3CH₂ linker, C4 or C5), 68.34 (CH₂, C1' linker), 65.01 (CH₂, C5' linker), 61.38 (CH₂, C6), 41.44 (CH₂, SCH₂(CH₂)₈CH₃ decanethiol), 41.14 & 41.10 (CH₂, C6' linker), 31.65 (CH₂, SCH₂CH₂(CH₂)₇CH₃ decanethiol), 29.23 (CH₂, SCH₂CH₂(CH₂)₇CH₃ decanethiol), 29.11 (CH₂, SCH₂CH₂(CH₂)₇CH₃ decanethiol), 29.02 (CH₂, SCH₂CH₂(CH₂)₇CH₃ decanethiol), 28.65 (CH₂, SCH₂CH₂(CH₂)₇CH₃ decanethiol), 28.07 (CH₂, SCH₂CH₂(CH₂)₇CH₃ decanethiol), 23.54 (CH₂, SCH₂CH₂(CH₂)₇CH₃ decanethiol), 22.33 (CH₂, SCH₂CH₂(CH₂)₇CH₃ decanethiol), 13.04 (CH₃, SCH₂CH₂(CH₂)₇CH₃ decanethiol). **¹¹B{¹H} NMR (128 MHz, CD₃OD)** δ 2.10 (d, $J = 48.0$ Hz). **¹⁹F{¹H} NMR (377 MHz, CD₃OD)** δ -139.01 (q, $J = 81.6, 22.1$ Hz). **IR** (neat, cm⁻¹): 3373, 2922, 2854, 1637, 1458, 1296, 1251, 1016, 982. **HRMS** (C₂₃H₄₆BF₃O₈S, MW 550.47); found m/z 573.28553 [M+Na]⁺ (vs 573.28508 calculated).

Synthesis of Glc7

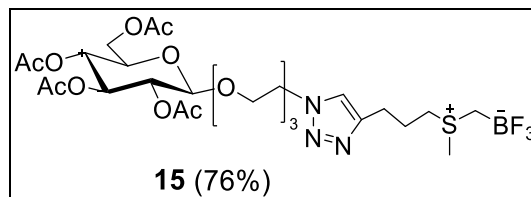


Compound **9.3** (48 mg, 0.07 mmol) reacted according to the general procedure **G** to give **Glc7** (37 mg, 98%) as a white foam.

$[\alpha]_D^{25}$: -9.6 ($c = 1.0$ g/100 mL, methanol).

$^1\text{H NMR}$ (400 MHz, CD_3OD) δ 4.32 (d, $J = 7.8$ Hz, 1H, H1), 4.17 – 3.99 (m, 3H, C-H mCb, H1'a linker), 3.94 (t, $J = 5.5$ Hz, 2H, 2H5' linker), 3.87 (dd, $J = 17.6, 6.8$ Hz, 1H, H6a), 3.83 – 3.65 (m, 8H, 3CH₂ linker, H6b, H1'b linker), 3.65 – 3.54 (m, 1H, H6'a linker), 3.37 (dd, $J = 8.0, 5.6$ Hz, 2H, H6'b linker, H3), 3.35 – 3.26 (m, 2H, H4, H5), 3.21 (t, $J = 8.4$ Hz, 1H, H2), 2.14 (br s, 1H, SCH₂B), 2.02 (br s, 1H, SCH₂B) + between 3.3 and 1.5 all signals are increased due to the presence of 9 B-H protons that appear as uneven base line. **$^{13}\text{C}\{^1\text{H}\}$ NMR (101 MHz, CD_3OD)** δ 103.06 (CH, C1), 76.57 (2CH, C3, C4 or C5), 73.69 (CH, C2), 70.22 (CH, C4 or C5), 70.14 (CH₂, C linker), 70.11 (CH₂, C linker), 70.04 (CH₂, C linker), 68.34 (CH₂, C1' linker), 65.87 (CH₂, C5' linker), 61.35 (CH₂, C6), 56.95 (2CH, mCb), 42.94 (CH₂, C6' linker). **$^{11}\text{B}\{^1\text{H}\}$ NMR (128 MHz, CD_3OD)** δ 2.14 (d, $J = 44.5$ Hz, 1B, SCH₂BF₃), -3.42 (s, 1B, mCb), -6.26 (s, 1B, mCb), -7.50 (s, 1B, mCb), -10.16 (s, 1B, mCb), -12.19 (s, 2B, mCb), -13.48 (s, 2B, mCb), -15.48 (s, 1B, mCb), -16.89 (s, 1B, mCb). **$^{19}\text{F}\{^1\text{H}\}$ NMR (376 MHz, CD_3OD)** δ -140.19 (d, $J = 54.2$ Hz). **IR** (neat, cm^{-1}): 3370, 3061, 2876, 2612, 1730, 1594, 1353, 1297, 1250, 1012, 986, 860. **HRMS** ($\text{C}_{15}\text{H}_{36}\text{B}_{11}\text{F}_3\text{O}_8\text{S}$, MW 552.41); found m/z 570.35258 [$\text{M}+\text{NH}_4$]⁺ (vs 570.35275 calculated).

Synthesis of **15**

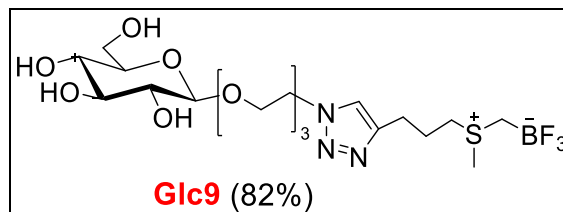


4 (240 mg, 0.47 mmol) reacted with **11** (90 mg, 0.47 mmol) according to the general procedure **H**. Purification over silica gel gave **15** (Rf product 0.4 in DCM:MeOH 95:5) as a white foam (246 mg, 76%).

$[\alpha]_D^{25}$: -12.6 (c = 1.0 g/100 mL, chloroform).

^1H NMR (400 MHz, CDCl_3) δ 7.72 (s, 1H, H triazole), 5.19 (t, J = 9.5 Hz, 1H, H3), 5.05 (t, J = 9.6 Hz, 1H, H4), 4.99 – 4.85 (m, 1H, H2), 4.65 – 4.44 (m, 3H, H1, 2H6' linker), 4.25 (dd, J = 12.1, 3.8 Hz, 1H, H6a), 4.12 (d, J = 12.0 Hz, 1H, H6b), 3.94 (d, J = 10.2 Hz, 1H, H1'a linker), 3.86 (br s, 2H, 2H5' linker), 3.71 (br s, 2H, H5, H1'b linker), 3.59 (d, J = 8.1 Hz, 6H, 3CH₂ linker), 3.22 (d, J = 35.9 Hz, 2H, TriazoleCH₂CH₂CH₂S), 2.92 (br s, 2H, TriazoleCH₂CH₂CH₂S), 2.77 (s, 3H, SCH₃), 2.37 – 2.17 (m, 2H, TriazoleCH₂CH₂CH₂S), 2.20 – 1.89 (m, 14H, SCH₂B, 4 CH₃). **$^{13}\text{C}\{^1\text{H}\}$ NMR (101 MHz, CDCl_3)** 170.63 (C, C=O), 170.21 (C, C=O), 169.46 (C, C=O), 169.40 (C, C=O), 100.85 (CH, H1), 72.73 (CH, C3), 71.77 (CH, C5), 71.24 (CH, C2), 70.54 (CH₂ linker), 70.51 (CH₂ linker), 70.15 (CH₂ linker), 69.32 (2CH₂, C1'linker, C5'linker), 68.40 (CH, C4), 61.95 (CH₂, C6), 50.49 (C6'linker), 43.13 (TriazoleCH₂CH₂CH₂S), 25.20 (SCH₃), 23.78 (TriazoleCH₂CH₂CH₂S), 23.50 (TriazoleCH₂CH₂CH₂S), 20.75 (CH₃), 20.70 (CH₃), 20.60 (2CH₃). **$^{11}\text{B}\{^1\text{H}\}$ NMR (128 MHz, CDCl_3)** δ 1.96 (br s). **$^{19}\text{F}\{^1\text{H}\}$ NMR (377 MHz, CDCl_3)** δ -137.04 (s). **IR** (neat, cm^{-1}): 2940, 2874, 1743, 1638, 1551, 1429, 1366, 1216, 1032, 985. **HRMS** ($\text{C}_{27}\text{H}_{43}\text{BF}_3\text{N}_3\text{O}_{12}\text{S}$, MW 701.51); found m/z 724.24963 [$\text{M}+\text{Na}$]⁺ (vs 724.25048 calculated).

Synthesis of **Glc9**



Compound 15 (46 mg, 0.07 mmol) reacted according to the general procedure **G** to give **Glc9** (28 mg, 82%) as a white foam.

$[\alpha]_D^{25}$: -8.9 (c = 1.0 g/100 mL, methanol).

^1H NMR (400 MHz, CD_3OD) δ 7.92 (s, 1H, H triazole), 4.64 – 4.54 (m, 2H, 2H6' linker), 4.32 (d, J = 7.8 Hz, 1H, H1), 4.06 – 3.97 (m, 1H, H1'a linker), 3.90 (dd, J = 12.0, 7.1 Hz, 3H, H6a, 2H5' linker), 3.78 – 3.62 (m, 8H, 3CH₂ linker, H1'b linker, H6b), 3.41 – 3.35 (m, 1H, H3), 3.30 (dd, J = 3.7, 2.1 Hz, 2H, H5, H4), 3.27 – 3.13 (m, 3H, H2, TriazoleCH₂CH₂CH₂S), 2.91 (t, J = 7.3 Hz, 2H, TriazoleCH₂CH₂CH₂S), 2.79 (s, 3H, SCH₃), 2.26 – 2.07 (m, 3H, TriazoleCH₂CH₂CH₂S, 1SCH₂B), 2.07 – 1.94 (m, 1H, 1SCH₂B). **$^{13}\text{C}\{^1\text{H}\}$ NMR (101 MHz, CD_3OD)** δ 145.34 (C, triazole), 123.30 (CH, triazole), 103.09 (CH, H1), 76.60 (2CH, C5 and C3), 73.70 (CH, C2), 70.25 (CH, C4), 70.02 (2CH₂ linker), 69.93 (CH₂ linker), 68.98 (C5'linker), 68.32 (CH₂, C1'linker), 61.35 (CH₂, C6), 50.01 (C6'linker), 42.45 (TriazoleCH₂CH₂CH₂S), 23.70 (SCH₃), 23.45* (TriazoleCH₂CH₂CH₂S), 23.32* (TriazoleCH₂CH₂CH₂S). * May be interchanged. **$^{11}\text{B}\{^1\text{H}\}$ NMR (128 MHz, CD_3OD)** δ 2.02 (dd, J = 95.3, 47.1 Hz). **$^{19}\text{F}\{^1\text{H}\}$ NMR (377 MHz, CD_3OD)** δ -139.26 (q, J = 88.7, 38.6 Hz). **IR** (neat, cm^{-1}): 3381, 2918, 1637, 1539, 1431, 1375, 1029, 820. **HRMS** ($\text{C}_{19}\text{H}_{35}\text{BF}_3\text{N}_3\text{O}_8\text{S}$, MW 533.37); found m/z 556.20871 [$\text{M}+\text{Na}$]⁺ (vs 556.20822 calculated).

2.2 Stability Evaluation

2 mg of the compound was dissolved in 900 μL of phosphate buffer 0.2M, then 100 μL of D_2O was added. The sample was transferred into an NMR test tube, and the ^{19}F NMR spectra were acquired at the given times (320 scans, 295 K). Between the acquisitions, the samples were stored at room temperature.

2.2.1 ^{19}F NMR kinetic analysis for Glc5

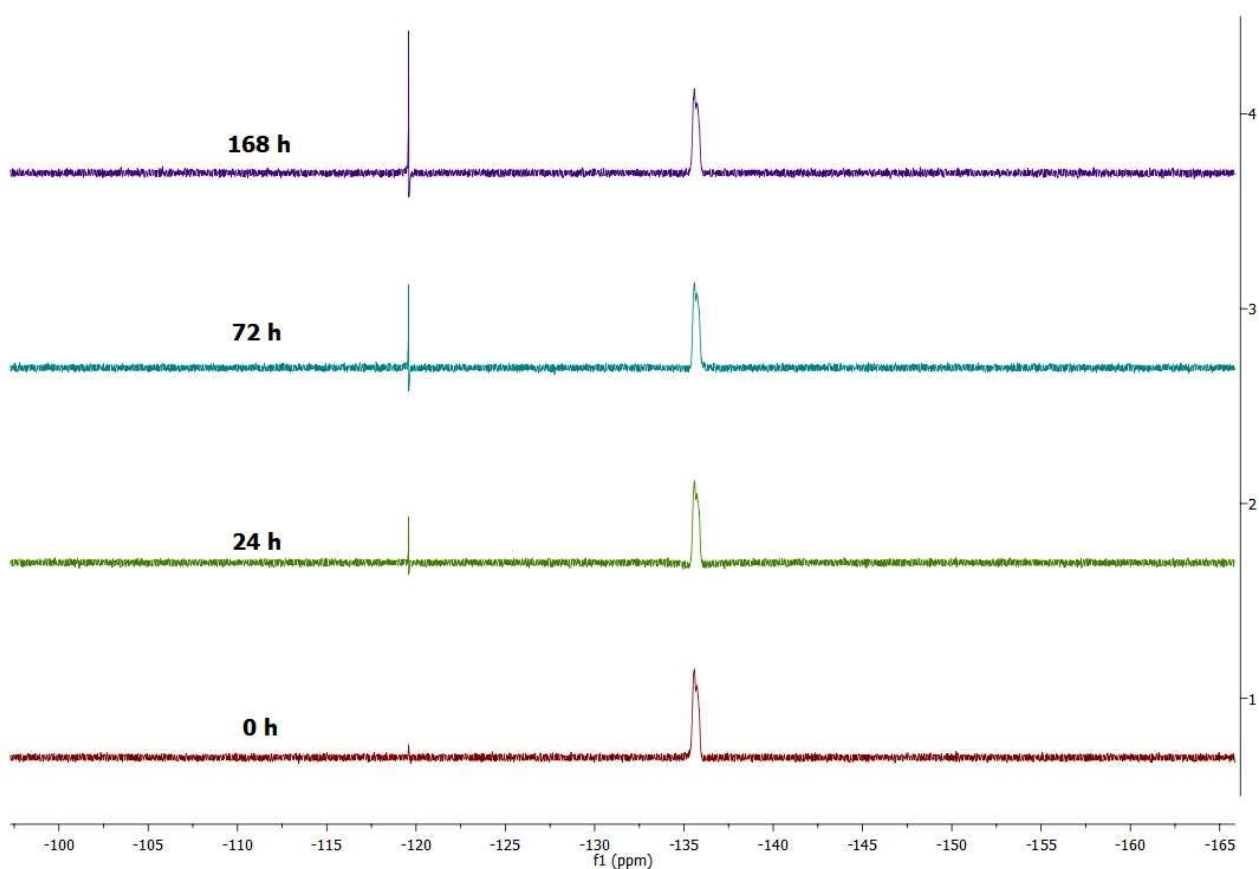


Figure 7 - ^{19}F -NMR spectra (^{19}F : -120 ppm, Glc5: -137 ppm)

2.2.2 ^{19}F NMR kinetic analysis for Glc6

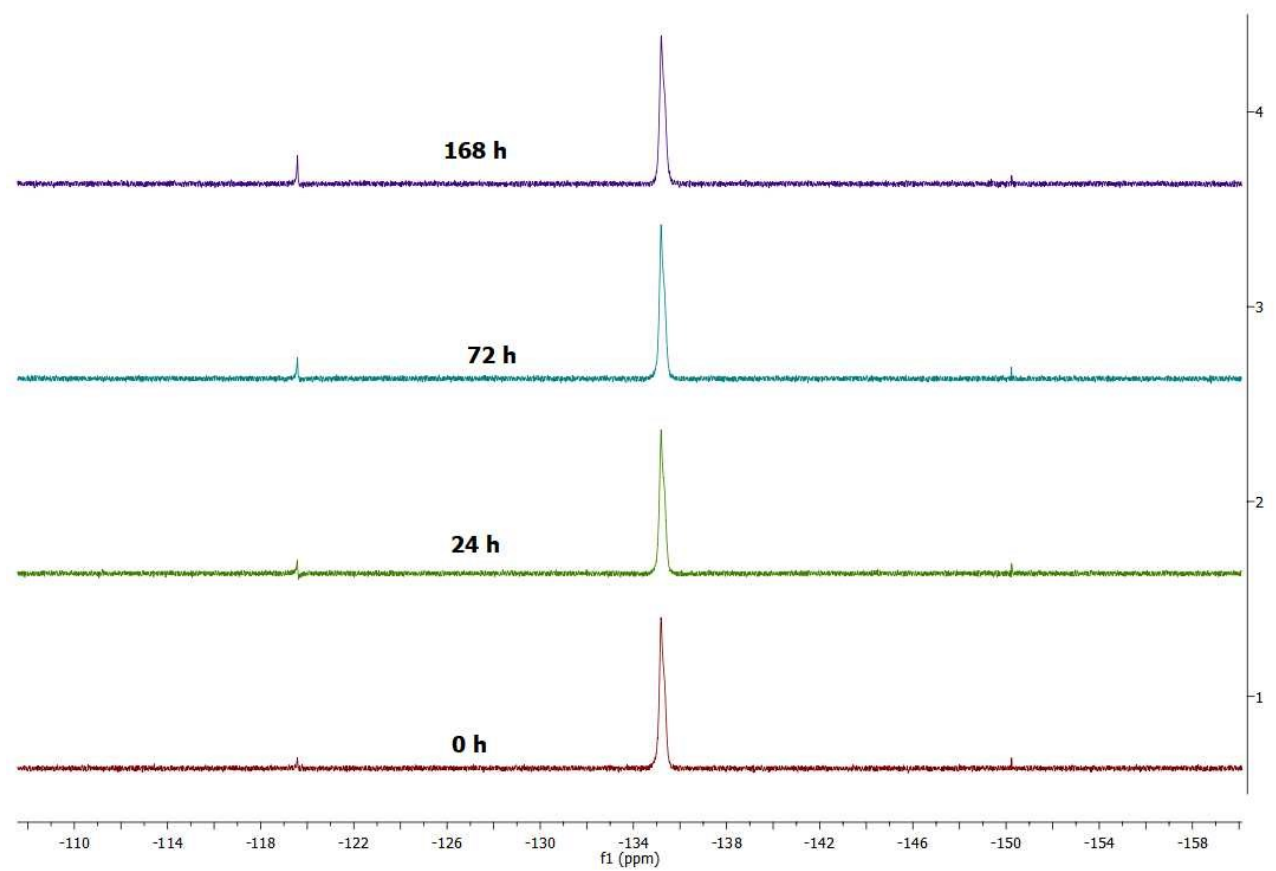


Figure 8 - ^{19}F -NMR spectra (^{19}F :-120 ppm, Glc6: -135 ppm)

2.2.3 ^{19}F NMR kinetic analysis for Glc7

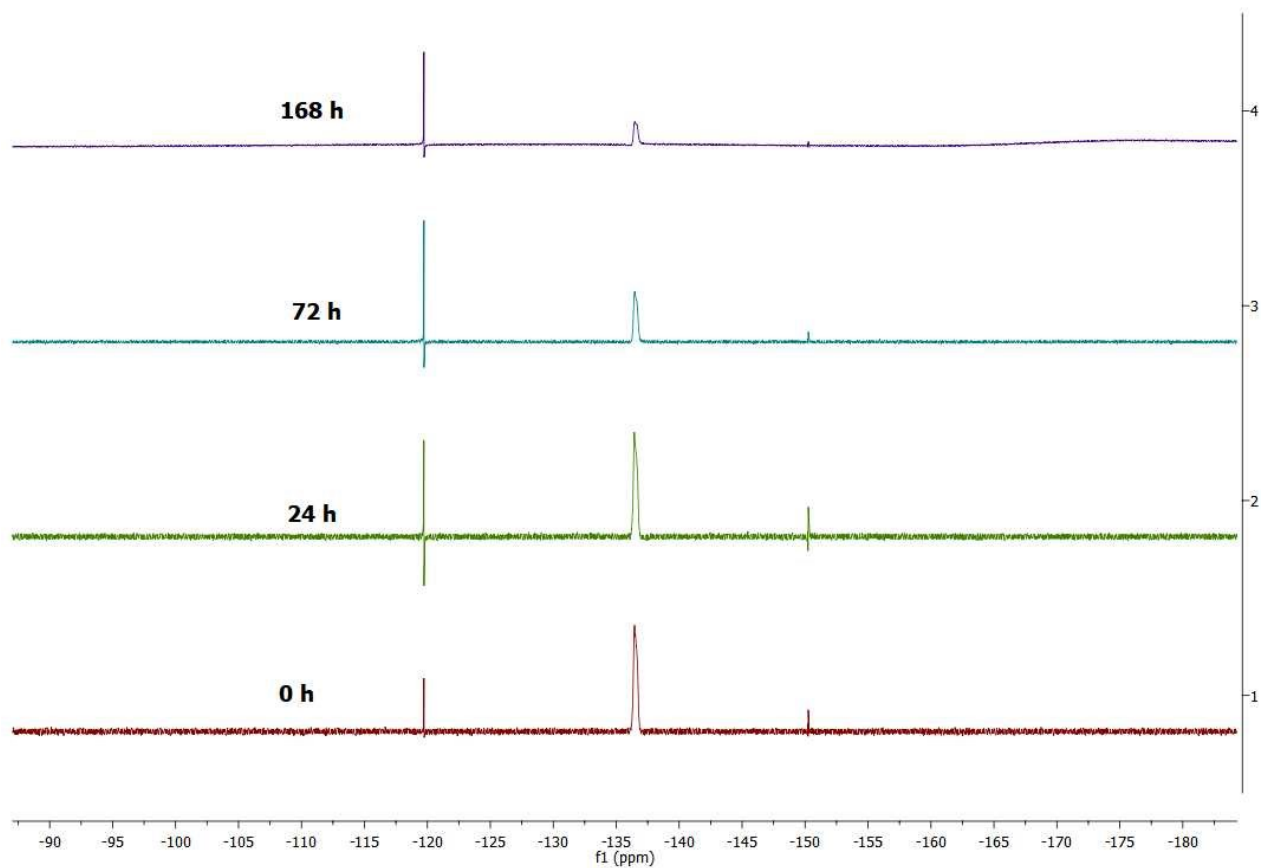


Figure 9 - ^{19}F -NMR spectra (^{19}F :- -120 ppm, Glc7: -135 ppm)

2.2.4 ^{19}F NMR kinetic analysis for Glc9

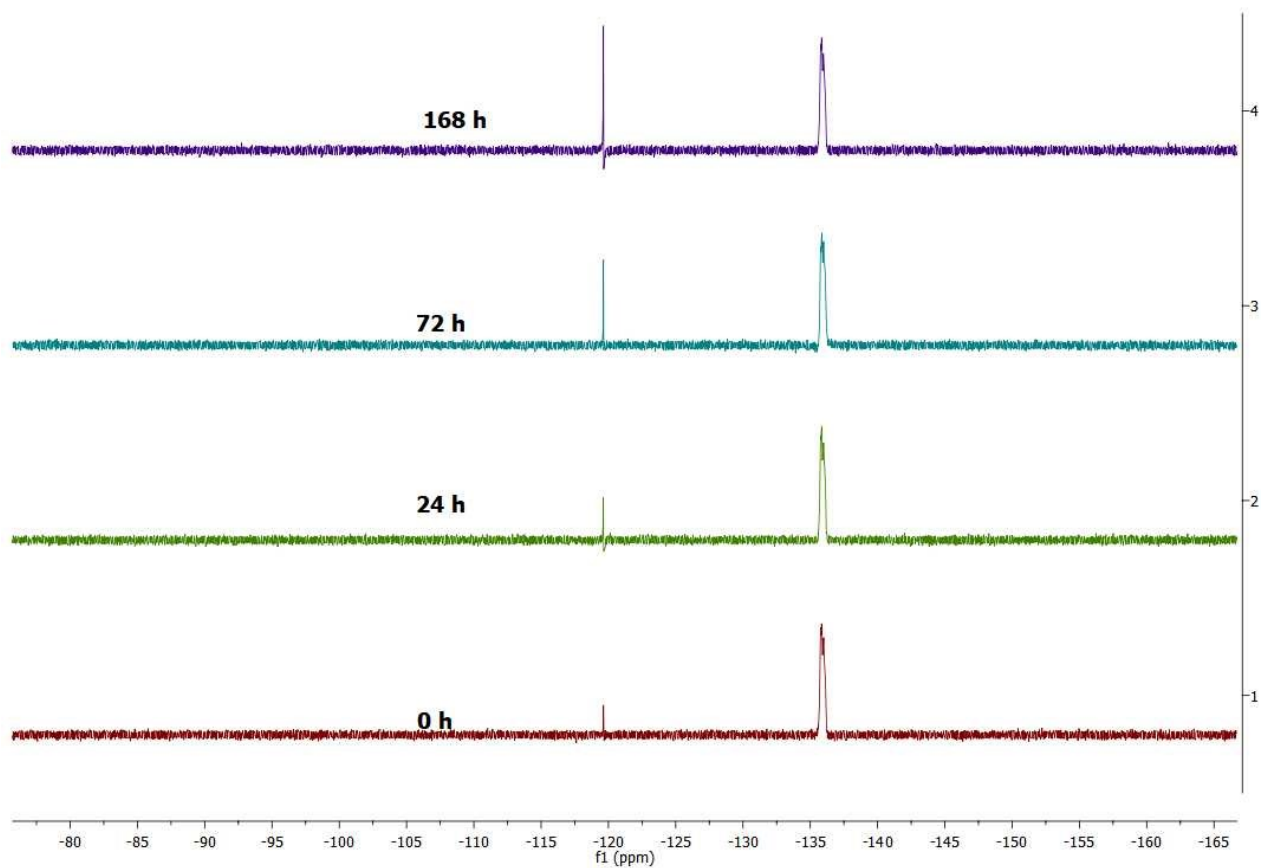


Figure 10 - ^{19}F -NMR spectra (^{19}F -: -120 ppm, Glc9: -135 ppm)

3. Nanomaterial decorated with borane structures

3.1 Chemistry

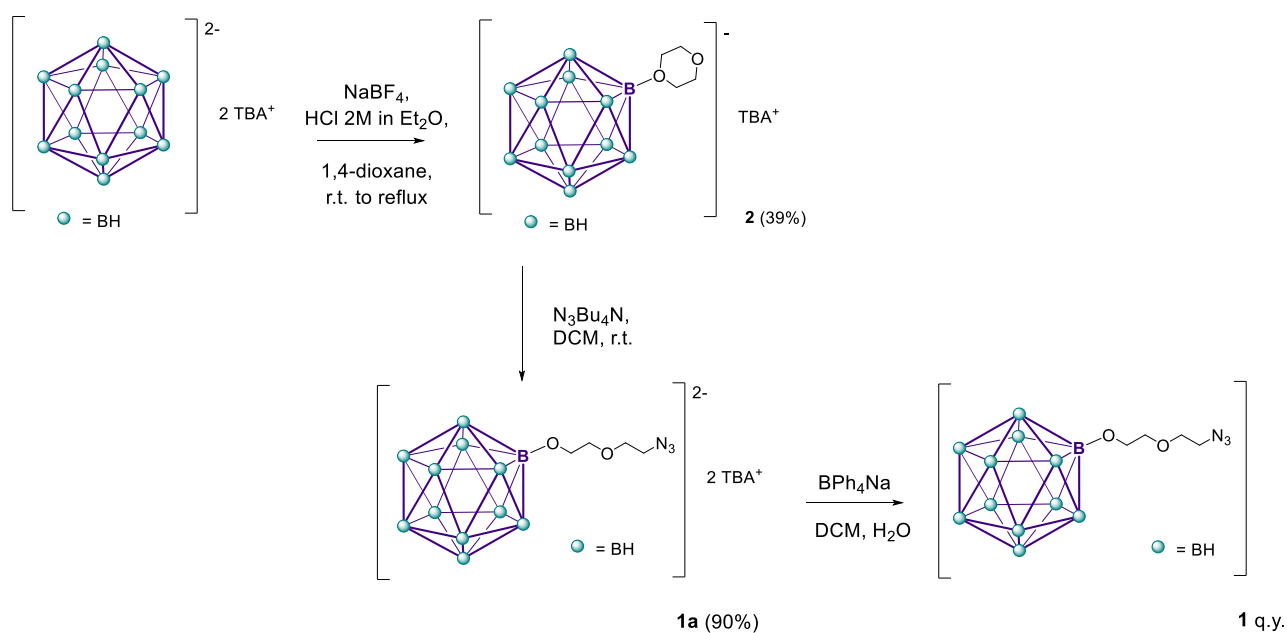
3.1.1 General

All reagents and solvents were purchased from Sigma-Aldrich (Milan) and used as supplied without further purification unless otherwise stated. Thin-layer chromatography was performed on silica gel plates with a fluorescent indicator (Merck, Milan) and visualized at the UV light (254 nm) and/or by staining in palladium (II) chloride acidic solution. 1,4-dioxane was purchased as anhydrous solvents and used as supplied. Dichloromethane (DCM) was refluxed with calcium hydride, then distilled.

All reactions (if not specifically containing water as reactant, solvent, or co-solvent) were performed under a nitrogen or argon atmosphere.

NMR spectra were recorded using a Bruker Avance Neo 400 MHz spectrometer (Bruker, Italy) or Bruker FT-NMR AVANCE DRX500 (Bruker, Italy).

3.1.2 Synthetic scheme



Scheme 1 – Synthesis of compound 1

3.1.3 Synthetic procedures

Synthesis of 2

A commercially available solution of HCl in Et₂O (2M, 1.4 mL) was added to a suspension of (Bu₄N)₂[B₁₂H₁₂] (710 mg, 1.13 mmol) and NaBF₄ (623mg, 5.67 mmol) in 35 ml of 1,4-dioxane. The reaction was heated at reflux for 3h. Then, it was cooled to room temperature, filtered (through Hirsh) and concentrated near to dryness under reduced pressure. The residue was dissolved in 10 mL of acetone, 15 mL of ethanol and 5 mL of water; and a precipitate was allowed to form overnight. The solution was concentrated under reduced pressure and the precipitate filtered, washed with a small amount of water and ethanol, and dried to give 210 mg (39%) of product **2**.

Characterization as described in the literature⁶.

Synthesis of Bu₄NN₃

Bu₄NOH (2.2 mL, 3.3 mmol) was added to a solution of NaN₃ (0.5g, 7.7 mmol) in water (7 mL). The reaction was stirred for 2h, then diluted with water and extracted with DCM (2 x 30 mL). The organic extract was concentrated to dryness and dried in vacuo to give the crude Bu₄NN₃ (728 mg).

Synthesis of 1a

A solution of Bu₄NN₃ (257 mg, 0.90 mmol) in DCM (3 mL) was added to a solution of **2** (200 mg, 0.42 mmol) in DCM (3 mL). The reaction mixture was stirred for 24h then washed with water (3 x 30 mL). The aqueous layer was extracted with DCM (3 x 20 mL) and the organic extracts were concentrated to dryness to give 287mg (90%) of product **1a**.

Characterization as described in the literature¹⁸³.

Synthesis of 1

A solution of BPh₄Na (5g/L, 17 mL, 0.25 mmol) in water was added to a solution of **1a** (100 mg, 0.13 mmol) in DCM (17 mL). The biphasic reaction mixture was stirred for 3h, then the two layers were divided. The aqueous layer was washed with DCM (2 x 30 mL), filtered, washed again with DCM (2 x 20 mL), and filtered. The aqueous layer was concentrated to dryness to give 40 mg of product **1**.

¹H NMR (500 MHz, CD₃OD+CDCl₃) δ 3.71 (d, *J* = 4.8 Hz, 2H, [B₁₁H₁₁]BOCH₂CH₂OCH₂CH₂N₃), 3.65 (dt, *J* = 15.1, 4.9 Hz, 4H, [B₁₁H₁₁]BOCH₂CH₂OCH₂CH₂N₃), 3.52 – 3.46 (m, 2H, [B₁₁H₁₁]BOCH₂CH₂OCH₂CH₂N₃), 1.87 – 0.55 (m, 11H, [B₁₁H₁₁]BOCH₂CH₂OCH₂CH₂N₃). **¹³C{¹H} NMR (500 MHz, CD₃OD+CDCl₃)** δ 71.58, 68.83, 67.25, 50.60. **¹¹B{¹H} NMR (128 MHz, CD₃OD+CDCl₃)** δ 6.35 (s, 1B), -16.62 (s, 6B), -18.02 (s, 5B), -23.02 (s, 1B). **¹¹B NMR (128 MHz, CD₃OD+CDCl₃)** δ 6.37 (s, 1B), -14.20 – -20.12 (m, 11B), -23.02 (d, *J* = 124.1 Hz, 1B). **HRMS** (C₄H₁₉B₁₂N₃Na₂O₂, MW 316.91); found *m/z* 340.23561 [M+Na]⁺ (vs 340.23542 calculated).

4. Carborane-containing drug analogs

4.1 Chemistry

4.1.1 General

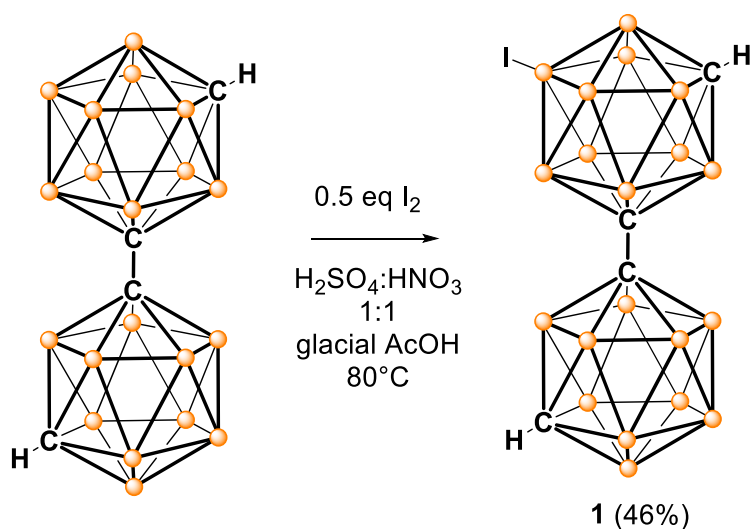
Standard Schlenk and vacuum-line techniques were employed for all manipulations of air- and moisture-sensitive compounds.

The NMR spectra were recorded with a Bruker AvanceDRX 400 spectrometer.

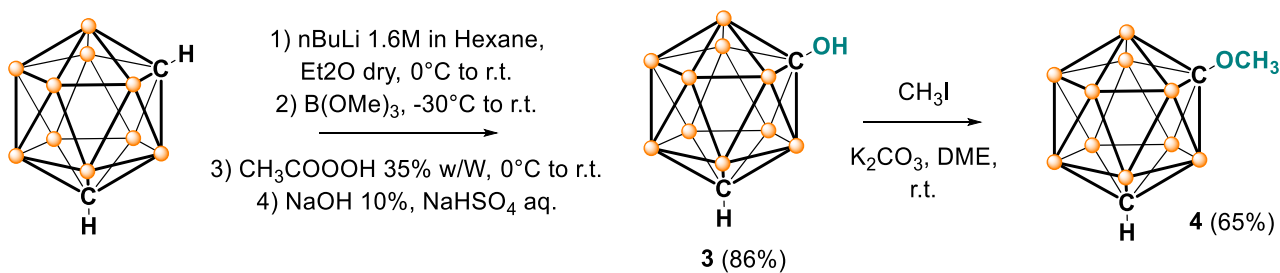
^1H NMR (400.13 MHz): internal standard solvent, external standard TMS.

The mass spectra were recorded with a Bruker Daltonics 7 Tesla APEX II (ESI) or Finnigan MAT MAT8200 (EI) spectrometer. The reported masses refer to the most intense peak of the isotopic pattern. Column chromatography was performed on silica gel 60 (230-400 mesh). Visualization of boron compounds was achieved with a 2 % solution of PdCl_2 in methanol.

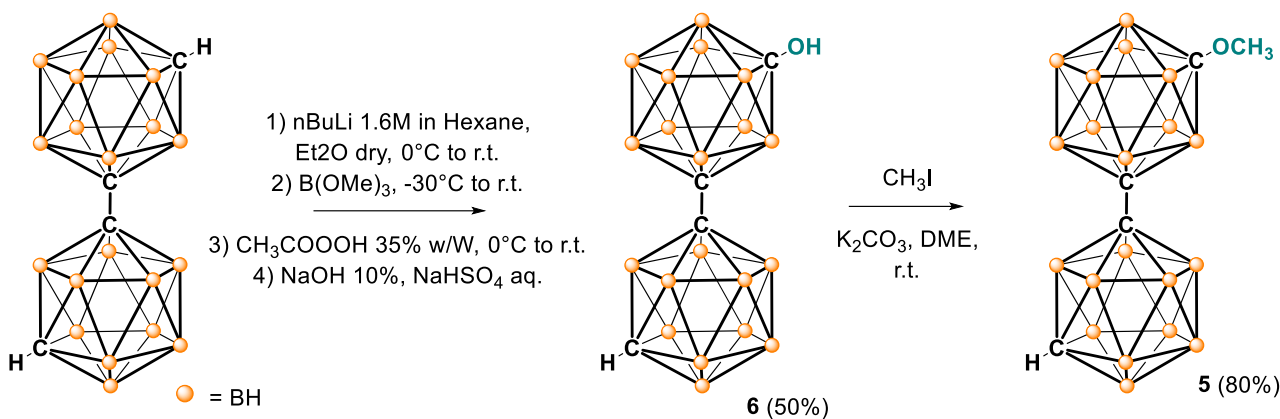
4.1.2 Synthetic scheme



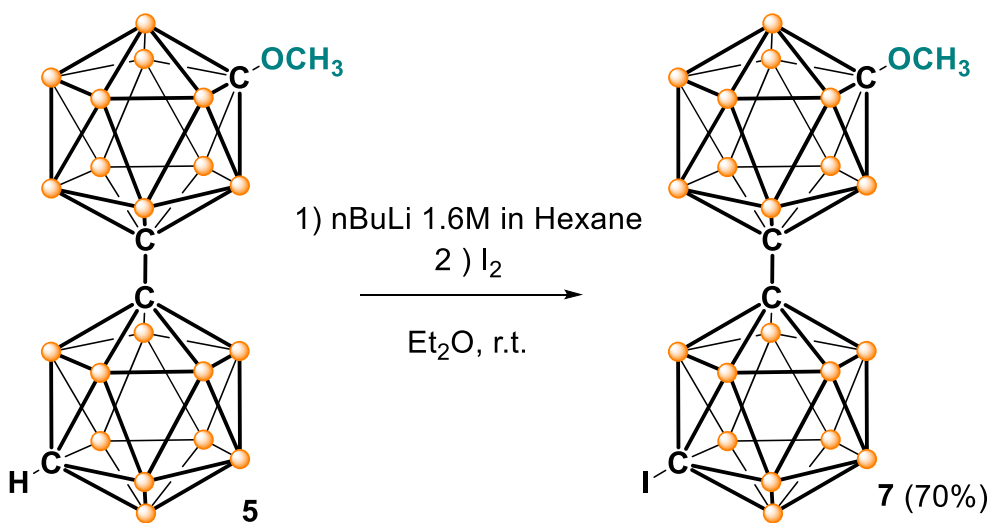
Scheme 1 – Synthesis of compound 1



Scheme 2 – Synthesis of compound 3 and 4



Scheme 3 – Synthesis of compound 6 and 5



Scheme 4 – Synthesis of compound 7

4.1.3 Synthetic procedures and characterizations

Synthesis of **1**

A 50 mL round-bottomed flask equipped with a dropping funnel was charged with the respective bis-mCb (1 mmol), elemental iodine (126 mg, 0.5 mmol), and glacial acetic acid (15 mL, 0.06M). The solution was warmed to 60 °C and then a mixture of concentrated H₂SO₄ and concentrated HNO₃ (3 mL; 50:50 v/v) was added dropwise in 40 min. After complete addition, the reaction mixture was stirred at 80 °C for 2 h. The mixture was cooled to room temperature and ice-cold water (200 mL) was added. During this addition, a colorless precipitate formed that was isolated by filtration through a glass frit. The crude product was washed with water (100 mL) and dissolved in diethyl ether (50 mL). The solution was treated with a dilute aqueous solution of sodium sulfite (10 mL, 0.1 M). The solution was dried with MgSO₄, filtered, and the solvent was removed under reduced pressure. The crude product was purified over silica gel (H: EA from 98:2 to 60:40) and gave 190 mg of product **1** (46%).

¹H NMR (400 MHz, CDCl₃) δ 3.07 (s, 1H, CH bis-mCb), 2.99 (s, 1H, CH bis-mCb), 3.32-1.02 (m, 21H, BH). **¹¹B{¹H} NMR (128 MHz, CDCl₃)** δ -2.21 (s, 1B), -3.22 (s, 2B), -6.78 (s, 2B), -7.67 (s, 2B), -8.67 (s, 1B), -9.64 (s, 2B), -10.65 (s, 2B), -12.55 (s, 1B), -13.67 (s, 2B), -14.51 (s, 2B), -16.43 (s, 2B), -23.89 (s, 1B, B-I). **¹¹B NMR (128 MHz, CDCl₃)** δ -0.50 – -4.87 (m, 3B), -5.23 – -12.39 (m, 9B), -14.91 (dd, J = 321.0, 196.9 Hz, 7B), -23.87 (s, 1B, B-I). **¹³C{¹H} NMR (101 MHz, CDCl₃)** δ 75.99, 73.76, 55.77, 55.03.

Synthesis of **3**

A solution of 1.6 M n-BuLi in n-hexane (7 mL, 11 mmol) was added to a solution of a *m*-carborane (1.5 g, 10 mmol) in 15 mL of dry ether at 0 °C under an N₂ atmosphere, and the mixture was stirred at room temperature for 2 h. After it was cooled to -30 °C, neat trimethyl borate (1.4 mL, 12 mmol) was added over 10 minutes. The mixture was warmed to r.t. overnight. Then, the reaction was cooled at 0°C and 5 mL of CH₃COOOH 35% w/W was added. The reaction mixture was stirred at room temperature for 24 h. Then, 20 mL of saturated NaHSO₃ aqueous solution and 30 mL of 10% NaOH solution were added dropwise. The stirring was continued at room temperature for 3 h, and the solution was extracted with ether. The organic layer was washed with water and brine, dried over MgSO₄, and concentrated. The residue was purified by column chromatography on silica gel with H: EA 9: 1 to give compound **3** (86%).

Characterization as described in the literature¹⁸⁸.

¹H NMR (400 MHz, CDCl₃) δ 3.64 (s, 1H), 2.84 (s, 1H, CH), 3.88 – 1.15 (m, J = 320.2 Hz, 12H). **¹¹B{¹H} NMR (128 MHz, CDCl₃)** δ -4.51 (s, 1B), -11.21 (s, 2B), -13.01 (s, 2B), -15.76 (s, 5B). **¹¹B NMR (128 MHz, CDCl₃)** δ -4.50 (d, J = 162.8 Hz, 1B), -11.23 (d, J = 169.5 Hz, 2B), -14.01 (d, J = 103.3 Hz, 2B), -15.75 (d, J = 181.0 Hz, 5B). **¹³C{¹H} NMR (101 MHz, CDCl₃)** δ 98.34, 62.83.

Synthesis of 4

To a solution of **3** (115 mg, 0.7 mmol) in anhydrous 1,2-dimethoxyethane (7 ml, 0.1M) under nitrogen atmosphere K_2CO_3 (135 mg, 1 mmol) was added. The mixture was stirred for 15 min and iodomethane (60 μ L, 1 mmol) was added. The reaction mixture was heated at 50 °C for 6 h. After cooling the mixture was filtered and the solvent was evaporated in vacuo. The residue was dissolved in DCM (20 ml), washed with water (2 \times 20 mL) and brine (20 mL). The organic phase was dried over $MgSO_4$ and evaporated under reduced pressure. The crude product was dissolved in DCM and filtered over a pad of silica gel to give **4** (88 mg, 65% yield).

1H NMR (400 MHz, $CDCl_3$) δ 3.36 (s, 3H, CH_3), 2.76 (s, 1H, CH), 3.73 – 1.09 (m, 14H). $^{11}B\{^1H\}$ NMR (128 MHz, $CDCl_3$) δ -6.26 (s, 1B), -12.61 (s, 2B), -13.42 (s, 2B), -15.27 (s, 1B), -16.16 (s, 4B). ^{11}B NMR (128 MHz, $CDCl_3$) δ -6.24 (d, J = 162.4 Hz, 1B), -11.20 – -18.52 (m, 9B). $^{13}C\{^1H\}$ NMR (101 MHz, $CDCl_3$) δ 108.07, 60.76, 50.49

Synthesis of 6

A solution of 1.6 M n-BuLi in n-hexane (770 μ L, 1.2 mmol) was added to a solution of a bis-*m*-carborane (335 mg, 1.2 mmol) in 5 mL of dry ether at 0 °C under an N_2 atmosphere, and the mixture was stirred at room temperature for 2 h. After it was cooled to -30 °C, neat trimethyl borate (150 μ L, 1.3 mmol) was added over 5 minutes. The mixture was warmed to r.t. overnight. Then, the reaction was cooled at 0°C and 560 μ L of CH_3COOOH 35% w/W was added. The reaction mixture was stirred at room temperature for 24 h. Then, 2 mL of saturated $NaHSO_3$ aqueous solution and 3 mL of 10% NaOH solution were added dropwise. The stirring was continued at room temperature for 3 h, and the solution was extracted with ether. The organic layer was washed with water and brine, dried over $MgSO_4$, and concentrated. The residue was purified by column chromatography on silica gel with H: EA from 98: 2 to 60: 40 to give compound **6** (50%).

1H NMR (400 MHz, Acetone) δ 3.85 (s, 1H), 2.93 (s, 1H, CH), 3.69 – 1.18 (m, 21H). $^{11}B\{^1H\}$ NMR (128 MHz, Acetone) δ -3.68 (s, 1B), -5.57 (s, 1B), -7.76 (s, 1B), -9.84 (s, 2B), -11.11 (s, 2B), -11.51 (s, 2B), -12.85 (s, 4B), -13.84 (s, 7B). ^{11}B NMR (128 MHz, Acetone) δ -3.73 (d, J = 171.0 Hz, 1B), -4.66 – -18.01 (m, 19B). $^{13}C\{^1H\}$ NMR (101 MHz, Acetone) δ 103.56, 74.27, 70.44, 55.00.

Synthesis of 5

To a solution of **6** (30 mg, 0.1 mmol) in anhydrous 1,2-dimethoxyethane (1 ml, 0.1M) under nitrogen atmosphere K_2CO_3 (16 mg, 0.1 mmol) was added. The mixture was stirred for 1h and iodomethane (22 μ L, 0.35 mmol) was added. The reaction mixture was stirred at r.t. for 24h. Then,

the reaction was filtered, and the solvent was evaporated in vacuo. The residue was dissolved in DCM (20 ml), washed with water (2 ×20 mL) and brine (20 mL). The organic phase was dried over MgSO₄ and evaporated under reduced pressure. The crude product was purified over silica gel (H: EA 98: 2) to give **5** (25 mg, 80% yield).

¹H NMR (400 MHz, CDCl₃) δ 3.33 (s, 3H, CH₃), 2.96 (s, 1H, CH), 3.79 – 0.98 (m, 24H). **¹¹B{¹H} NMR (128 MHz, CDCl₃)** δ -3.23 (s, 1B), -7.58 (s, 2B), -9.72 (s, 2B), -10.79 (s, 3B), -12.97 (s, 4B), -13.73 (s, 6B), -14.51 (s, 2B). **¹¹B NMR (128 MHz, CDCl₃)** δ -0.55 – -5.32 (m, 1B), -5.32 – -17.43 (m, 19B). **¹³C{¹H} NMR (101 MHz, CDCl₃)** δ 107.75, 74.24, 69.99, 60.91 (CH₃), 54.66 (CH).

Synthesis of **7**

A solution of 1.6 M n-BuLi in n-hexane (60 μL, 0.09 mmol) was added to a solution of a **5** (26 mg, 0.08 mmol) in 1 mL of dry ether at 0 °C under an N₂ atmosphere, and the mixture was stirred at room temperature for 2 h. After it was cooled to 0 °C, and I₂ (26 mg, 0.1 mmol) was added in one portion. Then, the reaction was stirred at room temperature for 1 h. At the end, the solution was diluted with ether and treated with a dilute aqueous solution of sodium sulfite (10 mL, 5%). The organic layer was dried over MgSO₄ and concentrated. The crude product was purified by column chromatography on silica gel with 100% Hexane to give compound **7** (70%).

¹H NMR (400 MHz, CDCl₃) δ 3.33 (s, 3H), 4.04 – 1.00 (m, 23H). **¹¹B{¹H} NMR (128 MHz, CDCl₃)** δ -2.68 (s, 1B), -5.06 (s, 1B), -7.38 (s, 1B), -8.63 (s, 3B), -9.66 (s, 3B), -10.32 (s, 2B), -11.45 (s, 1B), -12.91 (s, 4B), -13.62 (s, 4B). **¹¹B NMR (128 MHz, CDCl₃)** δ -3.75 (dd, *J* = 265.2, 138.0 Hz, 2B), -4.97 – -16.41 (m, 18B). **¹³C{¹H} NMR (101 MHz, CDCl₃)** δ 108.34, 69.28, 61.00.

F. References

- (1) Atkins, P.; Overton, T.; Rourke, J.; Weller, M.; Armstrong, F. *Shriver & Atkins' Inorganic Chemistry*, Fifth.; Oxford University Press, 2010.
- (2) *Royal Society of Chemistry - Boron*.
- (3) Molander, G. A.; Ellis, N. Organotrifluoroborates: Protected Boronic Acids That Expand the Versatility of the Suzuki Coupling Reaction. *Acc Chem Res* **2007**, *40* (4), 275–286. <https://doi.org/10.1021/ar050199q>.
- (4) Housecroft, C. E. Kenneth Wade (1932 - 2014) . *Angewandte Chemie International Edition* **2014**, *53* (23), 5742–5743. <https://doi.org/10.1002/anie.201404227>.
- (5) Wade, K. *The Structural Significance of the Number of Skeletal Bonding Electron-Pairs in Carboranes, the Higher Boranes and Borane Anions, and Various Transition-Metal Carbonyl Cluster Compounds*; 1971.
- (6) Sivaev, I. B.; Kulikova, N. Y.; Nizhnik, E. A.; Vichuzhanin, M. v.; Starikova, Z. A.; Semioshkin, A. A.; Bregadze, V. I. Practical Synthesis of 1,4-Dioxane Derivative of the Closo-Dodecaborate Anion and Its Ring Opening with Acetylenic Alkoxides. *J Organomet Chem* **2008**, *693* (3), 519–525. <https://doi.org/10.1016/j.jorganchem.2007.11.027>.
- (7) Grimes, R. N. Icosahedral Carboranes. In *Carboranes*; Elsevier, 2016; pp 283–502. <https://doi.org/10.1016/B978-0-12-801894-1.00009-3>.
- (8) Armstrong, A. F.; Valliant, J. F. The Bioinorganic and Medicinal Chemistry of Carboranes: From New Drug Discovery to Molecular Imaging and Therapy. *Dalton Transactions* **2007**, No. 38, 4240. <https://doi.org/10.1039/b709843j>.
- (9) Messner, K.; Vuong, B.; Tranmer, G. K. The Boron Advantage: The Evolution and Diversification of Boron's Applications in Medicinal Chemistry. *Pharmaceuticals*. MDPI March 1, 2022. <https://doi.org/10.3390/ph15030264>.
- (10) Schwarze, B.; Gozzi, M.; Hey-Hawkins, E. Half- and Mixed-Sandwich Transition Metal Dicarbolides and Nido-Carboranes(-1) for Medicinal Applications. In *Boron-Based Compounds*; John Wiley & Sons, Ltd: Chichester, UK, 2018; pp 60–108. <https://doi.org/10.1002/9781119275602.ch1.4>.
- (11) Satapathy, R.; Dash, B. P.; Mahanta, C. S.; Swain, B. R.; Jena, B. B.; Hosmane, N. S. Glycoconjugates of Polyhedral Boron Clusters. Dedicated to Professor Russell Grimes on the Occasion of His 80th Birthday. *Journal of Organometallic Chemistry*. Elsevier December 1, 2015, pp 13–23. <https://doi.org/10.1016/j.jorganchem.2015.06.027>.
- (12) Marepally, S. R.; Yao, M. L.; Kabalka, G. W. Boronated Carbohydrate Derivatives as Potential Boron Neutron Capture Therapy Reagents. *Future Medicinal Chemistry*. April 2013, pp 693–704. <https://doi.org/10.4155/fmc.13.39>.
- (13) Kellert, M.; Worm, D. J.; Hoppenz, P.; Sárosi, M. B.; Lönnecke, P.; Riedl, B.; Koebberling, J.; Beck-Sickinger, A. G.; Hey-Hawkins, E. Modular Triazine-Based Carborane-Containing Carboxylic Acids- Synthesis and Characterisation of Potential Boron Neutron Capture Therapy Agents Made of Readily Accessible Building Blocks. *Dalton Transactions* **2019**, *48* (29), 10834–10844. <https://doi.org/10.1039/c9dt02130b>.

- (14) Kellert, M.; Lönnecke, P.; Riedl, B.; Koebberling, J.; Hey-Hawkins, E. Enlargement of a Modular System-Synthesis and Characterization of an s-Triazine-Based Carboxylic Acid Ester Bearing a Galactopyranosyl Moiety and an Enormous Boron Load. *Molecules* **2019**, *24* (18). <https://doi.org/10.3390/molecules24183288>.
- (15) Worm, D. J.; Hoppenz, P.; Els-Heindl, S.; Kellert, M.; Kuhnert, R.; Saretz, S.; Köbberling, J.; Riedl, B.; Hey-Hawkins, E.; Beck-Sickinger, A. G. Selective Neuropeptide γ Conjugates with Maximized Carborane Loading as Promising Boron Delivery Agents for Boron Neutron Capture Therapy. *J Med Chem* **2020**, *63* (5), 2358–2371. <https://doi.org/10.1021/acs.jmedchem.9b01136>.
- (16) Das, B. C.; Ojha, D. P.; Das, S.; Evans, T. Boron Compounds in Molecular Imaging. In *Boron-Based Compounds*; John Wiley & Sons, Ltd: Chichester, UK, 2018; pp 205–231. <https://doi.org/10.1002/9781119275602.ch2.4>.
- (17) Valliant, J. F.; Guenther, K. J.; King, A. S.; Morel, P.; Schaffer, P.; Sogbein, O. O.; Stephenson, K. A. The Medicinal Chemistry of Carboranes. *Coord Chem Rev* **2002**, *232* (1–2), 173–230. [https://doi.org/10.1016/S0010-8545\(02\)00087-5](https://doi.org/10.1016/S0010-8545(02)00087-5).
- (18) Zaitsev, A. v.; Kononova, E. G.; Markova, A. A.; Shibaeva, A. v.; Kostyukov, A. A.; Egorov, A. E.; Kuzmin, V. A.; Shtil, A. A.; Ol'shevskaya, V. A. A Straightforward Approach to Carborane-Substituted BODIPY Derivatives via Nucleophilic Aromatic Substitution: Synthesis and Photodynamic Properties. *Dyes and Pigments* **2022**, *207*, 110711. <https://doi.org/10.1016/j.dyepig.2022.110711>.
- (19) Stockmann, P.; Gozzi, M.; Kuhnert, R.; Sárosi, M. B.; Hey-Hawkins, E. New Keys for Old Locks: Carborane-Containing Drugs as Platforms for Mechanism-Based Therapies. *Chemical Society Reviews*. Royal Society of Chemistry July 7, 2019, pp 3497–3512. <https://doi.org/10.1039/c9cs00197b>.
- (20) Endo, Y. *Boron-Based Compounds: Potential and Emerging Applications in Medicine*; 2018.
- (21) Wilkinson, S. M.; Gunosewoyo, H.; Barron, M. L.; Boucher, A.; McDonnell, M.; Turner, P.; Morrison, D. E.; Bennett, M. R.; McGregor, I. S.; Rendina, L. M.; Kassiou, M. The First CNS-Active Carborane: A Novel P2X₇ Receptor Antagonist with Antidepressant Activity. *ACS Chem Neurosci* **2014**, *5* (5), 335–339. <https://doi.org/10.1021/cn500054n>.
- (22) Endo, Y.; Iijima, T.; Yamakoshi, Y.; Yamaguchi, M.; Fukasawa, H.; Shudo, K. Potent Estrogenic Agonists Bearing Dicarba-Closo-Dodecaborane as a Hydrophobic Pharmacophore. *J Med Chem* **1999**, *42* (9), 1501–1504. <https://doi.org/10.1021/jm9900725>.
- (23) Lee, H.-R.; Kim, T.-H.; Choi, K.-C. Functions and Physiological Roles of Two Types of Estrogen Receptors, ER α and ER β , Identified by Estrogen Receptor Knockout Mouse. *Lab Anim Res* **2012**, *28* (2), 71. <https://doi.org/10.5625/lar.2012.28.2.71>.
- (24) Murphy, N.; McCarthy, E.; Dwyer, R.; Farràs, P. Boron Clusters as Breast Cancer Therapeutics. *J Inorg Biochem* **2021**, *218*, 111412. <https://doi.org/10.1016/j.jinorgbio.2021.111412>.
- (25) Chen, Y.; Du, F.; Tang, L.; Xu, J.; Zhao, Y.; Wu, X.; Li, M.; Shen, J.; Wen, Q.; Cho, C. H.; Xiao, Z. Carboranes as Unique Pharmacophores in Antitumor Medicinal Chemistry. *Mol Ther Oncolytics* **2022**, *24*, 400–416. <https://doi.org/10.1016/j.omto.2022.01.005>.
- (26) Kaise, A.; Ohta, K.; Endo, Y. Design, Synthesis, and Anti-Proliferative Activity of 1-(4-Methoxyphenyl)-12-Hydroxymethyl-p-Carborane Derivatives. *Eur J Med Chem* **2016**, *122*, 257–263. <https://doi.org/10.1016/j.ejmech.2016.06.029>.

- (27) Sedlák, D.; Wilson, T. A.; Tjarks, W.; Radomska, H. S.; Wang, H.; Kolla, J. N.; Leśnikowski, Z. J.; Špičáková, A.; Ali, T.; Ishita, K.; Rakotondraibe, L. H.; Vibhute, S.; Wang, D.; Anzenbacher, P.; Bennett, C.; Bartunek, P.; Coss, C. C. Structure–Activity Relationship of Para-Carborane Selective Estrogen Receptor β Agonists. *J Med Chem* **2021**, *64* (13), 9330–9353. <https://doi.org/10.1021/acs.jmedchem.1c00555>.
- (28) Fujii, S. Expanding the Chemical Space of Hydrophobic Pharmacophores: The Role of Hydrophobic Substructures in the Development of Novel Transcription Modulators. *Medchemcomm* **2016**, *7* (6), 1082–1092. <https://doi.org/10.1039/C6MD00012F>.
- (29) Useini, L.; Mojić, M.; Laube, M.; Lönnecke, P.; Dahme, J.; Sárosi, M. B.; Mijatović, S.; Maksimović-Ivanić, D.; Pietzsch, J.; Hey-Hawkins, E. Carboranyl Analogues of Mefenamic Acid and Their Biological Evaluation. *ACS Omega* **2022**, *7* (28), 24282–24291. <https://doi.org/10.1021/acsomega.2c01523>.
- (30) Hu, Z.; Yang, Y.; Zhao, Y.; Huang, Y. The Prognostic Value of Cyclooxygenase-2 Expression in Patients with Esophageal Cancer: Evidence from a Meta-Analysis. *OncoTargets and Therapy*. Dove Medical Press Ltd. June 9, 2017, pp 2893–2901. <https://doi.org/10.2147/OTT.S134599>.
- (31) Pu, D.; Yin, L.; Huang, L.; Qin, C.; Zhou, Y.; Wu, Q.; Li, Y.; Zhou, Q.; Li, L. Cyclooxygenase-2 Inhibitor: A Potential Combination Strategy With Immunotherapy in Cancer. *Front Oncol* **2021**, *11*. <https://doi.org/10.3389/fonc.2021.637504>.
- (32) Hawkey, C. J. COX-1 and COX-2 Inhibitors. *Best Pract Res Clin Gastroenterol* **2001**, *15* (5), 801–820. <https://doi.org/10.1053/bega.2001.0236>.
- (33) Burnier, M. The Safety of Rofecoxib. *Expert Opin Drug Saf* **2005**, *4* (3), 491–499. <https://doi.org/10.1517/14740338.4.3.491>.
- (34) El-Malah, A. A.; Gineinah, M. M.; Deb, P. K.; Khayyat, A. N.; Bansal, M.; Venugopala, K. N.; Aljahdali, A. S. Selective COX-2 Inhibitors: Road from Success to Controversy and the Quest for Repurposing. *Pharmaceuticals* **2022**, *15* (7), 827. <https://doi.org/10.3390/ph15070827>.
- (35) Arora, M.; Choudhary, S.; Singh, P. K.; Sapra, B.; Silakari, O. Structural Investigation on the Selective COX-2 Inhibitors Mediated Cardiotoxicity: A Review. *Life Sciences*. Elsevier Inc. June 15, 2020. <https://doi.org/10.1016/j.lfs.2020.117631>.
- (36) Buzharevski, A.; Paskaš, S.; Sárosi, M.-B.; Laube, M.; Lönnecke, P.; Neumann, W.; Murganić, B.; Mijatović, S.; Maksimović-Ivanić, D.; Pietzsch, J.; Hey-Hawkins, E. Carboranyl Derivatives of Rofecoxib with Cytostatic Activity against Human Melanoma and Colon Cancer Cells. *Sci Rep* **2020**, *10* (1), 4827. <https://doi.org/10.1038/s41598-020-59059-3>.
- (37) Scholz, M.; Blobaum, A. L.; Marnett, L. J.; Hey-Hawkins, E. Ortho-Carborane Derivatives of Indomethacin as Cyclooxygenase (COX)-2 Selective Inhibitors. *Bioorg Med Chem* **2012**, *20* (15), 4830–4837. <https://doi.org/10.1016/j.bmc.2012.05.063>.
- (38) Moss, R. L. Critical Review, with an Optimistic Outlook, on Boron Neutron Capture Therapy (BNCT). *Applied Radiation and Isotopes* **2014**, *88*, 2–11. <https://doi.org/10.1016/j.apradiso.2013.11.109>.
- (39) Xuan, S.; Vicente, M. da G. H. Recent Advances in Boron Delivery Agents for Boron Neutron Capture Therapy (BNCT). In *Boron-Based Compounds*; John Wiley & Sons, Ltd: Chichester, UK, 2018; pp 298–342. <https://doi.org/10.1002/9781119275602.ch3.2>.

- (40) Wang, S.; Zhang, Z.; Miao, L.; Li, Y. Boron Neutron Capture Therapy: Current Status and Challenges. *Frontiers in Oncology*. Frontiers Media S.A. March 31, 2022. <https://doi.org/10.3389/fonc.2022.788770>.
- (41) Sköld, K.; Gorlia, T.; Pellettieri, L.; Giusti, V.; H-Stenstam, B.; Hopewell, J. W. Boron Neutron Capture Therapy for Newly Diagnosed Glioblastoma Multiforme: An Assessment of Clinical Potential. *British Journal of Radiology* **2010**, *83* (991), 596–603. <https://doi.org/10.1259/bjr/56953620>.
- (42) Lan, T. L.; Chou, F. I.; Lin, K. H.; Pan, P. S.; Lee, J. C.; Huang, W. S.; Liu, Y. M.; Chao, Y.; Chen, Y. W. Using Salvage Boron Neutron Capture Therapy (BNCT) for Recurrent Malignant Brain Tumors in Taiwan. *Applied Radiation and Isotopes* **2020**, *160*. <https://doi.org/10.1016/j.apradiso.2020.109105>.
- (43) Barth, R. F.; Vicente, M. G. H.; Harling, O. K.; Kiger, W. S.; Riley, K. J.; Binns, P. J.; Wagner, F. M.; Suzuki, M.; Aihara, T.; Kato, I.; Kawabata, S. Current Status of Boron Neutron Capture Therapy of High Grade Gliomas and Recurrent Head and Neck Cancer. *Radiation Oncology*. August 29, 2012. <https://doi.org/10.1186/1748-717X-7-146>.
- (44) Suzuki, M.; Suzuki, O.; Sakurai, Y.; Tanaka, H.; Kondo, N.; Kinashi, Y.; Masunaga, S.; Maruhashi, A.; Ono, K. Reirradiation for Locally Recurrent Lung Cancer in the Chest Wall with Boron Neutron Capture Therapy (BNCT). *Int Cancer Conf J* **2012**, *1* (4), 235–238. <https://doi.org/10.1007/s13691-012-0048-8>.
- (45) Mishima, Y.; Kondoh, H.; Yoshino, K.; Hiratsuka, J. Current Clinical Paradigms in Melanoma BNCT. In *Frontiers in Neutron Capture Therapy*; Springer US: Boston, MA, 2001; pp 1365–1382. https://doi.org/10.1007/978-1-4615-1285-1_208.
- (46) Medina-Castro, D.; Vega-Carrillo, H. R.; Galicia-Aragón, J.; Soto-Bernal, T. G.; Baltazar-Raigosa, A. Beam Port Filters in a TRIGA MARK III Nuclear Reactor to Produce Epithermal Neutrons for BNCT. *Applied Radiation and Isotopes* **2022**, *179*. <https://doi.org/10.1016/j.apradiso.2021.110018>.
- (47) Moss, R. L. Critical Review, with an Optimistic Outlook, on Boron Neutron Capture Therapy (BNCT). *Applied Radiation and Isotopes* **2014**, *88*, 2–11. <https://doi.org/10.1016/j.apradiso.2013.11.109>.
- (48) Jin, W. H.; Seldon, C.; Butkus, M.; Sauerwein, W.; Giap, H. B. A Review of Boron Neutron Capture Therapy: Its History and Current Challenges. *Int J Part Ther* **2022**, *9* (1), 71–82. <https://doi.org/10.14338/ijpt-22-00002.1>.
- (49) Khodaei, T.; Inamdar, S.; Suresh, A. P.; Acharya, A. P. Drug Delivery for Metabolism Targeted Cancer Immunotherapy. *Adv Drug Deliv Rev* **2022**, *184*, 114242. <https://doi.org/10.1016/j.addr.2022.114242>.
- (50) Fu, Z.; Li, S.; Han, S.; Shi, C.; Zhang, Y. Antibody Drug Conjugate: The “Biological Missile” for Targeted Cancer Therapy. *Signal Transduction and Targeted Therapy*. Springer Nature December 1, 2022. <https://doi.org/10.1038/s41392-022-00947-7>.
- (51) Sauerwein, W. A. G.; Sancey, L.; Hey-Hawkins, E.; Kellert, M.; Panza, L.; Imperio, D.; Balcerzyk, M.; Rizzo, G.; Scalco, E.; Herrmann, K.; Mauri, P.; Palma, A. de; Wittig, A. Theranostics in Boron Neutron Capture Therapy. *Life*. MDPI AG April 1, 2021. <https://doi.org/10.3390/life11040330>.
- (52) Savolainen, S.; Kortensniemi, M.; Timonen, M.; Reijonen, V.; Kuusela, L.; Uusi-Simola, J.; Salli, E.; Koivunoro, H.; Seppälä, T.; Lönnroth, N.; Välimäki, P.; Hyvönen, H.; Kotiluoto, P.; Serén, T.; Kuronen, A.; Heikkinen, S.; Kosunen, A.; Auterinen, I. Boron Neutron Capture Therapy (BNCT) in Finland: Technological and Physical Prospects after 20 Years of Experiences. *Physica Medica*. May 2013, pp 233–248. <https://doi.org/10.1016/j.ejmp.2012.04.008>.

- (53) Li, L.; Li, J.; Shi, Y.; Du, P.; Zhang, Z.; Liu, T.; Zhang, R.; Liu, Z. On-Demand Biodegradable Boron Nitride Nanoparticles for Treating Triple Negative Breast Cancer with Boron Neutron Capture Therapy. *ACS Nano* **2019**, *13* (12), 13843–13852. <https://doi.org/10.1021/acsnano.9b04303>.
- (54) Chen, J.; Yang, Q.; Liu, M.; Lin, M.; Wang, T.; Zhang, Z.; Zhong, X.; Guo, N.; Lu, Y.; Xu, J.; Wang, C.; Han, M.; Wei, Q. Remarkable Boron Delivery of IRGD-Modified Polymeric Nanoparticles for Boron Neutron Capture Therapy. *Int J Nanomedicine* **2019**, *14*, 8161–8177. <https://doi.org/10.2147/IJN.S214224>.
- (55) Tsurubuchi, T.; Shirakawa, M.; Kurosawa, W.; Matsumoto, K.; Ubagai, R.; Umishio, H.; Suga, Y.; Yamazaki, J.; Arakawa, A.; Maruyama, Y.; Seki, T.; Shibui, Y.; Yoshida, F.; Zaboronok, A.; Suzuki, M.; Sakurai, Y.; Tanaka, H.; Nakai, K.; Ishikawa, E.; Matsumura, A. Evaluation of a Novel Boron-Containing α -D-Mannopyranoside for BNCT. *Cells* **2020**, *9* (5). <https://doi.org/10.3390/cells9051277>.
- (56) Dai, Q.; Yang, Q.; Bao, X.; Chen, J.; Han, M.; Wei, Q. The Development of Boron Analysis and Imaging in Boron Neutron Capture Therapy (BNCT). *Molecular Pharmaceutics*. American Chemical Society February 7, 2022, pp 363–377. <https://doi.org/10.1021/acs.molpharmaceut.1c00810>.
- (57) Barth, R. F.; Mi, P.; Yang, W. Boron Delivery Agents for Neutron Capture Therapy of Cancer. *Cancer Commun* **2018**, *38* (1), 1–15. <https://doi.org/10.1186/s40880-018-0299-7>.
- (58) Miller, H. C.; Miller, N. E.; Muetterties, E. L. Chemistry of Boranes. XX. Syntheses of Polyhedral Boranes. *Inorg Chem* **1964**, *3* (10), 1456–1463. <https://doi.org/10.1021/ic50020a026>.
- (59) Hatanaka, H.; Nakagawa, Y. Clinical Results of Long-Surviving Brain Tumor Patients Who Underwent Boron Neutron Capture Therapy. *International Journal of Radiation Oncology*Biophysics*Physics* **1994**, *28* (5), 1061–1066. [https://doi.org/10.1016/0360-3016\(94\)90479-0](https://doi.org/10.1016/0360-3016(94)90479-0).
- (60) Nakagawa, Y.; Pooh, K.; Kobayashi, T.; Kageji, T.; Uyama, S.; Matsumura, A.; Kumada, H. Clinical Review of the Japanese Experience with Boron Neutron Capture Therapy and a Proposed Strategy Using Epithermal Neutron Beams. *J Neurooncol* **2003**, *62* (1–2), 87–99. <https://doi.org/10.1007/BF02699936>.
- (61) Vos, M. J.; Turowski, B.; Zanella, F. E.; Paquis, P.; Siefert, A.; Hideghéty, K.; Haselsberger, K.; Grochulla, F.; Postma, T. J.; Wittig, A.; Heimans, J. J.; Slotman, B. J.; Vandertop, W. P.; Sauerwein, W. Radiologic Findings in Patients Treated with Boron Neutron Capture Therapy for Glioblastoma Multiforme within EORTC Trial 11961. *Int J Radiat Oncol Biol Phys* **2005**, *61* (2), 392–399. <https://doi.org/10.1016/j.ijrobp.2004.06.008>.
- (62) Snyder, H. R.; Reedy, A. J.; Lennarz, W. J. *Synthesis of Aromatic Boronic Acids Synthesis of Aromatic Boronic Acids. Aldehyde Boronic Acids and a Boronic Acid Analog of Tyrosine1*; 1958. <https://pubs.acs.org/sharingguidelines>.
- (63) Mishima, Y. Selective Thermal Neutron Capture Therapy of Cancer Cells Using Their Specific Metabolic Activities—Melanoma as Prototype. In *Cancer Neutron Capture Therapy*; Springer US: Boston, MA, 1996; pp 1–26. https://doi.org/10.1007/978-1-4757-9567-7_1.
- (64) Yoshino, K.; Suzuki, A.; Mori, Y.; Kakahana, H.; Honda, C.; Mishima, Y.; Kobayashi, T.; Kanda, K. Improvement of Solubility of P-Boronophenylalanine by Complex Formation with Monosaccharides. *Strahlenther Onkol* **165** (2–3), 127–129.
- (65) Kankaanranta, L.; Seppälä, T.; Koivunoro, H.; Välimäki, P.; Beule, A.; Collan, J.; Kortensniemi, M.; Uusi-Simola, J.; Kotiluoto, P.; Auterinen, I.; Sern, T.; Paetau, A.; Saarihahti, K.; Savolainen, S.; Joensuu, H. L-Boronophenylalanine-Mediated Boron Neutron Capture Therapy for Malignant Glioma Progressing

after External Beam Radiation Therapy: A Phase I Study. *Int J Radiat Oncol Biol Phys* **2011**, *80* (2), 369–376. <https://doi.org/10.1016/j.ijrobp.2010.02.031>.

- (66) Diaz, A. Z. Assessment of the Results from the Phase I/II Boron Neutron Capture Therapy Trials at the Brookhaven National Laboratory from a Clinician's Point of View. *J Neurooncol* **2003**, *62* (1–2), 101–109. <https://doi.org/10.1007/BF02699937>.
- (67) Goodman, J. H.; Yang, W.; Barth, R. F.; Gao, Z.; Boesel, C. P.; Staubus, A. E.; Gupta, N.; Gahbauer, R. A.; Adams, D. M.; Gibson, C. R.; Ferketich, A. K.; Moeschberger, M. L.; Soloway, A. H.; Carpenter, D. E.; Albertson, B. J.; Bauer, W. F.; Zhang, M. Z.; Wang, C. C. Boron Neutron Capture Therapy of Brain Tumors: Biodistribution, Pharmacokinetics, and Radiation Dosimetry of Sodium Borocaptate in Patients with Gliomas. *Neurosurgery* **2000**, *47* (3), 608–622. <https://doi.org/10.1097/00006123-200009000-00016>.
- (68) Koivunoro, H.; Hippeläinen, E.; Auterinen, I.; Kankaanranta, L.; Kulvik, M.; Laakso, J.; Seppälä, T.; Savolainen, S.; Joensuu, H. Biokinetic Analysis of Tissue Boron (¹⁰B) Concentrations of Glioma Patients Treated with BNCT in Finland. *Applied Radiation and Isotopes* **2015**, *106*, 189–194. <https://doi.org/10.1016/j.apradiso.2015.08.014>.
- (69) Chen, R.; Smith-Cohn, M.; Cohen, A. L.; Colman, H. Glioma Subclassifications and Their Clinical Significance. *Neurotherapeutics*. Springer New York LLC April 1, 2017, pp 284–297. <https://doi.org/10.1007/s13311-017-0519-x>.
- (70) Barth, R. F.; Grecula, J. C. Boron Neutron Capture Therapy at the Crossroads - Where Do We Go from Here? *Applied Radiation and Isotopes* **2020**, *160*. <https://doi.org/10.1016/j.apradiso.2019.109029>.
- (71) Yanagië, H.; Ogata, A.; Sugiyama, H.; Eriguchi, M.; Takamoto, S.; Takahashi, H. Application of Drug Delivery System to Boron Neutron Capture Therapy for Cancer. *Expert Opin Drug Deliv* **2008**, *5* (4), 427–443. <https://doi.org/10.1517/17425247.5.4.427>.
- (72) Maruyama, K. Intracellular Targeting Delivery of Liposomal Drugs to Solid Tumors Based on EPR Effects. *Advanced Drug Delivery Reviews*. March 18, 2011, pp 161–169. <https://doi.org/10.1016/j.addr.2010.09.003>.
- (73) Matsumura, Y. 35 Years of Discussions with Prof. Maeda on the EPR Effect and Future Directions. *Journal of Controlled Release* **2022**, *348*, 966–969. <https://doi.org/10.1016/j.jconrel.2022.06.035>.
- (74) Hu, K.; Yang, Z.; Zhang, L.; Xie, L.; Wang, L.; Xu, H.; Josephson, L.; Liang, S. H.; Zhang, M. R. Boron Agents for Neutron Capture Therapy. *Coordination Chemistry Reviews*. Elsevier B.V. February 15, 2020. <https://doi.org/10.1016/j.ccr.2019.213139>.
- (75) Ming, W.; Liu, X.; Friedrich, A.; Krebs, J.; Marder, T. B. The Borono-Strecker Reaction: Synthesis of α -Aminoboronates via a Multicomponent Reaction of Carbonyl Compounds, Amines, and B₂pin₂. *Org Lett* **2020**, *22* (2), 365–370. <https://doi.org/10.1021/acs.orglett.9b03773>.
- (76) He, T.; Musah, R. A. Evaluation of the Potential of 2-Amino-3-(1,7-Dicarba-Closo-Dodecaboranyl-1-Thio)Propanoic Acid as a Boron Neutron Capture Therapy Agent. *ACS Omega* **2019**, *4* (2), 3820–3826. <https://doi.org/10.1021/acsomega.8b03407>.
- (77) Semioshkin, A.; Nizhnik, E.; Godovikov, I.; Starikova, Z.; Bregadze, V. Reactions of Oxonium Derivatives of [B₁₂H₁₂]²⁻ with Amines: Synthesis and Structure of Novel B₁₂-Based Ammonium Salts and Amino Acids. *J Organomet Chem* **2007**, *692* (19), 4020–4028. <https://doi.org/10.1016/j.jorganchem.2007.06.001>.

- (78) Kabalka, G. W.; Wu, Z.; Yao, M. L. Synthesis of a Series of Boronated Unnatural Cyclic Amino Acids as Potential Boron Neutron Capture Therapy Agents. *Appl Organomet Chem* **2008**, *22* (9), 516–522. <https://doi.org/10.1002/aoc.1435>.
- (79) Barth, R. F.; Kabalka, G. W.; Yang, W.; Huo, T.; Nakkula, R. J.; Shaikh, A. L.; Haider, S. A.; Chandra, S. Evaluation of Unnatural Cyclic Amino Acids as Boron Delivery Agents for Treatment of Melanomas and Gliomas. *Applied Radiation and Isotopes* **2014**, *88*, 38–42. <https://doi.org/10.1016/j.apradiso.2013.11.133>.
- (80) Chandra, S.; Ahmad, T.; Barth, R. F.; Kabalka, G. W. Quantitative Evaluation of Boron Neutron Capture Therapy (BNCT) Drugs for Boron Delivery and Retention at Subcellular-Scale Resolution in Human Glioblastoma Cells with Imaging Secondary Ion Mass Spectrometry (SIMS). *J Microsc* **2014**, *254* (3), 146–156. <https://doi.org/10.1111/jmi.12126>.
- (81) Lunato, A. J.; Wang, J.; Woollard, J. E.; Anisuzzaman, A. K. M.; Ji, W.; Rong, F.-G.; Ikeda, S.; Soloway, A. H.; Eriksson, S.; Ives, D. H.; Blue, T. E.; Tjarks, W. Synthesis of 5-(Carboranylalkylmercapto)-2'-Deoxyuridines and 3-(Carboranylalkyl)Thymidines and Their Evaluation as Substrates for Human Thymidine Kinases 1 and 2. *J Med Chem* **1999**, *42* (17), 3378–3389. <https://doi.org/10.1021/jm990125i>.
- (82) Białek-Pietras, M.; Olejniczak, A. B.; Paradowska, E.; Studzińska, M.; Jabłońska, A.; Leśnikowski, Z. J. Synthesis, Susceptibility to Enzymatic Phosphorylation, Cytotoxicity and in Vitro Antiviral Activity of Lipophilic Pyrimidine Nucleoside/Carborane Conjugates. *J Organomet Chem* **2018**, *865*, 166–172. <https://doi.org/10.1016/j.jorganchem.2018.03.026>.
- (83) Agarwal, H. K.; Khalil, A.; Ishita, K.; Yang, W.; Nakkula, R. J.; Wu, L. C.; Ali, T.; Tiwari, R.; Byun, Y.; Barth, R. F.; Tjarks, W. Synthesis and Evaluation of Thymidine Kinase 1-Targeting Carboranyl Pyrimidine Nucleoside Analogs for Boron Neutron Capture Therapy of Cancer. *Eur J Med Chem* **2015**, *100*, 197–209. <https://doi.org/10.1016/j.ejmech.2015.05.042>.
- (84) Barth, R. F.; Yang, W.; Adams, D. M.; Rotaru, J. H.; Shukla, S.; Sekido, M.; Tjarks, W.; Fenstermaker, R. A.; Ciesielski, M.; Nawrocky, M. M.; Coderre, J. A. Molecular Targeting of the Epidermal Growth Factor Receptor for Neutron Capture Therapy of Gliomas. *Cancer Res* **2002**, *62* (11), 3159–3166.
- (85) Backer, M. v.; Gaynutdinov, T. I.; Patel, V.; Bandyopadhyaya, A. K.; Thirumamagal, B. T. S.; Tjarks, W.; Barth, R. F.; Claffey, K.; Backer, J. M. Vascular Endothelial Growth Factor Selectively Targets Boronated Dendrimers to Tumor Vasculature. *Mol Cancer Ther* **2005**, *4* (9), 1423–1429. <https://doi.org/10.1158/1535-7163.MCT-05-0161>.
- (86) Kimura, S.; Masunaga, S.; Harada, T.; Kawamura, Y.; Ueda, S.; Okuda, K.; Nagasawa, H. Synthesis and Evaluation of Cyclic RGD-Boron Cluster Conjugates to Develop Tumor-Selective Boron Carriers for Boron Neutron Capture Therapy. *Bioorg Med Chem* **2011**, *19* (5), 1721–1728. <https://doi.org/10.1016/j.bmc.2011.01.020>.
- (87) Yang, W.; Wu, G.; Barth, R. F.; Swindall, M. R.; Bandyopadhyaya, A. K.; Tjarks, W.; Tordoff, K.; Moeschberger, M.; Sferra, T. J.; Binns, P. J.; Riley, K. J.; Ciesielski, M. J.; Fenstermaker, R. A.; Wikstrand, C. J. Molecular Targeting and Treatment of Composite EGFR and EGFRVIII-Positive Gliomas Using Boronated Monoclonal Antibodies. *Clinical Cancer Research* **2008**, *14* (3), 883–891. <https://doi.org/10.1158/1078-0432.CCR-07-1968>.
- (88) Hanahan, D.; Weinberg, R. A. Hallmarks of Cancer: The Next Generation. *Cell* **2011**, *144* (5), 646–674. <https://doi.org/10.1016/j.cell.2011.02.013>.

- (89) Imperio, D.; Panza, L. Sweet Boron: Boron-Containing Sugar Derivatives as Potential Agents for Boron Neutron Capture Therapy. *Symmetry*. MDPI February 1, 2022. <https://doi.org/10.3390/sym14020182>.
- (90) Abbaszadeh, Z.; Çeşmeli, S.; Biray Avcı, Ç. Crucial Players in Glycolysis: Cancer Progress. *Gene*. Elsevier B.V. February 5, 2020. <https://doi.org/10.1016/j.gene.2019.144158>.
- (91) Hossain, F.; Andreana, P. R. Developments in Carbohydrate-Based Cancer Therapeutics. *Pharmaceuticals* **2019**, *12* (2). <https://doi.org/10.3390/ph12020084>.
- (92) Mullapudi, S. S.; Mitra, D.; Li, M.; Kang, E. T.; Chiong, E.; Neoh, K. G. Potentiating Anti-Cancer Chemotherapeutics and Antimicrobials: Via Sugar-Mediated Strategies. *Molecular Systems Design and Engineering*. Royal Society of Chemistry May 1, 2020, pp 772–791. <https://doi.org/10.1039/c9me00175a>.
- (93) Calvaresi, E. C.; Hergenrother, P. J. Glucose Conjugation for the Specific Targeting and Treatment of Cancer. *Chem Sci* **2013**, *4* (6), 2319–2333. <https://doi.org/10.1039/c3sc22205e>.
- (94) Imperio, D.; del Grosso, E.; Fallarini, S.; Lombardi, G.; Panza, L. Synthesis of Sugar-Boronic Acid Derivatives: A Class of Potential Agents for Boron Neutron Capture Therapy. *Org Lett* **2017**, *19* (7), 1678–1681. <https://doi.org/10.1021/acs.orglett.7b00382>.
- (95) Imperio, D.; del Grosso, E.; Fallarini, S.; Lombardi, G.; Panza, L. Anomeric Sugar Boronic Acid Analogues as Potential Agents for Boron Neutron Capture Therapy. *Beilstein Journal of Organic Chemistry* **2019**, *15*, 1355–1359. <https://doi.org/10.3762/bjoc.15.135>.
- (96) Itoh, T.; Tamura, K.; Ueda, H.; Tanaka, T.; Sato, K.; Kuroda, R.; Aoki, S. Design and Synthesis of Boron Containing Monosaccharides by the Hydroboration of D-Glucal for Use in Boron Neutron Capture Therapy (BNCT). *Bioorg Med Chem* **2018**, *26* (22), 5922–5933. <https://doi.org/10.1016/j.bmc.2018.10.041>.
- (97) Muz, B.; Azab, A. K.; Confalonieri, L.; del Grosso, E.; Fallarini, S.; Imperio, D.; Panza, L. Synthesis, Equilibrium, and Biological Study of a C-7 Glucose Boronic Acid Derivative as a Potential Candidate for Boron Neutron Capture Therapy. *Bioorg Med Chem* **2022**, *59*. <https://doi.org/10.1016/j.bmc.2022.116659>.
- (98) Imperio, D.; Muz, B.; Azab, A. K.; Fallarini, S.; Lombardi, G.; Panza, L. A Short and Convenient Synthesis of Closo-Dodecaborate Sugar Conjugates. *European J Org Chem* **2019**, *2019* (43), 7228–7232. <https://doi.org/10.1002/ejoc.201901412>.
- (99) Matović, J.; Järvinen, J.; Sokka, I. K.; Stockmann, P.; Kellert, M.; Imlimthan, S.; Sarparanta, M.; Johansson, M. P.; Hey-Hawkins, E.; Rautio, J.; Ekholm, F. S. Synthesis and in Vitro Evaluation of a Set of 6-Deoxy-6-Thio-Carboranyl d-Glucoconjugates Shed Light on the Substrate Specificity of the GLUT1 Transporter. *ACS Omega* **2022**, *7* (34), 30376–30388. <https://doi.org/10.1021/acsomega.2c03646>.
- (100) Backer, M. v.; Gaynutdinov, T. I.; Patel, V.; Bandyopadhyaya, A. K.; Thirumamagal, B. T. S.; Tjarks, W.; Barth, R. F.; Claffey, K.; Backer, J. M. Vascular Endothelial Growth Factor Selectively Targets Boronated Dendrimers to Tumor Vasculature. *Mol Cancer Ther* **2005**, *4* (9), 1423–1429. <https://doi.org/10.1158/1535-7163.MCT-05-0161>.
- (101) Wu, G.; Barth, R. F.; Yang, W.; Chatterjee, M.; Tjarks, W.; Ciesielski, M. J.; Fenstermaker, R. A. Site-Specific Conjugation of Boron-Containing Dendrimers to Anti-EGF Receptor Monoclonal Antibody

- Cetuximab (IMC-C225) and Its Evaluation as a Potential Delivery Agent for Neutron Capture Therapy. *Bioconjug Chem* **2004**, *15* (1), 185–194. <https://doi.org/10.1021/bc0341674>.
- (102) Saraf, S.; Jain, A.; Tiwari, A.; Verma, A.; Panda, P. K.; Jain, S. K. Advances in Liposomal Drug Delivery to Cancer: An Overview. *Journal of Drug Delivery Science and Technology*. Editions de Sante April 1, 2020. <https://doi.org/10.1016/j.jddst.2020.101549>.
- (103) Maitz, C. A.; Khan, A. A.; Kueffer, P. J.; Brockman, J. D.; Dixon, J.; Jalisatgi, S. S.; Nigg, D. W.; Everett, T. A.; Hawthorne, M. F. Validation and Comparison of the Therapeutic Efficacy of Boron Neutron Capture Therapy Mediated By Boron-Rich Liposomes in Multiple Murine Tumor Models. *Transl Oncol* **2017**, *10* (4), 686–692. <https://doi.org/10.1016/j.tranon.2017.05.003>.
- (104) Lee, W.; Sarkar, S.; Ahn, H.; Kim, J. Y.; Lee, Y. J.; Chang, Y.; Yoo, J. PEGylated Liposome Encapsulating Nido-Carborane Showed Significant Tumor Suppression in Boron Neutron Capture Therapy (BNCT). *Biochem Biophys Res Commun* **2020**, *522* (3), 669–675. <https://doi.org/10.1016/j.bbrc.2019.11.144>.
- (105) Kueffer, P. J.; Maitz, C. A.; Khan, A. A.; Schuster, S. A.; Shlyakhtina, N. I.; Jalisatgi, S. S.; Brockman, J. D.; Nigg, D. W.; Hawthorne, M. F. Boron Neutron Capture Therapy Demonstrated in Mice Bearing EMT6 Tumors Following Selective Delivery of Boron by Rationally Designed Liposomes. *Proc Natl Acad Sci U S A* **2013**, *110* (16), 6512–6517. <https://doi.org/10.1073/pnas.1303437110>.
- (106) Yoneoka, S.; Park, K.; Nakagawa, Y.; Ebara, M.; Tsukahara, T. Synthesis and Evaluation of Thermoresponsive Boron-Containing Poly(N-Isopropylacrylamide) Diblock Copolymers for Self-Assembling Nanomicellar Boron Carriers. *Polymers (Basel)* **2018**, *11* (1), 42. <https://doi.org/10.3390/polym11010042>.
- (107) Wang, J.; Chen, L.; Ye, J.; Li, Z.; Jiang, H.; Yan, H.; Stogniy, M. Yu.; Sivaev, I. B.; Bregadze, V. I.; Wang, X. Carborane Derivative Conjugated with Gold Nanoclusters for Targeted Cancer Cell Imaging. *Biomacromolecules* **2017**, *18* (5), 1466–1472. <https://doi.org/10.1021/acs.biomac.6b01845>.
- (108) Zhu, Y.; Lin, Y.; Zhu, Y. Z.; Lu, J.; Maguire, J. A.; Hosmane, N. S. Boron Drug Delivery via Encapsulated Magnetic Nanocomposites: A New Approach for BNCT in Cancer Treatment. *J Nanomater* **2010**, *2010*, 1–8. <https://doi.org/10.1155/2010/409320>.
- (109) Gilham, I. Theranostic an Emerging Tool in Drug Discovery and Commercialisation. *Drug Discovery World Fall* **2002**, 17–23.
- (110) Kelkar, S. S.; Reineke, T. M. Theranostics: Combining Imaging and Therapy. *Bioconjug Chem* **2011**, *22* (10), 1879–1903. <https://doi.org/10.1021/bc200151q>.
- (111) Kumar S, J. T. Theranostics: A Way of Modern Medical Diagnostics and the Role of Chitosan. *Journal of Molecular and Genetic Medicine* **2014**, *09* (01). <https://doi.org/10.4172/1747-0862.1000159>.
- (112) Gupta, A.; Sood, A.; Fuhrer, E.; Djanashvili, K.; Agrawal, G. Polysaccharide-Based Theranostic Systems for Combined Imaging and Cancer Therapy: Recent Advances and Challenges. *ACS Biomaterials Science and Engineering*. American Chemical Society June 13, 2022, pp 2281–2306. <https://doi.org/10.1021/acsbmaterials.1c01631>.
- (113) Indoria, S.; Singh, V.; Hsieh, M.-F. Recent Advances in Theranostic Polymeric Nanoparticles for Cancer Treatment: A Review. *Int J Pharm* **2020**, *582*, 119314. <https://doi.org/10.1016/j.ijpharm.2020.119314>.

- (114) Swierczewska, M.; Han, H. S.; Kim, K.; Park, J. H.; Lee, S. Polysaccharide-Based Nanoparticles for Theranostic Nanomedicine. *Adv Drug Deliv Rev* **2016**, *99*, 70–84. <https://doi.org/10.1016/j.addr.2015.11.015>.
- (115) Ichikawa, Y.; Kobayashi, N.; Takano, S.; Kato, I.; Endo, K.; Inoue, T. Neuroendocrine Tumor Theranostics. *Cancer Sci* **2022**, *113* (6), 1930–1938. <https://doi.org/10.1111/cas.15327>.
- (116) Levine, R.; Krenning, E. P. Clinical History of the Theranostic Radionuclide Approach to Neuroendocrine Tumors and Other Types of Cancer: Historical Review Based on an Interview of Eric P. Krenning by Rachel Levine. *Journal of Nuclear Medicine* **2017**, *58* (Supplement 2), 3S–9S. <https://doi.org/10.2967/jnumed.116.186502>.
- (117) Das, S.; Al-Toubah, T.; El-Haddad, G.; Strosberg, J. 177 Lu-DOTATATE for the Treatment of Gastroenteropancreatic Neuroendocrine Tumors. *Expert Rev Gastroenterol Hepatol* **2019**, *13* (11), 1023–1031. <https://doi.org/10.1080/17474124.2019.1685381>.
- (118) Protti, N.; Deagostino, A.; Boggio, P.; Alberti, D.; Crich, S. G. New Boronated Compounds for an Imaging-Guided Personalized Neutron Capture Therapy. In *Boron-Based Compounds*; John Wiley & Sons, Ltd: Chichester, UK, 2018; pp 389–415. <https://doi.org/10.1002/9781119275602.ch3.5>.
- (119) Coenen, H. H.; Ermert, J. Expanding PET-Applications in Life Sciences with Positron-Emitters beyond Fluorine-18. *Nuclear Medicine and Biology*. Elsevier Inc. January 1, 2021, pp 241–269. <https://doi.org/10.1016/j.nucmedbio.2020.07.003>.
- (120) Vaquero, J. J.; Kinahan, P. Positron Emission Tomography: Current Challenges and Opportunities for Technological Advances in Clinical and Preclinical Imaging Systems. *Annual Review of Biomedical Engineering*. Annual Reviews Inc. December 7, 2015, pp 385–414. <https://doi.org/10.1146/annurev-bioeng-071114-040723>.
- (121) Deng, X.; Rong, J.; Wang, L.; Vasdev, N.; Zhang, L.; Josephson, L.; Liang, S. H. Chemie Der Positronenemissionstomographie: Aktuelle Fortschritte Bei 11 C-, 18 F-, 13 N- Und 15 O-Markierungsreaktionen . *Angewandte Chemie* **2019**, *131* (9), 2604–2631. <https://doi.org/10.1002/ange.201805501>.
- (122) Burke, B. P.; Clemente, G. S.; Archibald, S. J. Boron-18F Containing Positron Emission Tomography Radiotracers: Advances and Opportunities. *Contrast Media and Molecular Imaging*. John Wiley and Sons Ltd March 1, 2015, pp 96–110. <https://doi.org/10.1002/cmml.1615>.
- (123) Ishiwata, K.; Ido, T.; Mejia, A. A.; Ichihashi, M.; Mishima, Y. Synthesis and Radiation Dosimetry of 4-Borono-2-[18F]Fluoro-d,l-Phenylalanine: A Target Compound for PET and Boron Neutron Capture Therapy. *Int J Rad Appl Instrum A* **1991**, *42* (4), 325–328. [https://doi.org/10.1016/0883-2889\(91\)90133-L](https://doi.org/10.1016/0883-2889(91)90133-L).
- (124) Evangelista, L.; Jori, G.; Martini, D.; Sotti, G. Boron Neutron Capture Therapy and 18F-Labelled Borophenylalanine Positron Emission Tomography: A Critical and Clinical Overview of Theliterature. *Applied Radiation and Isotopes* **2013**, *74*, 91–101. <https://doi.org/10.1016/j.apradiso.2013.01.001>.
- (125) Li, J.; Shi, Y.; Zhang, Z.; Liu, H.; Lang, L.; Liu, T.; Chen, X.; Liu, Z. A Metabolically Stable Boron-Derived Tyrosine Serves as a Theranostic Agent for Positron Emission Tomography Guided Boron Neutron Capture Therapy. *Bioconjug Chem* **2019**, *30* (11), 2870–2878. <https://doi.org/10.1021/acs.bioconjchem.9b00578>.

- (126) Li, Z.; Kong, Z.; Chen, J.; Li, J.; Li, N.; Yang, Z.; Wang, Y.; Liu, Z.; Cn, Y. 18F-Boromino Acid PET/CT in Healthy Volunteers and Glioma Patients. *Eur J Nucl Med Mol Imaging* **2021**, *48*, 3113–3121. <https://doi.org/10.1007/s00259-021-05212-7>/Published.
- (127) Kong, Z.; Li, Z.; Chen, J.; Liu, S.; Liu, D.; Li, J.; Li, N.; Ma, W.; Feng, F.; Wang, Y.; Yang, Z.; Liu, Z. Metabolic Characteristics of [18F]Fluoroboronotyrosine (FBY) PET in Malignant Brain Tumors. *Nucl Med Biol* **2022**, *106–107*, 80–87. <https://doi.org/10.1016/j.nucmedbio.2022.01.002>.
- (128) Pimlott, S. L.; Sutherland, A. Molecular Tracers for the PET and SPECT Imaging of Disease. *Chemical Society Reviews*. January 2011, pp 149–162. <https://doi.org/10.1039/b922628c>.
- (129) Kobayashi, T.; Sakurai, Y.; Ishikawa, M. A Noninvasive Dose Estimation System for Clinical BNCT Based on PG-SPECT-Conceptual Study and Fundamental Experiments Using HPGe and CdTe Semiconductor Detectors. *Med Phys* **2000**, *27* (9), 2124–2132. <https://doi.org/10.1118/1.1288243>.
- (130) Hales, B.; Katabuchi, T.; Hayashizaki, N.; Terada, K.; Igashira, M.; Kobayashi, T. Feasibility Study of SPECT System for Online Dosimetry Imaging in Boron Neutron Capture Therapy. *Applied Radiation and Isotopes* **2014**, *88*, 167–170. <https://doi.org/10.1016/j.apradiso.2013.11.135>.
- (131) Winkler, A.; Koivunoro, H.; Reijonen, V.; Auterinen, I.; Savolainen, S. Prompt Gamma and Neutron Detection in BNCT Utilizing a CdTe Detector. *Applied Radiation and Isotopes* **2015**, *106*, 139–144. <https://doi.org/10.1016/j.apradiso.2015.07.040>.
- (132) Manabe, M.; Sato, F.; Murata, I. Basic Detection Property of an Array-Type CdTe Detector for BNCT–SPECT – Measurement and Analysis of Anti-Coincidence Events. *Applied Radiation and Isotopes* **2016**, *118*, 389–394. <https://doi.org/10.1016/j.apradiso.2015.11.003>.
- (133) Kim, M.-S.; Shin, H.-B.; Choi, M.-G.; Monzen, H.; Shim, J. G.; Suh, T. S.; Yoon, D.-K. Reference Based Simulation Study of Detector Comparison for BNCT-SPECT Imaging. *Nuclear Engineering and Technology* **2020**, *52* (1), 155–163. <https://doi.org/10.1016/j.net.2019.07.002>.
- (134) Murata, I.; Kusaka, S.; Minami, K.; Saraue, N.; Tamaki, S.; Kato, I.; Sato, F. Design of SPECT for BNCT to Measure Local Boron Dose with GAGG Scintillator. *Applied Radiation and Isotopes* **2022**, *181*, 110056. <https://doi.org/10.1016/j.apradiso.2021.110056>.
- (135) Robertson, A. G.; Rendina, L. M. Gadolinium Theranostics for the Diagnosis and Treatment of Cancer. *Chemical Society Reviews*. Royal Society of Chemistry April 7, 2021, pp 4231–4244. <https://doi.org/10.1039/d0cs01075h>.
- (136) Nemoto, H.; Cai, J.; Nakamura, H.; Fujiwara, M.; Yamamoto, Y. The Synthesis of a Carborane Gadolinium-DTPA Complex for Boron Neutron Capture Therapy. *J Organomet Chem* **1999**, *581* (1–2), 170–175. [https://doi.org/10.1016/S0022-328X\(99\)00049-2](https://doi.org/10.1016/S0022-328X(99)00049-2).
- (137) Takahashi, K.; Nakamura, H.; Furumoto, S.; Yamamoto, K.; Fukuda, H.; Matsumura, A.; Yamamoto, Y. Synthesis and in Vivo Biodistribution of BPA–Gd–DTPA Complex as a Potential MRI Contrast Carrier for Neutron Capture Therapy. *Bioorg Med Chem* **2005**, *13* (3), 735–743. <https://doi.org/10.1016/j.bmc.2004.10.046>.
- (138) Alberti, D.; Deagostino, A.; Toppino, A.; Protti, N.; Bortolussi, S.; Altieri, S.; Aime, S.; Geninatti Crich, S. An Innovative Therapeutic Approach for Malignant Mesothelioma Treatment Based on the Use of Gd/Boron Multimodal Probes for MRI Guided BNCT. *Journal of Controlled Release* **2018**, *280*, 31–38. <https://doi.org/10.1016/j.jconrel.2018.04.043>.

- (139) Aime, S.; Barge, A.; Crivello, A.; Deagostino, A.; Gobetto, R.; Nervi, C.; Prandi, C.; Toppino, A.; Venturello, P. Synthesis of Gd(III)-C-Palmitamidomethyl-C'-DOTAMA-C 6-o-Carborane: A New Dual Agent for Innovative MRI/BNCT Applications. *Org Biomol Chem* **2008**, *6* (23), 4460–4466. <https://doi.org/10.1039/b808804g>.
- (140) Janasik, D.; Krawczyk, T. 19F MRI Probes for Multimodal Imaging**. *Chemistry - A European Journal*. John Wiley and Sons Inc January 24, 2022. <https://doi.org/10.1002/chem.202102556>.
- (141) Capuani, S.; Porcari, P.; Fasano, F.; Campanella, R.; Maraviglia, B. 10B-Editing 1H-Detection and 19F MRI Strategies to Optimize Boron Neutron Capture Therapy. *Magn Reson Imaging* **2008**, *26* (7), 987–993. <https://doi.org/10.1016/j.mri.2008.01.040>.
- (142) Porcari, P.; Capuani, S.; D'Amore, E.; Lecce, M.; la Bella, A.; Fasano, F.; Campanella, R.; Migneco, L. M.; Pastore, F. S.; Maraviglia, B. In Vivo 19F MRI and 19F MRS of 19F- Labelled Boronophenylalanine-Fructose Complex on a C6 Rat Glioma Model to Optimize Boron Neutron Capture Therapy (BNCT). *Phys Med Biol* **2008**, *53* (23), 6979–6989. <https://doi.org/10.1088/0031-9155/53/23/021>.
- (143) Ciardiello, A.; Altieri, S.; Ballarini, F.; Bocci, V.; Bortolussi, S.; Cansolino, L.; Carlotti, D.; Ciocca, M.; Faccini, R.; Facchetti, A.; Ferrari, C.; Ficcadenti, L.; Furfaro, E.; Giagu, S.; Iacoangeli, F.; Macioce, G.; Mancini-Terracciano, C.; Messina, A.; Milazzo, L.; Pacifico, S.; Piccolella, S.; Postuma, I.; Rotili, D.; Vercesi, V.; Voena, C.; Vulcano, F.; Capuani, S. Multimodal Evaluation of 19F-BPA Internalization in Pancreatic Cancer Cells for Boron Capture and Proton Therapy Potential Applications. *Physica Medica* **2022**, *94*, 75–84. <https://doi.org/10.1016/j.ejmp.2021.12.011>.
- (144) Hess, S.; Blomberg, B. A.; Rakheja, R.; Friedman, K.; Kwee, T. C.; Højlund-Carlsen, P. F.; Alavi, A. A Brief Overview of Novel Approaches to FDG PET Imaging and Quantification. *Clinical and Translational Imaging*. Springer-Verlag Italia s.r.l. 2014, pp 187–198. <https://doi.org/10.1007/s40336-014-0062-2>.
- (145) Pijl, J. P.; Nienhuis, P. H.; Kwee, T. C.; Glaudemans, A. W. J. M.; Slart, R. H. J. A.; Gormsen, L. C. Limitations and Pitfalls of FDG-PET/CT in Infection and Inflammation. *Seminars in Nuclear Medicine*. W.B. Saunders November 1, 2021, pp 633–645. <https://doi.org/10.1053/j.semnuclmed.2021.06.008>.
- (146) Jacobson, O.; Chen, X. PET Designated Flouride-18 Production and Chemistry. *Curr Top Med Chem* **2010**, *10* (11), 1048–1059. <https://doi.org/10.2174/156802610791384298>.
- (147) Vallabhajosula, S.; Solnes, L.; Vallabhajosula, B. A Broad Overview of Positron Emission Tomography Radiopharmaceuticals and Clinical Applications: What Is New? *Seminars in Nuclear Medicine*. July 2011, pp 246–264. <https://doi.org/10.1053/j.semnuclmed.2011.02.003>.
- (148) Bidesi, N. S. R.; Vang Andersen, I.; Windhorst, A. D.; Shalgunov, V.; Herth, M. M. The Role of Neuroimaging in Parkinson's Disease. *J Neurochem* **2021**, *159* (4), 660–689. <https://doi.org/10.1111/jnc.15516>.
- (149) Toch, S.-R.; Poussier, S.; Micard, E.; Bertaux, M.; van der Gucht, A.; Chevalier, E.; Marie, P.-Y.; Guedj, E.; Verger, A. Physiological Whole-Brain Distribution of [18F]FDOPA Uptake Index in Relation to Age and Gender: Results from a Voxel-Based Semi-Quantitative Analysis. *Mol Imaging Biol* **2019**, *21* (3), 549–557. <https://doi.org/10.1007/s11307-018-1256-1>.
- (150) Jacobson, O.; Kiesewetter, D. O.; Chen, X. Fluorine-18 Radiochemistry, Labeling Strategies and Synthetic Routes. *Bioconjug Chem* **2015**, *26* (1), 1–18. <https://doi.org/10.1021/bc500475e>.

- (151) Coenen, H. H. Fluorine-18 Labeling Methods: Features and Possibilities of Basic Reactions. In *PET Chemistry*; Springer Berlin Heidelberg; pp 15–50. https://doi.org/10.1007/978-3-540-49527-7_2.
- (152) Kelly, N. M.; Sutherland, A.; Willis, C. L. Syntheses of Amino Acids Incorporating Stable Isotopes. *Nat Prod Rep* **1997**, *14* (3), 205. <https://doi.org/10.1039/np9971400205>.
- (153) Li, X. G.; Haaparanta, M.; Solin, O. Oxime Formation for Fluorine-18 Labeling of Peptides and Proteins for Positron Emission Tomography (PET) Imaging: A Review. *Journal of Fluorine Chemistry*. Elsevier B.V. 2012, pp 49–56. <https://doi.org/10.1016/j.jfluchem.2012.07.005>.
- (154) Ajenjo, J.; Destro, G.; Cornelissen, B.; Gouverneur, V. Closing the Gap between ^{19}F and ^{18}F Chemistry. *EJNMMI Radiopharmacy and Chemistry*. Springer Science and Business Media Deutschland GmbH December 1, 2021. <https://doi.org/10.1186/s41181-021-00143-y>.
- (155) Fowler, J. S.; Ido, T. Initial and Subsequent Approach for the Synthesis of ^{18}F FDG. *Semin Nucl Med* **2002**, *32* (1), 6–12. <https://doi.org/10.1053/snuc.2002.29270>.
- (156) Forsback, S.; Eskola, O.; Haaparanta, M.; Bergmann, J.; Solin, O. Electrophilic Synthesis of 6-[^{18}F]Fluoro-L-DOPA Using Post-Target Produced [^{18}F]F $_2$. *Radiochim Acta* **2008**, *96* (12), 845–848. <https://doi.org/10.1524/ract.2008.1527>.
- (157) Eskola, O.; Grönroos, T. J.; Forsback, S.; Tuomela, J.; Komar, G.; Bergman, J.; Härkönen, P.; Haaparanta, M.; Minn, H.; Solin, O. Tracer Level Electrophilic Synthesis and Pharmacokinetics of the Hypoxia Tracer [^{18}F]EF5. *Mol Imaging Biol* **2012**, *14* (2), 205–212. <https://doi.org/10.1007/s11307-011-0484-4>.
- (158) Bratteby, K.; Shalgunov, V.; Herth, M. M. Aliphatic ^{18}F -Radiofluorination: Recent Advances in the Labeling of Base-Sensitive Substrates. *ChemMedChem* **2021**, *16* (17), 2612–2622. <https://doi.org/10.1002/cmdc.202100303>.
- (159) Chansaenpak, K.; Vabre, B.; Gabbai, F. P. [^{18}F]-Group 13 Fluoride Derivatives as Radiotracers for Positron Emission Tomography. *Chemical Society Reviews*. Royal Society of Chemistry February 21, 2016, pp 954–971. <https://doi.org/10.1039/c5cs00687b>.
- (160) Rosenthal, M. S.; Bosch, A. L.; Nickles, R. J.; Gatley, S. J. Synthesis and Some Characteristics of No-Carrier Added [^{18}F]Fluorotrimethylsilane. *Int J Appl Radiat Isot* **1985**, *36* (4), 318–319. [https://doi.org/10.1016/0020-708X\(85\)90094-8](https://doi.org/10.1016/0020-708X(85)90094-8).
- (161) Schirmacher, R.; Bradtmöller, G.; Schirmacher, E.; Thews, O.; Tillmanns, J.; Siessmeier, T.; Buchholz, H. G.; Bartenstein, P.; Wängler, B.; Niemeyer, C. M.; Jurkschat, K. ^{18}F -Labeling of Peptides by Means of an Organosilicon-Based Fluoride Acceptor. *Angewandte Chemie - International Edition* **2006**, *45* (36), 6047–6050. <https://doi.org/10.1002/anie.200600795>.
- (162) Zhu, J.; Chin, J.; Wängler, C.; Wängler, B.; Lennox, R. B.; Schirmacher, R. Rapid ^{18}F -Labeling and Loading of PEGylated Gold Nanoparticles for in Vivo Applications. *Bioconjug Chem* **2014**, *25* (6), 1143–1150. <https://doi.org/10.1021/bc5001593>.
- (163) Ting, R.; Adam, M. J.; Ruth, T. J.; Perrin, D. M. Arylfluoroborates and Alkylfluorosilicates as Potential PET Imaging Agents: High-Yielding Aqueous Biomolecular ^{18}F -Labeling. *J Am Chem Soc* **2005**, *127* (38), 13094–13095. <https://doi.org/10.1021/ja053293a>.
- (164) Perrin, D. M. Organotrifluoroborates as Prosthetic Groups for Single-Step ^{18}F -Labeling of Complex Molecules. *Current Opinion in Chemical Biology*. Elsevier Ltd August 1, 2018, pp 86–94. <https://doi.org/10.1016/j.cbpa.2018.03.001>.

- (165) Bernard-Gauthier, V.; Bailey, J. J.; Liu, Z.; Wängler, B.; Wängler, C.; Jurkschat, K.; Perrin, D. M.; Schirmmayer, R. From Unorthodox to Established: The Current Status of ¹⁸F-Trifluoroborate- And ¹⁸F-SiFA-Based Radiopharmaceuticals in PET Nuclear Imaging. *Bioconjugate Chemistry*. American Chemical Society February 17, 2016, pp 267–279. <https://doi.org/10.1021/acs.bioconjchem.5b00560>.
- (166) Ting, R.; Harwig, C. W.; Lo, J.; Li, Y.; Adam, M. J.; Ruth, T. J.; Perrin, D. M. Substituent Effects on Aryltrifluoroborate Solvolysis in Water: Implications for Suzuki-Miyaura Coupling and the Design of Stable ¹⁸F-Labeled Aryltrifluoroborates for Use in PET Imaging. *Journal of Organic Chemistry* **2008**, *73* (12), 4662–4670. <https://doi.org/10.1021/jo800681d>.
- (167) Li, Z.; Chansaenpak, K.; Liu, S.; Wade, C. R.; Conti, P. S.; Gabbai, F. P. Harvesting ¹⁸F-Fluoride Ions in Water via Direct ¹⁸F-¹⁹F Isotopic Exchange: Radiofluorination of Zwitterionic Aryltrifluoroborates and in Vivo Stability Studies. *Medchemcomm* **2012**, *3* (10), 1305–1308. <https://doi.org/10.1039/c2md20105d>.
- (168) Liu, Z.; Chao, D.; Li, Y.; Ting, R.; Oh, J.; Perrin, D. M. From Minutes to Years: Predicting Organotrifluoroborate Solvolysis Rates. *Chemistry - A European Journal* **2014**, *21* (10), 3924–3928. <https://doi.org/10.1002/chem.201405829>.
- (169) Liu, Z.; Pourghiasian, M.; Bénard, F.; Pan, J.; Lin, K.-S.; Perrin, D. M. Preclinical Evaluation of a High-Affinity ¹⁸F-Trifluoroborate Octreotate Derivative for Somatostatin Receptor Imaging. *Journal of Nuclear Medicine* **2014**, *55* (9), 1499–1505. <https://doi.org/10.2967/jnumed.114.137836>.
- (170) Liu, Z.; Pourghiasian, M.; Radtke, M. A.; Lau, J.; Pan, J.; Dias, G. M.; Yapp, D.; Lin, K. S.; Bénard, F.; Perrin, D. M. An Organotrifluoroborate for Broadly Applicable One-Step¹⁸F-Labeling. *Angewandte Chemie - International Edition* **2014**, *53* (44), 11876–11880. <https://doi.org/10.1002/anie.201406258>.
- (171) Kuo, H.-T.; Lepage, M. L.; Lin, K.-S.; Pan, J.; Zhang, Z.; Liu, Z.; Pryyma, A.; Zhang, C.; Merckens, H.; Roxin, A.; Perrin, D. M.; Bénard, F. One-Step ¹⁸F-Labeling and Preclinical Evaluation of Prostate-Specific Membrane Antigen Trifluoroborate Probes for Cancer Imaging. *Journal of Nuclear Medicine* **2019**, *60* (8), 1160–1166. <https://doi.org/10.2967/jnumed.118.216598>.
- (172) Medicines Agency, E. *Background Review for the Excipient Propylene Glycol*; 2014. www.ema.europa.eu/contact.
- (173) Banerjee, S. S.; Aher, N.; Patil, R.; Khandare, J. Poly(Ethylene Glycol)-Prodrug Conjugates: Concept, Design, and Applications. *J Drug Deliv* **2012**, *2012*, 1–17. <https://doi.org/10.1155/2012/103973>.
- (174) Salman, A. A.; Heidelberg, T. In Situ Functionalized Fluorescent Nanoparticles for Efficient Receptor Coupling. *Journal of Nanoparticle Research* **2014**, *16* (5). <https://doi.org/10.1007/s11051-014-2399-x>.
- (175) Schirmmayer, R.; Bradtmöller, G.; Schirmmayer, E.; Thews, O.; Tillmanns, J.; Siessmeier, T.; Buchholz, H. G.; Bartenstein, P.; Wängler, B.; Niemeyer, C. M.; Jurkschat, K. ¹⁸F-Labeling of Peptides by Means of an Organosilicon-Based Fluoride Acceptor. *Angewandte Chemie - International Edition* **2006**, *45* (36), 6047–6050. <https://doi.org/10.1002/anie.200600795>.
- (176) Krishnan, H. S.; Ma, L.; Vasdev, N.; Liang, S. H. ¹⁸F-Labeling of Sensitive Biomolecules for Positron Emission Tomography. *Chemistry - A European Journal*. Wiley-VCH Verlag November 7, 2017, pp 15553–15577. <https://doi.org/10.1002/chem.201701581>.

- (177) Guo, J. R.; Huang, H. Y.; Yan, Y. L.; Liang, C. F. Selective S-Deacetylation of Functionalized Thioacetates Catalyzed by Dy(OTf)₃. *Asian J Org Chem* **2018**, *7* (1), 179–188. <https://doi.org/10.1002/ajoc.201700481>.
- (178) Han, C. C.; Balakumar, R. Mild and Efficient Methods for the Conversion of Benzylic Bromides to Benzylic Thiols. *Tetrahedron Lett* **2006**, *47* (47), 8255–8258. <https://doi.org/10.1016/j.tetlet.2006.09.093>.
- (179) Li, Z.; Wang, Z.; Zhu, L.; Tan, X.; Li, C. Silver-Catalyzed Radical Fluorination of Alkylboronates in Aqueous Solution. *J Am Chem Soc* **2014**, *136* (46), 16439–16443. <https://doi.org/10.1021/ja509548z>.
- (180) Stenhagen, I. S. R.; Kirjavainen, A. K.; Forsback, S. J.; Jørgensen, C. G.; Robins, E. G.; Luthra, S. K.; Solin, O.; Gouverneur, V. [18F]Fluorination of an Arylboronic Ester Using [18F]Selectfluor Bis(Triflate): Application to 6-[18F]Fluoro-l-DOPA. *Chemical Communications* **2013**, *49* (14), 1386–1388. <https://doi.org/10.1039/c2cc38646a>.
- (181) Cecioni, S.; Oerthel, V.; Iehl, J.; Holler, M.; Goyard, D.; Praly, J. P.; Imberty, A.; Nierengarten, J. F.; Vidal, S. Synthesis of Dodecavalent Fullerene-Based Glycoclusters and Evaluation of Their Binding Properties towards a Bacterial Lectin. *Chemistry - A European Journal* **2011**, *17* (11), 3252–3261. <https://doi.org/10.1002/chem.201003258>.
- (182) Bencivenni, G.; Lanza, T.; Leardini, R.; Minozzi, M.; Nanni, D.; Spagnolo, P.; Zanardi, G. Tin-Free Generation of Alkyl Radicals from Alkyl 4-Pentynyl Sulfides via Homolytic Substitution at the Sulfur Atom. *Org Lett* **2008**, *10* (6), 1127–1130. <https://doi.org/10.1021/ol800046k>.
- (183) Orlova, A. v.; Kondakov, N. N.; Kimel, B. G.; Kononov, L. O.; Kononova, E. G.; Sivaev, I. B.; Bregadze, V. I. Synthesis of Novel Derivatives of Closo-Dodecaborate Anion with Azido Group at the Terminal Position of the Spacer. *Appl Organomet Chem* **2007**, *21* (2), 98–100. <https://doi.org/10.1002/aoc.1151>.
- (184) Nelyubin, A. v.; Selivanov, N. A.; Bykov, A. Y.; Klyukin, I. N.; Novikov, A. S.; Zhdanov, A. P.; Karpechenko, N. Y.; Grigoriev, M. S.; Zhizhin, K. Y.; Kuznetsov, N. T. Primary Amine Nucleophilic Addition to Nitrilium Closo-dodecaborate [B₁₂H₁₁Ncch₃]⁺: A Simple and Effective Route to the New Bnct Drug Design. *Int J Mol Sci* **2021**, *22* (24). <https://doi.org/10.3390/ijms222413391>.
- (185) Armstrong, A. F.; Valliant, J. F. The Bioinorganic and Medicinal Chemistry of Carboranes: From New Drug Discovery to Molecular Imaging and Therapy. *Dalton Transactions* **2007**, No. 38, 4240–4251. <https://doi.org/10.1039/b709843j>.
- (186) Himmelspach, A.; Finze, M. Dicarba-Closo-Dodecaboranes with One and Two Ethynyl Groups Bonded to Boron. *Eur J Inorg Chem* **2010**, No. 13, 2012–2024. <https://doi.org/10.1002/ejic.201000064>.
- (187) Dziedzic, R. M.; Saleh, L. M. A.; Axtell, J. C.; Martin, J. L.; Stevens, S. L.; Royappa, A. T.; Rheingold, A. L.; Spokoynny, A. M. B-N, B-O, and B-CN Bond Formation via Palladium-Catalyzed Cross-Coupling of B-Bromo-Carboranes. *J Am Chem Soc* **2016**, *138* (29), 9081–9084. <https://doi.org/10.1021/jacs.6b05505>.
- (188) Ohta, K.; Goto, T.; Yamazaki, H.; Pichierri, F.; Endo, Y. Facile and Efficient Synthesis of C-Hydroxycarboranes and C,C'-Dihydroxycarboranes. *Inorg Chem* **2007**, *46* (10), 3966–3970. <https://doi.org/10.1021/ic062025q>.
- (189) Green, K. Improved Metalation of 2,4,6-Tribromoanisole: Synthesis of 2-Methoxyresorcinol. *J Org Chem* **1991**, *56* (13), 4325–4326. <https://doi.org/10.1021/jo00013a052>.

- (190) Stogniy, M. Y.; Erokhina, S. A.; Sivaev, I. B.; Bregadze, V. I. Synthesis of C-Methoxy- and C,C'-Dimethoxy-Ortho-Carboranes. *J Organomet Chem* **2020**, 927. <https://doi.org/10.1016/j.jorganchem.2020.121523>.
- (191) Stadlbauer, S.; Lönnecke, P.; Welzel, P.; Hey-Hawkins, E. Bis-Carbaborane-Bridged Bis-Glycophosphonates as Boron-Rich Delivery Agents for BNCT. *European J Org Chem* **2010**, No. 16, 3129–3139. <https://doi.org/10.1002/ejoc.201000213>.
- (192) Cao, K.; Zhang, C. Advances in the Synthesis of Biscarboranes. *European J Org Chem* **2022**, 2022 (31). <https://doi.org/10.1002/ejoc.202200737>.
- (193) Zhang, S.; Moussodia, R. O.; Sun, H. J.; Leowanawat, P.; Muncan, A.; Nusbaum, C. D.; Chelling, K. M.; Heiney, P. A.; Klein, M. L.; André, S.; Roy, R.; Gabius, H. J.; Percec, V. Mimicking Biological Membranes with Programmable Glycan Ligands Self-Assembled from Amphiphilic Janus Glycodendrimers. *Angewandte Chemie - International Edition* **2014**, 53 (41), 10899–10903. <https://doi.org/10.1002/anie.201403186>.
- (194) Schofield, C. L.; Mukhopadhyay, B.; Hardy, S. M.; McDonnell, M. B.; Field, R. A.; Russell, D. A. Colorimetric Detection of Ricinus Communis Agglutinin 120 Using Optimally Presented Carbohydrate-Stabilised Gold Nanoparticles. In *Analytst*; Royal Society of Chemistry, 2008; Vol. 133, pp 626–634. <https://doi.org/10.1039/b715250g>.
- (195) Guliyev, R.; Ozturk, S.; Sahin, E.; Akkaya, E. U. Expanded Bodipy Dyes: Anion Sensing Using a Bodipy Analog with an Additional Difluoroboron Bridge. *Org Lett* **2012**, 14 (6), 1528–1531. <https://doi.org/10.1021/ol300260q>.
- (196) Gillespie, R. J.; Hartman, J. S.; Parekh, M. *Solvent Effects on the Boron-Fluorine Coupling Constant and on Fluorine Exchange in the Tetrafluoroborate Anion*; 1968; Vol. 46.
- (197) Imperio, D.; del Grosso, E.; Fallarini, S.; Lombardi, G.; Panza, L. Synthesis of Sugar–Boronic Acid Derivatives: A Class of Potential Agents for Boron Neutron Capture Therapy. *Org Lett* **2017**, 19 (7), 1678–1681. <https://doi.org/10.1021/acs.orglett.7b00382>.
- (198) Pereira de Freitas, R.; lehl, J.; Delavaux-Nicot, B.; Nierengarten, J. F. Synthesis of Fullerene Building Blocks Bearing Alkyne or Azide Groups and Their Subsequent Functionalization by the Copper Mediated Huisgen 1,3-Dipolar Cycloaddition. *Tetrahedron* **2008**, 64 (50), 11409–11419. <https://doi.org/10.1016/j.tet.2008.09.047>.
- (199) <https://www.nanalysis.com/nmready-blog/2018/1/25/a-bright-application> visited on 26.01.2023